Title
Modular Advanced Oxidation Processes Enabled by Cathodic Hydrogen Peroxide Production

Author
Barazesh, James Michael

Publication Date
2017

Peer reviewed|Thesis/dissertation

Modular Advanced Oxidation Processes Enabled by Cathodic Hydrogen Peroxide Production

By

James Michael Barazesh

A dissertation submitted in partial satisfaction of

the requirements for the degree of

Doctor of Philosophy

in

Engineering - Civil and Environmental Engineering

in the

Graduate Division

of the

University of California, Berkeley

Committee in charge:

Professor David L. Sedlak, Chair

Professor Kara L. Nelson

Professor Laura Lammers

Summer 2017

Modular Advanced Oxidation Processes Enabled by Cathodic Hydrogen Peroxide Production

James Michael Barazesh

Abstract

Modular Advanced Oxidation Processes Enabled by Cathodic Hydrogen Peroxide Production

by

James Michael Barazesh

Doctor of Philosophy in Engineering - Civil and Environmental Engineering

University of California, Berkeley

Professor David L. Sedlak, Chair

Point-of-entry and point-of-use drinking water treatment have emerged as an alternative means of providing potable water in locations where centralized water treatment is unable to provide safe water or where access to treated water is impractical. Although such systems could be useful in many applications, adoption of the technology requires cost-effective, reliable removal of pathogens, trace organic contaminants, and pollutant metals. Electrochemical water treatment technologies are advantageous for small-scale, distributed water treatment because they can be installed quickly without large capital investment and reactants can be generated on demand, solely though the input of electrical energy. However, their adoption has been hampered by a variety of issues including limited understanding of removal mechanisms, variable treatment efficiency, uncertainties about durability, and relatively high costs of operations associated with power consumption. For example, anodic treatment of water sources containing chloride and bromide has been shown to attenuate parent compounds but produce potentially toxic products under certain conditions, which could preclude consumption of treated water. Much of the prior work regarding electrochemical treatment has been purely empirical or has been conducted in simplified electrolytes that are not representative of conditions encountered in treatment systems. Therefore, this research attempts to bridge this gap by providing both a theoretical understanding and practical application of electrochemical treatment of natural waters. At the same time, we identify novel electrochemical remediation strategies that challenge the status quo and address the major limitations barring the uptake of anodic oxidation for the treatment of organic pollutants from waste streams.

To identify conditions which anodic oxidation would be appropriate for treatment of organic contaminants in various drinking water sources, electrolysis of a suite of trace organic contaminants including pharmaceuticals, pesticides, and personal care products was evaluated under representative conditions (Chapter 2). Key reaction pathways, including transformation on anode surfaces and reactions with homogenous species including hydroxyl radicals, carbonate radicals, chlorine, and bromine were assessed for different classes of contaminants on both titanium-iridium oxide (Ti-IrO_2) and boron-doped diamond electrodes. Assessment of transformation rates indicate that many of the contaminants were transformed by halide species and that halogenated byproducts such as trihalomethanes and haloacetic acids were often

produced in excess of drinking water quality standards prior to complete removal of the contaminant.

To provide a means of employing electrochemical treatment without the production of toxic disinfection byproducts, an alternative approach was developed by integrating cathodically-driven electrolysis with ultraviolet (UV) photolysis to produce a low-cost system capable of transforming trace organic contaminants (Chapter 3). Using a carbon-based gas-permeable cathode, hydrogen peroxide (H_2O_2) was produced from ambient air with high efficiency. H_2O_2-containing water was then exposed to UV irradiation followed by passage through an anode chamber. The performance of the system was evaluated using a suite of trace organic contaminants that spanned a range of reactivity with UV light and hydroxyl radical. Results indicate that organic contaminants could be removed in flow-through reactors without the formation of toxic byproducts at a lower cost and energy demand than observed in conventional anodic oxidation systems.

Finally, the cathode-driven electrolysis system was applied for the removal of toxic trace elements in drinking water sources. Initial experiments conducted in contaminated groundwater collected from Colusa, CA indicated that dissolved arsenic, lead, and copper were converted into colloid-associated forms that could be removed by filtration when water passed through the treatment system (Chapter 4). Results indicate that the pollutant elements were associated with iron-containing colloids which were formed when dissolved Fe(II) in the groundwater was exposed to O_2 and H_2O_2. Experiments conducted with water containing solutes typically present in groundwater were used to gain insight into the mechanism through which toxic elements were removed. These experiments demonstrated that UV light caused changes in natural organic matter that altered its affinity for iron, and that loss of ligating ability was accelerated in the presence of Ca^{2+} and Mg^{2+}.

Collectively, results of the experiments included in this dissertation indicate that the modular advanced oxidation system integrating electrolysis with UV photolysis holds promise as a point-of-use or point-of-entry treatment system. Under conditions expected in water treatment systems, the device is capable of simultaneously removing trace organic contaminants and pollutant metals. Additional research is needed to further develop and deploy the system to assess its performance under field conditions.

TABLE OF CONTENTS

LIST OF FIGURES

LIST OF TABLES

ACKNOWLEDGMENTS

This arduous journey over the past 5 years would not have been possible without the support from a myriad of different people. First, I would like the thank David Sedlak for being a phenomenal advisor and providing support and guidance while simultaneously allowing me to confront challenges independently using my own creativity. I would also like to acknowledge that I had the privilege to be under the tutelage of Tom Hennebel, who led me on my journey on using electrochemistry for water treatment. Carsten Prasse, Kara Nelson, Bryan McCloskey, Laura Lammers, and Ashok Gadgil all provided valuable insight and helped shape my research vision over the years.

I would also like the thank my fellow graduate students and post-doctoral researchers, especially Jannis Wenk, Jessica Ray, Tom Bruton, Joe Charbonnet, Will Tarpeh, Siva Bandaru Chelsea Preble, Mike Taptich, Emily Marron, and Flo Bonvin, for providing support and friendship during my time at Berkeley. Lara Davidge, my girlfriend, has encouraged me and I am thankful for her devotion while I pursued my Ph.D.

Finally, I would like to thank my parents, Reza and Lynn Barazesh, for always supporting me every step of the way. They have always been my source of inspiration and I could not be more thankful for the love they have given me and amazing opportunities they have allowed me to explore.

CHAPTER 1. Introduction

1.1 Water Challenges of an Urbanizing World

Amidst rapid population growth, urbanization, and climate change, the world is entering an era where water demand exceeds declining freshwater resources (Figure 1.1) (Gikas & Tchobanoglous, 2009; Englehardt *et al.*, 2013; Hering *et al.*, 2013; Bichai *et al.*, 2015; Chini *et al.*, 2016; Liu *et al.*, 2016). Globally, 500 million people currently reside in areas where water demand exceeds locally available, renewable water sources (Mekonnen & Hoekstra, 2016). Changing water consumption patterns associated with higher standards of living, as well as increasing water withdrawals for industrial and agricultural production, are projected to increase the global water demand by ~50% by 2030 and exacerbate this deficit (Gleeson *et al.*, 2012). At the same time, climate change is expected to affect the spatial and temporal variability of precipitation events, influencing the replenishment, distribution, and availability of water resources (Oki & Kanae, 2006).

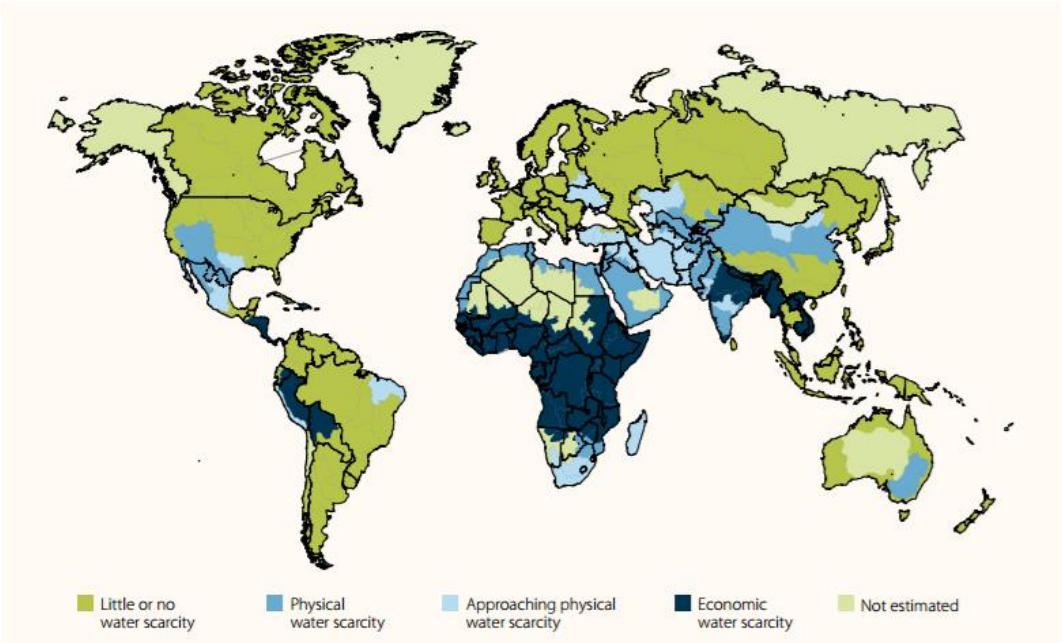

Figure 1.1. Global physical and economic water scarcity. Adapted from (World Water Assessment Programme, 2012).

This imbalance is further compounded by an outdated system of energy-intensive centralized water treatment and conveyance. Pumping costs associated with long-distance transport of treated water, often times over significant topographical elevations, negates the lower operational costs achieved at centralized treatment facilities due to economies of scale (Larsen *et al.*, 2016; Liu *et al.*, 2016). For example, the energy use associated with pumping water over the Tehachapi mountains to southern California is approximately 2.4 kWh per m^3, comparable to the energy required for seawater desalination (Nair *et al.*, 2014). Strategic changes in water resource management are needed to reliably provide potable water to cities and to

reduce the significant energy expenditure associated with importing, treating, and distributing water from centralized treatment facilities.

Small scale, decentralized approaches to water resources management that facilitate the use of nontraditional water sources, such as municipal wastewater, roof water, stormwater, and water from shallow aquifers, are promising alternatives as they can be installed rapidly without the significant capital costs required for centralized facilities (Dahlgren *et al.*, 2013; Larsen *et al.*, 2016). However, the presence of trace concentrations of organic contaminants (e.g., pesticides, solvents, pharmaceuticals) and toxic elements (e.g., arsenic, lead) pose threats to human health and challenge the viability of distributed treatment systems (Schwarzenbach *et al.*, 2006; Benotti *et al.*, 2008). Challenges and hazards associated with the transport, storage, and dosing of chemicals used in conventional treatment, such as chlorination and ozonation, limit the remediation processes that can be employed in decentralized systems (Larsen *et al.*, 2013).

1.2 Prevalence of Trace Organic Contaminants in the Environment

Worldwide, an estimated 80,000 organic chemicals, including pharmaceuticals, personal care products, and pesticides, are currently in daily use (Monteiro & Boxall, 2010). An estimated 300 million tons of synthetic compounds are continuously released to the aquatic environment annually from industrial and municipal discharges as well as nonpoint agricultural runoff (Schwarzenbach *et al.*, 2006). Depending on their chemical structure and polarity, many of these organic contaminants are recalcitrant and undergo incomplete removal in conventional wastewater treatment processes. For example, activated sludge used in secondary wastewater treatment typically removes less than 40% of influent trace organic contaminants (Daughton & Ternes, 1999; Oulton *et al.*, 2010). Accordingly, wastewater-derived organic contaminants and their metabolites have been detected in environmental surface waters at concentrations between 1 to 30,000 ng L^{-1} (Figure 1.2) (Kolpin *et al.*, 2002; Rice *et al.*, 2013; Bradley *et al.*, 2017).

The occurrence of one or more trace organic contaminants represents significant concerns for aquatic ecosystems. Of particular importance are pesticides/insecticides (e.g., atrazine, desulfinyl fipronil, metolachlor, glyphosate), steroid hormones (e.g., ethinyl estradiol, progesterone, testosterone), and detergent metabolites (e.g., triclosan) (Schwarzenbach *et al.*, 2006; Benotti *et al.*, 2008). For example, exposure of endocrine-active steroid hormones such as metformin and ethinyl estradiol induce upregulation of male intersex (i.e., fish feminization) at low ng L^{-1} concentrations (Purdom *et al.*, 1994; Niemuth *et al.*, 2015). Similarly, metabolites of the phenylpyrazole insecticide, fipronil, and neonicotinoid insecticide, imidacloprid, present significant toxicity to aquatic invertebrate ecosystems (Weston & Lydy, 2014; Morrissey *et al.*, 2015). Although the potential genotoxicological health risks of direct exposure of chemical-mixtures to humans are not fully understood, there is significant social and institutional concern over chronic exposure of endocrine-disrupting phenolic compounds and known carcinogens such as nitrosodimethylamine (NDMA) to reproductive impairment and increased cancer incidence (Mitch *et al.*, 2003; Benotti *et al.*, 2008). Indirectly, the presence of these antibiotics in wastewater effluent may lead to the selection of drug-resistant strains (Laxminarayan *et al.*, 2013). Accordingly, the presence of organic contaminant mixtures in streams and groundwater is unwarranted and threatens the adoption of distributed treatment systems if left unaddressed (Toze, 2006).

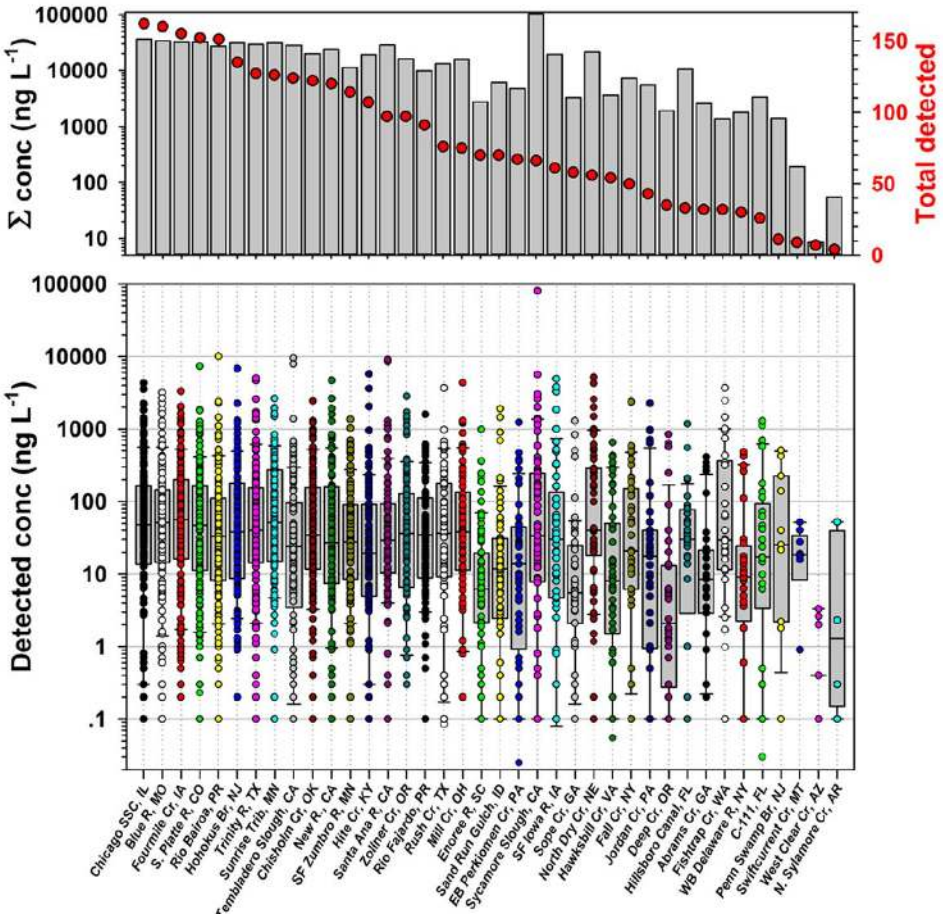

Figure 1.2. Top: Total numbers (red circles) and cumulative concentrations (ng L^{-1}; bars) of organic analytes detected in 38 streams sampled from 2012-2014. Bottom: Concentrations of individual organics detected (ng L^{-1}, circles) and range (whiskers, 5^{th}-95^{th} percentile; boxes 25^{th}-75^{th} percentile; solid line, median). Adapted from (Bradley *et al.*, 2017).

1.3 Treatment Technologies for the Removal of Trace Organic Contaminants

Trace organic contaminants can be removed from water by reactions with ozone or hydroxyl radicals formed from advanced oxidation processes (AOPs) applied in drinking water treatment, potable water reuse, and groundwater remediation (Huber *et al.*, 2003; Ternes *et al.*, 2003). However, ozone and ultraviolet light/hydrogen peroxide (i.e., UV/H_2O_2) require significant capital expenditure to retrofit existing wastewater treatment plant infrastructure and are complicated and operationally intensive, making them impractical for small-scale, point-of-use systems. Moreover, ozone can form the carcinogenic disinfection byproduct bromate during treatment of waters containing significant concentrations of bromide (Von Gunten & Oliveras, 1998). Although activated carbon can remove many trace organic contaminants from water, carbon cartridges require disposal and replacement once the sorption capacity is exceeded (Snyder *et al.*, 2007; Bonvin *et al.*, 2016). Other phase separation technologies using membrane treatment (e.g., microfiltration membrane bioreactors, carbon nanotubes) analogously suffer from flux losses after prolonged use due to membrane fouling (Shannon *et al.*, 2008).

Electrolysis is well suited for point-of-use treatment of contaminated water sources due to their small footprint, flexible design, and ability to generate reactive oxidants on demand. Previous research has demonstrated the ability of electrochemical systems to disinfect water and degrade a broad spectrum of organic contaminants (Bagastyo *et al.*, 2011; Butkovskyi *et al.*, 2014; Chaplin, 2014; Radjenovic & Sedlak, 2015; Barazesh *et al.*, 2016; Jasper *et al.*, 2016). Interest in electrochemical water treatment systems has been facilitated by the development of stable electrode materials, particularly boron-doped diamond and mixed-metal oxide anodes (e.g., IrO_2, RuO_2). Nonactive anodes (e.g., boron-doped diamond) exhibit high O_2 overpotentials (E_H ~ 2.0 V vs. SHE), enabling the partial oxidation of water at the anode surface to generate large yields of hydroxyl radicals (i.e., $HO^{\bullet}$) prior to O atom recombination to produce O_2 (Comninellis *et al.*, 2008). Although active anodes (e.g., IrO_2, RuO_2) exhibit lower yields of hydroxyl radicals (i.e., low O_2 overpotential; E_H ~ 1.5 V vs. SHE), they readily oxidize halide ions to form reactive species such as Cl_2, HOCl, and HOBr (Figure 1.3). Furthermore, direct electron transfer from organic pollutants to the anode surface results in transformation of contaminants that are otherwise recalcitrant to conventional oxidation techniques (e.g., perfluorinated organics) (Zhuo *et al.*, 2011).

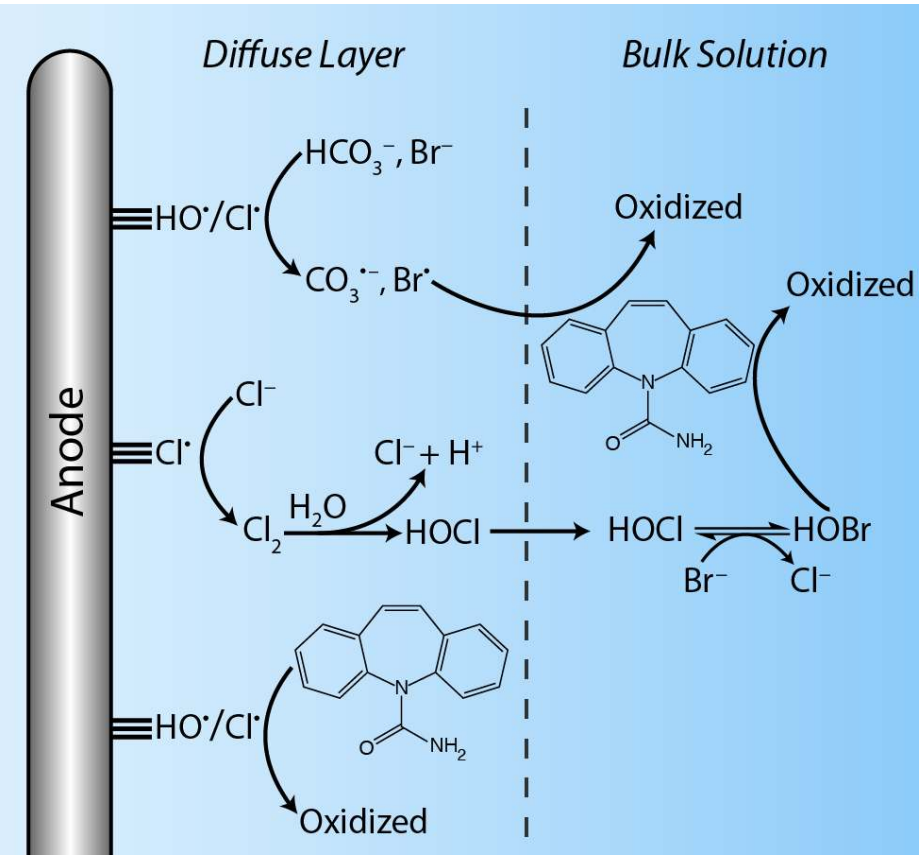

Figure 1.3. Production of oxidants and oxidation pathways of organic contaminants from dimensionally stable anodes. Adapted from (Barazesh *et al.*, 2016).

Despite its potential for application in distributed water treatment systems, electrolysis on anodes has not been widely adopted due to high capital costs of reactive electrodes, sluggish

mass transport to reactive surfaces, and production of toxic halogenated byproducts, such as bromate and perchlorate (Bergmann *et al.*, 2009; Azizi *et al.*, 2011). Furthermore, halogenation of aromatic contaminants often produces transformation products that may be more toxic than their parent compounds (Jasper *et al.*, 2016). For example, electrolysis of landfill leachate and reverse osmosis concentrate with boron-doped diamond electrodes resulted in the sequential halogenation of parent organic compounds to form trihalomethanes (THMs) and haloketones at concentrations exceeding drinking water standards (Anglada *et al.*, 2011; Lütke Eversloh *et al.*, 2015). Porous three-dimensional electrodes (Zaky & Chaplin, 2013), particulate electrodes (Zhu *et al.*, 2011), and electrochemical carbon nanotubes (Vecitis *et al.*, 2011) offer opportunities for increasing mass transfer and oxidation rates of contaminants. Such treatment technologies are still prone to byproduct formation and fouling during electrolysis when applied in drinking water sources containing high loadings of organic matter and halides. Successful implementation of point-of-use electrolysis therefore requires strategies to improve treatment efficacy and to minimize byproduct formation as well as new approaches that avoid the other limitations of oxidative electrochemical treatment.

1.4 Alternatives to Conventional Electrolysis

New approaches are needed that harness the intrinsic advantages of electrochemical systems (i.e., *in situ* chemical production) while simultaneously avoiding the pitfalls described above. One possible approach involves cathodic production of H_2O_2 from O_2. H_2O_2 produced in this manner has been used to generate oxidants through reactions with Fe(II) (i.e., the electro-Fenton system); however, production of H_2O_2 is most efficient at basic pH values while the Fenton reaction is inefficient at pH values above 5, resulting in low treatment efficiencies (Campos-Martin *et al.*, 2006; Brillas *et al.*, 2009). Additionally, the significant energy consumption associated with pumps and controllers needed to bubble air into solution to overcome the low solubility and sluggish diffusion of O_2 to the electrode increase energy consumption and capital costs (Campos-Martin *et al.*, 2006; Rozendal *et al.*, 2009; Modin & Fukushi, 2013; Yan *et al.*, 2014). Significant innovation is needed to create a suitable treatment technology for cathodic production of H_2O_2 in low ionic strength, circumneutral pH solutions without the consumption of large amounts of energy or production of solid waste.

To avoid the limitations of the Fenton reaction, it may be possible to produce hydroxyl radicals by exposing H_2O_2 to UV light:

$$H_2O_2 \xrightarrow{UV} 2\ HO^{\bullet}$$

This approach has been applied as an advanced oxidation process (AOP) in potable water reuse facilities and groundwater remediation systems (Comninellis *et al.*, 2008; Lee *et al.*, 2016). In distributed treatment systems, transport and storage of stock solutions of concentrated H_2O_2 is impractical due to the inherent instability of the compound. By using electrolysis cells designed specifically for cathodic production of H_2O_2 from O_2 followed by exposure to UV irradiation, it may be possible to employ the UV/H_2O_2 process remotely for distributed water treatment.

Investigation into the feasibility and reliability of new modular electrolysis systems to provide safe, potable water is needed to advance our understanding of situations when

electrochemical treatment is an appropriate solution and aid in the success of decentralized treatment uptake.

1.5 Motivation and Research Objectives

1.5.1 Motivation

Widespread adoption of decentralized drinking water treatment will require cost-effective, reliable technologies capable of operating without frequent maintenance or the need to replenish chemical reagents. The research described in this dissertation focuses on the use of an electrochemical system to remove trace contaminants typically present in drinking water sources with the objective of innovating in the space of low-energy, distributed water supply technologies. This will be accomplished by evaluating a novel system that combines *in situ* electrochemical production of H_2O_2 followed by UV irradiation and anodic treatment to remove trace organic contaminants and toxic trace elements from water. That said, a compressive understanding of anodic oxidation of organic contaminants is needed as a benchmark. Many previous studies of electrochemical systems were conducted in inert supporting electrolytes (i.e., $NaSO_4$, $NaClO_4$), often at ionic strengths well beyond those encountered in drinking waters. The few studies that have used authentic matrices have often failed to consider the fate of the parent compounds during transformation or the production of toxic byproducts. This research aims to resolve this disconnect by providing a mechanistic understanding of removal processes and treatment efficiencies when electrochemical treatment is applied using drinking water sources (Radjenovic & Sedlak, 2015). My specific objectives are as follows:

1.5.2 Objective 1: Determining the Fate of Oxidants in the Electrochemical Transformation of Trace Organic Contaminants During Anodic Oxidation of Natural Waters

The use of anodes to treat organic contaminants is a topic of considerable interest, especially in matrices with high conductivity such as industrial wastewater and reverse osmosis concentrate from municipal wastewater recycling (Bagastyo *et al.*, 2011; Butkovskyi *et al.*, 2014; Chaplin, 2014; Radjenovic & Sedlak, 2015). Although degradation of a diverse set of contaminants has been demonstrated in these matrices (Bagastyo *et al.*, 2011; Radjenovic *et al.*, 2011; Bagastyo *et al.*, 2013; Chaplin, 2014), the formation and fate of oxidants during treatment is poorly understood. Reactions of electrochemically-generated oxidants such as HOCl and $Cl_2^{\bullet-}$ with dissolved solutes, in particular natural organic matter (NOM), bromide, bicarbonate, and ammonium ions on the electrode surface can lead to the formation of secondary oxidants (e.g., $CO_3^{\bullet-}$, $NH_2^{\bullet}$) that could selectively react with certain trace organic compounds (Kiwi *et al.*, 2000; Grebel *et al.*, 2010; Rosario-Ortiz *et al.*, 2010; Jasper & Sedlak, 2013). Knowledge of the formation, reaction pathways, and fate of these species in electrochemical systems, as well as their propensity to form potentially toxic transformation products, is critical to identifying conditions under which anodic treatment will be practical. Therefore, the objective of this chapter was to gain insight into the role of different oxidants in contaminant transformation when electrolysis is employed for treatment of organic contaminants in waters containing halides and other solutes typically present in potential drinking water sources.

The effect of solution composition (Cl^-, HCO_3^-, NH_4^+) on the formation and fate of electrochemically-produced heterogeneous ($HO^\bullet_{ads}$, $Cl^\bullet_{ads}$) and homogenous (HOCl, HOBr) oxidants was evaluated on Ti-IrO_2 and boron-doped diamond electrodes using a suite of trace organic contaminants that exhibited varying reactivity with $HO^\bullet$, $CO_3^{\bullet-}$, HOCl and HOBr. Using this information, the contributions of reactions occurring on anode surfaces and in solution were used to predict contaminant removal in municipal wastewater effluent. Additionally, the formation of byproducts that could compromise the subsequent use of water was also evaluated. The approach employed in this study provides a means of identifying key reactions for different classes of contaminants and for predicting the conditions under which anodic treatment of wastewater will be practical.

1.5.3 Objective 2: Development and Testing of a Novel Electrochemical System Combining Cathodic H_2O_2 Production with UV Irradiation for the Removal of Trace Organic Contaminants

As described previously, the promise of anodic oxidation processes has been challenged by their low electro-active surface area and propensity to produce toxic halogenated byproducts during electrolysis of halide-containing waters. The objective of this phase of research was to evaluate the potential for employing cathodic production of H_2O_2 followed by UV photolysis as a novel, low cost means of transforming trace organic contaminants. A membrane-divided electrochemical cell employing an inexpensive carbon-based gas-permeable cathode was used to generate H_2O_2 from ambient air directly into water prior to exposure to UV irradiation and anodic pH adjustment (Figure 1.4).

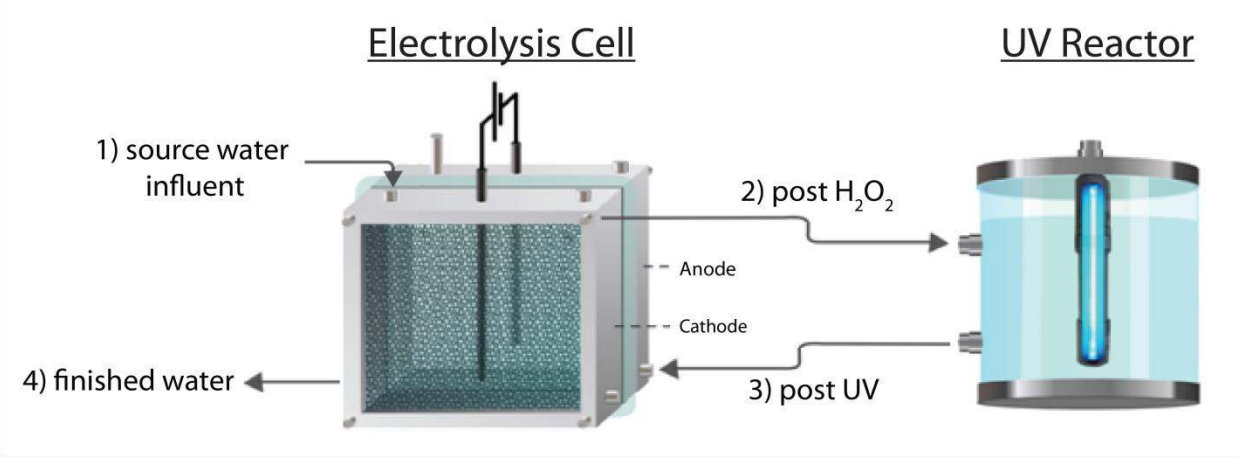

Figure 1.4. Schematic of the proposed modular advanced oxidation treatment system combining a dual-chambered electrolysis cell with low pressure mercury lamp.

Separation of anode and cathode chambers via a cation exchange membrane created a basic catholyte, which favored H_2O_2 production, while minimizing wasteful oxidation of H_2O_2 at the anode. Passage of the H_2O_2-containing catholyte through the anode following photolysis provided a means of quenching reactive chlorine and minimized the formation of halogenated byproducts. H_2O_2 production rates were quantified over a range of applied current densities and hydraulic residence times. The effectiveness of the technology was evaluated using a suite of trace contaminants that spanned a range of reactivity with UV light and hydroxyl radical ($HO^\bullet$)

in three different types of source waters (i.e., simulated groundwater, simulated surface water and municipal wastewater effluent) likely to be encountered in distributed water treatment systems. Results provided a basis for estimating the costs and energy use in the system.

1.5.4 Objective 3: Trace Element Removal in a Cathodic H_2O_2 / UV Irradiation Modular Electrolysis System

In addition to trace organic contaminants, drinking water sources often contain arsenic, lead, and other metals that pose health risks (Sansalone & Buchberger, 1997; Benotti *et al.*, 2009; Shi & Stone, 2009, 2009; Delaire *et al.*, 2015). Removal of arsenic and lead through coprecipitation with iron oxides is an effective means of removing trace elements, but it poses technical challenges with respect to management and disposal of contaminated solids, especially in distributed water treatment systems. Under conditions encountered in groundwater or organic-matter containing surface waters, high doses of iron are needed to remove oxyanions and metals due to the presence of iron-binding ligands in natural organic matter that inhibit iron oxide precipitation (Aiken *et al.*, 2011). Electrochemical and photochemical transformation of natural organic matter may oxidize iron-complexing ligands, thereby reducing the amount of iron needed to remove toxic trace elements.

The potential for using the modular advanced oxidation system to remove iron and trace elements was evaluated under conditions typically encountered in drinking water sources. Changes in the chemical composition and optical properties of iron-complexing ligands during treatment were evaluated using UV-visible spectroscopy, high resolution mass spectrometry, and electroanalytical techniques. Experiments conducted with differing concentrations of iron, organic matter, and divalent cations were used to assess the effect of solution chemistry on toxic trace element removal mechanisms. These data were used to assess the energy demand needed to achieve drinking water quality standards for arsenic in a representative, contaminated groundwater well in Colusa County, California.

CHAPTER 2. Electrochemical Transformation of Trace Organic Contaminants in the Presence of Halide and Carbonate Ions.

Reproduced with permission from Barazesh, J. M.; Prasse, C.; Sedlak, D. L. Electrochemical Transformation of Trace Organic Contaminants in the Presence of Halide and Carbonate Ions. *Environmental Science & Technology* **2016,** *50*, (18), 10143-10152.

2.1 Introduction

Electrochemical treatment of contaminated groundwater, industrial wastewater, and hazardous waste has gained interest as an alternative to advanced oxidation processes due to its ease of operation and ability to degrade a wide range of organic contaminants (Bagastyo *et al.*, 2011; Butkovskyi *et al.*, 2014; Chaplin, 2014; Radjenovic & Sedlak, 2015). In halide-free solutions, anodic treatment of contaminants proceeds through a combination of direct oxidation of compounds on the electrode surface and reaction with reactive species produced by partial oxidation of water. In particular, adsorbed hydroxyl radical ($HO^{\bullet}_{ads}$) has been invoked as an important oxidant generated at the surface of active electrodes (Comninellis, 1994; Chaplin, 2014).

When anodic treatment is performed in wastewaters and brines containing an abundance of halide ions, the rate of disappearance of organic contaminants often increases due to the formation of halogen-containing oxidants in the bulk solution, such as Cl_2, HOCl, and Br_2 (Bagastyo *et al.*, 2013; Butkovskyi *et al.*, 2014; Eversloh *et al.*, 2014; Eversloh *et al.*, 2015). Most researchers have ignored the possible role of adsorbed halogen species in contaminant transformation, despite their role as intermediates in the Volmer-Heyrovsky mechanism of electrochemical chlorine production (Krishtalik, 1981; Erenburg, 1984; Consonni *et al.*, 1987; Tomcsányi *et al.*, 1999; Ferro & De Battisti, 2002):

$$\equiv S + Cl^- \underset{k_{-1}}{\overset{k_1}{\leftrightarrow}} \equiv S(Cl^{\bullet}_{ads}) + e^- \quad (1)$$

$$\equiv S(Cl^{\bullet}_{ads}) + Cl^- \overset{k_2}{\rightarrow} \equiv S + Cl_2 + e^- \quad (2)$$

where ≡S corresponds to a surface lattice oxygen group that serves as the active site for the oxidation of chloride (Cho *et al.*, 2014). Formation of adsorbed chlorine atom ($Cl^{\bullet}_{ads}$) occurs at a much lower potential than $HO^{\bullet}_{ads}$ and therefore can be a significant anodic process, especially at the potentials used in electrochemical water treatment (Consonni *et al.*, 1987). Previously published data indicate that formation of Cl_2 (i.e., reaction 2) is limited by the rate of recombination of $Cl^{\bullet}_{ads}$ and the rate of diffusion of Cl_2 away from the electrode (Consonni *et al.*, 1987; Trasatti, 1987), enabling an accumulation of $Cl^{\bullet}_{ads}$ on anode surfaces (e.g., surface densities of up to 1.2×10^{-8} mol cm^{-2} have been observed on RuO_2 electrodes) (Tomcsányi *et al.*, 1999).

The importance of $Cl^{\bullet}_{ads}$ and other reactive halogens to contaminant transformation depends on their relative reactivity with halides and organic contaminants. In solution, chlorine atoms ($Cl^{\bullet}$) react with most organic contaminants at near-diffusion controlled rates (10^8 - 10^{10} M^{-1} s^{-1}) (Buxton *et al.*, 2000). However, other mechanisms of $Cl^{\bullet}_{ads}$ loss (e.g., recombination with $Cl^{\bullet}_{ads}$ to form Cl_2, propagation with Cl^- to form $Cl_2^{\bullet-}$, and reactions with other scavengers) may limit its role in contaminant transformation during electrochemical treatment. Nonetheless, there is evidence that $Cl^{\bullet}_{ads}$ formed via anodic oxidation may be important to contaminant transformation (Park *et al.*, 2009). Although the exact nature of adsorbed radicals (e.g., $HO^{\bullet}_{ads}$, $Cl^{\bullet}_{ads}$) is still unclear, it appears that they can play an important role in heterogeneous systems

and that their reactivity towards contaminants differs from that of their homogeneous analogues (Comninellis, 1994; Tojo *et al.*, 2004; Radjenovic & Sedlak, 2015).

Electrochemical treatment of waters containing elevated concentrations of dissolved solutes (e.g., brackish groundwater, wastewater effluent and reverse osmosis concentrate) can be affected by the matrix composition (Bagastyo *et al.*, 2011; Bagastyo *et al.*, 2013; Eversloh *et al.*, 2014; Eversloh *et al.*, 2015). In particular, reactions involving natural organic matter (NOM), bromide, bicarbonate, and ammonium ions on the electrode surface can lead to the formation of selective solution-phase oxidants (e.g., $CO_3^{\bullet-}$, $NH_2^{\bullet}$) that affect the rate of oxidation of certain trace organic compounds (Kiwi *et al.*, 2000; Grebel *et al.*, 2010; Rosario-Ortiz *et al.*, 2010; Jasper & Sedlak, 2013). Information on the formation and fate of these species in electrochemical systems is still limited.

The objective of this study was to gain insight into the role of different oxidants in contaminant transformation when electrolysis is employed for treatment of organic contaminants in waters containing halides and other solutes typically present in natural waters and municipal wastewater. By evaluating the oxidation of organic contaminants in the presence of various inorganic constituents, better strategies can be developed for assessing conditions under which electrochemical treatment is appropriate. To provide insight into the importance of transient species generated during electrolysis, both adsorbed to the electrode surface and in the bulk solution, the fate of a suite of trace contaminants exhibiting varying reactivity with different species was evaluated on two representative anodes (i.e., Ti-IrO_2 and boron-doped diamond) used in electrochemical water treatment.

2.2 Materials and Methods

2.2.1 Chemicals

All experiments were performed with reagent grade $NaHCO_3$, NaCl, NaBr, NH_4Cl, and $Na_2B_4O_7$ and analytical reference standards of organic contaminants (Sigma-Aldrich, St. Louis, MO). Chemical structures of trace organic contaminants studied are included in Table 2.1. Stable isotope-labeled analogues used as internal standards were obtained from Toronto Research Chemicals, Ontario, Canada. Suwannee River Humic Acid (SRHA) and Poly Lake Fulvic Acid (PLFA) were obtained from the International Humic Substances Society. Fluka analytical grade NaCl (< 0.001% Br^- by weight) was used for experiments performed with an electrolyte containing greater than 10 mM NaCl to minimize the possible effects of trace bromide impurities. NaOCl stock solutions were standardized monthly using N,N-diethyl-p-phenylenediamine (DPD) colorimetry.(Eaton *et al.*, 1998) Hypobromous acid (HOBr) stock solutions were prepared by adding 10% excess bromide to NaOCl solutions (Allard *et al.*, 2013). Grab samples of post-microfiltration wastewater effluent were obtained from the East Bay Municipal Utility District's wastewater treatment plant (Table 2.2; Oakland, CA).

Table 2.1. Chemical structures of test compounds

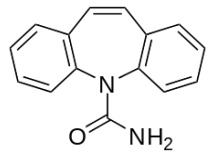

Carbamazepine (CBZ)

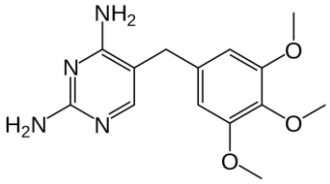

Trimethoprim (TMP)

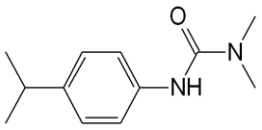

Isoproturon (ISO)

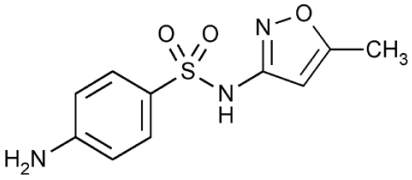

Sulfamethoxazole (SMX)

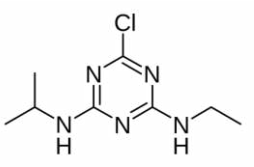

Atrazine (ATZ)

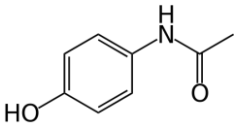

Acetaminophen (ACE)

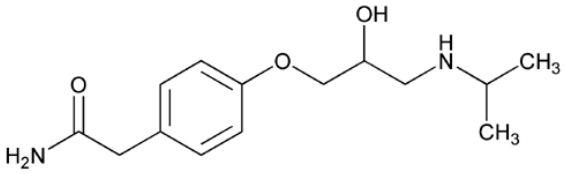

Atenolol (ATE)

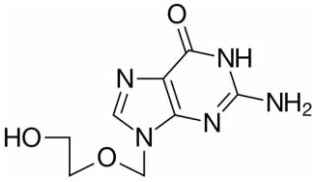

Acyclovir (ACY)

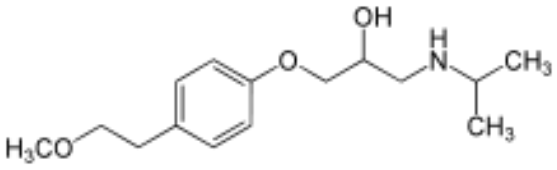

Metoprolol (MET)

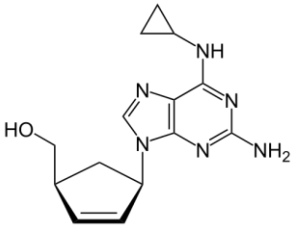

Abacavir (ABA)

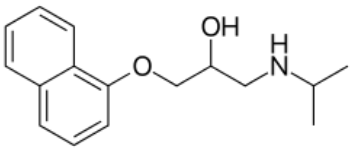

Propranolol (PRO)

Table 2.2. Composition of the wastewater effluent obtained from the East Bay Municipal Utilities District (EBMUD) wastewater treatment plant (Oakland, CA).

Cations (mM)	**Value**
Na^+	6.03
K^+	1.59
NH_4^+	0.41
Ca^{2+}	0.67
Mg^{2+}	0.69
Anions (mM)	
NO_3^-	0.032
NO_2^-	0.046
SO_4^{2-}	0.59
Cl^-	6.62
PO_4^{3-}	0.096
Br^-	0.007
Inorganic C (mM)	
HCO_3^-	5.1
CO_3^{2-}	LOD[a]
pH	7.2
DOC (mgC L^{-1})	9.5

[a]Limit of Detection (<0.1 mg L^{-1}).

2.2.2 Reaction Rate Constants for Organic Contaminants and Oxidants

Pseudo-first order rate constants for the reaction of test compounds with HOCl and HOBr were determined at pH 8.0 in 10 mM borate buffer. Solutions containing 10 µg L^{-1} of target compounds were amended with 0.1 to 1 mM NaOCl/NaOBr to initiate experiments, which were performed in triplicate. Samples were periodically collected, quenched with excess thiosulfate (3:1 thiosulfate-chlorine/bromine molar ratio), and analyzed for trace organic compounds.

2.2.3 Electrolysis Setup

Electrolysis experiments were carried out using either a Ti-IrO_2 mixed-metal oxide anode (64 cm^2; Magneto Special Anodes, Netherlands) or a BDD Diafilm EP anode (1.13 cm^2; Element 6; United States) in a single-chambered parallel plate electrochemical cell. In both cases, the anode was coupled with a stainless steel cathode of the same surface area (grade: 316L; Solana, Belgium; Figure 2.1). Electrolytes ($V_{TOT,Ti\text{-}IrO_2}$ = 250 mL; $V_{TOT,BDD}$ = 50 mL) were recirculated at a rate of 5 L h^{-1}. All experiments were performed at a fixed current of 80 A m^{-2} controlled by a multichannel potentiostat (Gamry Instruments Inc., Warminster, PA).

2.2.4 Electrolysis Experiments

Electrolysis experiments were conducted in a supporting electrolyte (10 mM borate buffer; pH 8.0 or 10.0) containing a mixture of 11 test compounds each at concentration of 10 µg L^{-1}. To elucidate the role of different solutes on transformation rates, the borate-buffered electrolyte was additionally modified with either NaCl, NH_4Cl, NaBr, $NaHCO_3$, or NOM. The

pH was monitored over the course of the experiment and never changed by more than 0.1 unit. Samples were periodically collected, quenched with excess thiosulfate (3:1 thiosulfate-chlorine molar ratio), and analyzed for trace organic compounds within 12 hours.

Experiments performed in the absence of current to assess sorption of contaminants to the anode indicated only modest losses of propranolol via adsorption ($k_{Ti\text{-}IrO_2} = 5.6 \times 10^{-4}\ s^{-1}$). To assess the influence of reduction on the cathode to observed transformation rates, electrolysis of NaCl was performed in a dual-chambered electrochemical cell separated by a cation exchange membrane (Ultrex CMI-7000, Membranes International Inc., Ringwood, NJ). HOCl production and contaminant transformation rates were nearly identical when experiments were conducted with the anode chamber isolated from the system, indicating cathodic reactions were unimportant to chlorine accumulation or contaminant transformation.

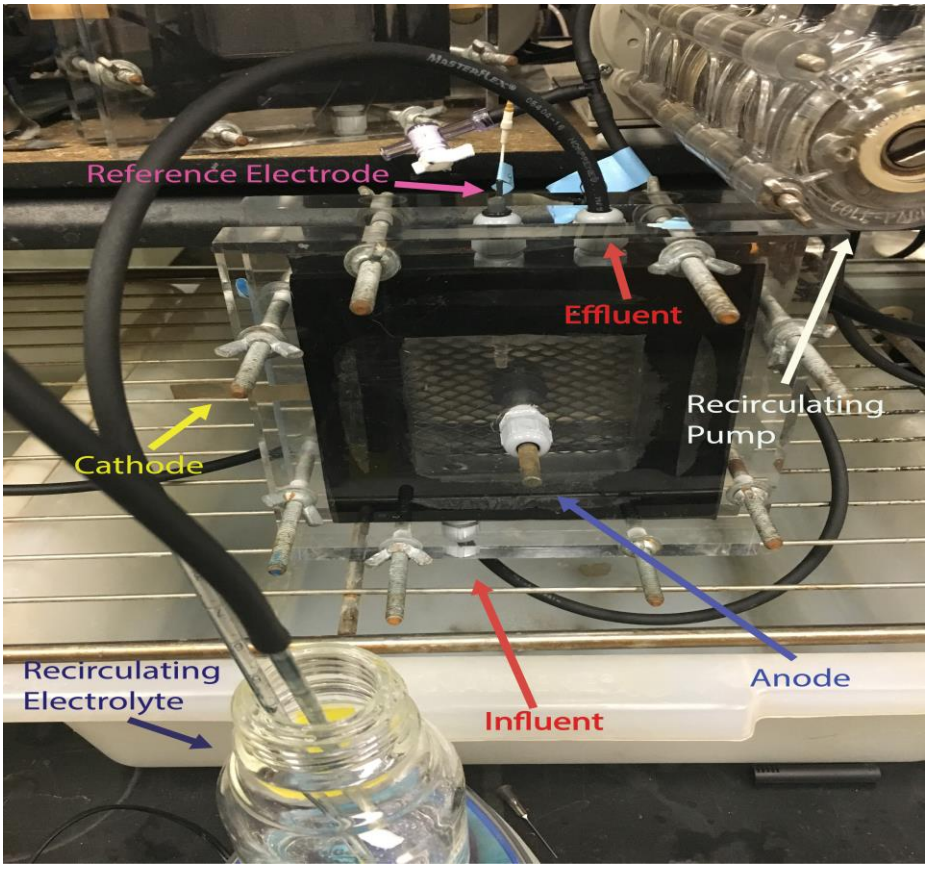

Figure 2.1: Laboratory setup used for anodic oxidation experiments.

Cyclic voltammograms to determine the potentials required for direct oxidation of organic compounds were performed in a pH 8.0, 1.5 M $NaClO_4$ electrolyte at a scan rate of 10 mV s^{-1} over a 2V potential range. Chronoamperometry experiments were performed to evaluate if inorganic solutes (e.g., HCO_3^-, Cl^-) underwent direct electron transfer on the anode. A potential of 1.55 V was applied using 0.5 M $NaClO_4$ at pH 8.0 until a stable current for water oxidation was reached (Azizi *et al.*, 2011). At this point, the electrolyte was amended with 50 mM HCO_3^-

or Cl^- and the current increase was measured. High concentration of solutes were used to prevent mass-transfer limitations at the anode surface.

2.2.5 Trace Organic Contaminant Removal via Electrolysis

Allyl alcohol (3-propenol, AA; 100 mM) or tertiary butanol (*t*-buOH; 100 mM) were used as selective quenchers to differentiate the importance of reactions involving adsorbed radicals (e.g., $Cl^{\bullet}_{ads}$ and $HO^{\bullet}_{ads}$) and dissolved radicals (e.g., $HO^{\bullet}$, $CO_3^{\bullet-}$) to contaminant electrolysis rates, respectively. Allyl alcohol was useful for probing surface-bound oxidants because the interaction of its π-orbitals with the positively charged anode surface and the high reactivity of the allylic carbon with oxidants allows it to react at the electrode surface (Celdran & Gonzalezvelasco, 1981; Pastor *et al.*, 1993). In contrast, saturated alcohols (i.e., *t*-buOH) do not react readily with electrode surfaces (Solomon & Madix, 1987), yet react rapidly with dissolved oxidants ($HO^{\bullet}$ and $Cl^{\bullet}$) and thus provide estimates of the importance of reactive solution phase intermediates. As allyl alcohol reacts rapidly with both heterogeneous and homogenous oxidants, transformation of the contaminants observed in the presence of high concentrations of allyl alcohol were ascribed exclusively to direct electron transfer.

The bulk solution steady-state concentration of $HO^{\bullet}$ ($[HO^{\bullet}]_{SS}$) was measured using *para*-chlorobenzoic acid (*p*CBA; 10 μM) as a probe ($k_{pCBA,\ HO\bullet} = 5 \times 10^9\ M^{-1}\ s^{-1}$) (Buxton *et al.*, 1988). Under the experimental conditions employed (i.e., $[Cl^-]$ =10 mM; pH 8.0), $Cl^{\bullet}$ in the bulk solution was converted rapidly to $Cl_2^{\bullet-}$, which is relatively unreactive with *p*CBA ($k_{pCBA,\ Cl_2\bullet-} = 3 \times 10^6\ M^{-1}\ s^{-1}$) (Buxton *et al.*, 1988). Control experiments in the presence of allyl alcohol indicated that direct oxidation of adsorbed *p*CBA was negligible, which agreed with published literature (Wang *et al.*, 2015).

Due to accumulation of HOCl, the contribution of free chlorine to compound oxidation increased with time (Eversloh *et al.*, 2015). This phenomenon was especially evident for compounds exhibiting high reactivity with HOCl (e.g., sulfamethoxazole, abacavir, acylovir, trimethoprim). For these compounds, deviations from first-order disappearance ($0.95 < r^2 < 0.98$) were observed.

2.2.6 Quantification of Surface Titanol Group Density

The surface density of adsorbed oxidants is needed to determine if they are present at high enough concentrations to play a role in oxidation relative to their homogeneous analogues. Ion-exchange capacity provides a means of estimating active surface area of oxide electrodes (Trasatti & Petrii, 1991). The density of electrocatalytic sites for the formation of surface hydroxyl and chlorine radical (i.e., ≡TiOH) (Erenburg, 1984; Trasatti, 1987; Cho & Hoffmann, 2014) was determined using the toluidine blue O (TBO) colorimetric method (Ray *et al.*, 2012). Briefly, electrodes were submerged in 0.05 mM TBO at pH 10.0 for 24 h at 30°C to promote TBO adsorption to surface functional groups (i.e., $\equiv TiO^-$). Excess TBO was rinsed off with 1 M NaOH and adsorbed TBO was subsequently desorbed in 8 mL of 50% acetic acid. Samples were vortexed for 10 min prior to spectroscopic measurement at 633 nm.

2.2.7 Analytical Methods

Free chlorine and TBO concentrations were measured with a Shimadzu UV-2600 spectrophotometer using the DPD method at 515 nm (Eaton *et al.*, 1998) and the TBO method at 633 nm, respectively (Ray *et al.*, 2012). Test compounds were quantified by HPLC/MS-MS in the multiple reaction monitoring (MRM) mode using an Agilent 1200 series HPLC system with a Hydro-RP column (150 x 3mm, 4uM; Phenomenex, Aschaffenburg, Germany) coupled to a 6460 triple quadropole tandem mass spectrometer as described previously (Jasper *et al.*, 2014). *p*CBA was quantified on a high-performance liquid chromatography (HPLC) system equipped with UV detection at 254 nm (Agilent 1260 Infinity). Analytical details and compound specific parameters are provided in Section A.2.1 of the Appendix.

Trihalomethanes (THMs) and haloacetic acids (HAA's) were also measured during electrolysis. THM's (1 mL sample aliquots) were extracted using pentane (2 mL) and the organic phase was centrifuged for 5 min and 5000 RPM and collected for analysis. HAA samples (1 mL) were amended with 0.5 g of sodium sulfate, acidified with 0.1 mL of concentrated sulfuric acid, and extracted using 2 mL of methyl tert-butyl ether. HAAs and THMs were analyzed by gas chromatography coupled to a mass spectrometer (GC/MS) in selected ion monitoring mode (SIM) using previously reported methods (Xie, 2001; Weinberg *et al.*, 2002).

2.3 Results and Discussion

Electrolysis rates for organic contaminants in the presence of halide and carbonate ions includes transformation via direct electron transfer in addition to contributions from reactive oxygen species ($HO^{\bullet}_{ads}$, $HO^{\bullet}$), reactive halide species ($Cl^{\bullet}_{ads}$, $Cl_2^{\bullet-}$, HOX), and $CO_3^{\bullet-}$. Experiments performed with quencher compounds detailed in the materials and methods section were used to isolate reactive dissolved and adsorbed species and gain insight into their contribution to electrolysis rates.

2.3.1 Oxidation of Trace Organic Contaminants by Dissolved Oxidants

Reaction rates for the test compounds with HOCl and HOBr varied by more than three orders of magnitude, exhibiting faster kinetics for compounds containing electron-rich aniline and deprotonated amine moieties (Figure 2.2). Bimolecular rate constants for HOCl with test compounds were in good agreement with previously reported data. Second-order reaction rate constants obtained from previous publications for trace organic contaminants with $HO^{\bullet}$ approached diffusion-controlled rates (10^9 - 10^{11} M^{-1} s^{-1}) (Acero *et al.*, 2000; Huber *et al.*, 2003; Jasper & Sedlak, 2013; De Laurentiis *et al.*, 2014; Prasse *et al.*, 2015), while rates of reaction with $CO_3^{\bullet-}$ ranged between 10^6 to 10^9 M^{-1} s^{-1} (Canonica *et al.*, 2005; Jasper & Sedlak, 2013; Prasse *et al.*, 2015), reflecting the selectivity of $CO_3^{\bullet-}$ with the previously mentioned electron-rich structural moieties, such as the reactive cyclopropyl and amino-adenine moieties of abacavir and the guanine moiety present in acyclovir (Prasse *et al.*, 2015).

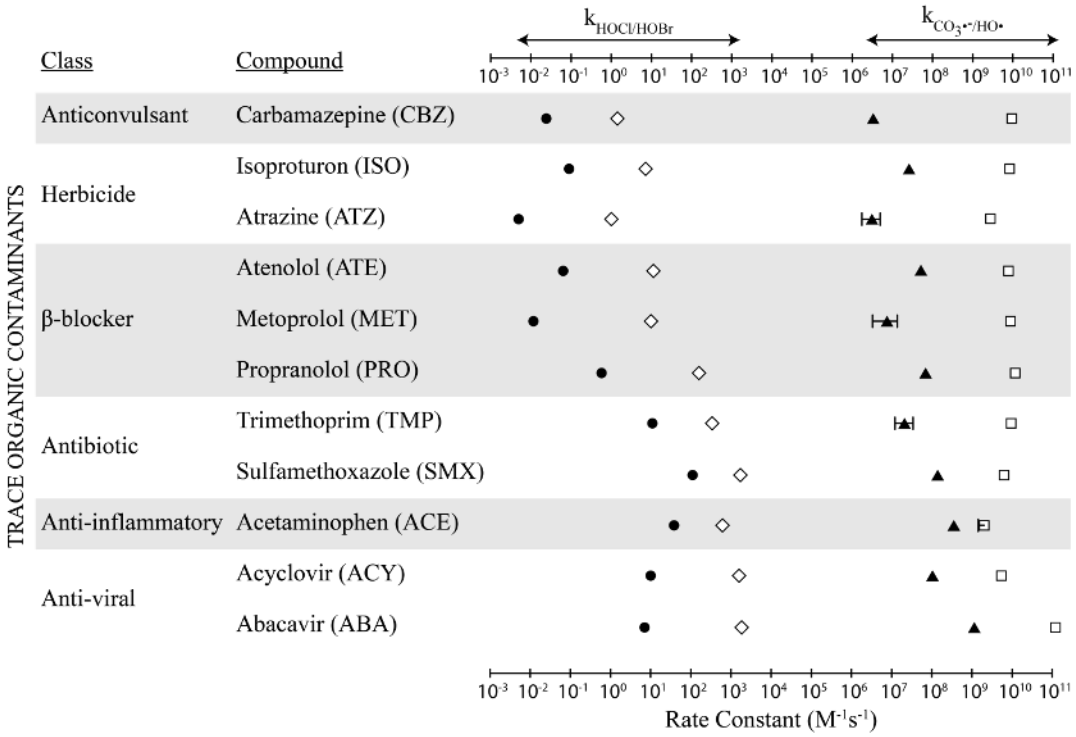

Figure 2.2: Bimolecular rate constants for the reaction between HOCl (●), HOBr (◊), $CO_3^{\bullet-}$ (▲), and $HO^{\bullet}$ (□) with trace organic contaminants. Rate constants for HOCl/HOBr were determined at pH 8.0. Error bars represent ± one standard deviation. In some cases, error bars are smaller than the data points.

2.3.2 Oxidation of Trace Organic Contaminants on Ti-IrO_2 Electrode Surfaces

HOCl production rates were fully inhibited by allyl alcohol ($k_{AA,\ Cl^{\bullet}} \approx 6 \times 10^8\ M^{-1}\ s^{-1}$) but were unaltered in the presence of *t*-buOH ($k_{t\text{-butanol},\ Cl^{\bullet}} = 1.5 \times 10^9\ M^{-1}\ s^{-1}$) (Gilbert *et al.*, 1988), thus confirming the selective reactivity of allyl alcohol with surface-bound oxidants (i.e., $Cl^{\bullet}_{ads}$; Figure 2.3). This was further supported by identical contaminant loss rates observed in borate, NaCl, and $NaHCO_3$ electrolytes in the presence of allyl alcohol, suggesting transformation was solely attributable to direct electron transfer from the anode to yield intermediate radical cations (Figure 2.4) (Chaplin, 2014). Cyclic voltammetry scans using acetaminophen as a probe compound indicated that oxidation via direct oxidation of the adsorbed organics occurred at potentials above +0.75 V (Figure 2.5).

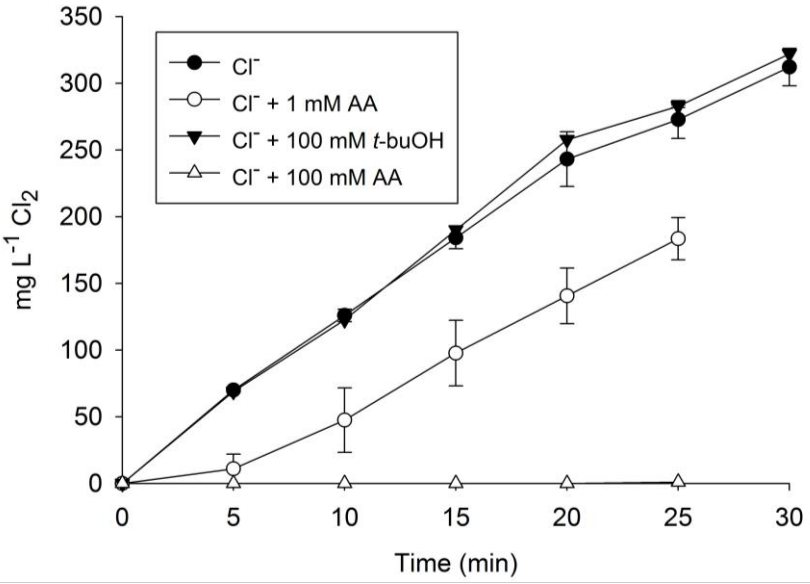

Figure 2.3: HOCl production on a Ti-IrO_2 electrode in a 10 mM chloride electrolyte in the presence of quenchers.

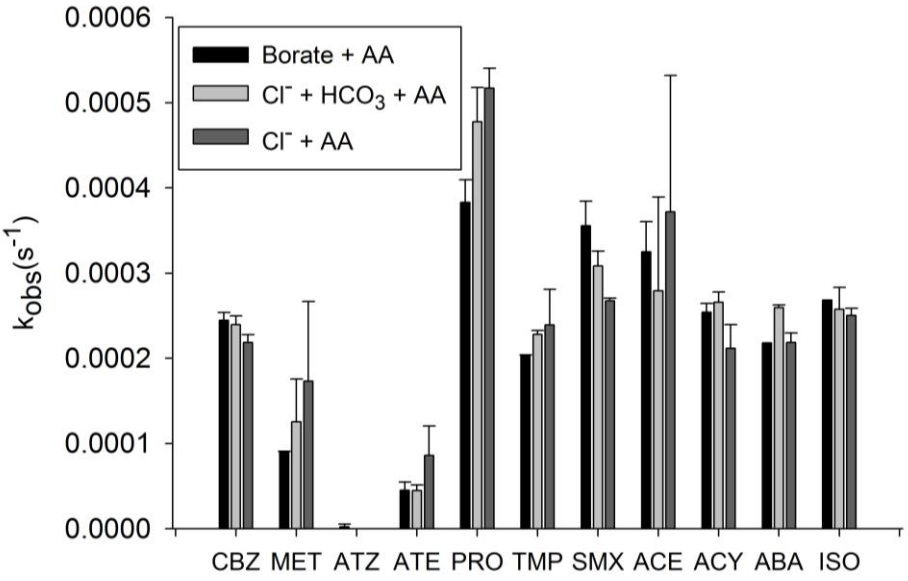

Figure 2.4: Removal rates of trace organic contaminants (s^{-1}) on Ti-IrO_2 electrode in the presence of 100 mM allyl alcohol.

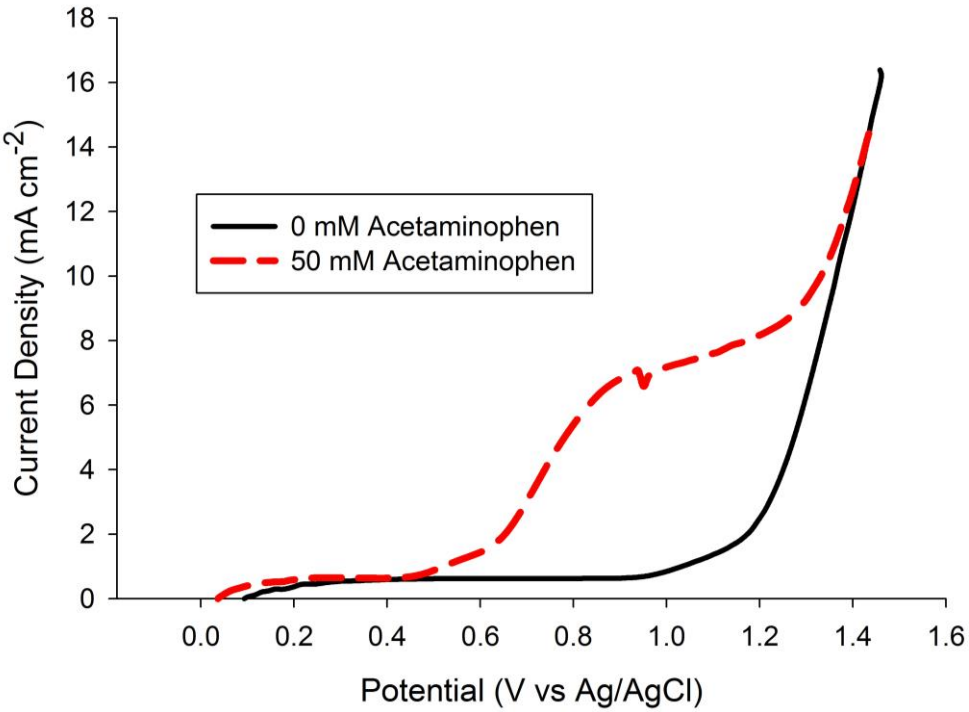

Figure 2.5: Cyclic Voltammogram in the presence and absence of acetaminophen in a pH 8, 1.5 M $NaClO_4$ electrolyte at a scan rate of 10 mV s^{-1}.

2.3.3 Impact of Solutes on Electrochemical Transformation of Contaminants

The observed loss rates for the trace contaminants in borate buffer at pH 8.0 ranged from 3.4×10^{-5} to 7.3×10^{-3} s^{-1} (Figure 2.6). In general, the relatively slow rate of contaminant removal on Ti-IrO_2 can be attributed to the low $HO^{\bullet}_{ads}$ production at an anodic potential of ~1.70 V at pH 8.0 (See Section A.2.2 of the Appendix). Loss rates for the organic compounds were not affected by addition of *t*-buOH, indicating that contribution of dissolved $HO^{\bullet}$ (measured $[HO^{\bullet}]_{SS} = 3.2 \times 10^{-15}$ M) to overall compound loss was small relative to surface-bound oxidation processes (i.e., direct electron transfer and reactions with $HO^{\bullet}_{ads}$). The negligible importance of dissolved $HO^{\bullet}$ was consistent with the short lifetimes of the reactive radical (i.e., < 1µs) relative to the time needed for diffusion out of the boundary layer (Azizi *et al.*, 2011; Chaplin, 2014).

The very slow rate of removal of atrazine (ATZ) was attributed to the stability of the s-triazine ring to electrochemical oxidation, as shown in previous studies (Acero *et al.*, 2000; Malpass *et al.*, 2006; Balci *et al.*, 2009; Oturan *et al.*, 2012). Similarly, the slow rate of loss of atenolol (ATE; pK_A 9.6) and metoprolol (MET; pK_A 9.1) at pH 8.0 was likely related to electrostatic repulsion between the positively charged anode surface and protonated amine functional groups. When the experiment was repeated at pH 10.0, the removal rate of atenolol and metoprolol increased by 330% and 190%, respectively (Figure 2.7).

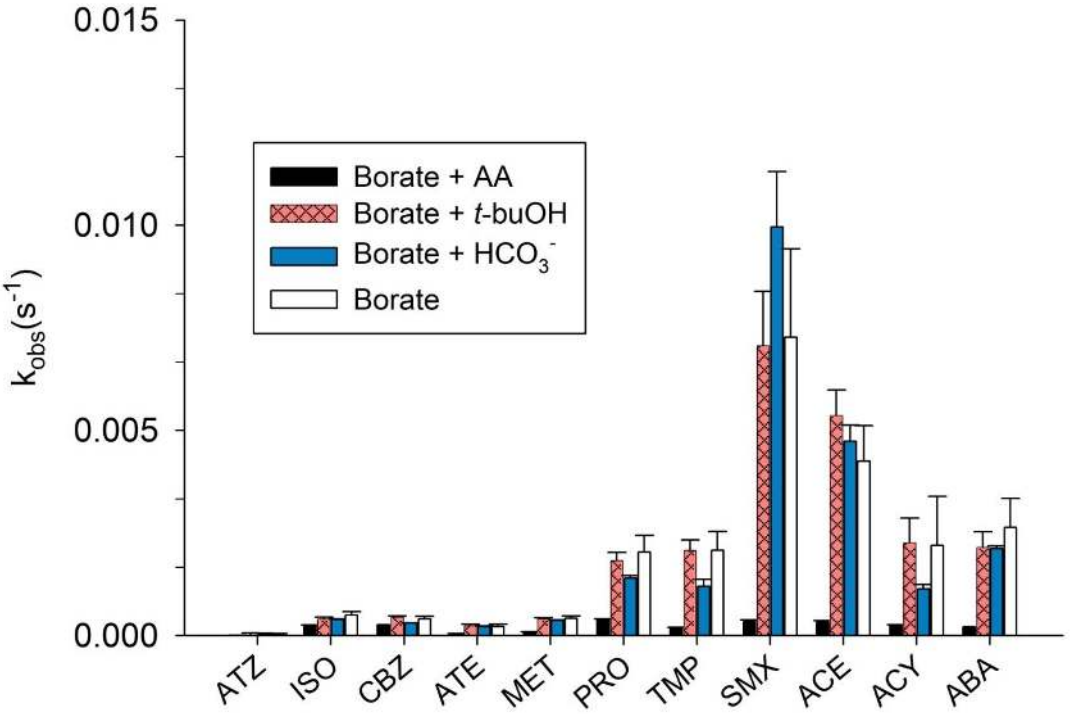

Figure 2.6: Observed first-order loss rates of trace organic contaminants on the Ti-IrO_2 electrode in 10 mM borate (pH 8.0) amended with 100 mM allyl alcohol (AA), 100 mM tertiary butanol *(t*-buOH), and 10 mM HCO_3^-. Error bars represent ± one standard deviation

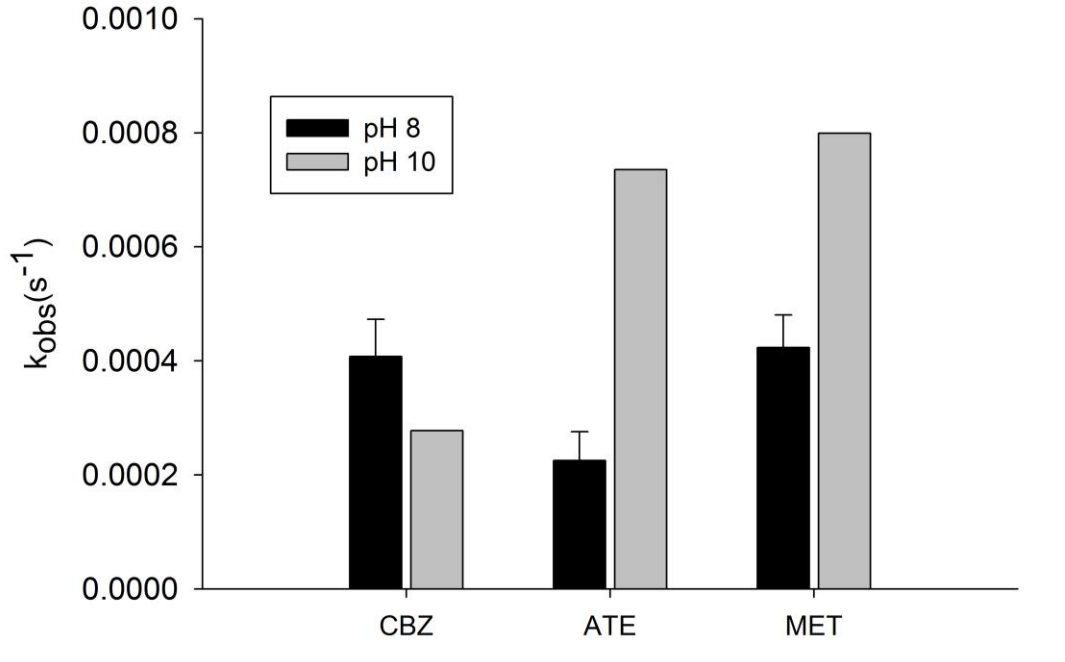

Figure 2.7: Removal rates of electron-poor trace organic contaminants (s^{-1}) on Ti-IrO_2 electrode at pH 8 and pH 10 borate-buffered electrolyte.

Significantly reduced rates of removal of propranolol (PRO), trimethoprim (TMP), sulfamethoxazole (SMX), acetaminophen (ACE), acyclovir (ACY), and abacavir (ABA) in the presence of allyl alcohol indicated that $HO^{\bullet}_{ads}$ contributed greatly to transformation (>85%; Figure 2.6). In contrast, removal of isoproturon (ISO) and carbamazepine (CBZ) was only partially inhibited by allyl alcohol suggesting that reactions with $HO^{\bullet}_{ads}$ are less important for these compounds (< 45%). Differences in relative reactivities among structurally similar aromatic amides with small variations in electron density (e.g., ACE and ISO) implied that $HO^{\bullet}_{ads}$ is more selective than its dissolved counterpart. Unlike ISO, the phenolic functional group present in ACE was more susceptible to electrophilic attack by $HO^{\bullet}_{ads}$. The high reactivity of $HO^{\bullet}_{ads}$ with SMX can most likely be attributed to the electron-rich aniline and/or isoxazole moiety.

Effect of Chloride. The addition of 10 mM chloride dramatically enhanced the loss rates of all trace organic contaminants relative to those observed in the borate-buffered electrolyte (i.e., 4 - 20 times increase; Figure 2.8). Contaminant removal was not affected by the presence of *t*-buOH, suggesting that contribution of dissolved $HO^{\bullet}$ and $Cl_2^{\bullet-}$ to the transformation process was negligible (measured $[HO^{\bullet}]_{SS} = 1.3 \times 10^{-14}$ M; Figure 2.9).

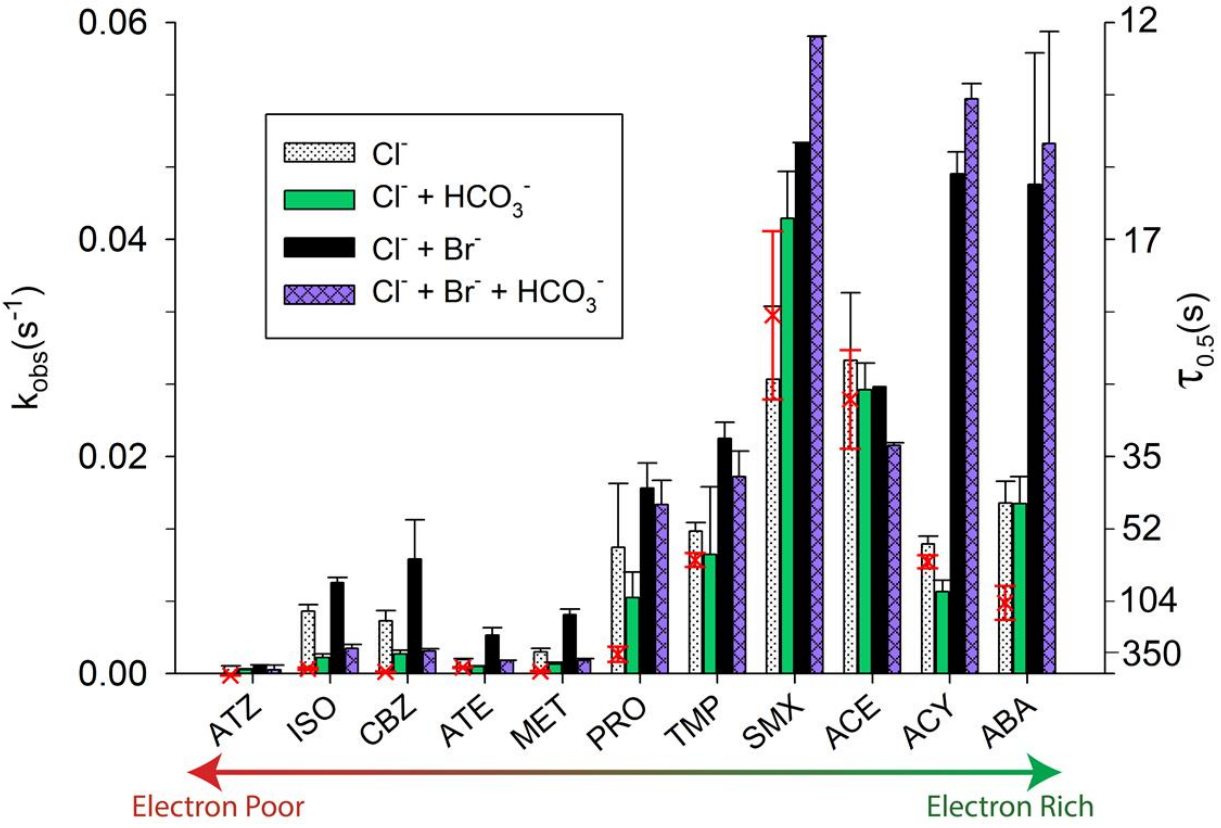

Figure 2.8: Observed first-order loss rates of trace organic contaminants on the Ti-IrO_2 electrode at pH 8.0 in 10 mM NaCl in the presence and absence of 20 µM NaBr and/or 10 mM HCO_3^-. Error bars represent ± one standard deviation. Red ×'s correspond to predicted first-order loss rates for 10 mM NaCl.

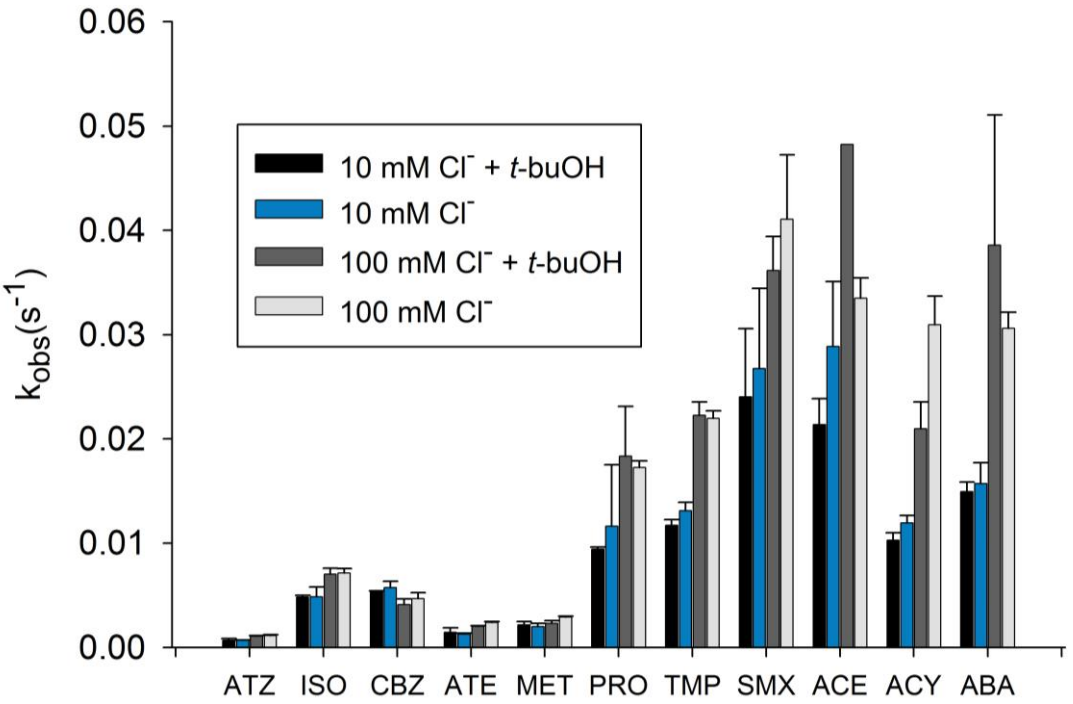

Figure 2.9: Pseudo-first order degradation rate of trace organic contaminants (s^{-1}) on Ti-IrO_2 electrode in NaCl electrolytes in the and absence of *t*-buOH.

Compounds containing strong electron-donating moieties, such as deprotonated amines (TMP, ACY, ABA), anilines (SMX), methoxy-naphtalenes (PRO), and phenolic groups (ACE), were removed faster due to rapid reactions with electrochemically generated HOCl (Figure 3.1). With the exception of abacavir and propranolol, estimates of transformation rates due to direct electron transfer, $HO^{\bullet}_{ads}$, and HOCl agreed to within 20% of observed values (Figure 2.8):

$$k_{pred} \approx k_{DET} + k_{HO^{\bullet}_{ads}} + k_{HOCl}[HOCl] \quad (3)$$

where k_{pred} is the predicted transformation rate (s^{-1}), k_{DET} and $k_{HO^{\bullet}_{ads}}$ are the transformation rates due to direct electron transfer and surface-bound oxidants, respectively, determined previously in borate buffered electrolyte (s^{-1}) in the presence and absence of allyl alcohol, and k_{HOCl} is the bimolecular rate constant of contaminants with HOCl (M^{-1} s^{-1}; See Table A.2 of Section A.2.3 of the Appendix for rate constants). Use of equation (3) significantly underpredicted transformation rates for CBZ, MET, and ATZ, suggesting that reactive species other than $HO^{\bullet}_{ads}$ (< 20%) or HOCl (< 25%) were responsible for the increase in transformation rates upon addition of Cl^-. For these compounds, differences in predicted and observed removal were ascribed to reaction with $Cl^{\bullet}_{ads}$, which accounted for the majority of the observed loss (i.e., > 50%; See Table A3 of Section A2.4 of the Appendix).

Estimates of the surface density of adsorbed chlorine atom can be made using the current efficiency for chlorine production with the total active surface hydroxyl group density (i.e., [≡TiOH]) on the Ti-IrO_2 electrode, which was determined to be $5.44 \pm 0.37 \times 10^{-8}$ moles cm^{-2}. This value agreed with reported surface densities of oxide electrocatalysts for similar types of mixed metal oxide electrodes (RuO_2 ~ 4×10^{-8} moles cm^{-2}) (De Battisti *et al.*, 2001; Ferro & De

Battisti, 2002). Given a 23% current efficiency in a 10 mM NaCl electrolyte, we estimate steady-state $Cl^{\bullet}_{ads}$ densities of 1.25×10^{-8} mol cm^{-2}, which agree with surface densities of 1.2×10^{-8} mol cm^{-2} determined with *in-situ* thin gap radiotracer methods using ^{36}Cl at similar chloride concentrations (Tomcsányi *et al.*, 1999).

Rates of removal of trace organic contaminants, with the exception of CBZ, increased between 16 to 160% as chloride concentrations increased from 10 to 100 mM (Figure 2.10). Faster removal rates can be explained by an increase in current efficiency for the two-electron transfer from Cl^- to Cl_2 (i.e., from 23% to 60%) as the chloride concentration was increased by an order of magnitude, resulting in greater chlorine atom surface density and a factor of three increase in HOCl production rates (Figure 2.11). The relatively small increases in HOCl production at higher chloride concentrations were attributable to mass-transfer limitations as well as an inversely proportional relationship between the rate-determining electrochemical desorption step of $Cl^{\bullet}_{ads}$ (i.e., k_2) and chloride concentration (Trasatti, 1987). Removal rates decreased by 38-69% for the entire suite of trace organic contaminants at lower chloride concentrations characteristic of groundwater or surface water (i.e., ~ 1 mM) due to low faradaic efficiency for chlorine evolution (<5%; data not shown).

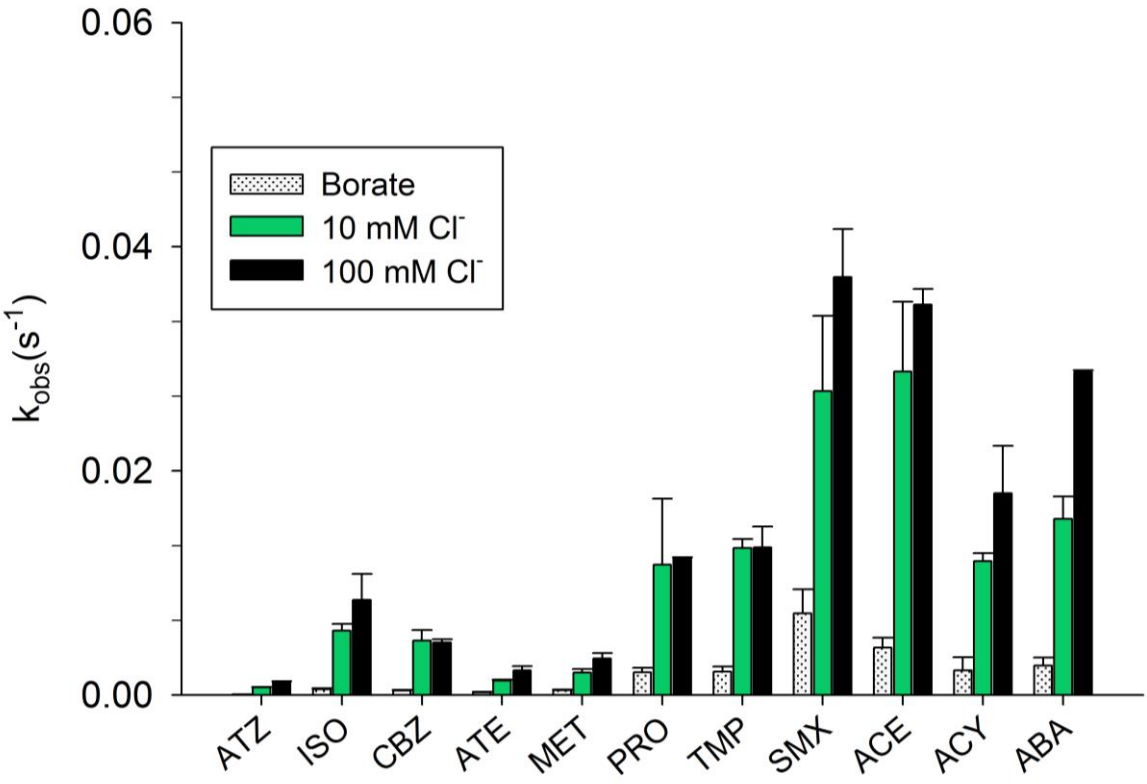

Figure 2.10: Observed first-order loss rates of trace organic contaminants on the Ti-IrO_2 electrode at pH 8.0 in borate buffer, 10 mM NaCl, and 100 mM NaCl. Error bars represent ± one standard deviation.

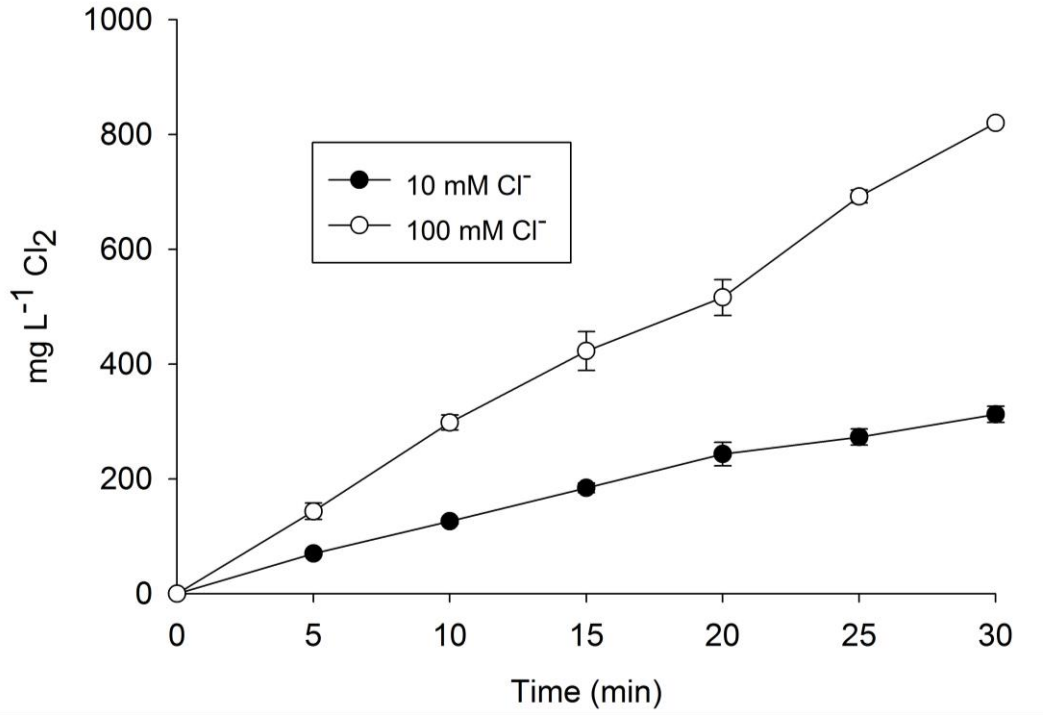

Figure 2.11: HOCl production on a Ti-IrO_2 electrode in a 10 mM and 100 mM chloride electrolyte.

Effect of Bromide. The addition of 20 µM Br^- to a 10 mM NaCl solution resulted in the increased removal rates for all of the trace organic contaminants (Figure 2.8). In this system, bromide rapidly reacted with hypochlorous acid to produce hypobromous acid (HOBr) (Kumar & Margerum, 1987):

$$HOCl + Br^- \xrightarrow{k=1.6-2.95\times10^3\ M^{-1}\ s^{-1}} HOBr + Cl^- \quad (4)$$

Given that reaction 3 is fast compared to the rate of oxidation of contaminants, and considering the rapid rate of HOCl production (i.e., HOCl is in excess), it is likely that essentially all of the Br^- was converted to HOBr within seconds of the initiation of electrolysis (i.e., [HOBr] ≈ [Br^-] = 20 µM) (Allard *et al.*, 2013). The observed transformation rates for compounds containing strong electron-donating moieties agreed well with predicted removal rates estimated by considering only the contribution of HOX to oxidation (i.e., $k_{obs} \approx k_{HOCl}[HOCl] + k_{HOBr}[HOBr]$; Figure 2.12). Because k_{HOBr} values were much greater than k_{HOCl} values (Figure 1), the presence of trace concentrations of Br^- increased the rate of removal of the organic contaminants (+10% to +285%) despite HOBr only accounting for a small portion of the total HOX. Notably, removal rates of contaminants in 10 mM NaCl with 20 µM NaBr were faster than those observed in 100 mM NaCl, suggesting that trace HOBr will displace HOCl as the most important HOX species in reverse osmosis concentrate from municipal wastewater, which typically contains over 40 µM Br^- (Eversloh *et al.*, 2015; Winid, 2015), and brines from shale gas production (>100 µM Br^-) (Warner *et al.*, 2013).

Again, transformation rates for ATZ, ISO, CBZ, ATE, and MET increased slightly despite being relatively unreactive with HOX (i.e., $k_{HOCl}[HOCl] + k_{HOBr}[HOBr] << k_{obs}$).

Experiments conducted in borate amended with 20 µM NaBr showed negligible HOX production (<1 µM detection limit); however, removal rates were similar to those observed in the 10 mM NaCl/20 µM Br^- electrolyte ([HOBr ≈ 20 µM]; Figure 2.13). Results suggest that for less reactive compounds (i.e., $k_{HOBr} < 10\ M^{-1}\ s^{-1}$), surface-bound reactive bromine species (i.e., $Br^{\bullet}_{ads}$) possibly contributed to oxidation (Ferro & Battisti, 2004; Ferro *et al.*, 2005).

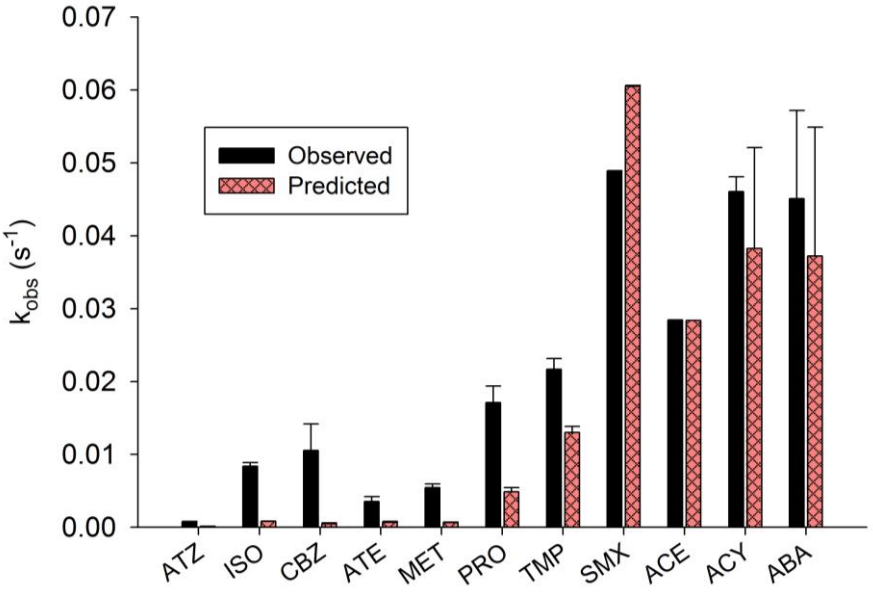

Figure 2.12: Predicted and measured pseudo-first order degradation rates for test compounds buffered at pH 8 on a Ti-IrO_2 electrode. [Cl^-] = 10 mM, [Br^-] = 20 µM.

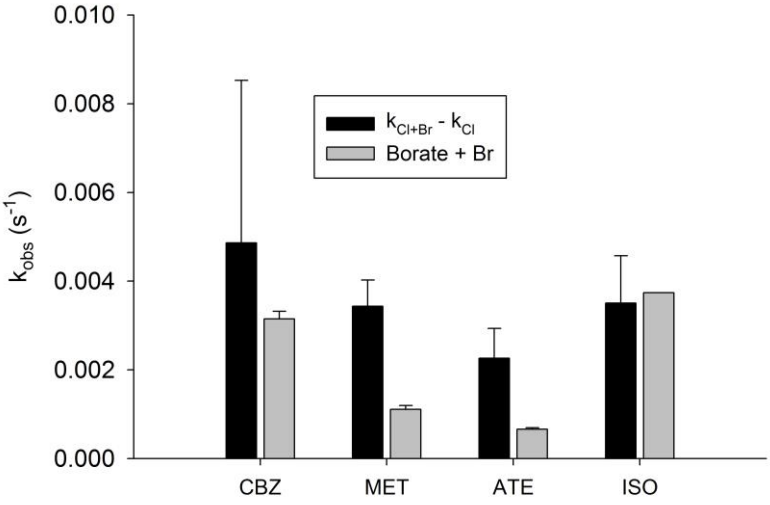

Figure 2.13: Pseudo-first order rate constants of select trace compounds at pH 8 on a Ti-IrO_2 electrode. Black bars are the difference between pseudo-first order rate constants between a 10 mM NaCl electrolyte with a 10 mM NaCl electrolyte containing 20 µM NaBr. Grey bars are the observed pseudo-first order rate constants in a 20 mM borate electrolyte in the presence of 20 µM bromide. Results indicate that formation of $Br^{\bullet}_{ads}$ via oxidation of trace amounts of bromide on the electrode can contribute to contaminant removal. HOBR production was not observed in the 20 µM bromide electrolyte.

Effect of Bicarbonate. The addition of 10 mM HCO_3^- decreased the loss rates of ATZ, ISO, CBZ, ATE, and MET by approximately 50 to 75% relative to removal rates in 10 mM NaCl (Figure 3.7). Although adsorption of anions with a stronger affinity for electrode surface functional sites, such as sulfate and phosphate, slows the rate formation of HOCl,(Trasatti, 1987) HOCl accumulation rates only decreased by approximately 25% in the presence of 10 mM HCO_3^- (Figure 2.14).

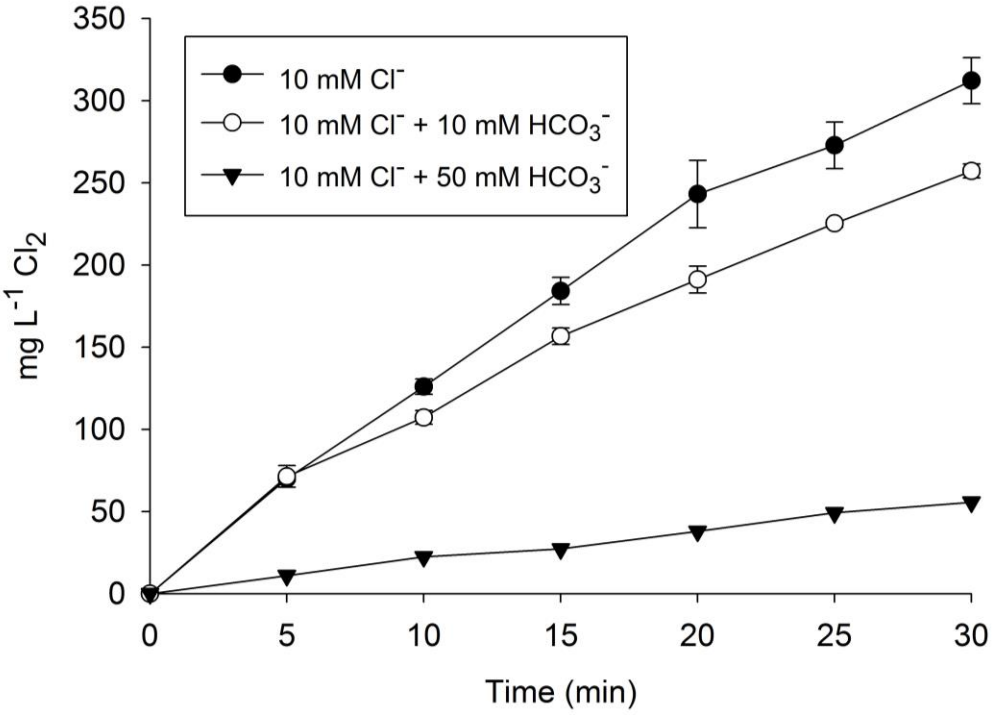

Figure 2.14: Production of HOCl as a function of time in the presence of carbonates.

The blockage of oxidation sites by adsorbed HCO_3^- was ruled out as the mechanism for the observed decreased transformation rates of the former compounds as the transformation rates of HOCl-reactive ABA, ACY, ACE, and SMX showed negligible or slightly increased removal when HCO_3^- was increased to 50 mM despite an approximately 85% decrease in chlorine production (Figure 2.14). The variability in transformation rates in the presence of HCO_3^- was likely attributable to the scavenging of $Cl^{\bullet}_{ads}$ by HCO_3^-:

$$Cl^{\bullet}_{ads} + HCO_3^- \xrightarrow{k_{homogenous}=2.2\times10^8\ M^{-1}\ s^{-1}} Cl^- + H^+ + CO_3^{\bullet-} \quad (5)$$

$CO_3^{\bullet-}$ reacts slowly with ATZ, ISO, CBZ, ATE, and MET (Figure 2.2). The effect of HCO_3^- on the rate of transformation of ABA, ACY, ACE, SMX was negligible due to the high reactivity of these compounds with $CO_3^{\bullet-}$. Unlike the situation in the NaCl electrolyte, decreases in removal rates after addition of *t*-buOH to the carbonate-containing electrolyte confirmed a shift from adsorbed oxidants to dissolved oxidants (i.e., $CO_3^{\bullet-}$; $k_{CO_3^{\bullet-},t\text{-buOH}} = 1.6 \times 10^2\ M^{-1}\ s^{-1}$; Figure 2.15 (Buxton *et al.*, 1988). Results from chronoamperometric experiments did not indicate a current increase upon the addition of HCO_3^- to an inert supporting electrolyte, suggesting that $CO_3^{\bullet-}$ was not formed through direct electron transfer on the anode (Figure 2.16) (Azizi *et al.*, 2011).

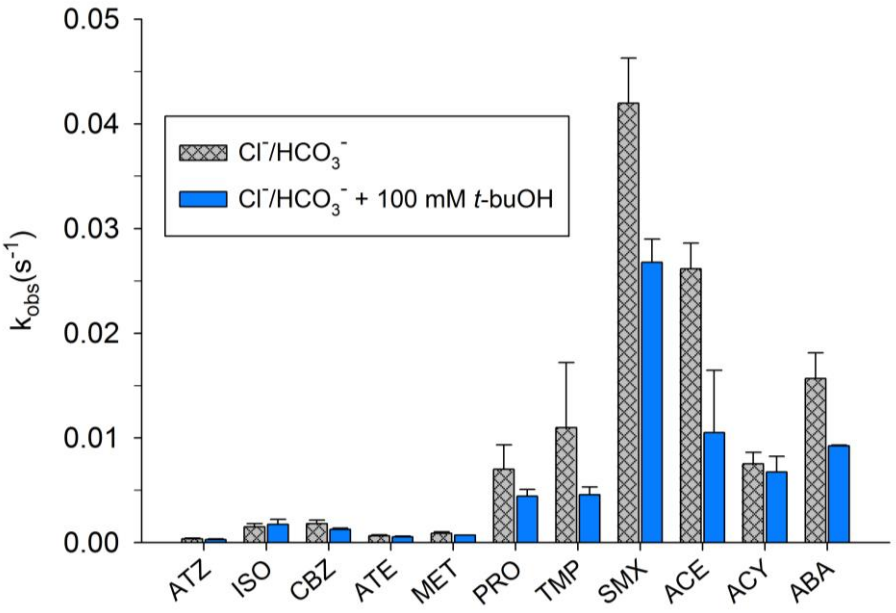

Figure 2.15: Observed pseudo-first order removal rates of trace organic contaminants on a Ti-IrO_2 electrode in 10 mM NaCl and 10 mM $NaHCO_3$ electrolyte in the presence and absence of 100 mM *t*-buOH.

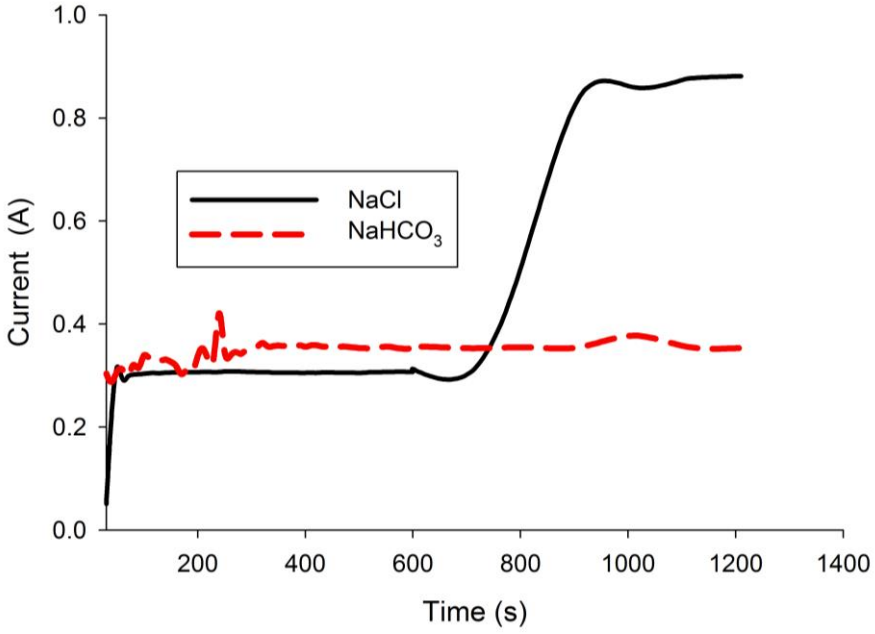

Figure 2.16: Chronoamperometry experiments performed at a potential of 1.55 V in a 0.5 M $NaClO_4$ electrolyte at pH 8 on a Ti-IrO_2 electrode. After a stable current for water oxidation was reached (~10 min) the electrolyte was amended with 50 mM HCO_3^- or Cl^-.

Experiments conducted in borate-buffered electrolyte with and without 10 mM HCO_3^- did not show a similar effect of HCO_3^- on the removal of contaminants observed in the NaCl electrolyte,

plausibly due to the lower reactivity of HCO_3^- with $HO^\bullet$ compared to $Cl^\bullet$ ($k_{HCO_3^-,HO^\bullet} = 8.5 \times 10^6$ M^{-1} s^{-1}; Figure 2.6).

Further insight into $CO_3^{\bullet-}$ formation as a scavenging mechanism for adsorbed halide radicals can be obtained by observing the effect of HCO_3^- on contaminant transformation rates in the 10 mM NaCl/20 µM NaBr matrix. Linear correlations were observed between the carbonate radical rate constant (i.e., $k_{CO_3^{\bullet-}}$) and the change in pseudo-first order removal rates when 10 mM HCO_3^- was amended to a 10 mM NaCl electrolyte ($r^2 = 0.41$, Figure 2.17) and to a 10 mM NaCl/20 µM NaBr electrolyte (r^2=0.63, Figure 2.18). These results indicate that despite the previously observed improvement in efficacy from the electrolysis of halide ions, the efficiency of the treatment is compound-specific when performed in the presence of moderate amounts of bicarbonate due to formation of more selective oxidants (Figure 2.19). Consequently, electrolysis of electron-rich organic contaminants with $k_{CO_3^{\bullet-}}$ greater than 10^8 M^{-1} s^{-1} (e.g., sulfonamides, antiviral nucleoside analogs) will require similar or less electrolysis time than in the absence of HCO_3^-. Conversely, electron-poor compounds that react with $CO_3^{\bullet-}$ at rates below 10^7 M^{-1} s^{-1} (e.g., β-blockers, triazine herbicides) have reduced rates of transformation and will require slightly longer treatment times for adequate compound removal in the presence of HCO_3^-.

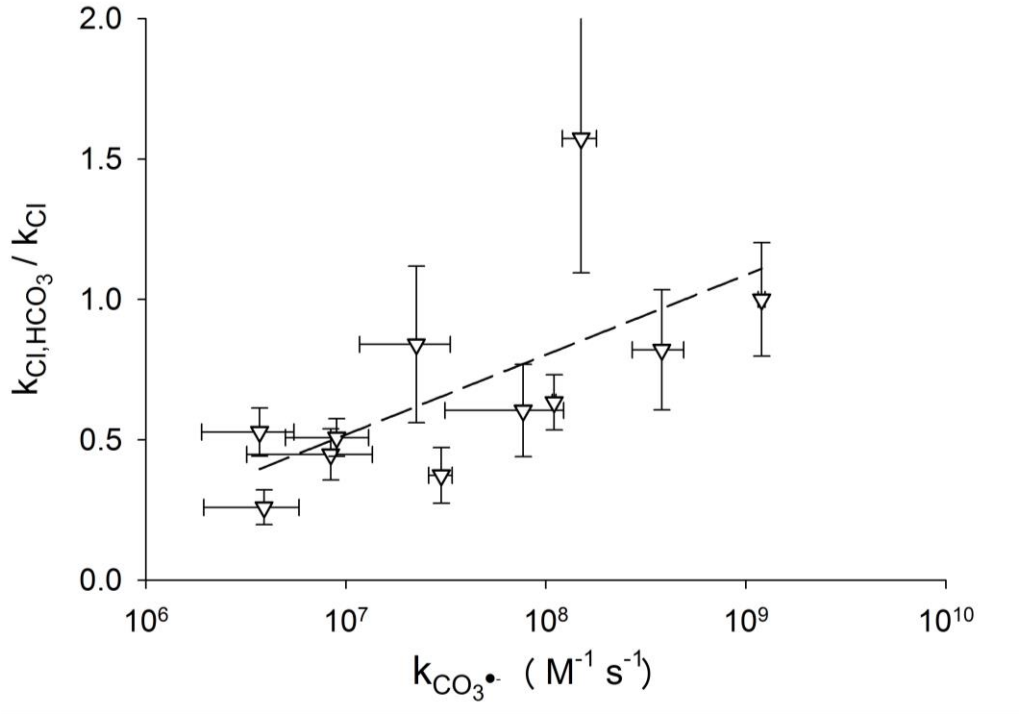

Figure 2.17: Relationship between the contaminant-specific bimolecular carbonate radical rate constant ($k_{CO_3^{\bullet-}}$) with the relative change in pseudo-first order removal rates when a 10 mM NaCl electrolyte (k_{Cl}) was amended with 10 mM HCO_3^- (k_{Cl,HCO_3^-}).

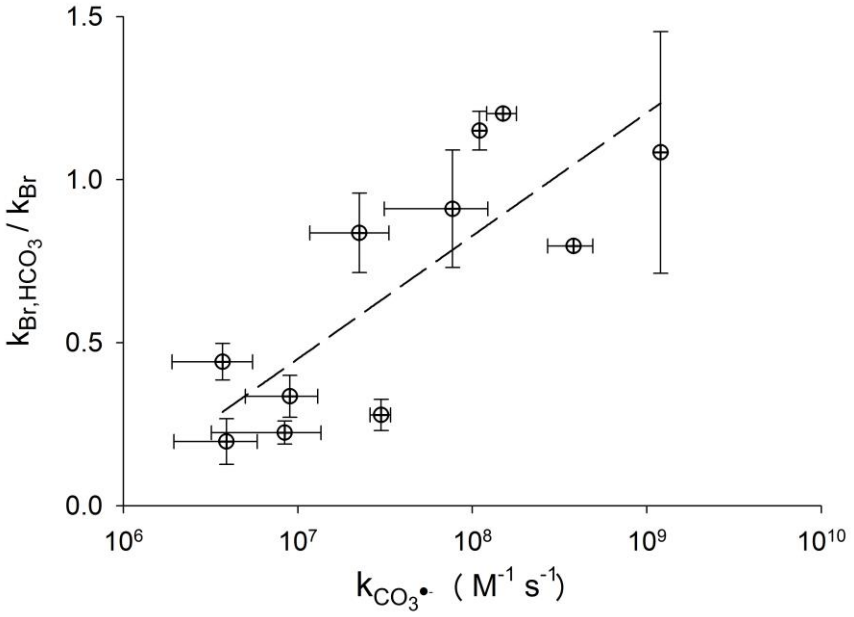

Figure 2.18: Relationship between the contaminant-specific bimolecular carbonate radical rate constant ($k_{CO_3^{\bullet-}}$) with the relative change in pseudo-first order removal rates when a 10 mM NaCl/20 µM NaBr electrolyte (k_{Br}) was amended with 10 mM HCO_3^- (k_{Br,HCO_3^-}).

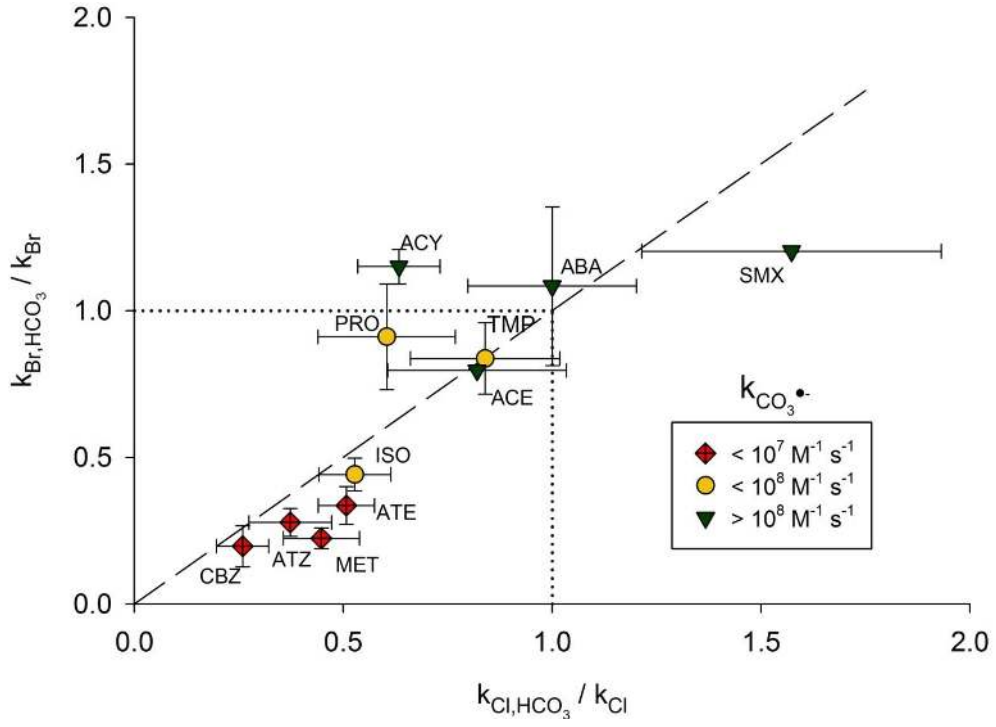

Figure 2.19: Relationship between the changes in pseudo-first order degradation rates when 10 mM HCO_3^- was amended to a 10 mM NaCl electrolyte (k_{Cl,HCO_3}/ k_{Cl}; x-axis) and to a 10mM NaCl/20 µM NaBr electrolyte (k_{Br,HCO_3}/ k_{Br}; y-axis) on a Ti-IrO_2 electrode at pH 8.0. Error bars represent ± one standard deviation.

Effect of Ammonia. In the presence of ammonia, the rate of transformation of TMP, SMX and ACE decreased due to the formation of combined chlorine (i.e., NH_2Cl), which is less reactive with these compounds than HOCl (Figure 2.20) (Dodd & Huang, 2004; Pinkston & Sedlak, 2004; Dodd & Huang, 2007). The removal rates of the remaining compounds ($k_{HOCl} < 10\ M^{-1}\ s^{-1}$) were unchanged or increased slightly in the presence of ammonia. Partial inhibition of transformation rates in the presence of *t*-buOH indicated a shift from adsorbed to dissolved oxidants (Figure 2.20). The enhanced rate of transformation observed in the presence of ammonia for some compounds may have been attributable to the formation of reactive nitrogen species (e.g., $NH_2^{\bullet}$, $NO^{\bullet}$, $NO_2^{\bullet}$) from the reaction of NH_3/NH_4^+ with $HO^{\bullet}$ ($k_{NH_3,HO^{\bullet}} = 1.0 \times 10^8\ M^{-1}\ s^{-1}$) (Neta *et al.*, 1978; Huang *et al.*, 2008) or $Cl^{\bullet}$ (Cho & Hoffmann, 2014; Cho *et al.*, 2014). The aminoperoxy radical ($NH_2O_2^{\bullet}$,ε_{350}~700 $M^{-1}\ cm^{-1}$) (Giguère & Herman, 1976) formed from the reaction between $NH_2^{\bullet}$ and O_2 in 1 M NH_3 was detected spectroscopically in both a UV/H_2O_2 control and 10 mM Cl^- electrolysis experiments at pH 8.0 and 10.5 (Figure 2.21). Furthermore, formation of NO_2^-/NO_3^- was observed, which is consistent with $NH_2^{\bullet}$ oxidation to $NH_2O_2^-$ and decomposition in solution (Figure 2.22) (Huang *et al.*, 2008).

Significant increases in the removal rates for the β-blockers (+85-370%) is consistent with the modest reactivity of $NH_2^{\bullet}$ with secondary amines (10^4-$10^5\ M^{-1}\ s^{-1}$) (Dodd *et al.*, 2008). The observed increase in transformation rates of contaminants containing weakly electron-donating moieties (CBZ, MET, ATE, ATZ) in NH_4Cl relative to NaCl was absent upon addition of NOM (5 mgC L^{-1}), highlighting the plausible contribution of dissolved secondary reactive nitrogen species ($k_{NH_2^{\bullet},NOM}$= 1 L $mg^{-1}\ s^{-1}$) to oxidation (Figure 2.23) (Dodd *et al.*, 2008). These findings suggest that reactive nitrogen species will not play an important role in the removal of these compounds during the treatment of natural waters.

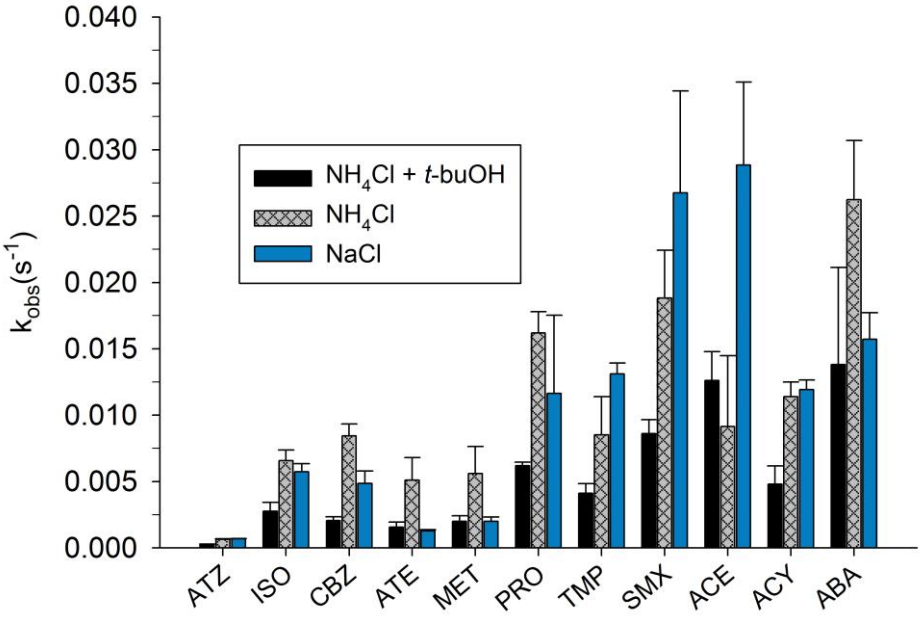

Figure 2.20: Pseudo-first order degradation rates of trace contaminants in 10 mM NaCl and 10 mM NH_4Cl in the presence and absence of 100 mM *t*-buOH on a Ti-IrO_2 electrode at pH 8.

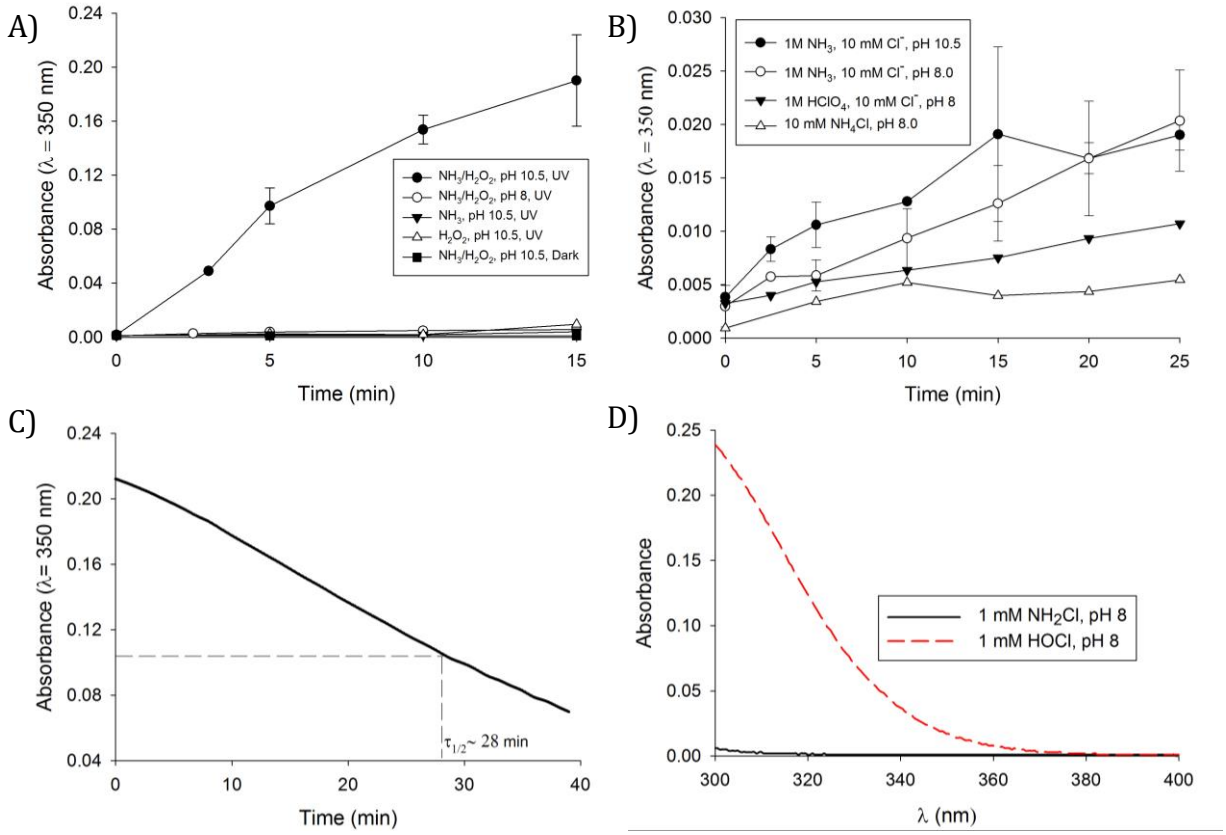

Figure 2.21: Kinetic absorption profiles recorded at 350 nm of solutions exposed to A) UV irradiance and B) electrolysis on a Ti-IrO_2 electrode. C) Transient absorption decay at 350 nm of the 1M NH_3/H_2O_2 pH 10.5 solution following exposure to 15 minutes of UV irradiance. D) pH-dependent absorption spectra of 1mM NH_2Cl and HOCl.

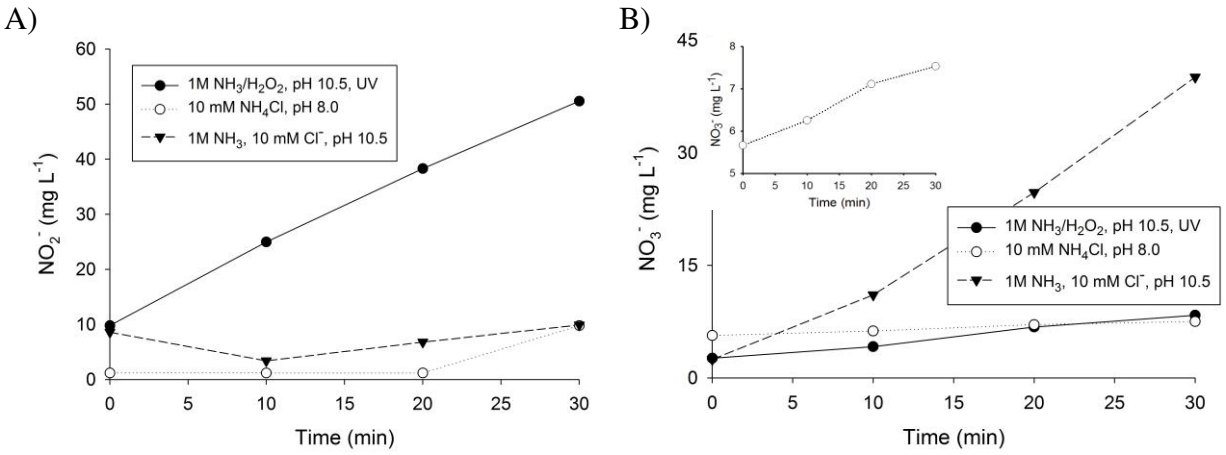

Figure 2.22: Concentration profiles of A) nitrite and B) nitrate formed from the decomposition of $NH_2^{\bullet}$ into $NH_2O_2^-$ in both a UV/H_2O_2 control experiment and on a Ti-IrO_2 electrode. Inset: The concentration profile of nitrate for the electrolysis of 10 mM NH_4Cl zoomed in.

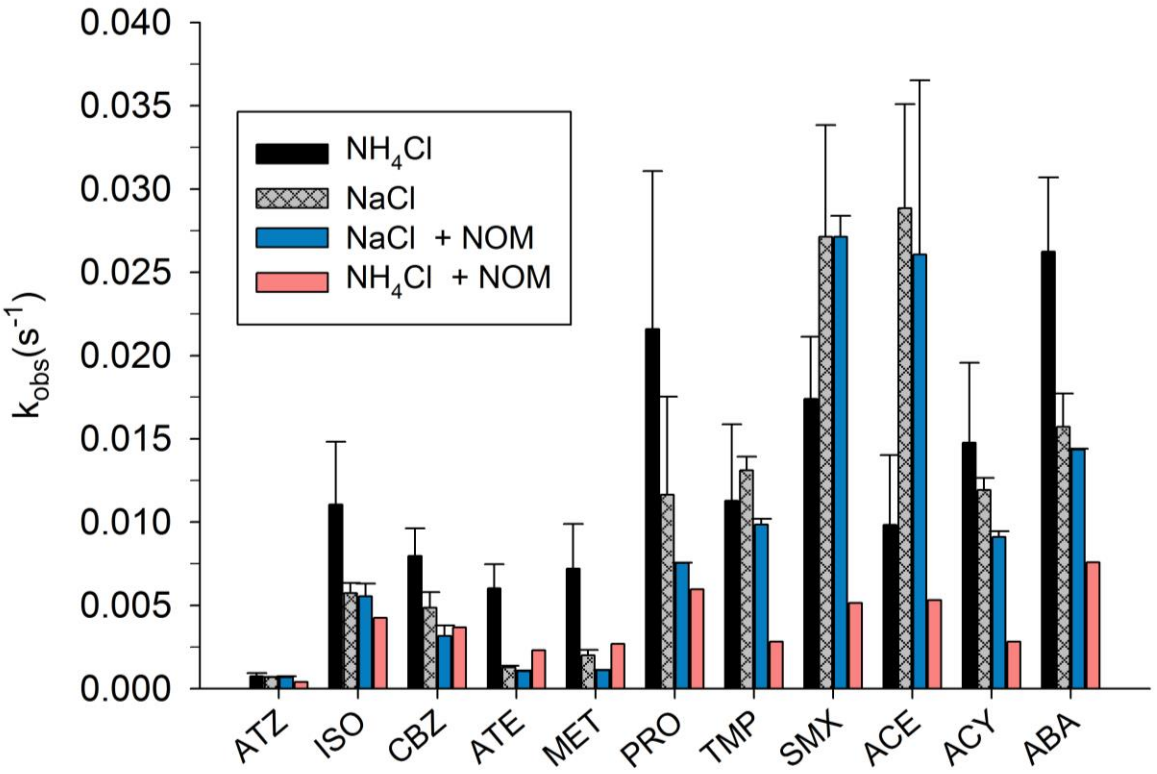

Figure 2.23: Pseudo-first order degradation rates of trace contaminants in 10 mM NaCl and 10 mM NH_4Cl in the presence and absence of 5 mgC L^{-1} Suwannee River Humic Acid (SRHA) on a Ti-IrO_2 electrode at pH 8.

Effect of Natural Organic Matter. Reaction of HOCl with Suwannee River Humic Acid (SRHA; 5 mgC L^{-1}) decreased HOCl evolution with increasing electrolysis time (-22%; Figure 2.24A). The absence of significant differences in HOCl concentration at short electrolysis times indicated that NOM competition with chloride for direct electrolysis sites and interaction with adsorbed oxidants was negligible (See Section A.2.5 of the Appendix for calculation). Accordingly, compounds transformed primarily through reactions with surface-bound oxidants (e.g., CBZ, MET, ATZ) were unaffected by the presence of NOM (Figure 2.24B).

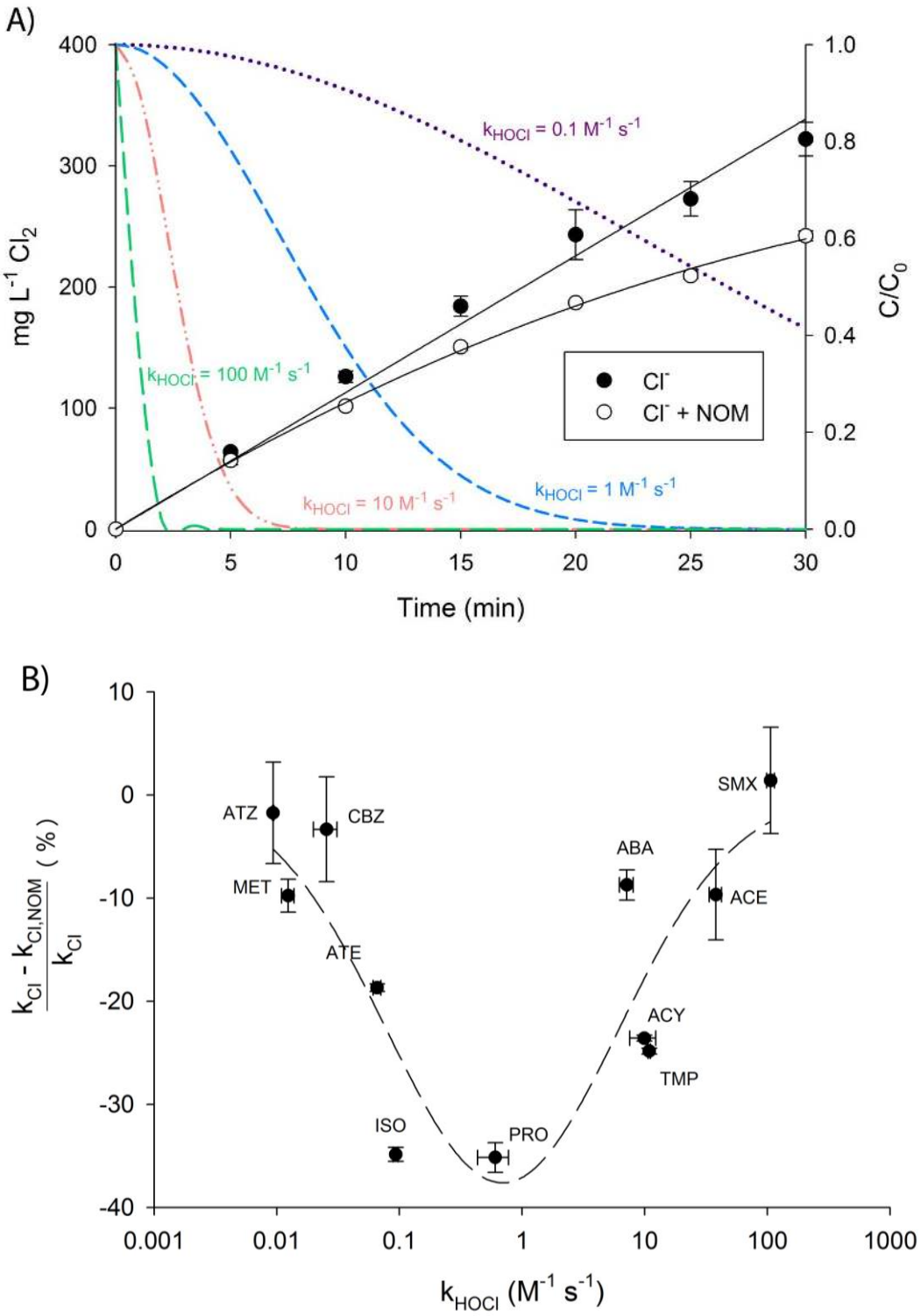

Figure 2.24: (A) Residual HOCl as a function of time in the presence and absence of 5 mg L^{-1} Suwannee River Humic Acids on Ti-IrO_2 during electrolysis of a 10 mM NaCl electrolyte (left axis). Modelled loses of organic contaminants exhibiting varying reactivity with HOCl (right axis). (B) Percent reduction of removal rates of trace organic contaminants in a pH 8.0, 10 mM NaCl electrolyte when amended with 5 mgC L^{-1} SRHA on Ti-IrO_2. Dashed lines show the fitted lognormal distribution (r^2 = 0.71). Error bars represent ± one standard deviation.

An absence of inhibitory effects of humic substances on transformation rates for compounds exhibiting rapid kinetics with HOCl (k_{HOCl} > 10 M^{-1} s^{-1}; SMX, ABA, ACE) was consistent with their elimination prior to significant loss of HOCl by reactions with phenolic, quinone, and amine moieties present in NOM (Figure 2.24A). Compounds exhibiting intermediate reactivity with HOCl (k_{HOCl} = 0.1-10 M^{-1} s^{-1}; PRO, TMP, ACY, ISO) exhibited up to 40% slower removal rates in the presence of NOM. Comparable transformation rates using less aromatic Pony Lake Fulvic Acid precluded the role of inhibition from reversion of partially-oxidized compounds to parent compounds via reactions with antioxidant moieties present in NOM (Figure 2.25) (Wenk *et al.*, 2011; Wenk & Canonica, 2012; Wenk *et al.*, 2013).

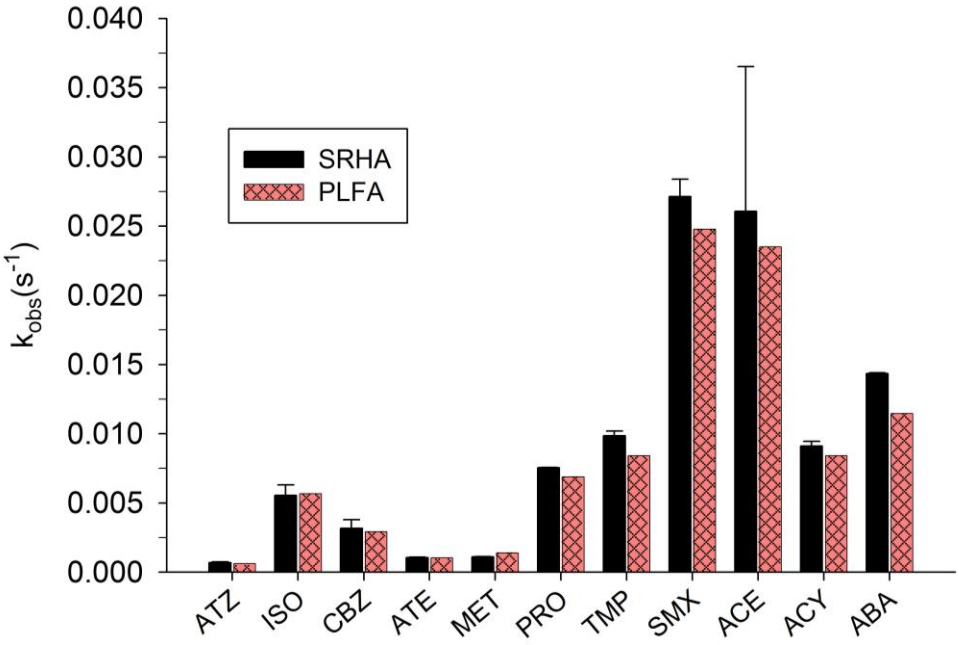

Figure 2.25: Pseudo-first order degradation rates of trace contaminants in 10 mM NaCl in the presence of 5 mgC L^{-1} Suwannee River Humic Acid (SRHA) or Pony Lake Fulvic Acid (PLFA) on a Ti-IrO_2 electrode at pH 8.

2.3.4 Impact of Anode Material on Electrochemical Transformation of Contaminants

Different electrode materials exhibit wide variations in their ability to oxidize water to hydroxyl radical (i.e., the O_2 overpotential varies) as well as the nature of the interaction between the adsorbed radicals and the electrode surface (Chaplin, 2014; Radjenovic & Sedlak, 2015). For example, BDD electrodes tend to be better suited for contaminant degradation than Ti-IrO_2 in the absence of chloride due to their ability to produce higher yields of weakly adsorbed $HO^{\bullet}$ (Comninellis, 1994). Significant increases were observed in surface-area normalized removal rates (100 - 2500%) on BDD relative to Ti-IrO_2 in borate-buffered electrolyte, consistent with a higher production of $HO^{\bullet}$ (φ_{anode} = 4.0 V vs. SHE, measured $[HO^{\bullet}]_{SS} = 2.8 \times 10^{-14}$ M; Figure 2.26). Consequently, transformation rates decreased (~85%) to rates of direct electrolysis upon addition of *t*-buOH. Partial inhibition (57±15%) of both contaminant oxidation rates and $[HO^{\bullet}]_{SS}$ occurred during the electrolysis of borate in the presence of SRHA. Steady-state $HO^{\bullet}$ concentration in the presence of SRHA was roughly 2 orders of magnitude greater than expected ($k_{HO^{\bullet},SRHA} = 5.7 \times 10^{8}$ L M_C^{-1} s^{-1}; See Section A.2.6 of the Appendix for calculations), plausibly

due the slow diffusion of high-molecular weight NOM into the reactive zone adjacent to the electrode (Dodd *et al.*, 2008).

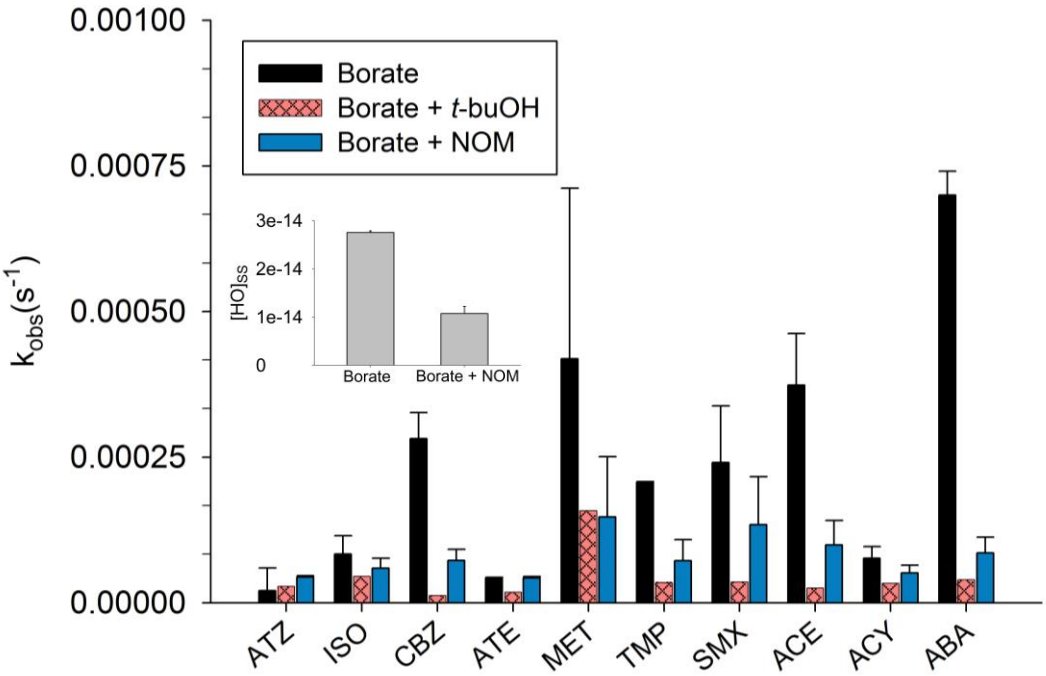

Figure 2.26: Pseudo-first order degradation rates of trace contaminants on a BDD electrode in a pH 8 borate-buffered electrolyte in the presence of 5 mgC L^{-1} Suwannee River Humic Acid, and 100 mM *t*-buOH, Inset: steady-state $HO^{\bullet}$ concentration.

The presence of chloride increased contaminant removal rates (Figure 2.27), although lower current efficiency was measured for Cl_2 production (7.8%) on BDD relative to Ti-IrO_2. Inhibition of HOCl production in the presence of *t*-buOH suggests the formation pathway involves dissolved species,(Kim *et al.*, 2014) thus the applicability of *t*-buOH to elucidate respective oxidation pathways (i.e., reactive radicals from HOX) is limited. Nonetheless, the dissolved oxidants (e.g., $HO^{\bullet}$, $Cl_2^{\bullet-}$, HOCl) contributed significantly to contaminant transformation, as evidenced by a 20-98% reduction in electrolysis rates observed in the presence of *t*-buOH (Figure 2.27). Interestingly, the absence of a strong effect of NOM on HOCl production despite the importance of dissolved oxidants in this system suggests that the interaction of reactive halide species (i.e., $Cl^{\bullet}$ and $Cl_2^{\bullet-}$) with NOM is slow (Figure 2.28) (Grebel *et al.*, 2010; Jasper & Sedlak, 2013; Barazesh *et al.*, 2015). This was consistent with minimal effects of NOM on the transformation rates of electron-poor contaminants during electrolysis (Figure 2.29) and UV photolysis (Figure 2.30) in the presence of halides. Similar to Ti-IrO_2, the removal of compounds with bimolecular rate constants for reaction with $CO_3^{\bullet-}$ below 10^6 M^{-1} s^{-1} (e.g., CBZ and ATZ) was inhibited when the chloride electrolyte was amended with carbonate (data not shown).

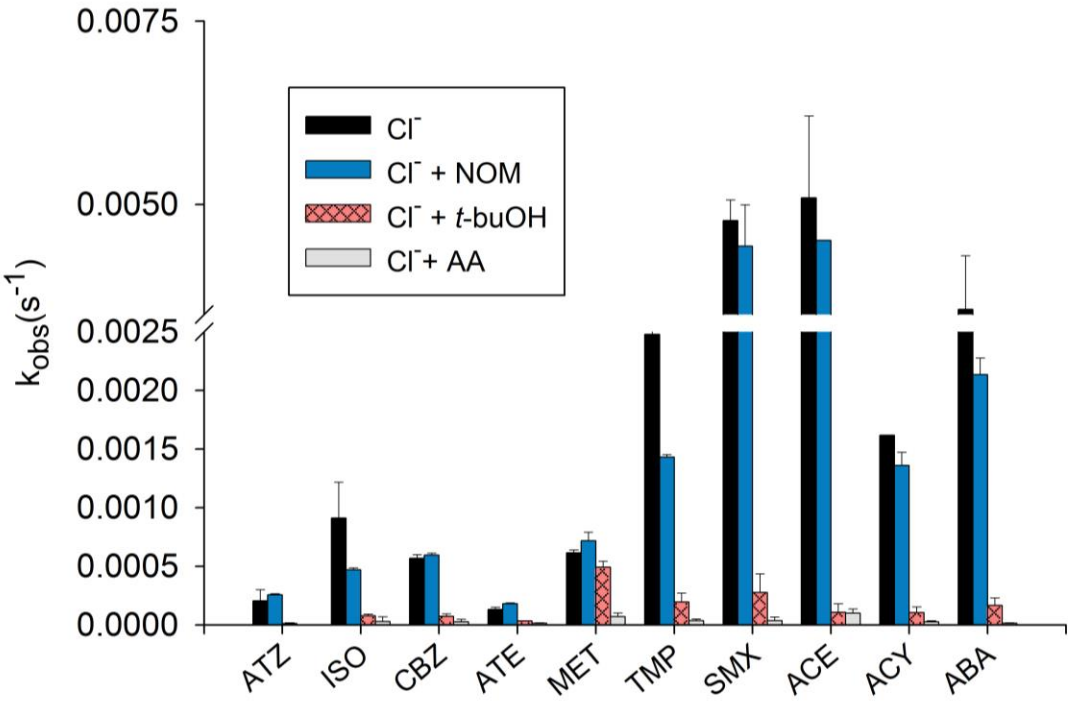

Figure 2.27: Pseudo-first order degradation rates of trace contaminants on a BDD electrode in a 10 mM NaCl electrolyte in the presence of 5mgC L^{-1} Suwannee River Humic Acid, 100 mM *t*-buOH, and 100 mM allyl alcohol.

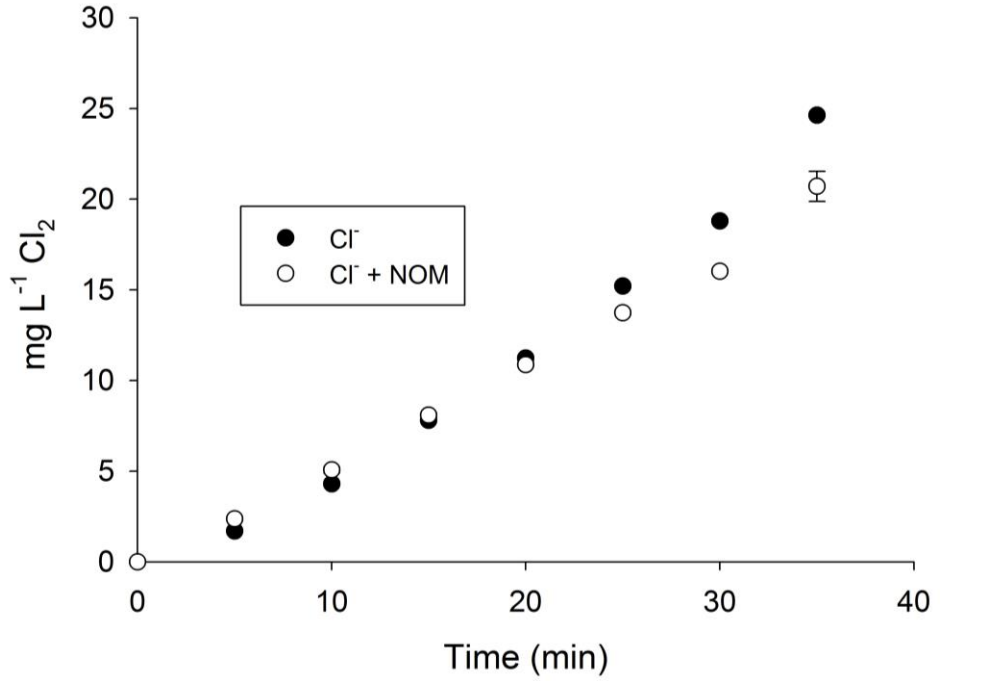

Figure 2.28: Production of HOCl as a function of time in the presence of 5 mg L^{-1} Suwannee River Humic Acids on BDD.

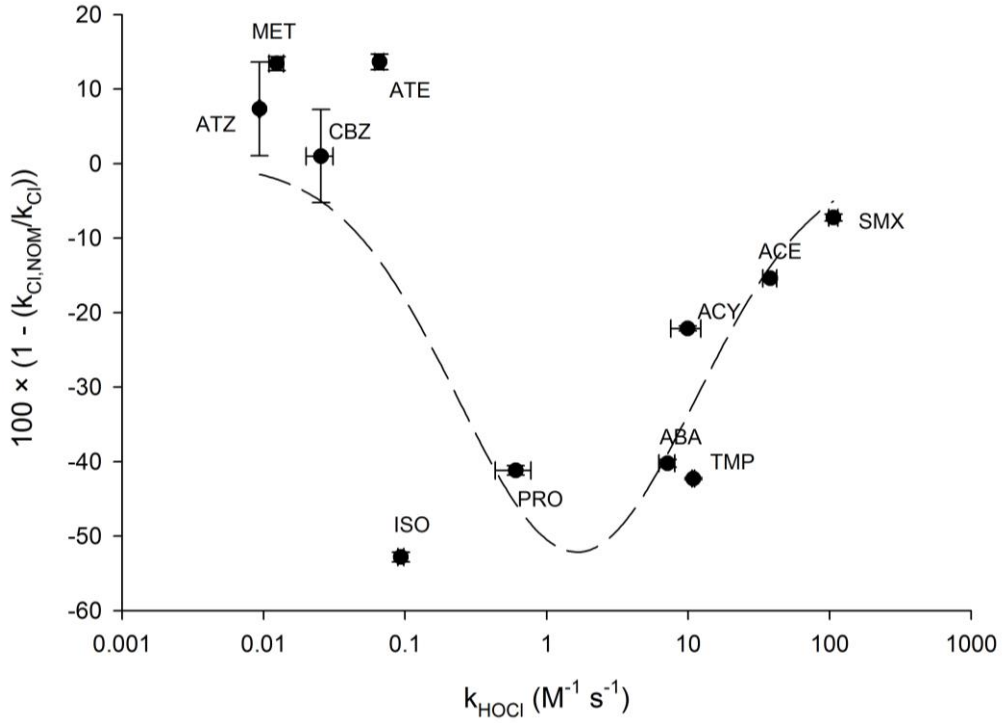

Figure 2.29: Percent reduction of removal rates of trace organic contaminants in a pH 8, 10 mM NaCl electrolyte when amended with 5 mgC L^{-1} SRHA on a BDD electrode. Dashed line shows the fitted lognormal distribution (r^2 = 0.58).

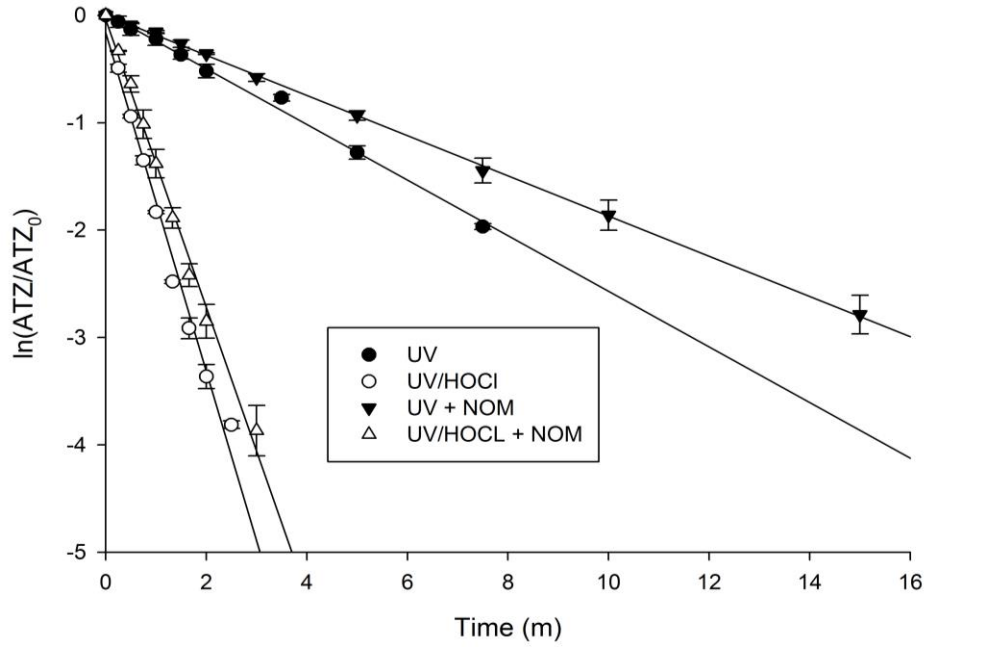

Figure 2.30: Pseudo-first order atrazine (ATZ) degradation rates by UV photolysis and UV/HOCl in the presence and absence of NOM. $Cl_2^{\bullet-}$ exhibits a much higher reactivity with electron-rich organic contaminants than with NOM (i.e., $k_{Cl_2^{\bullet-},NOM} < k_{Cl_2^{\bullet-},organics}$), as is evident from identical increases in ATZ degradation rates in UV/HOCl solutions relative to direct UV photolysis (556 ± 38%) in both the presence and absence of 1.5 mg L^{-1} NOM.

2.3.5 Removal of Trace Organic Contaminants from Municipal Wastewater Effluent

To gain insight into the potential for using anodes to transform contaminants under realistic operating conditions, an experiment was conducted in 0.45 µm-filtered municipal wastewater ($[Cl^-]$= 6.6 mM; $[Br^-]$ = 7 µM; [NOM] = 9.5 mgC L^{-1}; See Table 2.2 for full composition) with the Ti-IrO_2 anode (Figure 2.31). Predicted removal rates for contaminants included contributions from direct electron transfer, dissolved $HO^\bullet$, $CO_3^{\bullet-}$, and reactions with dissolved HOCl and HOBr (See Section A.2.7 of the Appendix for calculations). Due to inability to quantify $[CO_3^{\bullet-}]_{SS}$ with probe compounds (i.e., *N,N*-dimethylaniline) (Neta *et al.*, 1988; Deborde & von Gunten, 2008) in the presence of HOCl, the influence of $CO_3^{\bullet-}$ on removal rates was estimated by correcting the predicted contributions from direct electron transfer, $HO^\bullet$, HOCl, and HOBr with compound-specific scaling factors determined in Figure 2.19 (i.e., $k_{Br,HCO_3}/ k_{Br)}$. The contribution of $Cl^\bullet_{ads}$ was excluded from the model due to the absence of reliable estimates of bimolecular rate constants for organic compounds with $Cl^\bullet_{ads}$. Therefore, the underprediction of contaminant removal rates maybe attributable to the contribution of $Cl^\bullet_{ads}$ and related halogen radical species.

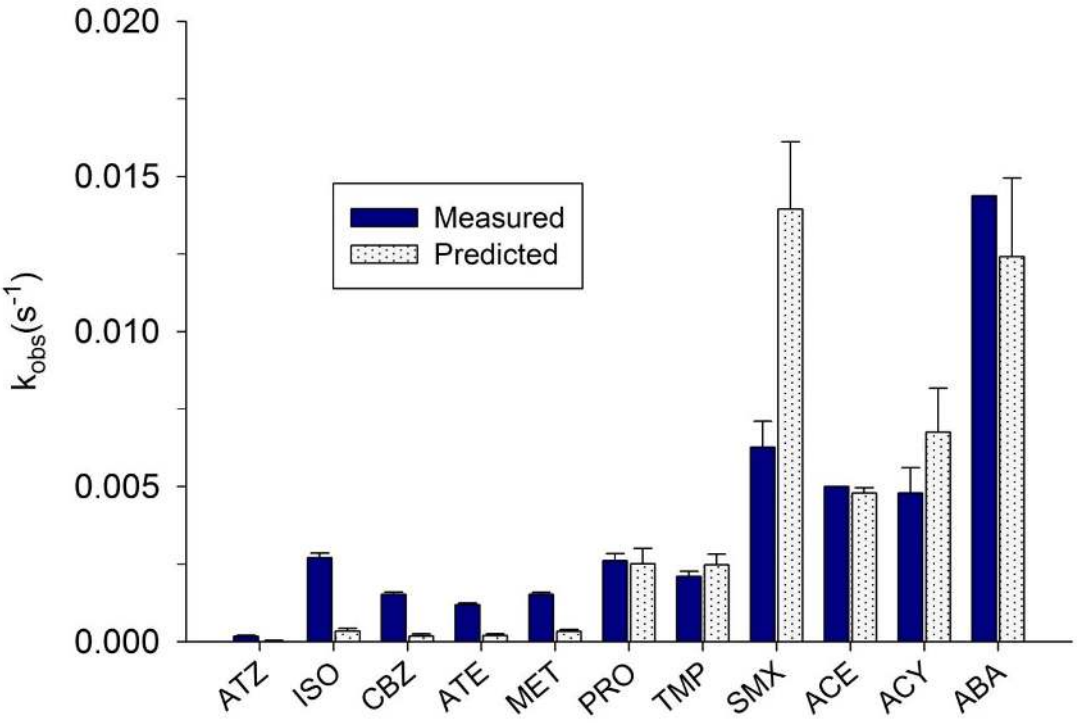

Figure 2.31: Predicted and measured pseudo-first order removal rates for test compounds in pH 8.0 buffered municipal wastewater effluent on a Ti-IrO_2 electrode. Error bars represent ± one standard deviation.

In the municipal wastewater effluent, the rate of production of HOCl was slower than that observed in 10 mM NaCl due to the formation of chloramines ($[NH_2Cl]$ = 0.26 mM), as well as slight inhibition in production due to the presence of NOM (9.5 mgC L^{-1}; Figure 2.32). The formation of combined chlorine did not increase contaminant removal rates due to its low

reactivity with organic compounds ($k_{NH_2Cl,organics}$ < 0.05 M^{-1} s^{-1}) (Dodd & Huang, 2004; Pinkston & Sedlak, 2004; Dodd & Huang, 2007).

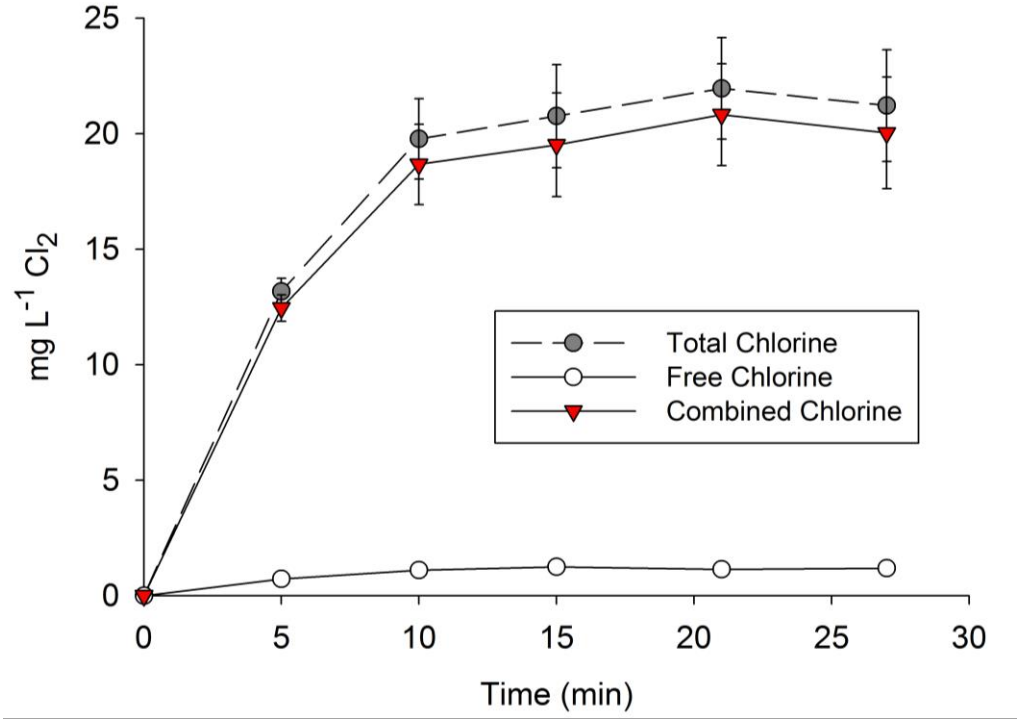

Figure 2.32: Production of free and combined chlorine as a function of time in municipal wastewater effluent on a Ti-IrO_2 electrode.

As expected, transformation rates were significantly underpredicted for those compounds that were less reactive with HOCl and HOBr (i.e., k_{HOCl} < 1 M^{-1} s^{-1}) due to unaccounted for contributions from $CO_3^{\bullet-}$, $Cl^{\bullet}_{ads}$, and $Br^{\bullet}_{ads}$. Predicted rates agreed well for compounds that exhibited high reactivity with HOCl/HOBr (PRO, TMP, ACY, and ABA) with the exception of SMX, which was removed at a slower rate than predicted by the combination of direct electron transfer and reactions with HOX. In the absence of NH_3, the predicted transformation rate agreed within 5% of the observed rate of SMX removal (Figure 2.8). The discrepancy between measured and predicted transformation rates highlights the need to consider the effects of additional solutes like NH_4^+ and SO_4^{2-} on oxidants, especially for electron-poor contaminants.

2.3.6 Electrolysis Transformation Products.

Chlorinated and brominated trace organic transformation products were detected during the electrolysis of municipal wastewater (Figure 2.33). Sequential halogenation of aromatic compounds has been implicated in elevating product toxicity relative to the parent compound and ultimately may propagate to form trihalomethanes (THM's) and haloacetic acids (HAA's; Figure 2.34) (Liu & Zhang, 2014). Following anodic treatment of municipal wastewater, THM's and HAA's were detected at 55 µg L^{-1} and 480 µg L^{-1}, respectively, the latter of which was greatly in excess of the EPA maximum contaminant level ($\Sigma[THM]_{MCL}$ = 80 µg L^{-1}; $\Sigma[HAA]_{MCL}$ =60 µg L^{-1}). In addition to organic disinfection byproducts, electrolysis of municipal wastewater

resulted in the production of the inorganic contaminant bromate at concentrations significantly in excess of the existing standard (10 µg L^{-1}; Figure 2.35).

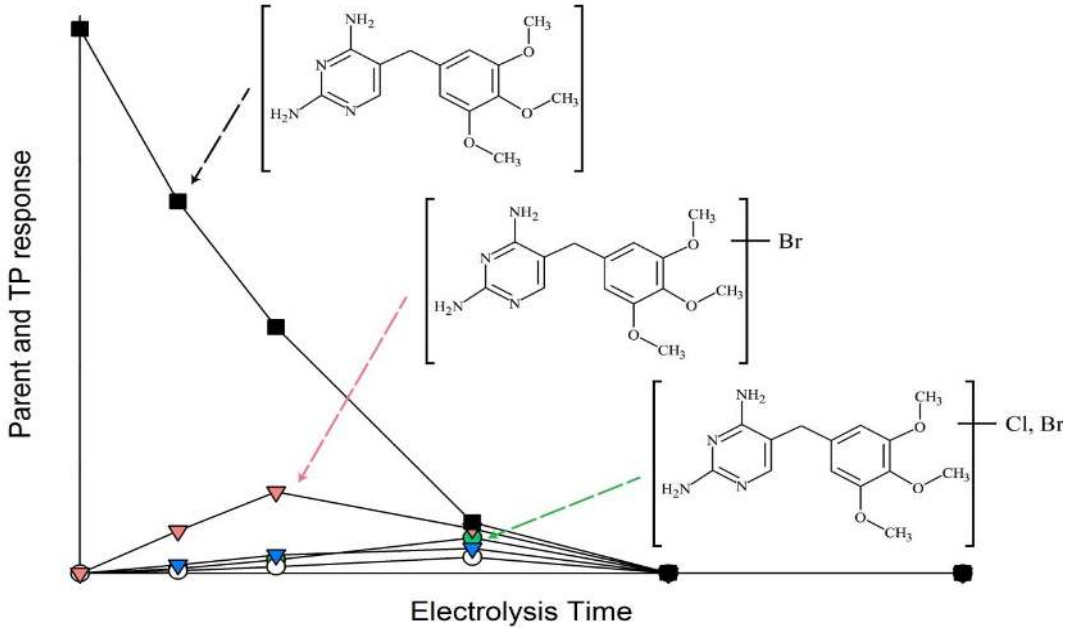

Figure 2.33: Trimethoprim transformation product formation during the electrolysis of municipal wastewater effluent.

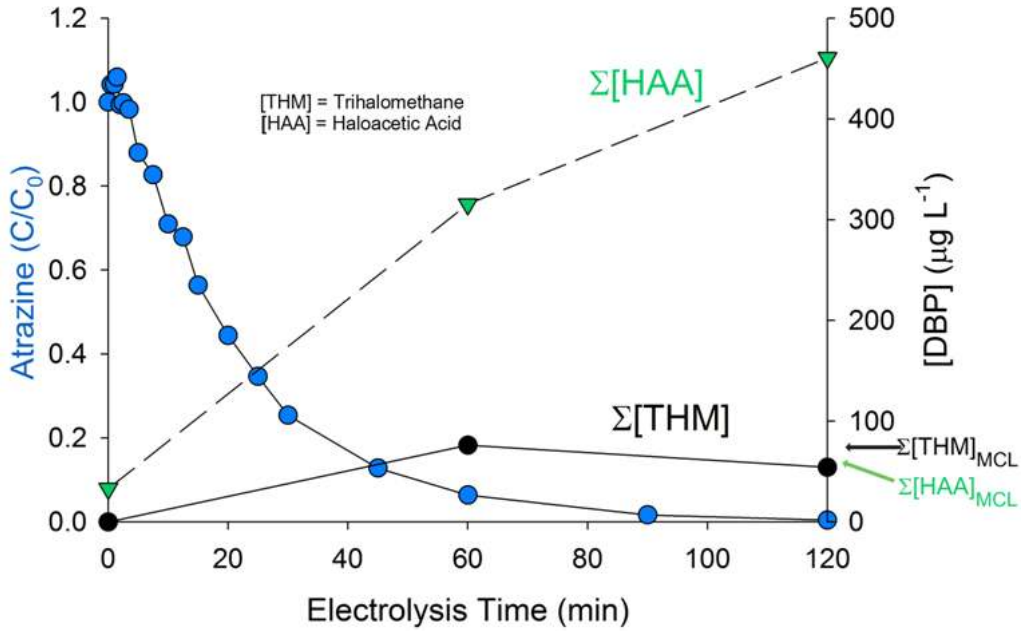

Figure 2.34: Production of trihalomethanes (THMs) and haloacetic acids (HAAs) during the electrolysis of municipal wastewater effluent.

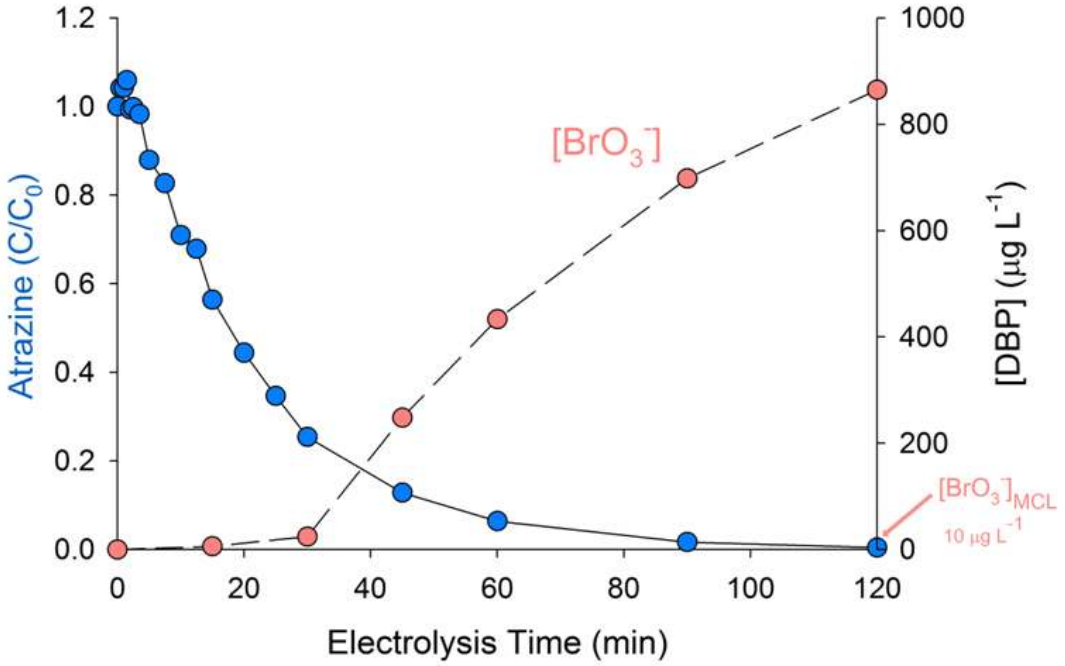

Figure 2.35: Production of bromate during the electrolysis of municipal wastewater effluent.

2.3.7 Environmental Implications

The efficiency with which contaminants are transformed on anodes depends upon the composition of the matrix and the nature of the anode. Higher salinity matrices, such as reverse osmosis concentrate from municipal wastewater and industrial wastewaters, are well suited for electrochemical treatment due to the lower energy demand in conductive matrices. For these waters, faster removal rates will be observed for many compounds due to the presence of Cl^- and Br^-. For compounds that do not react quickly with HOCl or HOBr, removal may be hampered by the presence of HCO_3^- which can scavenge reactive species like $Cl^\bullet$ and reduce the rate of transformation of prevalent electron-poor contaminants such as β-blockers (Kostich *et al.*, 2014) and triazine herbicides (Solomon *et al.*, 1996). The predominance of reactions occurring on the electrode for contaminants containing weakly-donating moieties suggesting benefits of designing treatment systems with high surface area per volume of water treated. Optimization of the treatment of wastewater effluent and reverse osmosis concentrate may require the removal of NH_4^+ and NOM.

In addition to electro-generated oxidants, toxic inorganic ions (e.g., chlorate, perchlorate, and bromate) (Bergmann *et al.*, 2014) and halogenated transformation products may be formed on all types of anodes (Farhat *et al.*, 2015; Radjenovic & Sedlak, 2015). The concentration of these contaminants depends upon the nature of the electrode, solution composition, and the applied current. This could limit the application of the technology and additional research is needed to develop tools to balance the benefits of efficient contaminant removal with the risks associated with formation of toxic byproducts.

CHAPTER 3. A Modular Advanced Oxidation Process Enabled by Cathodic Hydrogen Peroxide Production

Reproduced with permission from Barazesh, J. M.; Hennebel, T.; Jasper, J. T.; Sedlak, D. L., Modular Advanced Oxidation Process Enabled by Cathodic Hydrogen Peroxide Production. *Environmental Science & Technology* **2015,** *49*, (12), 7391-7399.

3.1 Introduction

Distributed water treatment systems offer a potential means of exploiting alternative water sources, including municipal wastewater effluent, roof water, stormwater and water from shallow aquifers (Larsen *et al.*, 2013). Unfortunately, alternative water sources often contain trace concentrations of organic contaminants (e.g., pesticides, solvents, pharmaceuticals, disinfection byproducts) (Benotti *et al.*, 2009). As a result, distributed treatment is often seen as an impractical means of providing potable water. Previous attempts to develop point-of-use treatment systems capable of removing trace organic contaminants prior to nonpotable reuse have employed electrochemical processes (Hernandez-Leal *et al.*, 2011; Butkovskyi *et al.*, 2014), but these systems suffer from limitations including the production of toxic byproducts, an inability to remove recalcitrant compounds and high cost of treatment (Chaplin, 2014) (Chapter 2).

Trace organic contaminants can be removed from water by exposure to hydroxyl radicals ($HO^{\bullet}$) in advanced oxidation processes (AOPs) (Pereira *et al.*, 2007; Pereira *et al.*, 2007; Rosario-Ortiz *et al.*, 2010; Shu *et al.*, 2013). In full-scale potable water reuse systems, trace organic contaminants are frequently removed by addition of a modest concentration of H_2O_2 (e.g., 3 mg/L) followed by exposure to UV light. This approach offers numerous benefits over other AOPs in terms of energy consumption, reliability and production of toxic byproducts (Katsoyiannis *et al.*, 2011). Although UV/H_2O_2 is a well established technology in centralized treatment facilities, challenges associated with the transport and storage of H_2O_2 make it an impractical solution for distributed treatment systems (Campos-Martin *et al.*, 2006). Electrochemical production of H_2O_2 from O_2 is an attractive alternative means of producing H_2O_2 if it can be achieved without the consumption of large amounts of energy or the formation of toxic byproducts (Campos-Martin *et al.*, 2006).

Electrochemical production of low concentrations of H_2O_2 can be achieved by several different approaches. Systems in which oxygen is bubbled into a solution prior to reduction on an electrode surface consume a considerable amount of energy due to the low solubility of oxygen and the need to ensure that it reaches the electrode surface. Bubbling air or pure oxygen into a solution is also an impractical approach for H_2O_2 production in decentralized systems because it requires pumps and controllers. Furthermore, the yield of H_2O_2 from reduction of O_2 is often quite low, which greatly increases electricity consumption (Campos-Martin *et al.*, 2006; Rozendal *et al.*, 2009; Modin & Fukushi, 2013; Yan *et al.*, 2014). Recently, gas diffusion electrodes have been used to generate H_2O_2 without a need to bubble air or oxygen into a solution (Campos-Martin *et al.*, 2006; Rozendal *et al.*, 2009; Modin & Fukushi, 2013). Most of the research in this area has been focused on producing concentrated H_2O_2 solutions by using highly conductive solutions or organic solvents (Rozendal *et al.*, 2009; Yan *et al.*, 2014). Cathodic production of H_2O_2 for the removal of organics has typically been used for electro-Fenton treatment; however, differences in pH needed for the optimal kinetics of the two reactions (i.e., production of H_2O_2 is most efficient at basic pH values and Fenton's reaction is more effective at acidic pH values) results in inefficient oxidation of trace organics if pH correction is not performed (Campos-Martin *et al.*, 2006; Brillas *et al.*, 2009). To produce low concentrations of H_2O_2 in water immediately prior to an AOP, the cathode must be capable of producing H_2O_2 in a low ionic strength, poorly-buffered solution at circumneutral pH values.

Furthermore, increases in pH that occur in the cathode chamber due to consumption of protons must be compensated for by a subsequent treatment process if the water is to be sent into a water distribution system.

The purpose of this study was to evaluate a system that combines *in situ* electrochemical production of H_2O_2 followed by UV irradiation and anodic pH adjustment as a cost-effective means of removing trace organic contaminants from water. This new system, which also inactivates waterborne pathogens and transforms photolabile contaminants through exposure to UV light, can be controlled by varying the production of H_2O_2 through adjustment of the applied current. To provide insight into the performance of the system under conditions likely to be encountered in distributed water treatment systems, three representative source waters (i.e., synthetic surface water, synthetic groundwater, and municipal wastewater effluent) were tested and compared to an electrolyte solution consisting of dilute sodium chloride. The performance of the system was investigated in terms of contaminant removal and energy consumption.

3.2 Materials and Methods

3.2.1 Chemicals

All experiments were performed at room temperature (23±2 °C) with chemicals of reagent grade or higher (Sigma-Aldrich, St. Louis, MO). The composition of the waters used is summarized in Table 3.1.

Table 3.1. Composition of the waters

Cations (mM)	Electrolyte	Surface Water	Ground Water	WWTP Effluent[b]
Na^+	12.5	1.12	0.0256	13.9
K^+	0	0.234	0.11	0.41
Ca^{2+}	0	2.55	0.81	1.8
Mg^{2+}	0	0.383	0.5	1.68
Anions (mM)				
NO_3^-	0	0.234	0.11	1.63
SO_4^{2-}	0	0.558	0.2	1.68
Cl^-	12.5	1.15	0.6	9.35
PO_4^{3-}	0	0	0.0128	0.069
Ionic Strength[a]	12.5	13.2	6.6	25.6
TIC (mM)	0	2.42	3.89	5.00
DOC (mg/L)	0	1.55	0	4.91

[a]Carbonate contribution to ionic strength calculated using speciation the speciation of TIC at the initial pH of the waters. [b]Nitrified wastewater effluent was obtained from the Discovery Bay municipal wastewater treatment plant (Discovery Bay, CA).

3.2.2 Electrochemical Cell and UV Reactor

Experiments were carried out in a two-chambered parallel plate electrochemical cell consisting of two square Perspex frames (internal dimensions: $8 \times 8 \times 1.9$ cm^3) separated by a cation exchange membrane (Ultrex CMI-7000, Membranes International Inc., Ringwood, NJ). The frames were bolted together between two square Perspex side plates, creating anode and cathode compartments that each had effective volumes of 122 mL (Figure 3.1). A solid plate was used for the anode frame, while the cathode chamber was bolted with a hollow side plate allowing for one side of the gas diffusion cathode to be exposed to air. A Ti mesh electrode coated with an Ir mixed-metal oxide was used as the anode (dimensions: 7.8×7.8 cm; 1 mm thickness; specific surface area 1.0 m^2 m^{-2}, Magneto Special Anodes, Netherlands). The anode and cathode had projected electrode surface areas of 64 cm^2. The UV reactor consisted of a 1 L brown glass bottle ($V_{effective}$ = 925 ml) containing a low-pressure UV lamp (arc length = 16.5 cm, optical path length = 4.3 cm) used typically for swimming pool disinfection (G23 Odyssea Pool Lamp, 9W, Odyssea Aquarium Appliance Co., Ltd., Guangdong, China; Figure 3.1).

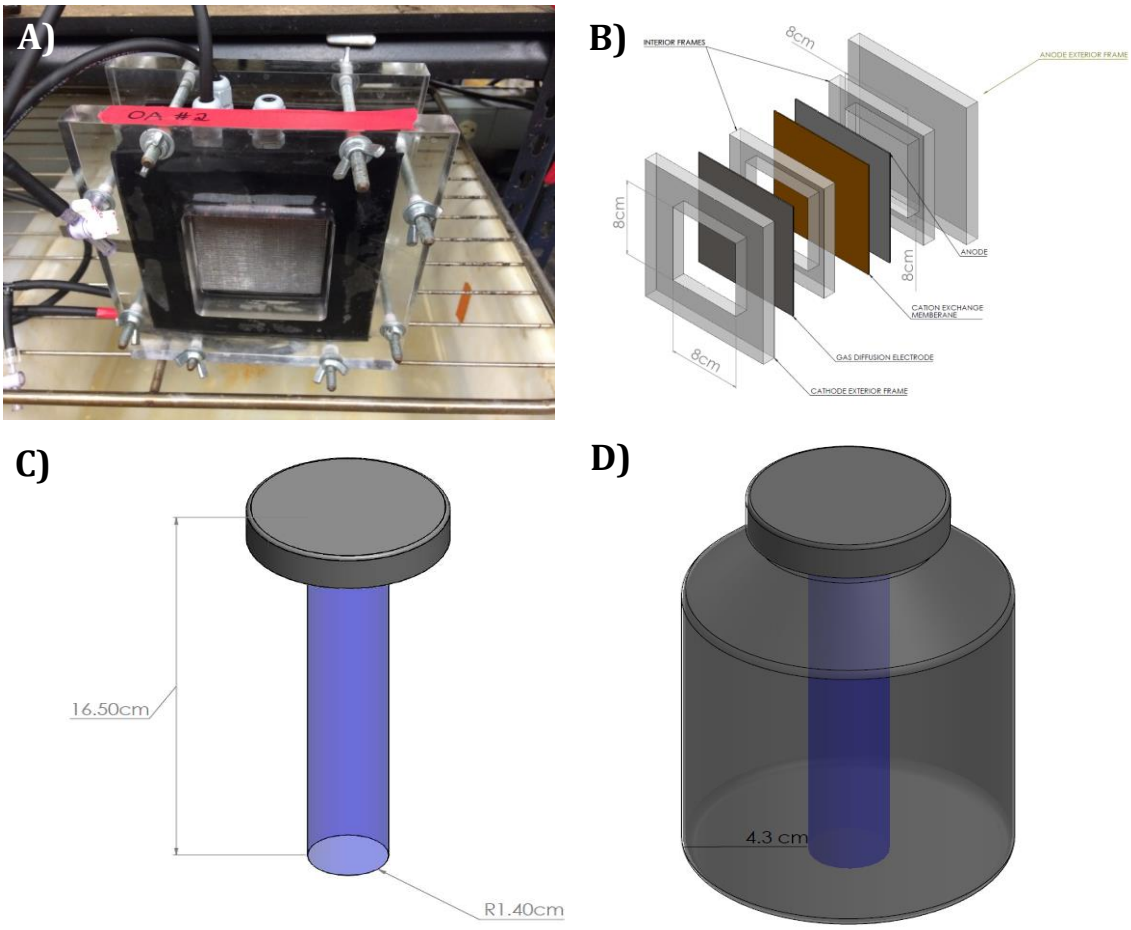

Figure 3.1: (a) Photo of the electrochemical cell, (b) blown up schematic of the cell components, (c) Low pressure UV lamp (G23 Odyssea Pool Lamp, 9W, electrical efficiency = 27%), (d) UV reactor.

3.2.3 Gas Diffusion Cathode Fabrication

The gas diffusion cathode was created by modifying carbon fiber paper (AvCarb P75T, $10 \times 10 cm^2$, Fuel Cell Store, College Station, TX) with a conductive, hydrophobic support layer and a carbon catalyst (Modin & Fukushi, 2013). The air-facing side of the cathode was prepared by coating a mixture of 60 wt% PTFE and 30 wt% graphite powder (200 mesh, Alfa Aesar, Ward Hill, MA) onto one side of the carbon base layer. The cathode was then air-dried at room temperature, followed by sintering at 350°C for 40 minutes. The liquid-facing side was prepared by applying a mixture of 3 mL propanol with 150 mg carbon black (Cabot Black Pearls 2000, Cabot, Boston, MA) and 50 mg PTFE onto the other side of the carbon base layer. The cathode was again air-dried at room temperature, followed by sintering at 350°C for 40 minutes.

3.2.4 Experimental Approach

Electrolysis experiments were performed at fixed currents controlled by a multichannel potentiostat (Gamry Instruments Inc., Warminster, PA). Water entered the cathode compartment operating in a flow-through mode with hydraulic residence times (HRT) ranging from 1.5 to 5.0 minutes (120 - 35 L d^{-1}). Cathode effluent was supplied to the UV reactor and then passed through the anode of the electrochemical cell. The applied charge density (ρ_q, C L^{-1}) was expressed as a product of the current density (I, A m^{-2}), electrode surface area (A, m^2) and the hydraulic residence time (t, s) normalized by the half chamber reactor volume (V, L):

$$\rho_q = \int \frac{I(t) * A}{V} * dt = \frac{IAt}{V} \quad (1)$$

Source waters were amended with a mixture of ten test compounds each at a concentration of 10 µg L^{-1}. For each experiment, samples were collected prior to the electrochemical cell, after passing through the cathode chamber, after the UV reactor, and after passing through the anode. At least 3.5 L of the test solution was passed through the system prior to collection of a sample. Samples were analyzed for H_2O_2, trace organic compounds, and pH. 1.9 mL-subsamples to be analyzed for trace organic compounds were mixed with 0.1 mL of methanol to quench radical reactions that could occur prior to analysis. H_2O_2 and pH were measured within 5 minutes, whereas trace contaminants were stored for a maximum of eight hours. Experiments quantifying H_2O_2 production in the varying waters were performed with applied cathodic current densities from 0 - 30 A m^{-2} under varying flow regimes (35 - 120 L d^{-1}). To assess the long-term cathode performance, 6000 L of 5 mM Na_2SO_4 in tap water (alkalinity = 0.34 mM, $[Ca^{2+}]$ = 0.2 mM) was run through the cell continuously at an applied current density of 15 A m^{-2} at a fixed flow rate of 120 L d^{-1}. Samples were collected daily and analyzed for H_2O_2. The effects of dissolved oxygen concentration on H_2O_2 production were evaluated by sparging source water with N_2 to remove O_2. The rate of production of H_2O_2 remained unchanged under N_2-sparged conditions.

3.2.5 Analytical Methods

H_2O_2 and free chlorine were measured with a Shimadzu UV-2600 spectrophotometer with the titanium (IV) sulfate method at 405 nm and the N,N-diethyl-p-phenylenediamine (DPD) method at 515 nm, respectively (Eisenberg, 1943; American Public Health *et al.*, 2005). Determination of free chlorine was performed in the absence of H_2O_2 to eliminate the positive interference of H_2O_2 with DPD (Dotson *et al.*, 2010). The UV absorbance of the four source

waters was measured with a Shimadzu UV-2600 spectrophotometer. Dissolved organic carbon (DOC) and dissolved inorganic carbon (DIC) were measured using a Shimadzu TOC-V analyzer. NO_3^-, Cl^-, and SO_4^{2-} were analyzed using a Dionex DX-120 ion chromatograph with an AS19G column. K^+, Na^+, Ca^{2+}, and Mg^{2+} were analyzed using a Dionex ICS-2000 ion chromatograph with a CS12A column. Fluence rate values were determined by chemical actinometry using 10 μM atrazine as an actinometer (ε_{254}=3860 M^{-1} cm^{-1}, ϕ_{254}= 0.046 mol Ei^{-1}, buffered at pH = 8 using a borate buffer; details of the calculation in the SI) (Bolton & Linden, 2003; Canonica *et al.*, 2008). Conductivity was measured with an Ultrameter II 4P (Myron L Company, Carlsbad, CA). Test compounds were quantified in multiple reaction monitoring (MRM) mode with an Agilent 1200 series HPLC system coupled to a 6460 triple quadropole tandem mass spectrometer (HPLC-MS/MS), as described previously (Jasper *et al.*, 2014). Analytical details and compound specific parameters are provided in section A.2.1 of the Appendix.

3.2.6 Electrochemical Power Calculations

The gas diffusion electrode was polarized cathodically against a Ag/AgCl reference electrode (+0.197 V vs. SHE; BASi, USA). The full cell potential between the working (i.e., cathode) and counter (i.e., anode) electrodes was measured in a two-electrode setup. The total system power (P_{total},W) is a combination of the UV lamp power and the electrochemical cell power, which can be expressed as a product of the current density (I, A m^{-2}), cell potential (V_{cell}), and the electrode surface area (A, m^2) :

$$P_{total} = I * A * V_{cell} + P_{lamp} \quad (2)$$

3.3 Results and Discussion

3.3.1 Hydrogen Peroxide Production as Function of Current in Varying Source Waters

Hydrogen peroxide concentrations (Figure 3.2) and production rates (Figure 3.3) were determined for an array of charge densities that were achieved from combinations of current densities (0-30 A m^{-2}) and cathode chamber retention times (1.5-5 min). A linear relationship between H_2O_2 production and applied charge density was observed at charge densities greater than 50 C L^{-1}, independent of how the charge was obtained (i.e., high current density and short retention times or low current density and long retention times):

$$\mathbf{[H_2O_2] = 0.0048 * \rho_q \quad (50 \leq \rho_q \leq 375\ C\ L^{-1})} \quad (3)$$

where ρ_q is the specific charge density applied in C L^{-1} and $[H_2O_2]$ is the hydrogen peroxide concentration in mM. For all of the waters tested, the coulombic efficiency of O_2 reduction to H_2O_2 averaged 88.8 ± 1.8 % at charge densities greater than 50 C L^{-1} (Figure 3.4). At lower charge densities, lower coulombic efficiencies were observed (note the deviation from the linear fit in Figure 1A at charge densities below 50 C L^{-1}). The observed increased coulombic efficiencies at higher charge densities agreed with previously published data for electrochemical synthesis of H_2O_2 using a gas diffusion electrode composed of a fluorocarbon binder and

activated carbon catalyst fed with conductive, alkaline solutions (Foller & Bombard, 1995; Campos-Martin *et al.*, 2006; Yan *et al.*, 2014).

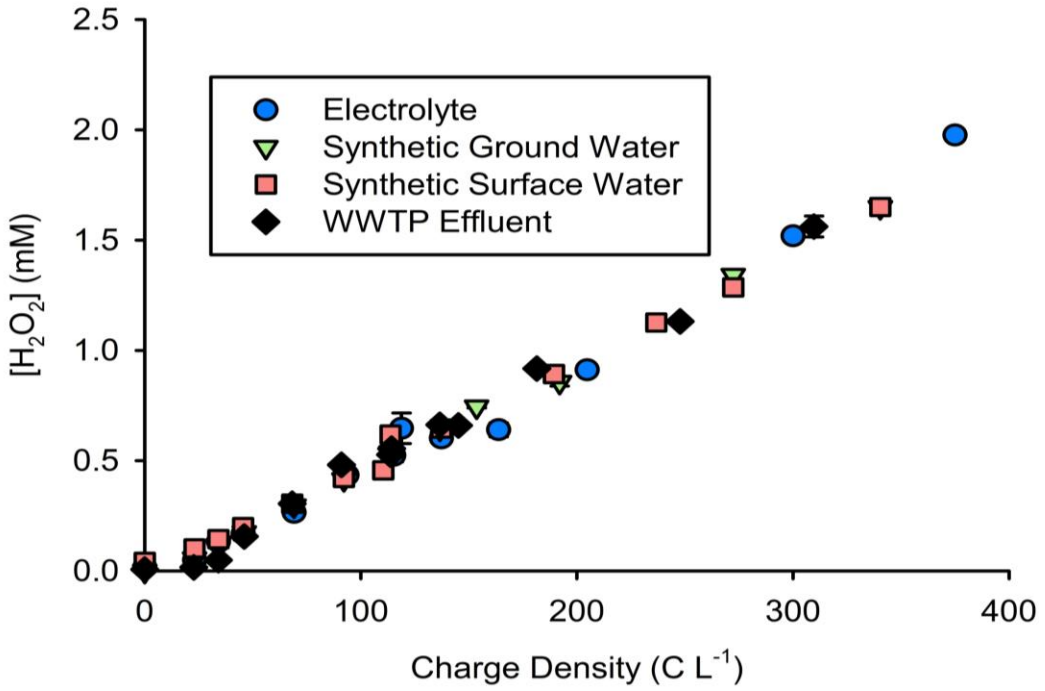

Figure 3.2: Production of hydrogen peroxide as a function of applied charge density (WWTP: wastewater treatment plant).

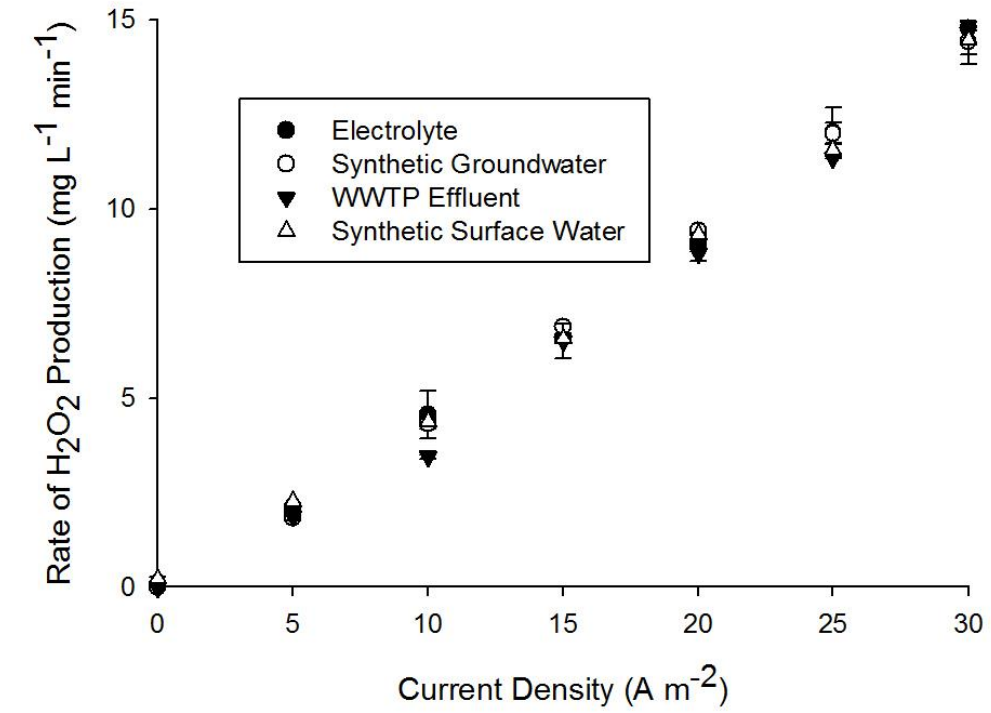

Figure 3.3: Hydrogen peroxide production rate as a function of current density (WWTP: wastewater treatment plant).

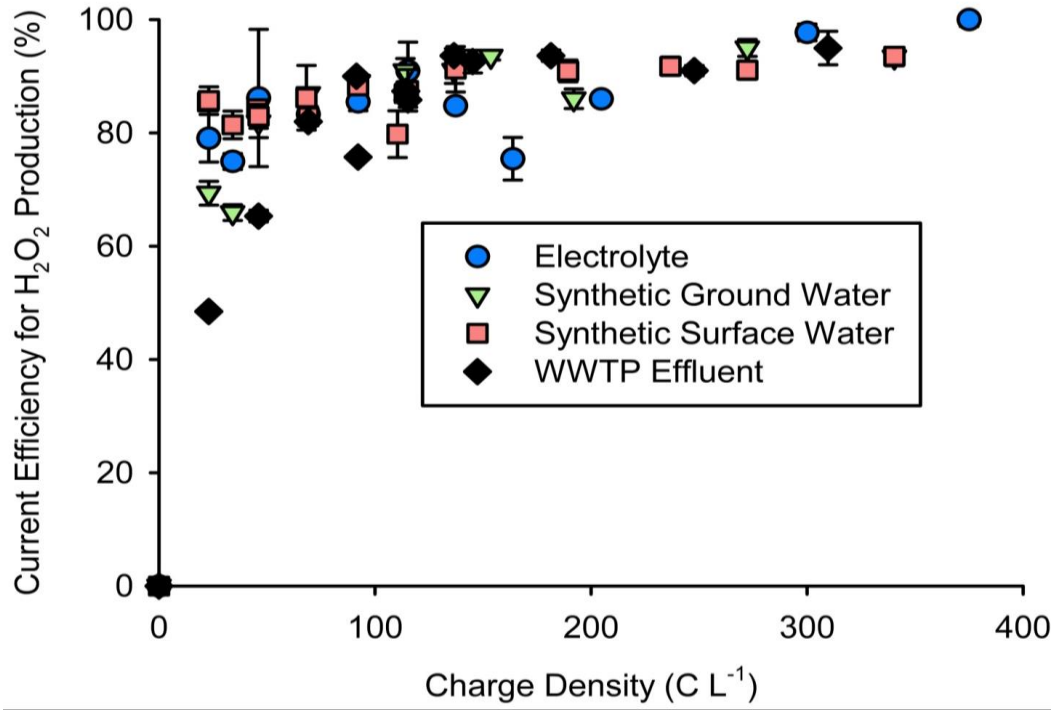

Figure 3.4: Coulombic efficiency for H_2O_2 production as a function of applied charge density (WWTP: wastewater treatment plant).

H_2O_2 production was independent of the type of source water used despite the substantial variability in the composition of the matrices (Tables 3.1 and 3.2). This suggests that H_2O_2 production was not affected by pH, the presence of natural organic matter (NOM), dissolved ions, or conductivity over the range of applied charge studied. Although H_2O_2 production was not influenced by influent water quality, the cell potential, and therefore energy consumption, was affected by the conductivity of the source waters. Higher ionic strength waters exhibited lower ohmic resistances and therefore operated at lower cell potentials, thus decreasing their energy consumption. For a given applied charge, the power required decreased with increased conductivity (synthetic surface water > synthetic groundwater > wastewater effluent ≅ electrolyte; Figure 3.5). Even for low conductivity surface water, however, the energy consumption for hydrogen peroxide production at a flow rate of 120 L d^{-1} was still relatively low (0.018 - 0.31 kWh m^{-3} for $5 < I < 30$ A m^{-2}), indicating that *in-situ* H_2O_2 production required much less energy than operation of the UV lamp (1.8 kWh m^{-3}; calculations provided the Section A3.1 of the Appendix).

The H_2O_2 production rate increased linearly with applied current density, with a maximum of between 14.4 and 14.8 mg H_2O_2 L^{-1} min^{-1} at 30 A m^{-2} for all of the waters tested (Figure 3.3). In full-scale AOP systems (e.g., the Orange County Water District's Groundwater Replenishment System), 3 mg H_2O_2 L^{-1} (0.09 mM) is typically applied (DDB Engineering, 2013). This concentration can be obtained with the gas diffusion electrode at an applied current density of only 4.14 A m^{-2} at a hydraulic residence time of 1.5 min. Under these conditions, this benchtop system could process approximately 120 L of water per day while consuming approximately 1.7 Wh to produce H_2O_2.

Table 3.2. Composition and Properties of the Tested Waters

	Property				Scavenging Compound			
Water Matrix	UV absorbance$_{254nm}$ (cm^{-1})	Conductivity ($\mu S\ cm^{-1}$)	$pH_{initial}$	TIC ($mEq\ L^{-1}$)	[DOC] ($mgC\ L^{-1}$)	H_2O_2 (mM)[b]	HCO_3^- (mM)	CO_3^{2-} (mM)
Electrolyte	0	1515	5.36	0	0	0 - 0.54	0	0
Synthetic Groundwater	0.0027	440.6	8.69	3.9	0.1	0 - 0.54	3.79	0.09
Synthetic Surface Water	0.131	360.4	8.55	2.4	1.6	0 - 0.54	2.35	0.04
Wastewater Effluent	0.137	2040	8.17	5.0	4.9	0 - 0.54	4.90	0.03
Rate Constant								
$k_{HO\bullet,cont}$ ($M^{-1}\ s^{-1}$)	-	-		-	9.8×10^3 [a]	2.7×10^7	8.5×10^6	3.9×10^8

[a] $k_{HO\bullet,NOM}$ rate constant is given in L $mgC^{-1}s^{-1}$. [b] $[H_2O_2]$ is variable and dependent on the applied current density.

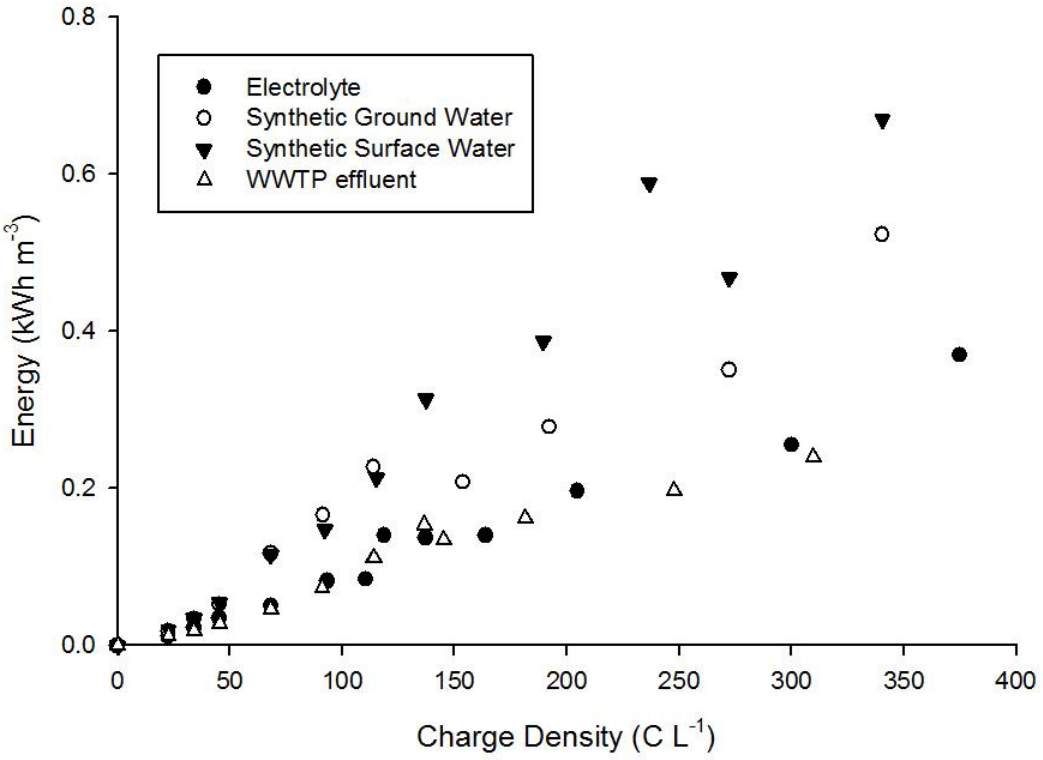

Figure 3.5: Energy demand of the electrochemical cell per m^3 of treated water as a function of applied charge density (WWTP: wastewater treatment plant).

3.3.2 Trace Organic Contaminant Removal by Electro-generated H_2O_2 and UV Irradiation

The removal of trace organic contaminants involved direct photolysis, reactions with $HO^\bullet$ produced by photolysis of H_2O_2 in the UV chamber, and direct oxidation of contaminants on the anode. At the fluence employed in the UV chamber (F_0 ~ 3000 mJ cm^{-2}), direct photolysis only removed those compounds that exhibited high quantum yields and strong light absorbance at 254 nm (Figure 3.6). Among the compounds tested, carbamazepine exhibited the lowest tendency for direct transformation by UV light (< 30% removal for all matrices), while more photoreactive compounds, such as sulfamethoxazole, propranolol, and atrazine, displayed higher removals (55 - 99%). Unlike the variability of the compounds with respect to direct photolysis, the suite of trace organics all reacted with $HO^\bullet$ at near diffusion controlled rates (10^9 - 10^{10} M^{-1} s^{-1}; Table 3.3). As a result of its low reactivity with UV light, carbamazepine removal in the presence of H_2O_2 and UV light provided useful information on the transformation of organic contaminants by $HO^\bullet$.

Table 3.3. Compound Specific Properties

	Property						
Compound	ε_{254} (M^{-1} cm^{-1})[a]	Φ_{254} (mol Ei^{-1})[a]	pK_a	log K_{ow}	$k_{HO\bullet}$,cont (M^{-1} s^{-1})	$k_{CO3\bullet-}$,cont (M^{-1} s^{-1})	k_{HOCl},cont (M^{-1} s^{-1})
Atenolol	5.27×10^{2}	1.1×10^{-2}	9.6	0.2-0.5	7.5×10^{9} [b]	5.9×10^{7} [d]	1.7×10^{-2} [i]
Trimethoprim	2.64×10^{3}	1.49×10^{-3}	9.5	1.9-2.3	8.7×10^{9} [c]	3.5×10^{7} [d,h]	1.6×10^{2} [j]
Metoprolol	1.9×10^{2}	1.18×10^{-2}	9.1	3.4	8.4×10^{9} [d]	-	1.7×10^{-2} [i]
Sulfamethoxazole	6.92×10^{3}	9.0×10^{-2}	7.4	0.9	5.9×10^{9} [d]	4.4×10^{8} [d]	6.17×10^{2} [j]
Propranolol	1.03×10^{3}	5.2×10^{-3}	5.6	0.9	1.1×10^{10} [d]	4.6×10^{8} [d]	7.5×10^{0} [i]
Carbamazepine	5.27×10^{2}	1.3×10^{-4}	13.9	2.5	9.1×10^{9} [d]	2.3×10^{6} [d]	< 0.1 [k]
Atrazine	3.86×10^{3}	4.6×10^{-2}	3.2	2.7	3×10^{9} [e]	-	-
Ibuprofen	1.24×10^{3}	1.12×10^{-2}	4.91	2.5	6.7×10^{9} [f]	-	< 0.1 [k]
Gemfibrozil	n.d.	1.23×10^{-2}	4.77	4.8	1.0×10^{10} [g]	-	7.3×10^{-1} [i]

[a] (Jasper *et al.*, 2014). [b] (Salgado *et al.*, 2013). [c] (Baeza & Knappe, 2011). [d] (Jasper & Sedlak, 2013). [e] (Acero *et al.*, 2000). [f] (Shu *et al.*, 2013). [g] (Razavi *et al.*, 2009). [h] (Zhang *et al.*, 2015). [i] (Pinkston & Sedlak, 2004). [j] (Deborde & von Gunten, 2008). [k] (Lee & von Gunten, 2010).

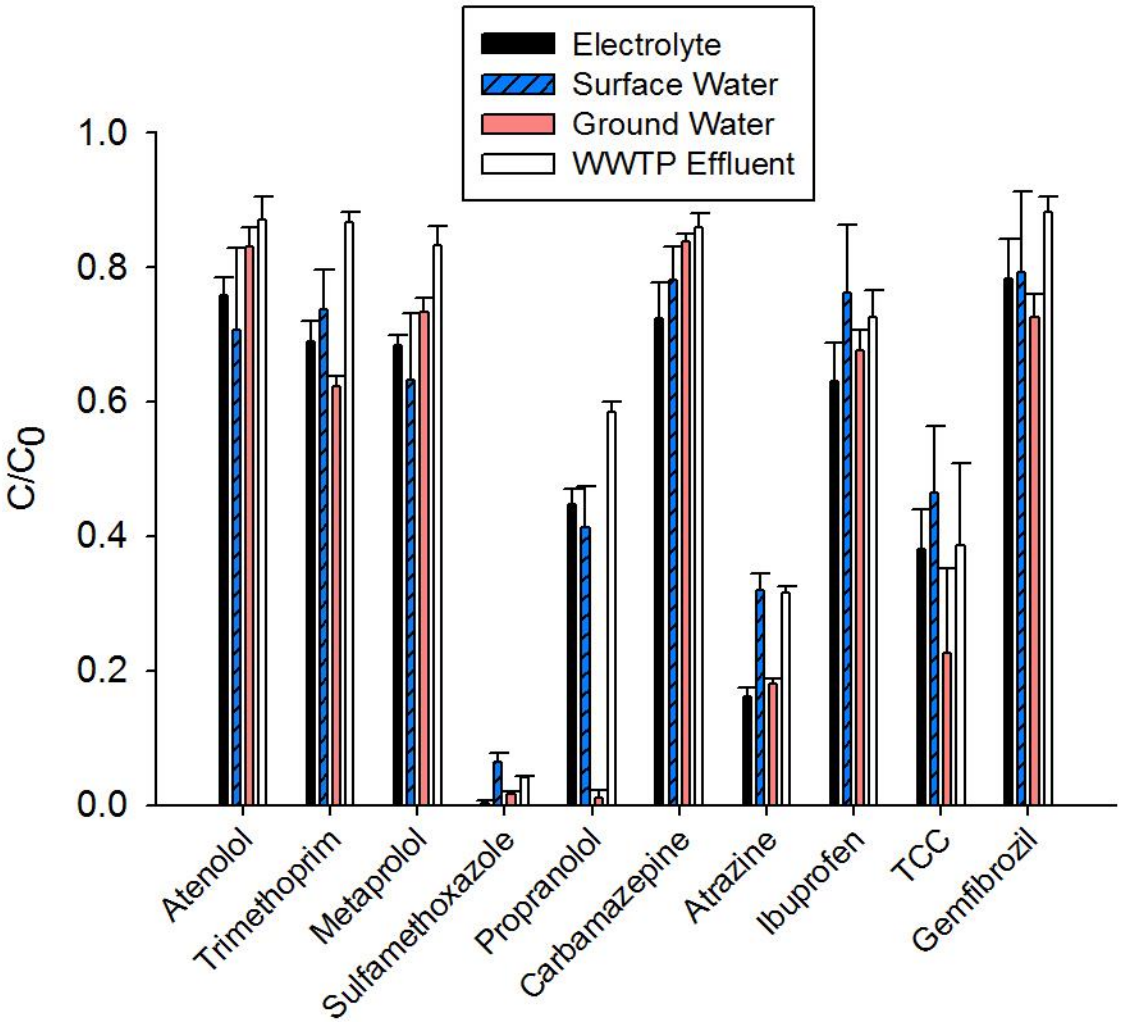

Figure 3.6: Normalized removal of organic contaminants by UV photolysis (no H_2O_2 present) (WWTP: wastewater treatment plant).

The extent of removal of carbamazepine varied among the different matrices (Figure 3.7). The presence of $HO^{\bullet}$ scavengers explained much of the variability. In the absence of current (and therefore H_2O_2), the variability of carbamazepine transformation was predominately influenced by the screening of light, as accounted for by the water factor [Bolton & Linden, 2003),(R.P. Schwarzenbach, 2002)]:

$$\text{water factor} = \frac{[1-10^{-1.2\alpha z}]}{(2.3)(1.2)\alpha z} \quad (4)$$

where z is the mixed water body depth (m) and α is the attenuation coefficient of the water body. The water factor, which was primarily influenced by the amount of NOM, followed the trend: electrolyte (0.998) > groundwater (0.985) > synthetic surface water (0.598) > wastewater effluent (0.508). Transformation of carbamazepine solely in the presence of UV light varied from 22 ± 5 % in the electrolyte solution to 15 ± 4 % in the wastewater effluent. The observed removal of carbamazepine in the surface water and wastewater effluent, however, was greater than suggested from the water factor. This may be explained by the generation of $HO^{\bullet}$

and ^{3}DOM* produced from NOM sensitization by UV light, which can be significant at UV fluences employed in AOPs (Dong & Rosario-Ortiz, 2012; Lester *et al.*, 2013).

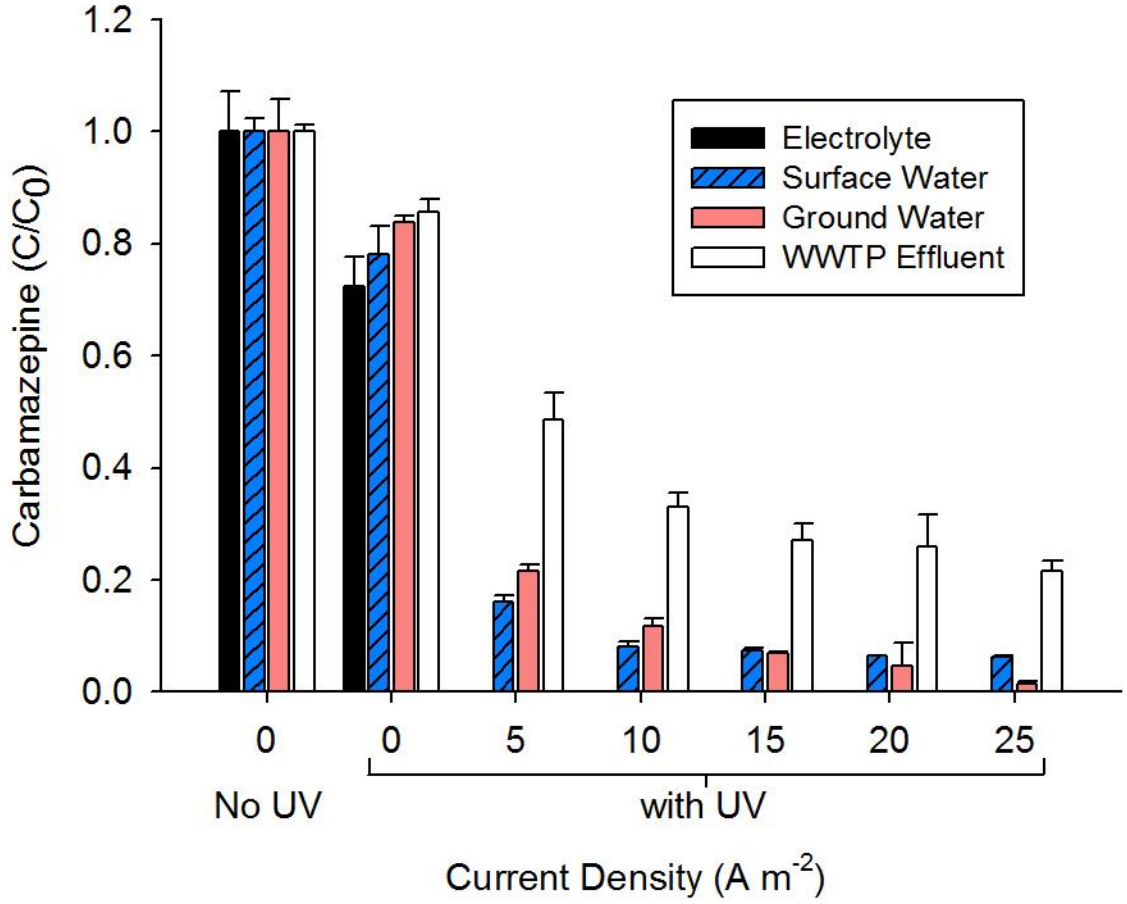

Figure 3.7: Removal of carbamazepine as a function of current density for the four types of source waters (WWTP: wastewater treatment plant).

The rate of transformation of trace contaminants increased with current density due to additional $HO^{\bullet}$ production that occurred at higher H_2O_2 concentrations (See Tables A3.1-A3.4 for raw values). Complete carbamazepine transformation was observed after the UV treatment chamber at an applied current density of 5 A m^{-2} for the electrolyte. For the three representative source waters, carbamazepine transformation increased to 98.7 ± 0.6 % for groundwater, 93.3 ± 1.0 % for surface water, and 78.5 ± 1.9 % for wastewater effluent as the current increased to 25 A m^{-2}. Organic compounds that have lower reaction rate constants with $HO^{\bullet}$ and are not susceptible to direct photolysis will require higher current densities to achieve a similar level of treatment.

The fraction of $HO^{\bullet}$ that reacted with the contaminants can be estimated by considering the concentrations and rate constants for reactions of different solutes with $HO^{\bullet}$:

$$\text{fraction } HO^{\bullet} \text{ to contaminants} = \frac{\sum k_{HO^{\bullet},cont}[Cont]}{\sum k_{HO^{\bullet},s}[S]} \quad (5)$$

Where $k_{OH^\bullet,S}$ and $k_{HO^\bullet,cont}$ are the second order reaction rate constants of scavengers and contaminants with $HO^\bullet$, respectively, and [S] is the concentration of the scavenger (e.g., HCO_3^-, CO_3^{2-}, NOM, H_2O_2; Tables 3.2 and 3.3).

Effect of H_2O_2 on Treatment Efficiency. At increasing H_2O_2 concentrations, a trade-off exists between additional transformation of trace organics by $HO^\bullet$ produced from H_2O_2 photolysis and greater radical scavenging and light screening by H_2O_2 (Sharpless & Linden, 2003). Therefore, despite linear increases in H_2O_2 production with current density, there is a diminishing benefit to the treatment. As H_2O_2 increased from 0.09 mM (4.14 A m^{-2}) to 0.54 mM (25 A m^{-2}), the fraction of $HO^\bullet$ reacting with contaminants decreased by 20 %, 21 %, and 10 % for the surface water, groundwater, and wastewater effluent, respectively. At 0.54 mM H_2O_2 (25 A m^{-2}), there was a 4.0 %, 4.7 %, and 3.8 % reduction in direct photolysis rates of contaminants from additional light screening by H_2O_2 for the surface water, groundwater, and wastewater effluent, respectively (details of $HO^\bullet$ branching ratio and direct photolysis calculations are included in Sections A3.3 and A3.4 of the Appendix, respectively).

Effect of pH on Treatment Efficiency. At pH 8, approximately 6.7%, 6.5%, and 2.9% of $HO^\bullet$ reacted with the organic contaminants in the UV reactor at an initial H_2O_2 concentration of 3 mg L^{-1} (0.09 mM) for the surface water, groundwater, and wastewater effluent, respectively. At pH 10, the fraction of $HO^\bullet$ reacting with trace organic contaminants decreased to 0.9%, 0.6%, and 0.4% for the three source waters, respectively. The significant decrease in $HO^\bullet$ reacting with the trace organic contaminants was due to scavenging by carbonate at the higher pH values. The product of this reaction, $^\bullet CO_3^-$, can play a significant role in the transformation of certain organic compounds (e.g., propranolol and sulfamethoxazole; Table 3.3) (Jasper & Sedlak, 2013). As a result of differences in alkalinity of the different source waters, the importance of carbonate scavenging and $^\bullet CO_3^-$ reactions depends on the source water composition and the applied current density (i.e., higher applied currents result in greater pH increases in the cathode chamber). Although nitrite is an effective scavenger of $HO^\bullet$ ($k_{HO\bullet,NO2-} = 6 \times 10^9$ M^{-1} s^{-1}), less than 0.3% of the generated $HO^\bullet$ would be scavenged by nitrite at concentrations typically found in nitrified wastewater effluent (i.e., ~0.1 mg L^{-1}). The formation of halogen radicals from reactions between $HO^\bullet$ and halide ions (chloride and bromide) should only be significant at low pH values and therefore will have a negligible impact on contaminant transformation at the circumneutral and basic pH values observed in this system (Grebel *et al.*, 2010).

3.3.3 Anodic pH Adjustment

The generation of H_2O_2 by the cathode consumed protons and increased the solution pH (reaction 6). In the anode, oxidation reactions produced protons and lowered the solution pH (reaction 7):

$$\mathbf{O_2 + 2e^- + 2H^+ \leftrightarrow H_2O_2} \quad \textbf{(Cathode)} \tag{6}$$

$$\mathbf{H_2O \leftrightarrow \frac{1}{2}O_2 + 2e^- + 2H^+} \quad \textbf{(Anode)} \tag{7}$$

$$\mathbf{2Cl^- \leftrightarrow Cl_2 + 2e^-} \quad \textbf{(Anode)} \tag{8}$$

$$\mathbf{Cl_2 + H_2O \leftrightarrow HOCl + H^+ + Cl^-} \tag{9}$$

For the production of 3 mg L^{-1} (0.09 mM) of H_2O_2 at a current density of 4.14 A m^{-2}, approximately 0.20 mEq L^{-1} of protons should have been consumed or produced at the cathode and anode, respectively. To maintain electroneutrality, a net migration of protons occurred from the anode chamber to the cathode chamber via the cation exchange membrane. In addition to protons, cations that were present at higher concentrations (e.g., Na^+, Ca^{2+}, Mg^{2+}) also carried ionic charge through the membrane satisfying electroneutrality in the cathode chamber while creating a proton deficit in the cathode chamber (Rozendal *et al.*, 2006).

As a result of differences in buffering among matrices, the solution pH should have increased more in the cathode chamber for waters with low alkalinity. The pH in the cathode chamber increased for each of the waters as the current increased from 0 to 25 A m^{-2} (Figure 3.8). The magnitude of pH increase was most pronounced for the electrolyte and surface water (alkalinity = 0 mM and 2.45 mM, respectively) with post-cathode pH values ranging from 10 to 10.5, while the pH never exceeded 9.9 and 9.2 in the groundwater (alkalinity = 3.89 mM) and the municipal wastewater effluent (alkalinity = 4.97 mM), respectively. The pH increases following the cathode resulted in supersaturation with respect to calcite ($CaCO_{3(s)}$) in the groundwater (log SI > 1.31), surface water (log SI > 1.58), and wastewater effluent (log SI > 1.09) beginning at a current density of 5 A m^{-2}. This reaction could result in scaling on the cathode or the ion exchange membrane that might eventually affect system performance. Loss of $CaCO_{3(s)}$ from the system could also result in an overall decrease in pH as water passed through the treatment system. For example, if the surface water solution reached equilibrium at the current density needed to produce 3 mg L^{-1} (0.09 mM) of H_2O_2, 0.74 mmoles (74 mg) of calcite would precipitate for each liter of water treated and the pH would have dropped from 9.82 to 7.23. On the basis of the observed pH values it is evident that equilibrium was not achieved. However, additional research is needed to assess the importance of calcite precipitation to scaling and pH control.

To readjust the solution pH, water leaving the UV reactor was passed through the anode chamber. If no mineral precipitation occurred in the cathode and UV chambers the final pH should have been equal to the influent pH. A slight decrease in pH was observed in all solutions to which current was applied, with greater pH decreases at higher current densities occurring in the least buffered of the three environmental matrices (i.e., surface water). Under the conditions that would likely be used for treatment (i.e., 5 - 10 A m^{-2} and short hydraulic residence times) the final pH was approximately equal to the initial pH.

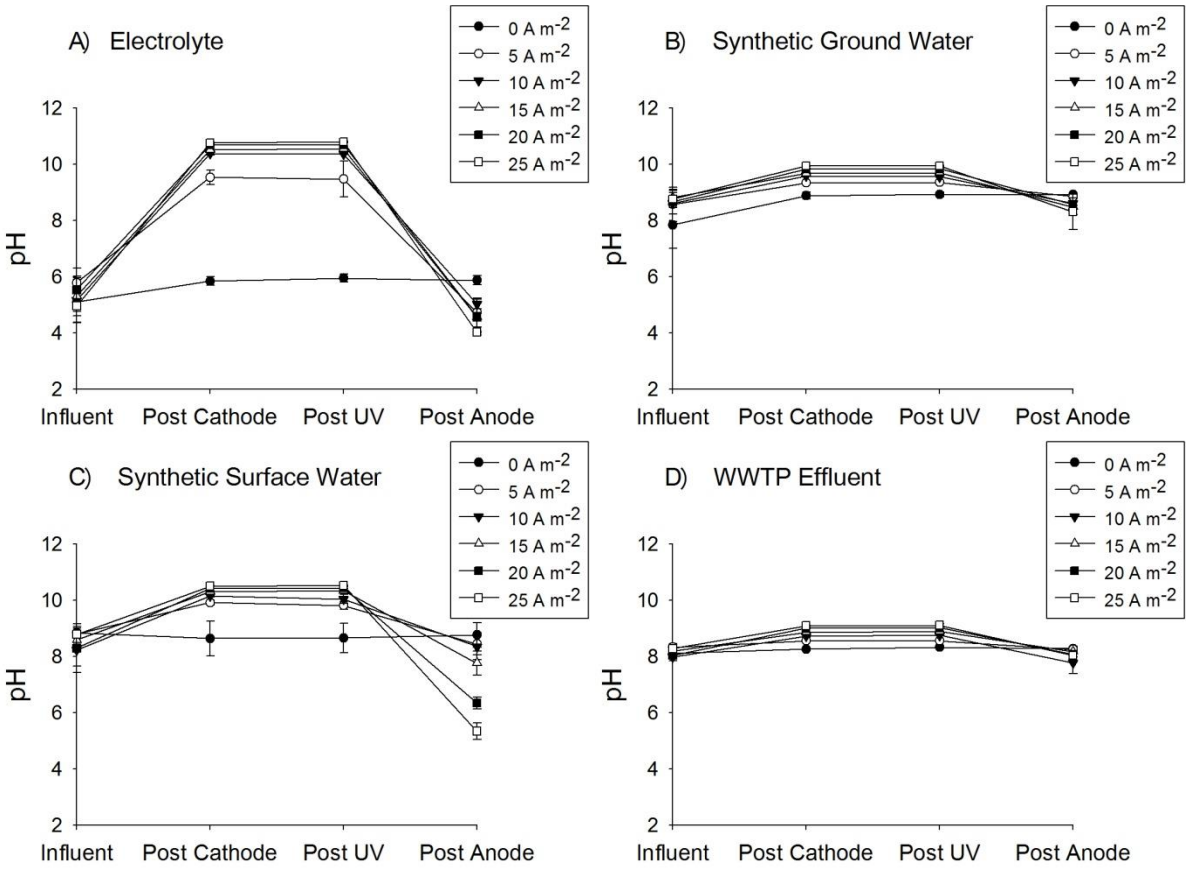

Figure 3.8: pH change of the source waters prior to entering the electrochemical cell, after passing through the cathode chamber, after the UV reactor, and after the anode as a function of current density (WWTP: wastewater treatment plant).

3.3.4 Anodic Quenching of Residual Hydrogen Peroxide

Due to the relatively low molar absorptivity of H_2O_2 at 254 nm (ε_{254} = 18.6 M^{-1} cm^{-1}) and the limited residence times in the UV reactor (τ = 660 s), much of the H_2O_2 passed through the UV chamber without undergoing photolysis. For solutions with relatively low light screening (i.e., electrolyte, synthetic groundwater and synthetic surface water) between 40 and 50% of the H_2O_2 was photolyzed at current densities ranging from 5 to 25 A m^{-2} (Figure 3.9 and Figure 3.10). As expected, less H_2O_2 photolysis occurred in municipal wastewater effluent due to light screening.

In practice, many centralized treatment plants employ reducing agents (e.g., bisulfite), chlorine, or activated carbon to remove residual H_2O_2 before distribution (Watts *et al.*, 2012). The use of activated carbon or the addition of chemicals, however, may be impractical in a distributed treatment system. Partial removal of H_2O_2 occurred when the solution passed through the anode, especially in the electrolyte solution (Figure 3.9 and Figure 3.10). Anodic removal of H_2O_2 increased with increasing current density (Figure 3.10). In the NaCl electrolyte solution, up to 0.12 mM of H_2O_2 was removed at 25 A m^{-2}. For the three source waters, however, the anode only removed about 25% of the amount removed in the electrolyte.

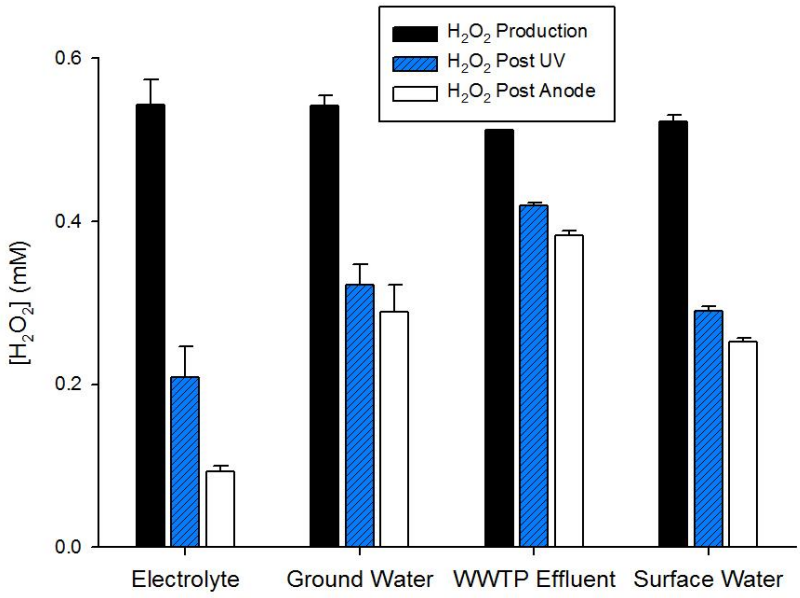

Figure 3.9: Production of H_2O_2 in the cathode, residual H_2O_2 after the UV cell and residual H_2O_2 after the anode for the four types of source waters at applied current density of 25 A m^{-2}.

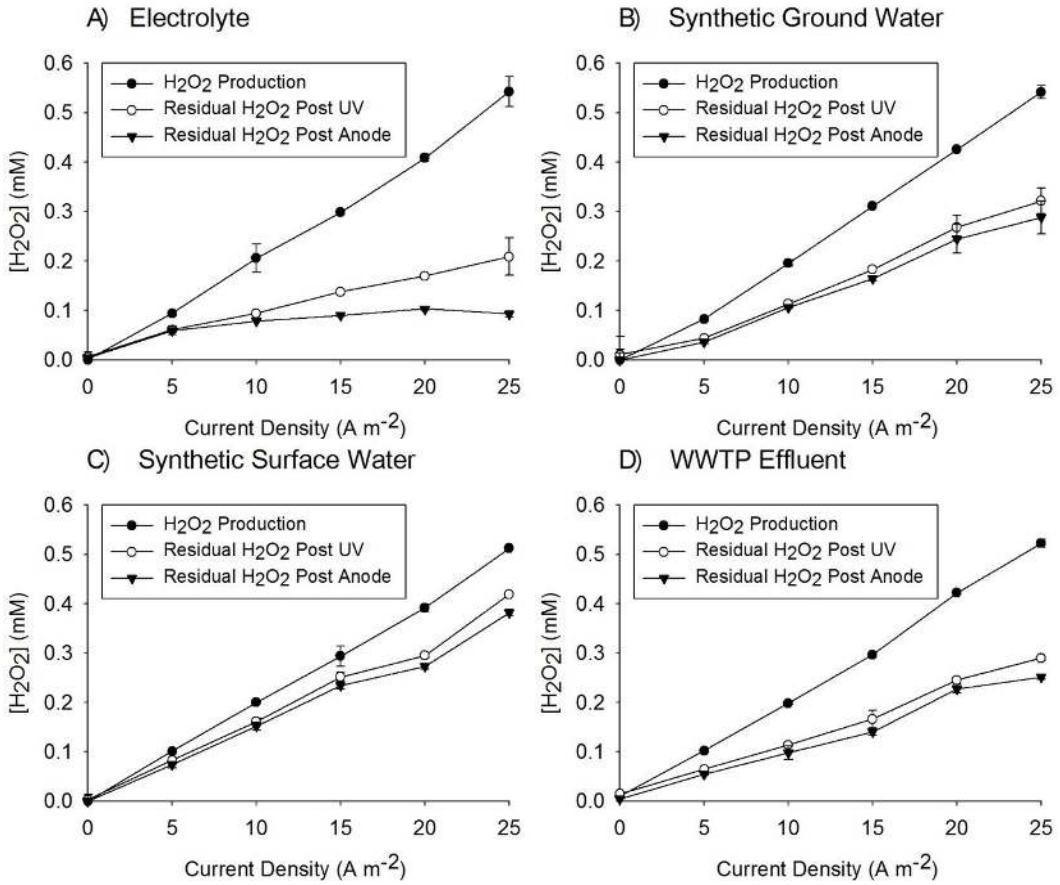

Figure 3.10: Production of H_2O_2 in the cathode, residual H_2O_2 after the UV cell and residual H_2O_2 after the anode for the four types of source waters at applied current densities from 0 to 25 A m^{-2} (WWTP: wastewater treatment plant).

Removal of H_2O_2 in the anode was attributable to a combination of direct anodic oxidation and reactions with oxidants produced on the anode surface. For example, oxidation of chloride can result in the production of hypochlorous acid (HOCl; $pK_a = 7.6$) (Reactions 8,9). Hypochlorite reacts rapidly with hydrogen peroxide under alkaline conditions with the bimolecular rate constant increasing from 196 M^{-1} s^{-1} to 7.5×10^3 M^{-1} s^{-1} from pH 6 to 9 (see Section A3.5 of the Appendix for calculation of the pH-dependent bimolecular rate constant) (Connick, 1947; Held *et al.*, 1978; VonGunten & Oliveras, 1997):

$$OCl^- + H_2O_2 \rightarrow Cl^- + O_2 + H_2O \quad (10)$$

Although Ti-IrO_2 electrodes have a high electrocatalytic activity with respect to chlorine evolution, only modest concentrations of chlorine were produced in control experiments at varying chloride concentrations due to the short hydraulic residence times and relatively low current densities applied (Szpyrkowicz *et al.*, 2005; Jeong *et al.*, 2009; Bagastyo *et al.*, 2011) (Table 3.4).

Table 3.4. Chloride-Chlorine Electrochemical Oxidation

	Current Density (A m^{-2})				
[Cl^-] (mM)	2.5	5	10	15	25
0.5	0	0	0	0	0
5	0	0	0.79	17	34
10	0	0	3.9	25	41
15	0	0	7.9	32	61

Free chlorine production (as µM Cl[I]) in the anode chamber as a function of applied current density and chloride concentration. Experiments were performed with a stainless steel cathode to prevent H_2O_2 formation, which interferes with the chlorine measurement.

To separate the effects of reactive halogen species from direct electrode oxidation on the removal of H_2O_2, experiments were repeated using an inert electrolyte (i.e., Na_2SO_4; Figure 3.11). H_2O_2 removal was independent of applied current density with 37 ± 2 µM H_2O_2 removed from 5 to 25 A m^{-2}; a concentration equivalent to the observed H_2O_2 removal in the anode for the three source waters in Figure 3.9. Given the low chloride concentrations (< 1 mM) of the simulated surface water and groundwater, it is not surprising that OCl^- production was low and only a small quantity of H_2O_2 was removed in the anode.

Despite the electrolyte and municipal wastewater effluent having roughly the same concentration of chloride, H_2O_2 removal was significantly higher in the electrolyte control than in the wastewater effluent, suggesting that reactive halogen species did not play an important role in H_2O_2 removal in the wastewater effluent matrix. NOM is an effective sink of HOCl/OCl^-; however, under the experimental conditions used in this study, the half-life of HOCl/OCl^- with respect to its reaction with H_2O_2 was much shorter than that predicted for NOM (i.e., 1.39 s and 49.3 s, respectively, as described in the Appendix) (Zhai *et al.*, 2014). As a result, NOM is only a minor sink for HOCl/OCl^- in the presence of H_2O_2. This was consistent with observations from experiments in which H_2O_2 removal decreased by less than 40% (58 µM) when NOM was added to a solution containing a fixed concentration of chloride at a current density of 25 A m^{-2}, suggesting that NOM is only partially responsible for the difference in H_2O_2 removal between the two solutions (Figure 3.11).

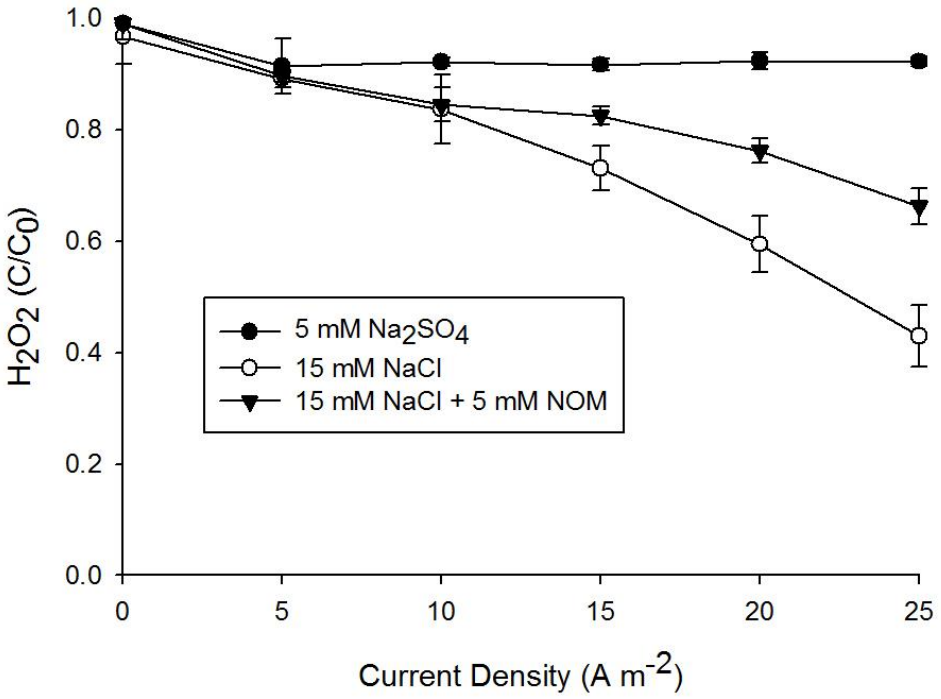

Figure 3.11: Normalized H_2O_2 removal in the anode as a function of current density in the presence and absence of chloride or natural organic matter (HRT = 1.5 min, $[H_2O_2]_0$ = 10 mg L^{-1} (0.294mM)) (WWTP: wastewater treatment plant).

The apparent discrepancy between municipal wastewater effluent and the sodium chloride solution may be partially attributable to differences in pH values in the anode chamber (Consonni *et al.*, 1987). At higher pH values, like those found in the municipal wastewater effluent after anodic treatment, there is a larger driving force for oxygen evolution compared to Cl_2 production:

$$O_2 + 4H^+ + 4e^- \leftrightarrow H_2O \quad E_H^\circ = 1.23\ V \tag{11}$$

$$Cl_2 + 2e^- \leftrightarrow 2Cl^- \quad E_H^\circ = 1.36\ V \tag{12}$$

Experiments conducted in the anode chamber at different pH values confirmed that chlorine production increased substantially as pH dropped from 9 to 7 (Figure 3.12). Due to the presence of bicarbonate in the municipal wastewater effluent, the anode pH was considerably higher (i.e., ~8) during treatment than in the unbuffered NaCl electrolyte, where pH decreased to approximately 6 during anodic treatment. As a result, considerably more HOCl/OCl^- was produced in the anode chamber when the electrolyte was treated.

Total hydrogen peroxide removal in the system (i.e., photolysis and anodic loss) was 48 ± 5 % for the simulated groundwater, 49 ± 3 % for the simulated surface water, and 25 ± 3% for the wastewater effluent for the array of current densities tested. At the current density required to produce 3 mg L^{-1} (0.09 mM) H_2O_2, water leaving the treatment system effluent contained 1.5 to 2.3 mg L^{-1} H_2O_2. Although H_2O_2 does not pose a health risk at these concentrations, its presence in potable water may be undesirable. In a point-of-use water treatment system it might be possible to remove the excess H_2O_2 by passing it through activated carbon or a high surface area

catalyst consisting of metal oxide (Salem *et al.*, 2000) or silver (Anipsitakis & Dionysiou, 2004). Alternatively, the efficiency of chloride oxidation in the anode chamber might be improved through the use of three-dimensional or porous electrodes that reduce mass transfer limitations or through the use of more catalytic anode materials (Chaplin, 2014).

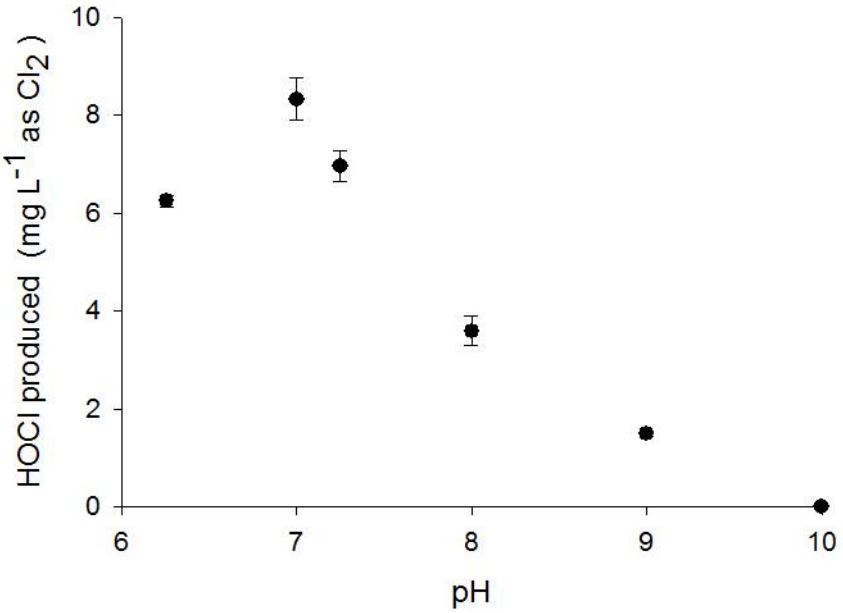

Figure 3.12: HOCl produced as a function of anodic pH at an applied current density of 25 A m^{-2} ($[Cl^-]_0$ = 10 mM). pH was buffered using 20 mM carbonate buffer (6) and borate buffer (7-10) (WWTP: wastewater treatment plant).

3.3.5 Anodic Transformation of Trace Organic Contaminants

Despite only accounting for a small fraction of the total removal observed in the treatment system, the anode did transform some of the compounds. Experiments conducted in the absence of UV exposure with solutions amended with 10 µg L^{-1} of trace organic contaminants indicated that direct anodic oxidation resulted in the removal of up to 20 % of certain trace organics (e.g., propranolol) at a current density of 25 A m^{-2} (Figure 3.13). Oxidation of organic compounds on the anode could be increased through the use of inactive anodes (e.g., boron-doped diamond, doped-SnO_2, PbO_2) (Szpyrkowicz *et al.*, 2005; Chaplin, 2014). These electrodes, however, have higher capital and operating costs than Ti-IrO_2 electrodes.

Although carbamazepine is relatively unreactive with hypochlorite, other compounds (e.g., propranolol and sulfamethoxazole) react with HOCl (Table 3.3). However, the presence of H_2O_2 reduced the importance of reactions between trace organics and chlorine species generated at the anode because chlorine preferentially reacts with H_2O_2. As a result, nearly all of the observed loss of the test compounds in the anode chamber was due to direct oxidation on the anode surface. This observation was consistent with experiments comparing anodic removal of trace organics in the presence and absence of H_2O_2 (Figure 3.14).

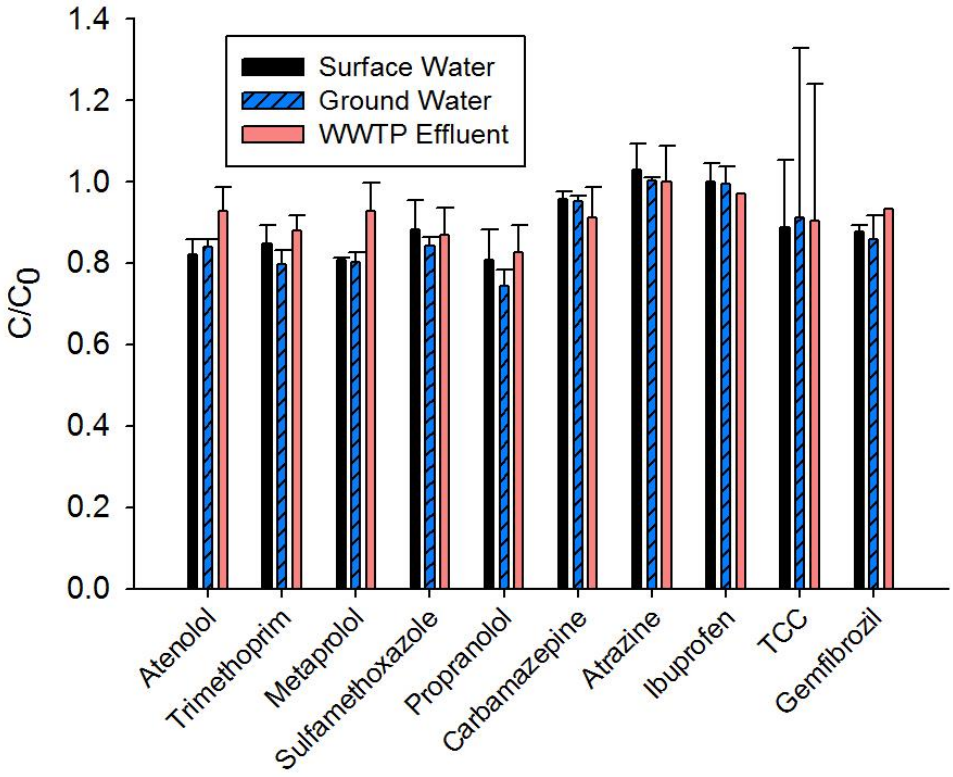

Figure 3.13: Direct oxidation of trace organic contaminants at 25 A m^{-2} for the 3 representative source waters (HRT = 1.5 min, $[H_2O_2]_0$ = 10 mg L^{-1} (0.294mM)). In the presence of H_2O_2 all HOCl/OCl^- is scavenged and removal of the trace organic contaminants is due to direct anodic oxidation (WWTP: wastewater treatment plant).

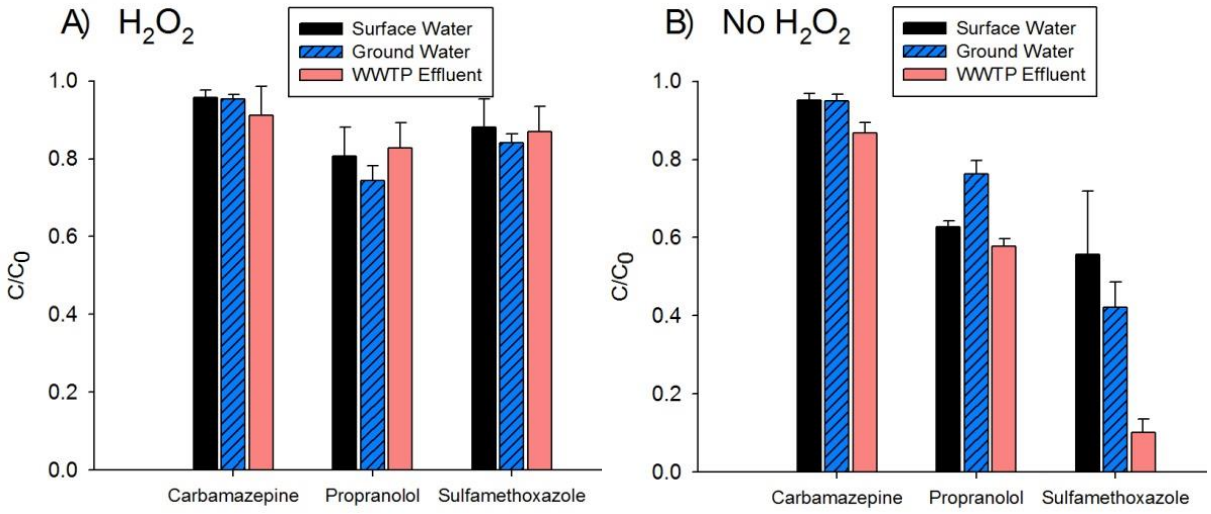

Figure 3.14: Anodic removal of carbamazepine, propranolol, and sulfamethoxazole in (a) the presence of H_2O_2 (10 mg L^{-1}, chlorine scavenged) and in (b) the absence of H_2O_2 (no chlorine scavenged) at 25 A m^{-2} (HRT = 1.5 min). In the presence of H_2O_2, removal of the trace organic contaminants was due to direct anodic oxidation. In the absence of H_2O_2, removal was due to a combination of direct oxidation and reaction with chlorine. The three compounds were selected because they exhibit varying reactivities with chlorine ($k_{HOCl,carbamazepine} < k_{HOCl,propranolol} < k_{HOCl,sulfamethoxazole}$; see Table S3) (WWTP: wastewater treatment plant).

3.3.6 Long-term Cathode Performance

The performance of gas diffusion electrodes can decrease over time due to clogging of the pores by precipitates, fouling with NOM as well as charge transfer resistance attributable to the loss of conductive graphite paste(Zhang *et al.*, 2011). In a long term trial, cathode performance (i.e., H_2O_2 production at a fixed current density) decreased by less than 2% after 6000 L of tap water amended with 5 mM Na_2SO_4 was passed through the system at an applied current density of 15 A m^{-2} (Figure 3.15). Calcium carbonate scaling due to the elevated pH and migration of calcium ions in the tap water into the cathode chamber was observed on the interior of the cathode. Nonetheless, H_2O_2 production was unaffected during this 50-day test. Additional experiments are needed to assess the importance of scaling and the efficacy of simple descaling approaches (i.e., polarization reversal) over longer time periods and more realistic operating conditions.

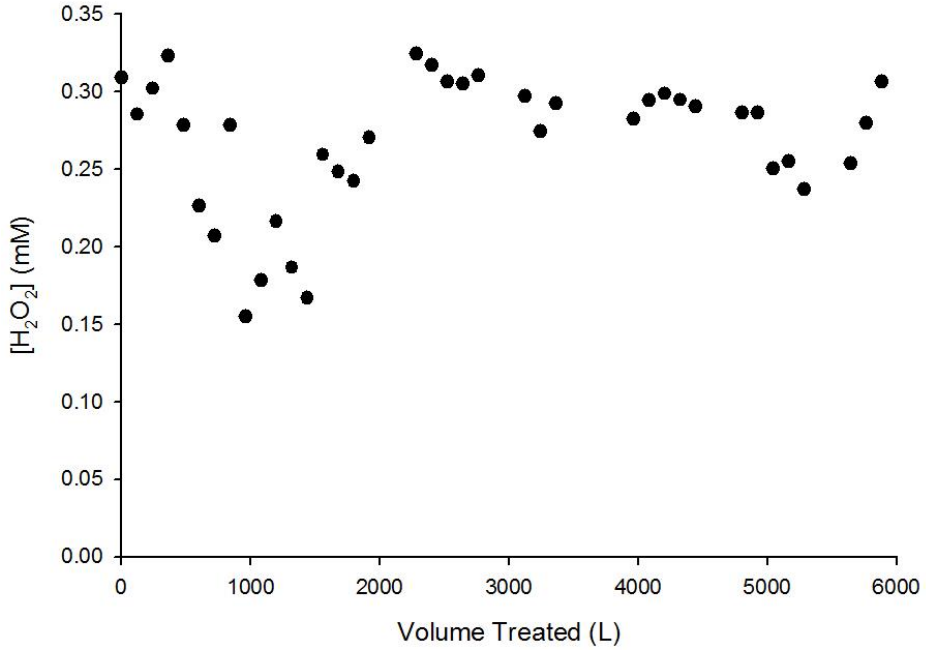

Figure 3.15: Measured long term cathode performance at 15 A m-2 (Catholyte/Anolyte = Tap water + 5mM Na2SO4, alkalinity = 0.34 mM, [Ca2+] = 0.2 mM, Q = 120 L d-1). Predicted H2O2 production was 0.29 mM (WWTP: wastewater treatment plant).

3.3.7 System Energy Consumption

The treatment system used electricity to produce the oxidant (i.e., H_2O_2) and to convert it into $HO^{\bullet}$ (i.e., the UV lamp). Electrical energy per order (E_{EO}) is a useful figure of merit for comparing the efficiency and cost of the treatment system with other AOPs. E_{EO} is the electrical energy (in kWh) required to reduce a contaminant concentration by one order of magnitude in 1 m^3 of water (Cater *et al.*, 2000; Bolton *et al.*, 2001; Bolton & Stefan, 2002):

$$E_{EO} = \frac{P}{Q \log\left(\frac{C_0}{C}\right)} \quad (13)$$

where P (kW) is the electrical power for the electrochemical cell and UV lamp, Q ($m^3\ h^{-1}$) is the system flow rate, and C_0 and C (M) are the initial and final contaminant concentrations. Without the production of H_2O_2, E_{EO} values ranged from 16.8 ± 0.3 to 28.1 ± 0.2 kWh m^{-3} order $^{-1}$, with larger amounts of energy needed to transform contaminants in waters that contained high concentrations of $HO^{\bullet}$ scavengers and chromophores (i.e., municipal wastewater effluent and synthetic groundwater; Figure 3.16).

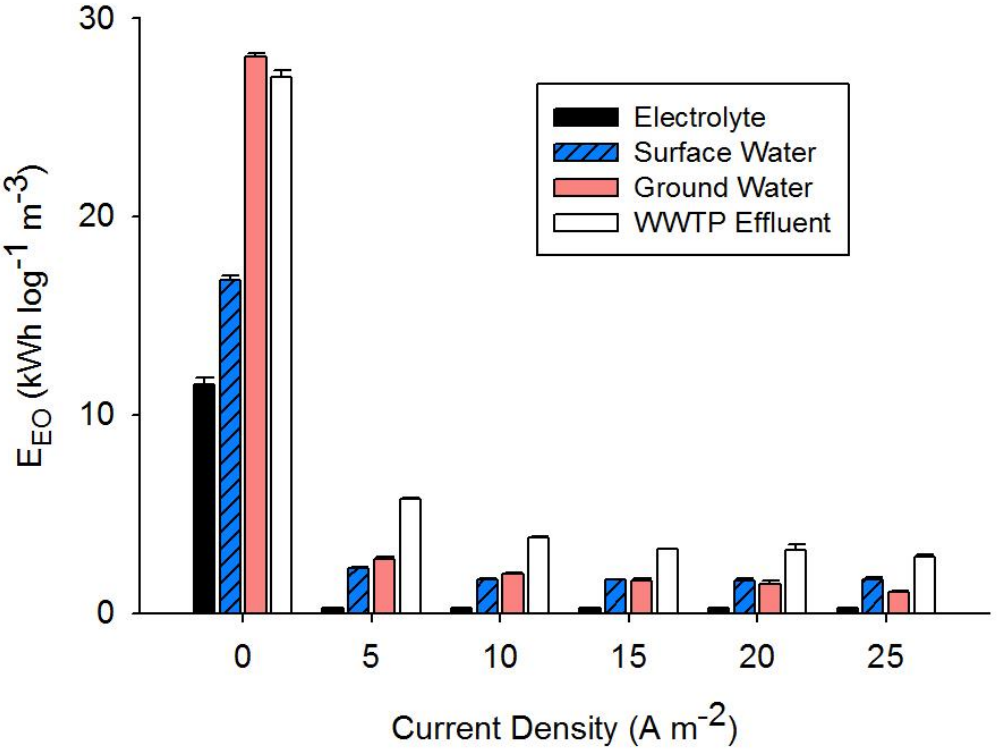

Figure 3.16: Electrical energy per order (E_{EO}) for the removal of carbamazepine as a function of current density (WWTP: wastewater treatment plant).

A substantial decrease in E_{EO} occurred when current was applied to the electrochemical cell (i.e., from 0 to 5 A m^{-2}). As current density increased from 5 to 25 A m^{-2} the E_{EO} decreased by less than 11%. These data indicate that the UV-H_2O_2 AOP system is much more efficient than the use of UV alone and that there is a marginal benefit associated with the production of higher H_2O_2 concentrations in the cathode because the reactions become less efficient at higher concentrations of H_2O_2. Only 8-14% of the energy demand was attributable to the electrochemical production of H_2O_2, with the majority of the energy required for the operation of the low-pressure UV lamp. At a current density of 25 A m^{-2}, an energy requirement of 1.08 ± 0.1 to 2.84 ± 0.1 kWh m^{-3} $order^{-1}$ was observed, which was similar to results from previous studies of the transformation of trace organic compounds by UV/H_2O_2 in different source waters (Katsoyiannis *et al.*, 2011).

The high coulombic efficiency and low current densities result in a low-cost means of H_2O_2 production even for treatment of water with low conductivity. For comparison, electrochemically produced H_2O_2 costs between 0.1-0.3 \$ kg^{-1}, while H_2O_2 produced by the anthraquinone process typically costs between 1-2 \$ kg^{-1}(Jones, 1999). When considering the lack of a need to transport, store, and handle H_2O_2 as well as modest capital and operational costs, the modular AOP treatment system can be a competitive technology for point-of-use treatment at a household and community level or even for wellhead treatment of trace organic contaminants present in potable water sources. As H_2O_2 production was directly proportional to current density, the treatment system could be scaled up by using faster flow rates accompanied by higher applied current densities or by increasing surface area of the cathode. To obtain the equivalent contaminant removal after scale-up, optimization of the UV reactor geometry would be required. Additional research is needed to assess long-term system performance under realistic operating conditions.

3.3.8 Comparison with Conventional Anodic Oxidation

Comparison of conventional of anodic oxidation with the cathodic H_2O_2/UV system for the removal of the same suite of contaminants in WWTP effluent revealed that the latter system is more energy efficient (Figure 3.17). Measured values for the modular advanced oxidation system were well within the range of EEO's reported for onsite electrolysis of micropollutants in gray water (1-14 kWh m^{-3} $order^{-1}$) (Butkovskyi *et al.*, 2014).

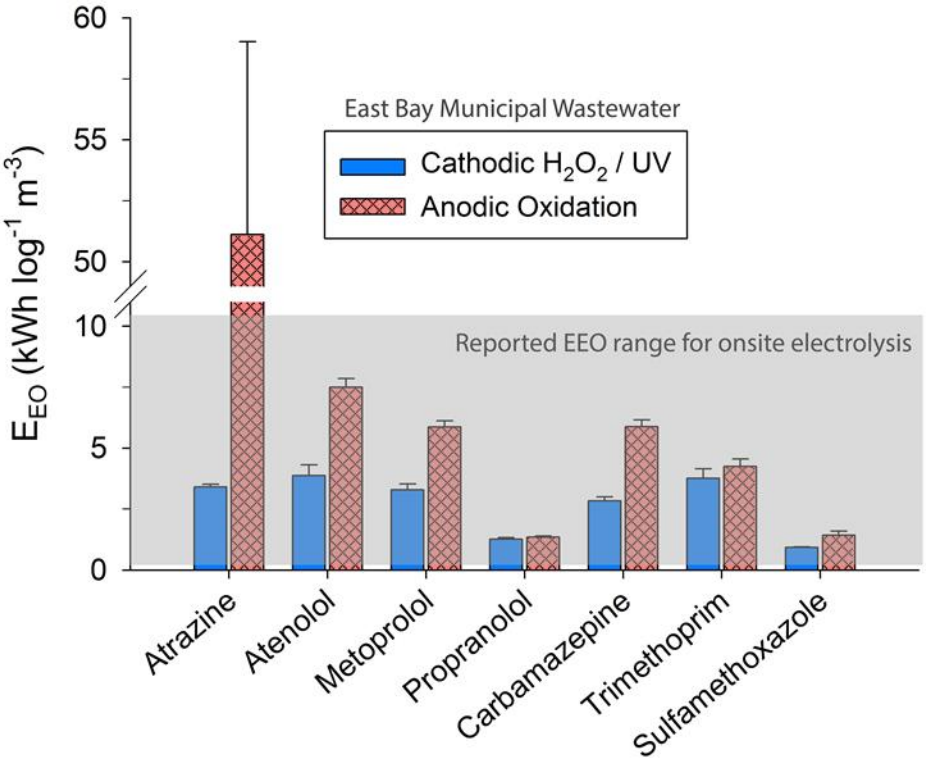

Figure 3.17: Electrical energy per order (E_{EO}) for the removal of select trace organic contaminants using conventional anodic oxidation with a Ti-IrO_2 electrode as well as the cathodic H_2O_2/UV system in municipal wastewater effluent.

Additionally, the cathodic H_2O_2/UV system produced significantly less chlorinated and brominated trace organic transformation products during the electrolysis of municipal wastewater. Following treatment of municipal wastewater, THM's and HAA's were both detected at 1.6 µg L^{-1}, substantially below their EPA maximum contaminant levels ($\Sigma[THM]_{MCL}$ = 80 µg L^{-1}; $\Sigma[HAA]_{MCL}$ =60 µg L^{-1}). Furthermore, bromate and chlorate were detected at low µg L^{-1} concentrations (<0.1 and 2.6 µg L^{-1}, respectively). Low concentrations of halogenated disinfection byproducts were accomplished due to the low residence time in the anodic chamber as well as quenching of any HOCl by H_2O_2. These findings help broaden the potential applications of electrolysis, providing insight into a new technology that can be used as an alternative to conventional anodic oxidation for the removal of trace organic contaminants.

CHAPTER 4. Trace Element Removal in Distributed Drinking Water Treatment Systems by Cathodic H_2O_2 Production and UV Photolysis

To be submitted with permission from Prasse, C.; Wenk, J.; Remucal, C.; Berg, S; Sedlak, D. L.

4.1 Introduction

Inadequate access to clean drinking water is one of the most globally pervasive problems. Amidst rapid population growth, urbanization, and climate change, water demand exceeds available freshwater resources in many locations (Vörösmarty *et al.*, 2000; Hering *et al.*, 2013). Continued reliance on difficult-to-maintain, energy-intensive centralized water treatment and conveyance systems may not be a viable option, especially in an era when reduction in energy and greenhouse gas emissions is a high priority (Larsen *et al.*, 2016; Liu *et al.*, 2016). For example, the energy use associated with pumping water over the Tehachapi mountains in southern California is approximately 2.4 kWh per m^3, which is comparable to the energy required for seawater desalination (Nair *et al.*, 2014). New water resource management strategies are needed to reliably provide potable water to cities and to reduce the energy expenditure associated with importing, treating, and distributing water from centralized treatment facilities.

Small scale, point-of-use and point-of-entry drinking water treatment systems may facilitate the use of nontraditional water sources, such as municipal wastewater, roof water, stormwater, and water from shallow aquifers. Such systems are particularly attractive in new developments because they can be installed rapidly without the significant capital costs required for centralized facilities (Dahlgren *et al.*, 2013; Larsen *et al.*, 2016). Despite their attractiveness, the presence of trace concentrations of organic contaminants (e.g., pesticides, solvents, pharmaceuticals), toxic trace elements (e.g., arsenic, lead), and waterborne pathogens call into question the viability of distributed drinking water treatment systems (Schwarzenbach *et al.*, 2006; Benotti *et al.*, 2008). Furthermore, challenges associated with the transport, storage, and use of chemicals typically employed in drinking water treatment, such as chlorine, activated carbon, and alum, limit the types of processes that can be employed in distributed water systems (Larsen *et al.*, 2013).

Electrolysis and UV treatment are well suited for distributed drinking water treatment systems due to their small footprint, flexible design, and intrinsic advantages of low cost and lack of chemical consumption. For example, we recently developed a device capable of treating up to 250 L d^{-1} of water contaminated by trace organic contaminants by employing cathodically-driven electrolysis for H_2O_2 production followed by UV photolysis with a modest energy consumption (~3-7 kWh log^{-1} m^{-3}) (Barazesh *et al.*, 2015). The UV fluence delivered by the systems (~3000 mJ cm^{-2}) was sufficient to disinfect most source waters. However, the ability of the system to remove trace elements from alternative water sources was not evaluated.

A common means of removing toxic trace elements from water is through coprecipitation or adsorption onto iron oxides. Although effective, this approach poses technical challenges with respect to management and disposal of contaminated solids generated from iron addition, especially in distributed water treatment systems (McKenzie, 1980; Dixit & Hering, 2003; van Genuchten *et al.*, 2012). Under conditions encountered in groundwater or organic-matter containing surface waters, relatively high doses of iron (i.e., > 100 μM) are typically needed to remove oxyanions and metals due to the presence of iron-complexing ligands in NOM that decrease the mineral saturation index and inhibit iron oxide precipitation (Barbeau, 2006; Aiken *et al.*, 2011). Electrochemical and photochemical treatment may transform iron-complexing ligands, thereby reducing the amount of iron needed to produce particulate iron oxides that can remove toxic trace elements.

Previous research has demonstrated that photochemical reactions alter the structure of NOM in a manner that lowers its affinity for Fe(III) (Barbeau, 2006; Aiken *et al.*, 2011; Fujii *et al.*, 2015). Although the rates of sunlight photolysis of Fe(III)-NOM complexes in natural waters are relatively slow, the application of low pressure Hg lamps, which emit UV light at 254 nm, could drive many of these same processes at higher rates in engineered treatment systems (Figure 4.1). Despite a reasonably well-defined understanding of photochemical reactions of iron and organic matter in natural systems (Sharpless *et al.*, 2014; Rosario-Ortiz & Canonica, 2016), the potential for exploiting these processes to enhance iron oxide precipitation and trace element uptake during water treatment has not been considered.

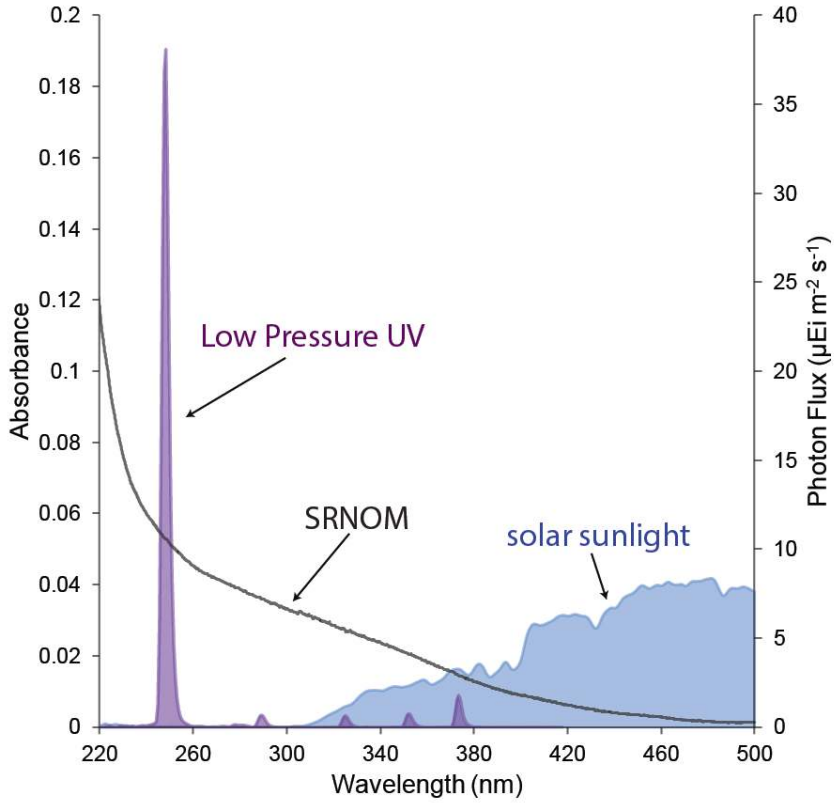

Figure 4.1. Absorbance Spectra of Suwannee River Natural Organic Matter (pH 9; 1 mg L^{-1}; left y-axis) and spectral photon flux of solar sunlight and from a low-pressure UV lamp (right y-axis).

The objective of this research was to evaluate the potential of using cathodically-produced H_2O_2 and UV light to enhance the removal of dissolved trace elements in the presence of NOM and low concentrations of iron (i.e., ~ 10 µM). To assess the role of solution conditions on the process, experiments were performed in authentic groundwater as well as synthetic groundwater containing varying concentrations of NOM and divalent cations (e.g., Ca^{2+}, Mg^{2+}). Furthermore, changes in electronic absorption spectra, intramolecular electron transfer properties, and mass spectra were measured to gain insight into the effect treatment on the molecular composition of NOM.

4.2 Materials and Methods

4.2.1 Chemicals

All experiments were performed with reagent grade $NaHCO_3$, NaCl, NaBr; ACS grade trace elements ($Pb(NO_3)_2$, $CuCl_2$, Na_3AsO_3); and alkali earth metals ($Ca(NO_3)_2$, $Mg(NO_3)_2$) obtained from Sigma-Aldrich (St. Louis, MO). Suwannee River Natural Organic Matter (2R101N) was obtained from the International Humic Substances Society. Stock solutions of trace metals (100 µM in 1% HNO_3; pH ≈ 1.7) and anoxic stock solutions of ferrous iron ($FeSO_4$; 100 mM) were used to prevent precipitation and/or metal oxidation prior to addition to solutions. The addition of trace elements from acidic stock solutions lowered the initial pH of solutions by approximately 0.5 units. UV photolysis of NO_3^- counter-ions increased the rate of formation of $HO^\bullet$ by less than 0.1% relative to $HO^\bullet$ formed from the photolysis of H_2O_2 generated in the cathode (See Section A.4.1 of the Appendix for calculations).

4.2.2 Solutions

Experiments were conducted with arsenic-contaminated groundwater collected from Colusa County, California (Table 4.1). To elucidate the role of different solutes on metal redox reactions and complexation, additional experiments were conducted with a synthetic groundwater solution prepared in Milli-Q water with added NOM and major ions (i.e., Na^+, Ca^{2+}, Mg^{2+}, Fe^{2+}, HCO_3^-, Cl^-, and Br^-) at concentrations comparable to those detected in the authentic groundwater. In some experiments, concentrations of Ca^{2+} and Mg^{2+}, Fe^{2+}, or NOM were varied. Synthetic groundwater solutions were amended with 1 µM of dissolved As(III), Pb(II), and Cu(II) from acidic stock solutions, whereas authentic groundwater was modified with only 1 µM of dissolved Pb(II) and Cu(II).

Table 4.1. Composition of authentic and synthetic groundwater.

Ion	Colusa County GW	Synthetic
Ca^{2+}	273.5 ± 0.35 µM	0 - 250 µM
Mg^{2+}	272 ± 0.96 µM	0 - 250 µM
SO_4^{2-}	33.1 ± 0.42 µM	0 µM
Cl^-	240 ± 7.2 µM	500 µM
Br^-	0.6 ± 0.09 µM	0.5 µM
PO_4^{3-}	510 ± 120 µM	0 µM
SiO_2	700 ± 245 µM	0 µM
DIC	5.84 ± 0.03 mM	5 mM
DOC	0.88 ± 0.34 µM	1 µM
pH	7.3 ± 0.2	7.8
Trace Metal		
Fe	11.0 ± 2.7 µM	10 µM
As	0.36 ± 0.03 µM	1 µM
Cu	0.07 ± 0.02 µM	1 µM
Pb	0.01 ± 0.0 µM	1 µM

4.2.3 Photolysis and Electrolysis Experiments

Experiments to assess trace element removal were performed in a previously described point-of-use treatment system (Barazesh *et al.*, 2015). As described previously, the device consisted of dual-chambered electrolysis cell employing a carbon-based gas-permeable cathode to generate H_2O_2 from ambient air directly in the solution prior to exposure to low-pressure UV irradiation in a batch reactor. After UV treatment, the water passed through an anode chamber where pH returned to its initial value (See Figure 1.4 for process schematic, sampling locations, and flow). Samples (10 mL) for analysis of pH, H_2O_2, UV-visible absorbance, and trace elements were collected prior to treatment and after each treatment step starting approximately 30 minutes after treatment was initiated. Under the constant current densities (25 A m^{-2}) and system flow rate (121 L d^{-1}) used in these experiments 510 ± 41 μM of H_2O_2 was produced in the solution (i.e., the columbic efficiency was 86%). Subsequent UV irradiation ($E_{254}° = 0.107$ mEi m^2 s^{-1}) resulted in photolysis of approximately 35% of the electrochemically-generated H_2O_2 as well as other photolytic processes (e.g., photolysis of Fe(III)-NOM complexes, production of reactive oxygen species by sensitization of chromophoric NOM) (Wenk *et al.*, 2011; Lester *et al.*, 2013; Sharpless *et al.*, 2014).

To differentiate between the effects of H_2O_2 photolysis and other processes, a series of experiments were performed with a stainless-steel cathode that reduced O_2 to H_2O without producing substantial concentrations of H_2O_2 (i.e., $[H_2O_2] < 1$ μM). Experiments also were conducted in the presence of the selective quenchers of reactive oxygen species and excited NOM, including sodium azide (NaN_3; 50 μM) and isoprene (500 μM) to scavenge $^1O_2$ and ^{3}NOM, respectively (Zafiriou *et al.*, 1998; Goldstone & Voelker, 2000; Wenk *et al.*, 2011; Lester *et al.*, 2013; Sharpless *et al.*, 2014; Rosario-Ortiz & Canonica, 2016). The quenchers were selected due to their hydrophilic nature, low reactivity with H_2O_2, and minimal light absorption at 254 nm (Figure 4.2) (Rosario-Ortiz & Canonica, 2016). Superoxide radical (O_2^-) was assumed to play an insignificant role in photochemical processes due to its catalytic dismutation in the presence of elevated concentrations of dissolved Cu^{2+}(Zafiriou *et al.*, 1998; Goldstone & Voelker, 2000).

4.2.4 NOM Characterization by Mass Spectrometry

NOM chemical composition was evaluated by Fourier transform-ion cyclotron resonance mass spectrometry (FT-ICR MS). To prepare samples, NOM was concentrated using solid phase extraction (SPE) as described previously (Dittmar *et al.*, 2008). Approximately 250 mL of sample was acidified to pH 2 ± 0.1 using 1 M HCl. Acidified samples were passed through Agilent Bond Elut-PPL cartridges (500 mg; 6 mL) that had been washed with methanol. Following extraction, the cartridges were rinsed with 0.01 M HCl and air dried. DOM was eluted with 2 mL of methanol and stored in the dark at 4°C.

Prior to FT-ICR MS analysis, samples were diluted 1:10 in a 60:40 acetonitrile:Milli-Q matrix. Samples were introduced into a SolariX XR 12T FT-ICR MS (Bruker) via a Triversa NanoMate sample delivery system (Advian). The accumulation time was set to 0.01 second for each sample and 350 scans were collected. The gas pressure was 0.3 psi and -1.4 kV was applied for the electrospray.

Peaks over a range from 200 to 600 *m/z* and a relative intensity of 0.0001% were exported to *R* for processing. Nominal masses of peaks were determined by adding the mass of a proton and a linear calibration was applied, as described previously (Maizel & Remucal, 2017). Formulas containing C, H, O, and ^{13}C were considered for matching. For a match to be considered successful, the error had to be less than 0.2 ppm and at least two homologous series had to be identified (CH_4 versus O or ± CH_2) (Kujawinski & Behn, 2006; Koch *et al.*, 2007). Weighted averages of NOM molecular weight, H/C ratio, and O/C ratio were calculated using the peak intensity and the molecular weight, H/C ratio, or O/C ratio of a given chemical formula, respectively (See Section A.4.2 of the Appendix for calculations).

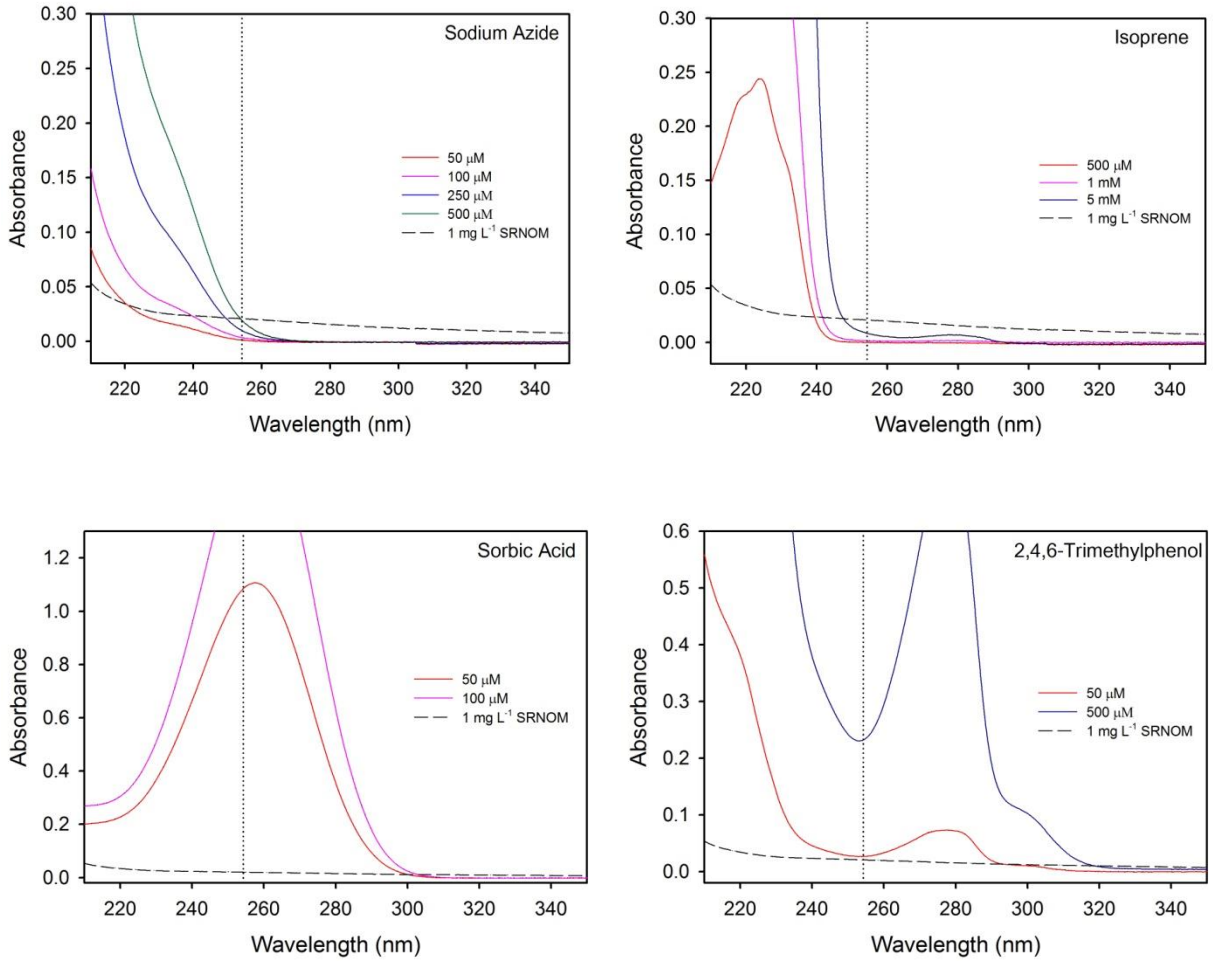

Figure 4.2. Electronic absorption spectra of 1 mg L^{-1} Suwannee River NOM (dashed line) and photochemically-produced reactive intermediates: (A) sodium azide ($^1O_2$ quencher), (B) isoprene (^{3}NOM quencher), (C) 2,4,6-trimethylphenol (^{3}NOM quencher), and (D) sorbic acid (^{3}NOM quencher). Dotted line corresponds to 254 nm.

4.2.5 Optical and Electrochemical Properties of Fe-NOM Complexes

To quantify changes in the molecular composition of NOM during treatment, UV-visible absorption spectra of authentic and synthetic groundwater samples were filtered and analyzed at each sampling location in the treatment system. Concentrated NaOH was used to adjust the sample pH to 9.0 prior to measurement of spectra from 240 to 500 nm. To assess light absorption solely by NOM, absorption due to Ca^{2+}, Mg^{2+}, H_2O_2, and NO_3^- was subtracted from the spectra prior to analysis (Figure 4.3). Differential absorbance spectra (Δabs) were calculated by subtracting specific absorbance (i.e., $A(\lambda)$) between the influent (i.e., untreated water) and effluent (i.e., post-anode). Spectral slope coefficients of the NOM absorbance spectra were calculated by non-linear least squares fitting of a single exponential model between 275 and 295 nm ($S_{275\text{-}295}$) and between 240 and 500 nm ($S_{240\text{-}500}$).

$$a(\lambda) = a(\lambda_{ref})\exp(-S(\lambda - \lambda_{ref})$$

where λ_{ref} = 350 nm. Changes in spectral slopes and differential absorption spectra were used in conjunction with data on chemical composition determined by FT-ICR MS to assess shifts in NOM aromaticity and molecular weight during treatment, as described previously (Twardowski *et al.*, 2004; Helms *et al.*, 2008; Wenk *et al.*, 2013).

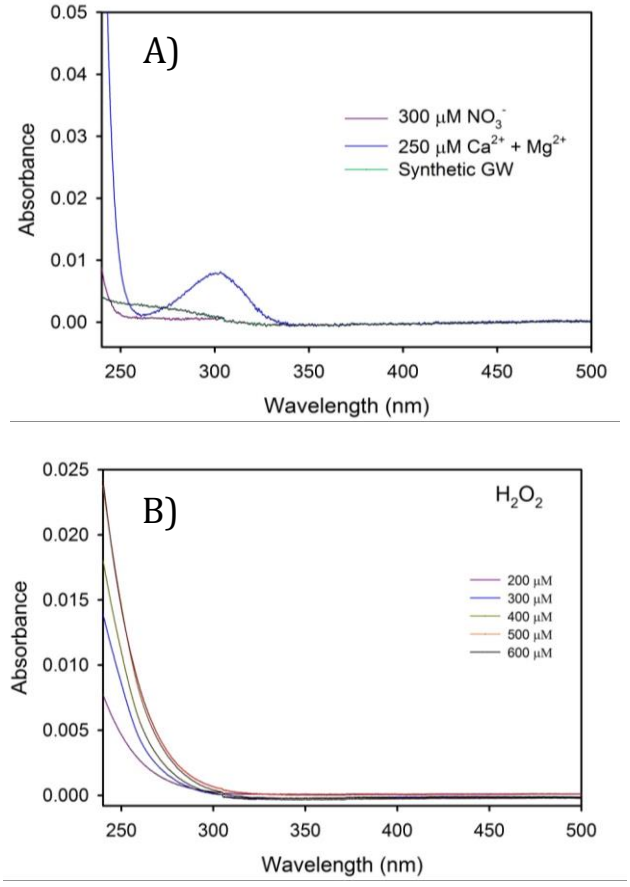

Figure 4.3. Electronic absorption spectra of the (A) background ionic constituents and (B) electro-generated H_2O_2.

To characterize the redox properties of NOM and metal-NOM complexes, cyclic voltammograms (CVs) were collected in anhydrous dimethyl sulfoxide (DMSO; 50 mL) containing 5 mM tetrabutylammonium hexaflurophosphate (NBu_4PF_6) as the supporting electrolyte. Experiments were performed in a 3-electrode setup employing Pt wires as the working and counter electrodes (0.25 mm diameter) along with a nonaqueous Ag/Ag^+ reference electrode (BASi) (Nurmi & Tratnyek, 2002). Experiments were performed at a scan rate of 10 mV s^{-1} starting from the open-circuit potential (~0 to -0.1 V) and scanned cathodically over a 2V potential range. CVs were collected for electrolytes containing Suwannee River NOM (90 mg L^{-1}; ~45 mgC L^{-1})(Appiani *et al.*, 2014) in the presence of 1 mM $Ca(Cl)_2$, $Mg(Cl)_2$, and/or $Fe(Cl)_3$. Spectra were corrected for the background spectra of DMSO. Prior to each CV, electrodes were sonicated in 50:50 CH_3OH/H_2O and electrolytes were purged with argon to remove O_2. The ferrocene/ferrocenium and benzoquinone/hydroquinone redox couples were used as reference reactions to validate the methodology and electrode response in the aprotic solvents (Nurmi & Tratnyek, 2002).

In addition, linear sweep voltammetry was employed to determine if trace element removal occurred via sorption and direct reduction on the cathode. Voltammograms indicated that the reduction of O_2 to H_2O_2 was the main reduction reaction and direct trace metal reduction was negligible at the potentials employed in the experiments (Figure 4.4).

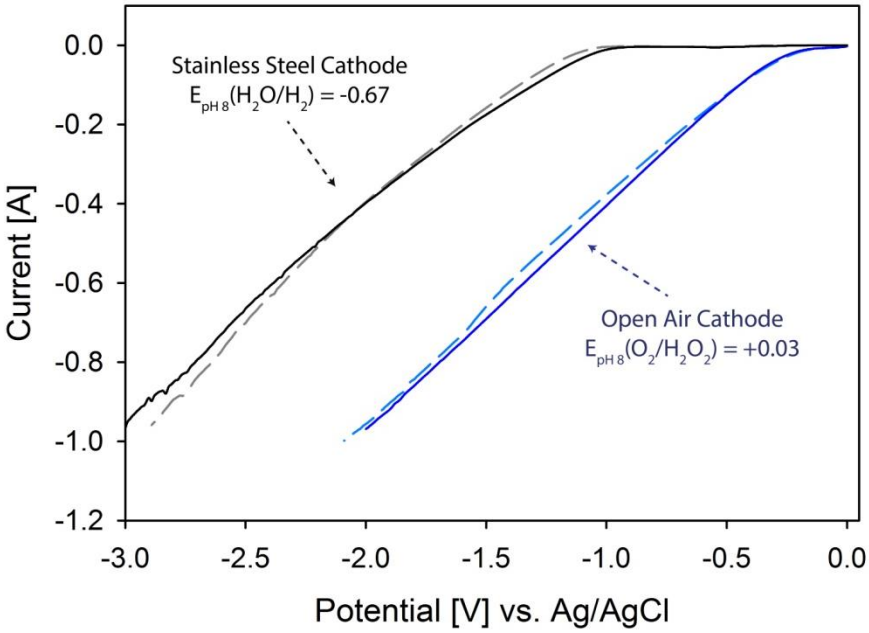

Figure 4.4. Linear sweep voltammogram of a stainless steel cathode and open air cathode in the absence (solid lines) and presence (dashed lines) of 50 mg L^{-1} Cu^{2+}, Pb^{2+}, and As in a 0.1 M $NaClO_4$ electrolyte containing 0.1 M borate buffer (pH 8).

To investigate the importance of ligand-to-metal charge transfer (LMCT) photoreduction reactions, solutions of synthetic groundwater containing NOM (1 mg L^{-1}; ~0.5 mgC L^{-1}) were irradiated with UV light in batch experiments conducted in the presence of the Fe(II)-complexing compound, ferrozine (FZ_3; 100 µM) (Barbeau, 2006; Fujii *et al.*, 2008; Fujii *et al.*, 2015). Fe(II) production was quantified in the presence and absence of Ca^{2+} and Mg^{2+}.

Production rates of the Fe(II)-FZ_3 complex from Fe(III)-NOM were determined spectroscopically at 562 nm and corrected for light screening by FZ_3 ($\varepsilon_{FZ_3,\lambda=254nm} = 12900\ M^{-1}\ cm^{-1}$; Figure 4.5) (Viollier *et al.*, 2000). Experiments were performed at pH 6.5 to minimize oxidation of Fe(II) by O_2 prior to complexation of the metal by ferrozine.

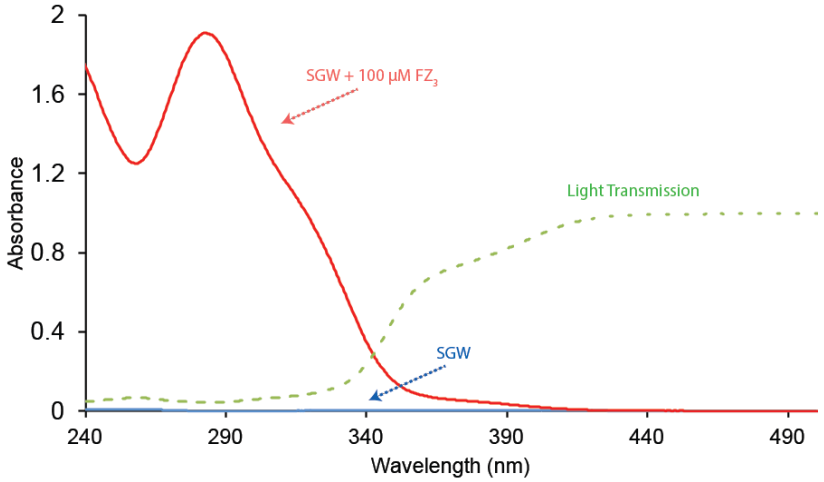

Figure 4.5: Absorption spectra of synthetic ground water (SGW) in the presence and absence of 100 µM ferrozine at pH 6.5 as well as the light transmission through the solution at different wavelengths.

4.2.6 Analytical Methods

H_2O_2, dissolved organic carbon, and dissolved inorganic carbon were measured using standard methods (American Public Health *et al.*, 2005). Unfiltered and filtered (0.22 µm nylon filters) water samples for measurement of total and dissolved As, Cu, Fe, and Pb, respectively, were digested with 1% HNO_3 prior to analysis by inductively coupled plasma mass spectrometry (ICP-MS, Agilent). Absorption spectra were recorded with a UV-2600 spectrophotometer (Shimadzu) using 1 cm quartz-glass cuvettes. Spectral irradiance of the UV lamp (G23 Odyssea Pool Lamp, 9W) and a collimated beam Oriel solar simulator (Spectra Physics 91194) were measured with a spectroradiometer (RPS 380, international light). Fluence was determined by chemical actinometry using 10 µM atrazine (ε_{254}=3860 $M^{-1}\ cm^{-1}$, ϕ_{254}= 0.046 mol Ei^{-1}) in 1 mM borate buffer (pH 8) (Barazesh *et al.*, 2015). Atrazine was quantified by multiple reaction monitoring (MRM) mode with an Agilent 1200 series HPLC system coupled to a 6460 triple quadropole tandem mass spectrometer (HPLC-MS/MS).

4.3 Results and Discussion

4.3.1 Speciation and Fate of Iron and Trace Elements during Treatment

Separation of cathodic (i.e., production of H_2O_2) and anodic (i.e., evolution of O_2) redox reactions via a cation exchange membrane led to significant fluctuations of pH during the treatment process: influent (7.8 ± 0.2), post-cathode (pH 9.3 ± 0.3), post-UV (pH 9.1 ± 0.3) and post-anode (pH 7.7 ± 0.2). Over this pH range, the predicted equilibrium solubility of Fe(III)

ranges from 0.008 µM to 0.064 µM, ignoring the effects of NOM on [Fe^{3+}]. As a result, in experiments employing synthetic groundwater in the absence of organic matter the solution was supersaturated with respect to amorphous $Fe(OH)_{3(s)}$. Under these conditions, nearly all of the iron was converted to filterable forms (i.e., [Fe] = 0.182 ± 0.05 µM; Figure 4.6).

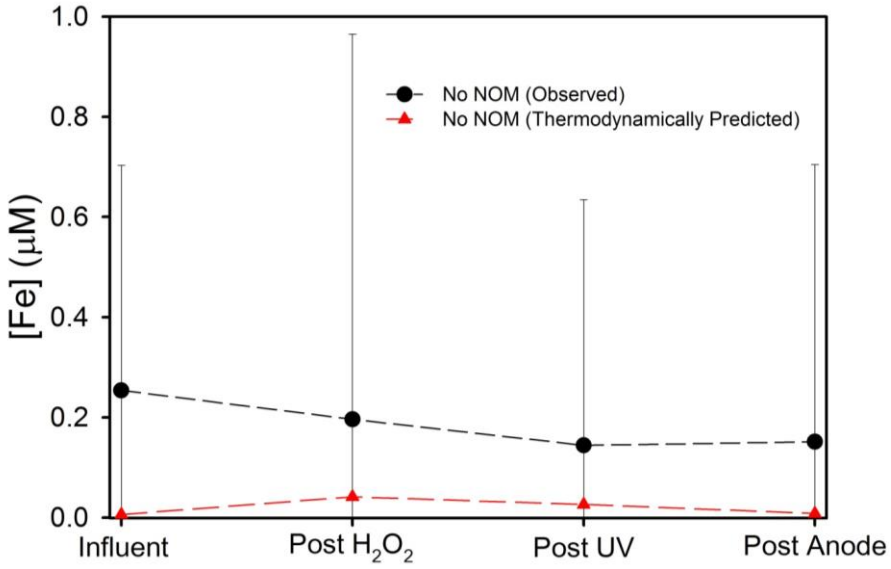

Figure 4.6: Predicted and measured concentrations of filterable dissolved iron during treatment of synthetic groundwater in the absence of natural organic matter.

Conversely, in synthetic and authentic groundwater matrices containing approximately 1 mg L^{-1} organic matter and approximately 10.5 µM of total iron, approximately 60% of the Fe passed through a 0.22 µm filter (Figure 4.7). Significantly higher concentrations of dissolved iron compared to thermodynamically predicted concentrations indicated either the formation of soluble Fe(III)-NOM complexes or stabilization of sub-micron colloids by NOM and inhibition of particle aggregation (Aiken *et al.*, 2011). Complexation of iron in the Fe(III) oxidation state was consistent with the higher stability constants of NOM with Fe(III) (log β ~ 40-49) relative to Fe(II) (log β ~ 13) and supported by negligible detection of Fe(II)-FZ_3 (data not shown) (Milne *et al.*, 2003; Rose, 2003).

In the absence of applied current or UV light (i.e., control conditions), iron removed by filtration (i.e., approximately 4.5 µM) did not change as authentic groundwater passed through the treatment system (Figure 4.7). Exposure of authentic groundwater to UV light in the absence of H_2O_2 (i.e., experiments conducted with a stainless steel cathode) or with the electrochemical system operating in the absence of UV light (i.e., EC only) resulted in the formation of an additional 4 µM of Fe that could be removed by filtration. Although the oxidation of iron-chelating hydroquinone (E_H° = +0.82 V)(Steenken & Neta, 1982) and catecholate moieties (E_H° = +0.84 V) (Steenken & Neta, 1982) by H_2O_2 (E_H° ($H_2O_2/HO_2^{\bullet -}$) = +1.51 V) (Steenken & Neta, 1982) is thermodynamically feasible, these reactions are usually slow (~ 2 M^{-1} s^{-1}) (Brunmark & Cadenas, 1987). Therefore, the simultaneous increased Fe removal and loss of H_2O_2 (i.e., 58 ± 17 µM; Figure 4.8) observed from dark experiments conducted in the absence of UV irradiation

may be attributable to the decomposition of H_2O_2 on the surface of iron colloids yielding reactive $HO^{\bullet}$ capable of oxidizing Fe-coordinating moieties (Kwan & Voelker, 2002).

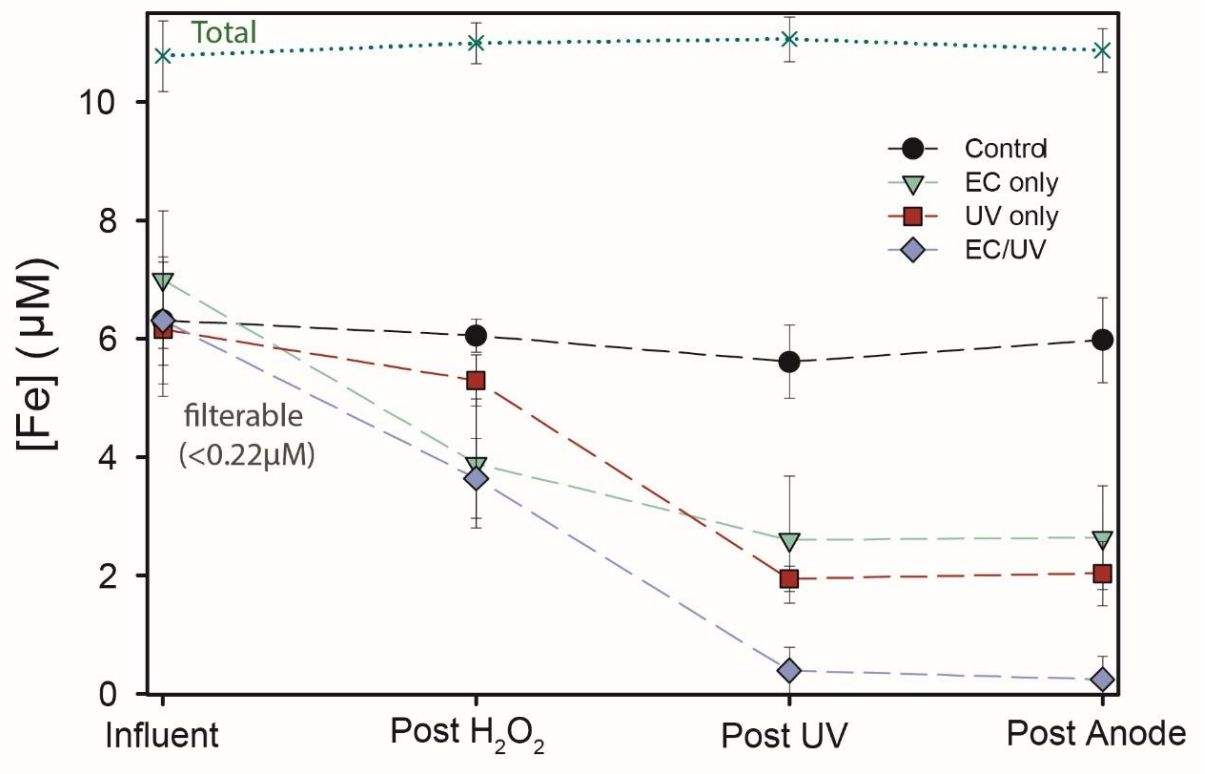

Figure 4.7: Concentration of dissolved and total (i.e., dissolved and colloidal) Fe during treatment of authentic groundwater under different reactor configurations.

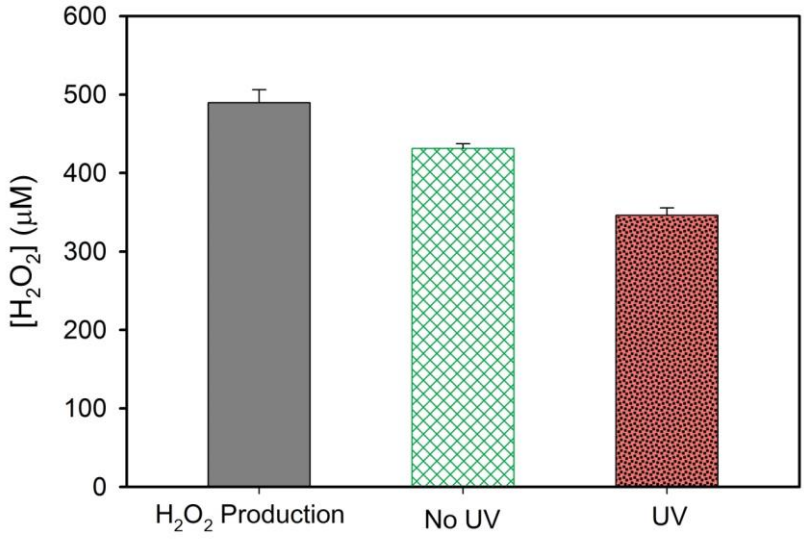

Figure 4.8: H_2O_2 production and effluent concentration leaving the system during dark and irradiated treatment of authentic groundwater from Colusa County, CA.

Simultaneous electrochemical and photochemical treatment (i.e., EC/UV) resulted in nearly complete conversion of the Fe into forms that were removed by filtration. Analysis of unfiltered samples of authentic groundwater subjected to electrochemical and UV treatment and allowed to settle overnight revealed approximately 90% removal of total Fe (i.e., dissolved and colloidal) from the bulk solution (Figure 4.9). Therefore, for the purposes of this study, removal describes the conversion of Fe and toxic trace elements (*vide infra*) into filterable forms that, given sufficient holding time, will settle out of solution.

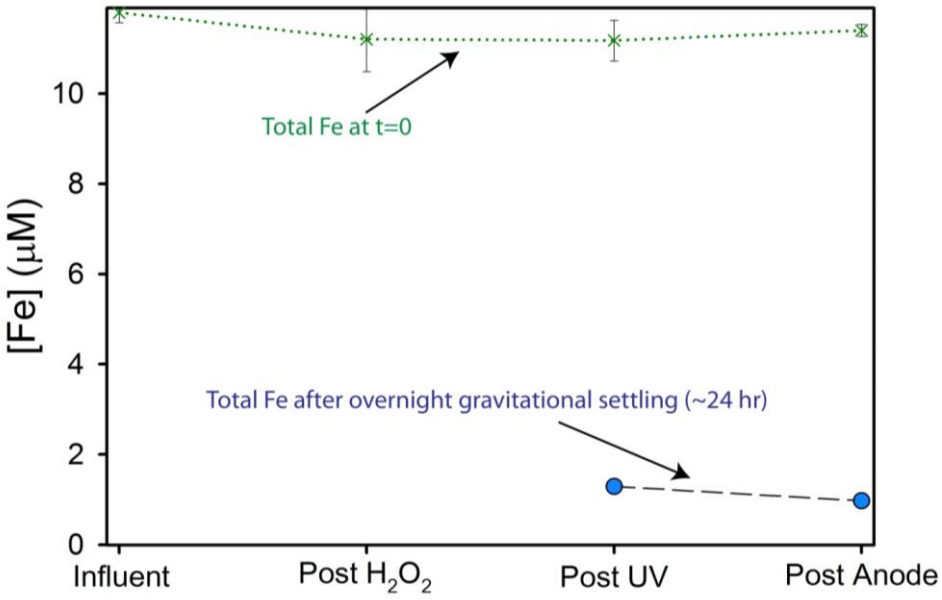

Figure 4.9: Total iron concentration after treatment followed by overnight gravitational settling of authentic groundwater.

Linear correlations were observed between the increase in Fe removal and the removal of trace elements from solution (Figure 4.10). Pb^{2+} was most efficiently removed (mol_{Pb}:mol_{Fe} of 0.089 ± 0.007), followed by Cu^{2+} (mol_{Cu}:mol_{Fe} of 0.070 ± 0.005) and As (mol_{As}:mol_{Fe} of 0.041 ± 0.009). For Pb^{2+} and Cu^{2+}, no difference was observed between experiments conducted in authentic (checkered symbols) and simulated groundwater (solid symbols) despite variability in their composition, suggesting that adsorption or coprecipitation was not influenced by other solutes such as silicate (i.e., SiO_4^{4-}) and phosphate (i.e., PO_4^{3-}). In contrast, As removal decreased substantially (i.e., decrease in mol_{As}:mol_{Fe} by -70%) in authentic groundwater, likely due to competition between oxyanions for metal adsorption sites on hydrous ferric oxide precipitates (Rose *et al.*, 1997; Doelsch *et al.*, 2000).

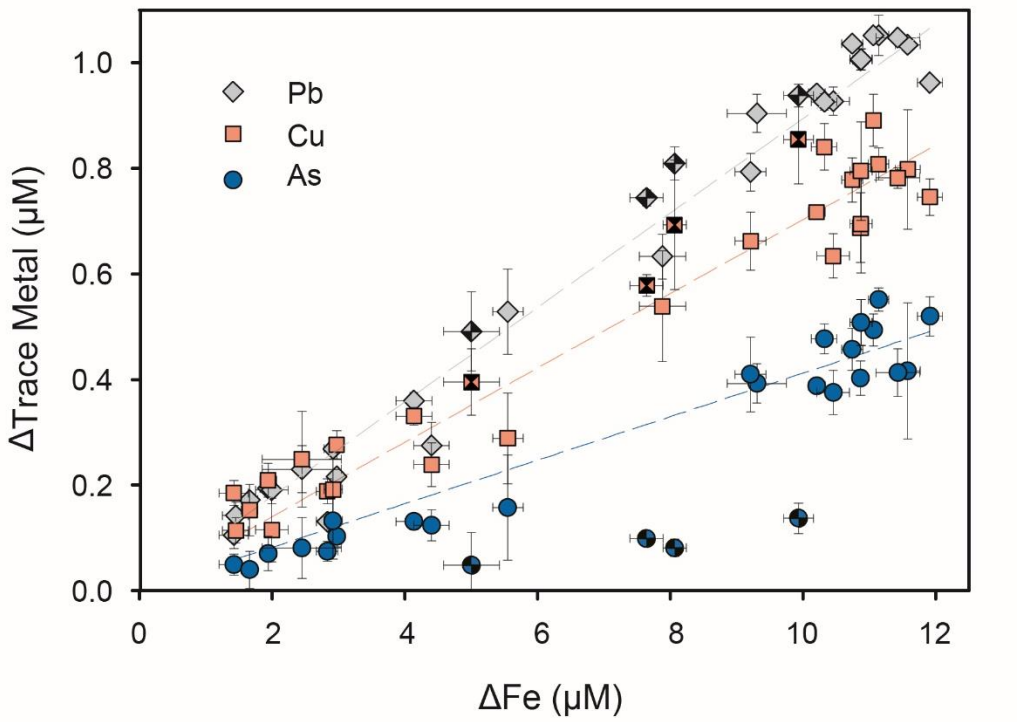

Figure 4.10: Correlation between Fe removal with Pb, Cu, and As removal observed for synthetic (solid symbols) and authentic matrices (checked symbols).

4.3.2 Photochemical Transformation of Fe(III)-Complexes

As described above, cathodically-produced H_2O_2 and photochemical reactions alter the macromolecular structure and functional group chemistry of natural organic matter in a manner that decreases its ability to prevent Fe(III)-oxide formation. To gain insight into the mechanisms that led to the transformation of the NOM complexes and increase in filterable Fe following treatment, experiments were repeated in synthetic groundwater. Although reactions with H_2O_2 contributed to Fe removal in authentic groundwater, its effect on Fe was absent in synthetic matrices (Figure 4.11). While the reason for this discrepancy is unknown, oxidation of NOM induced by H_2O_2 may vary depending on solution chemistry and among NOM sources. Because UV photolysis showed the same effect in both the authentic and synthetic matrices and the photoreactivity of NOM has been well documented (Del Vecchio & Blough, 2002; Sharpless *et al.*, 2014), changes in NOM molecular composition and optical properties during UV treatment were investigated in detail.

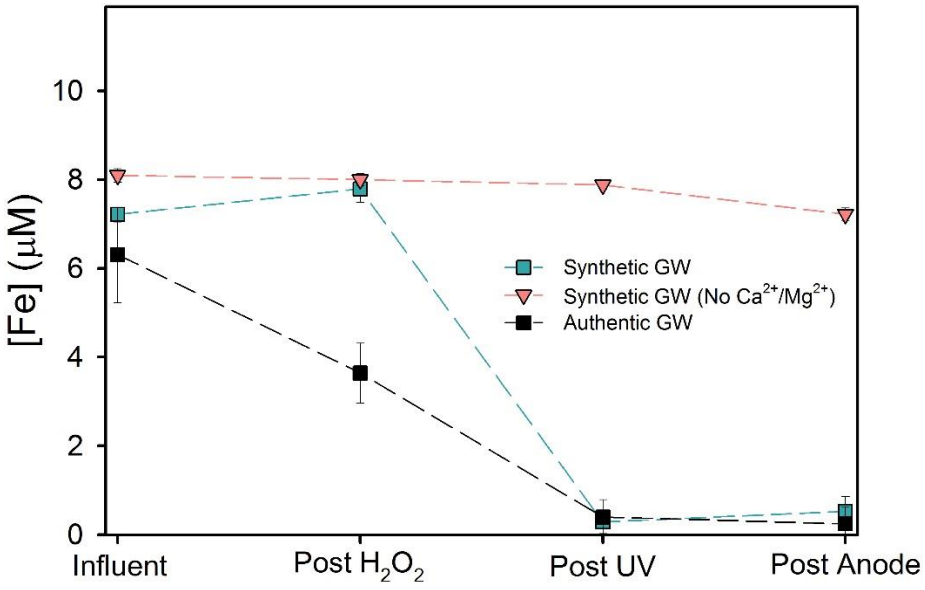

Figure 4.11: Measured concentrations of filterable dissolved iron during treatment of both synthetic and authentic groundwaters.

Analysis of FT-ICR MS data revealed 1455 chemical formulas in irradiated and non-irradiated authentic groundwater, of which 763 (i.e., 52%) of the peaks were common to both, 248 (i.e., 17%) peaks were observed only in the non-irradiated solution, and 444 (i.e., 31%) peaks were unique to the irradiated solution (Table 4.2).

Table 4.2. FT-ICR characterization of authentic GW from Colusa County, CA exposed to UV irradiation.

			Molecular Weight (Da)		H/C Ratio		O/C Ratio	
	Individual Peaks		Average	Stdev	Average	Stdev	Average	Stdev
Total	Non-Irradiated	1011	399.4614	81.5683	1.1707	0.1526	0.5193	0.1257
	Irradiated	1207	346.9095	70.7139	1.1133	0.2333	0.4880	0.1210
	Individual Peaks		Average	Stdev	Average	Stdev	Average	Stdev
Common	Non-Irradiated	763	385.5017	72.1991	1.1720	0.2079	0.5179	0.1220
	Irradiated	763	383.9748	70.7703	1.1771	0.2103	0.5235	0.1129
	Individual Peaks		Average	Stdev	Average	Stdev	Average	Stdev
Unique	Non-Irradiated	248	503.4796	71.6408	1.1509	0.2270	0.5393	0.1397
	Irradiated	444	358.6309	104.2617	1.2420	0.3050	0.4761	0.1529

Although interpretation of FT-ICR data requires caution because only compounds amenable to ionization (e.g., carboxylic acids) are detected, and thus only capture a subset of the total chemical formulas (Stenson *et al.*, 2002), results can provide insight into the changes in chemical composition that occurred during irradiation. For example, photolysis of authentic groundwater decreased the average molecular weight of detected peaks from 399.5 Da to 346.9 Da, with a greater loss of intensity for higher molecular weight formulas common to both dark

and light-exposed solutions (Figure 4.12). Similarly, approximately 70% of the peaks that completely disappeared upon UV irradiation were in the high molecular weight fraction (i.e., molecular weight formulas > 500 Da; Figure 4.13).

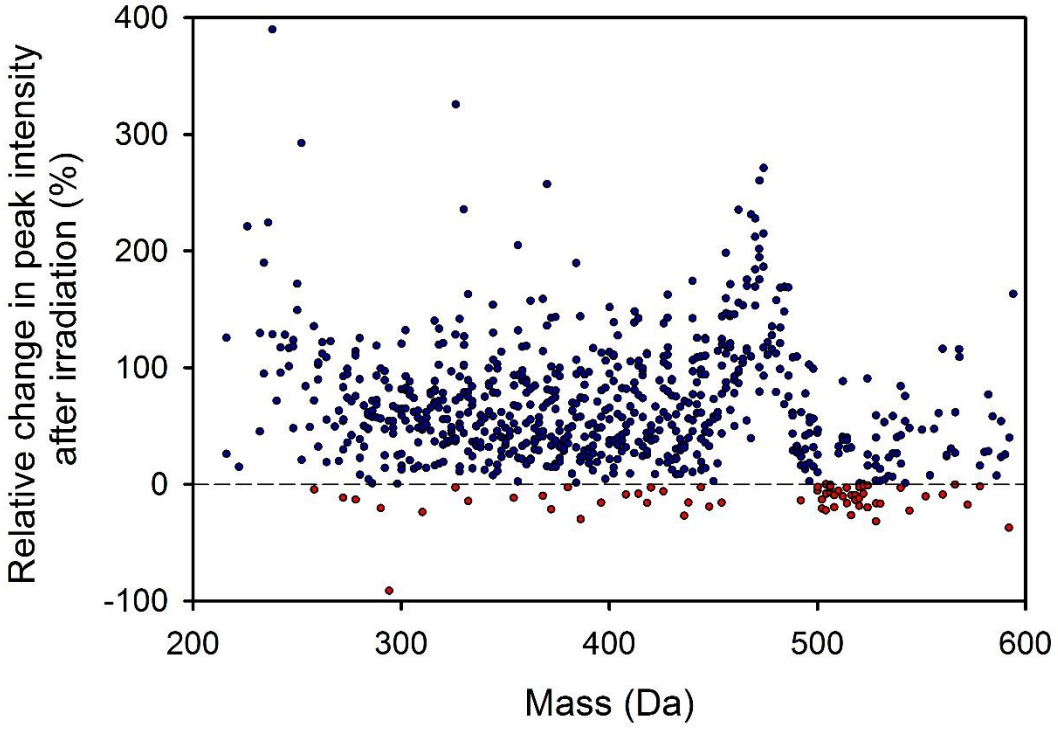

Figure 4.12: Loss (red circles) or gain (blue circles) in relative peak intensity after UV irradiation of authentic groundwater. Only chemical formulas common to both the virgin and irradiated solution are depicted.

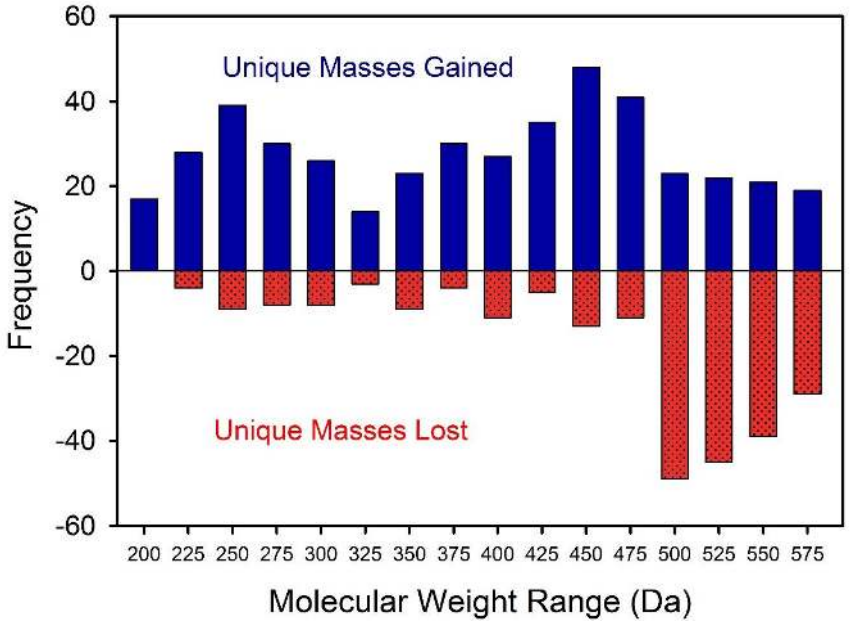

Figure 4.13: Distribution of unique masses lost (red) and gained (blue) during the photolysis of groundwater from Colusa County, CA (~1 mg L^{-1} NOM).

The apparent decreases in molecular weight upon irradiation are in agreement with an increase in spectral slope values observed in the UV-visible spectra (i.e., $S_{240\text{-}500}$ and $S_{275\text{-}295}$; Figure 4.14) (Helms *et al.*, 2008; Wenk *et al.*, 2013). Absorbance loss over the entire UV-visible spectrum (i.e., photobleaching; Figure 4.15), shifts in chemical compositions to slightly higher H/C ratios (Figure 4.16), and decreases in double bond equivalents (i.e., 9.40 to 8.71; Table 4.3) were consistent with ring cleavage or loss of aromaticity of chromophores (Ward & Cory, 2016; Maizel & Remucal, 2017).

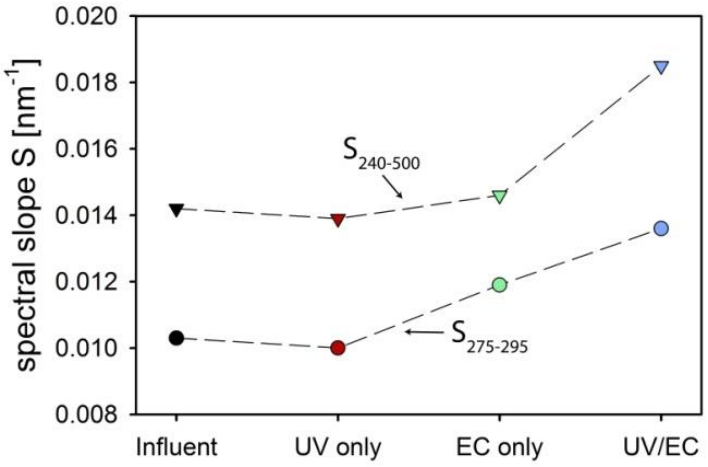

Figure 4.14: Spectral slope values (nm^{-1}) of authentic groundwater from Colusa County, CA following different treatment regimes (~1 mg L^{-1} NOM). Changes in the spectral slopes, S, were fitted over the wavelength intervals from 275 to 295 nm and from 240 to 500 nm.

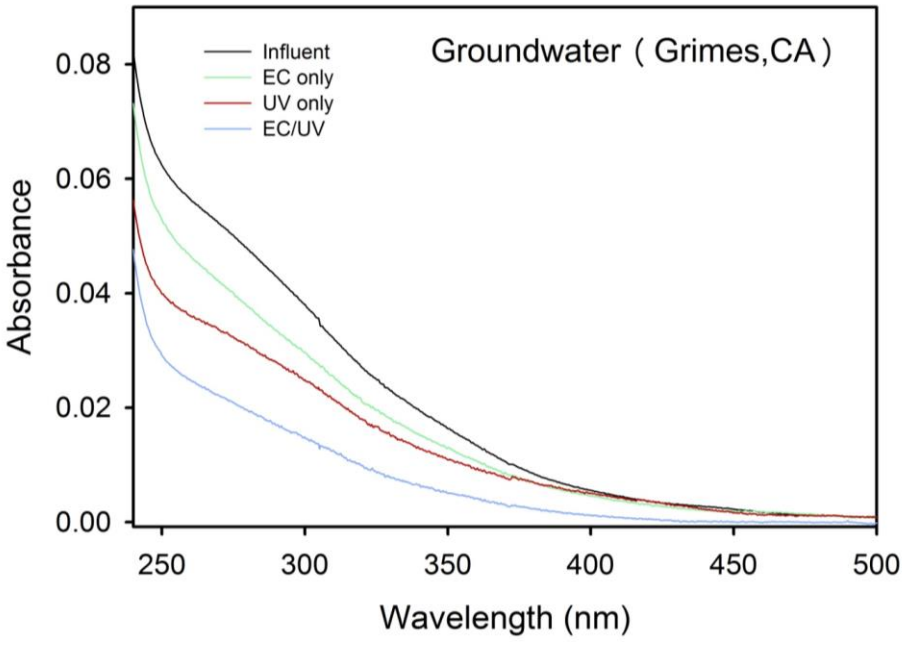

Figure 4.15: Effects of chemical treatment on the absorption spectra of authentic groundwater from Colusa County, CA (~1 mg L^{-1} NOM).

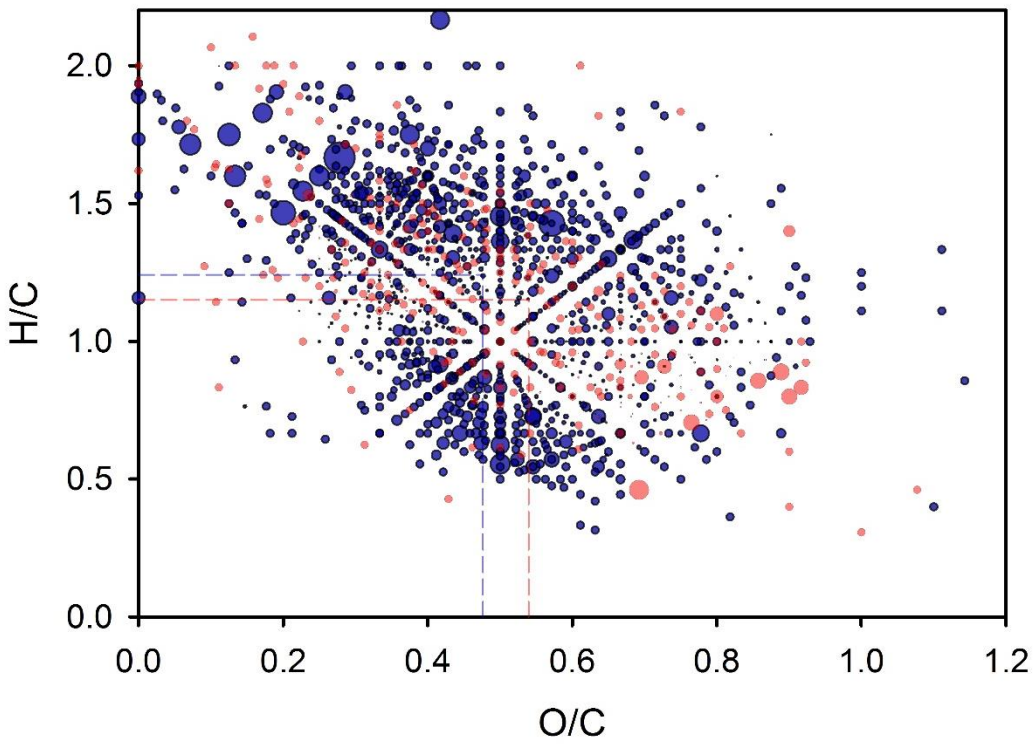

Figure 4.16: Van Krevelen diagrams of chemical formulas that were either unique to the non-irradiated authentic groundwater or decreased in intensity following irradiation (red circles) or were unique to the irradiated solution or increased in intensity following irradiation (blue circles). Bubble size is proportional to the peak intensity. Dashed lines correspond to the weighted average H/C and O/C ratios.

Table 4.3. Changes in Double Bond Equivalents determined using the FT-ICR data for Suwanee River NOM in the presence and absence of 10 µM Fe, 250 µM Ca^{2+}, and 250 µM Mg^{2+}, as well as authentic groundwater, exposed to UV Irradiation.

	Double Bond Equivalents	
	Non-Irradiated	Irradiated
NOM	9.601	8.407
Fe	8.602	8.184
Fe, Ca, Mg	8.445	8.051
Authentic GW	9.404	8.708

Mass spectra shifts in NOM to lower O/C ratios (i.e., average 0.063 lower) following exposure to UV irradiation provided additional insights into the photooxidation pathway of Fe complexing moieties in the NOM complexes (Figure 4.16). Photochemical loss of carboxyl moieties to produce hydrocarbons and CO_2 results in a 2:1 ratio of oxygen to carbon loss (Ward & Cory, 2016). Due to the fact that carboxylates (Kinniburgh *et al.*, 1996; Milne *et al.*, 2003), and structurally similar α-hydroxy acids moieties (Faust & Zepp, 1993), are the dominant metal-coordinating functional groups in NOM, these shifts in chemical composition are consistent with a photodecarboxylation mechanism previously proposed by Ward and Cory (Ward & Cory,

2016). Consequently, oxidation of Fe-coordinating moieties following light-exposure of Fe(III)-NOM complexes could help explain the in Fe-binding ability. To test this hypothesis, previously treated synthetic groundwater was filtered, respiked with 10 µM Fe(II), and subjected to a second pass through the treatment system (Figure 4.17). Results from UV-visible spectroscopy suggest that although NOM is present (Figure 4.18), filterable dissolved iron concentrations at all sampling locations were indistinguishable from control experiments performed with synthetic groundwater in the absence of NOM (Table 4.4), confirming an irreversible loss of Fe(III)-binding ability after the first exposure to UV light.

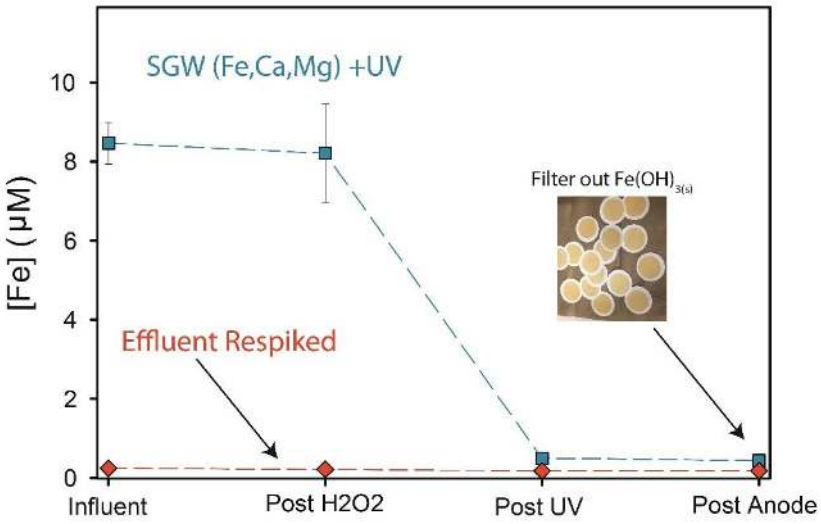

Figure 4.17: Concentration of dissolved (filterable) Fe in synthetic groundwater containing Ca^{2+} and Mg^{2+} exposed to the combined EC/UV treatment system. After the first pass, effluent iron oxides were filtered through a 0.22 µm filter, respiked with 10 µM Fe(II), and subjected through the treatment system for a second time.

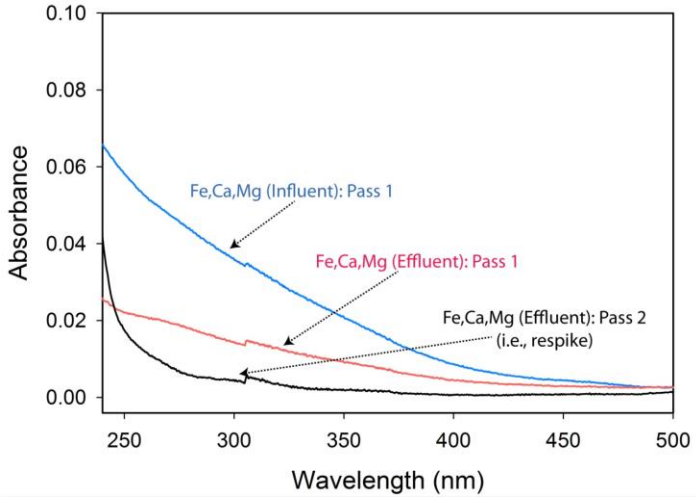

Figure 4.18: Absorption spectra of synthetic groundwater containing Fe^{2+}, Ca^{2+}, and Mg^{2+} exposed to the combined EC/UV treatment system. Two passes of synthetic groundwater solution through the treatment system were performed. After the first pass, effluent iron oxides were filtered through a 0.22 µm filter and respiked with 10 µM Fe(II).

Table 4.4. Total and dissolved iron measured during respike experiments.

		Total Fe (μM)	Dissolved Fe (μM)			
		Influent	Influent	Post H_2O_2	Post UV	Effluent
FCM + NOM Pass 1	Average	10.898	8.461	8.208	0.495	0.441
	Standard	0.213	0.529	1.250	0.007	0.120
FCM + NOM Pass 2[a]	Average	11.762	0.242	0.216	0.176	0.184
	Standard	0.181	0.028	0.103	0.008	0.044
No NOM[b]	Average	11.578	0.249	0.192	0.141	0.148
	Standard	0.297	0.007	0.027	0.005	0.021

[a]For Pass 2, effluent of Pass 1 was filtered through a 0.22 μm filter, respiked with ~ 10 μM Fe, and exposed to the treatment system for a second time. [b]No NOM corresponds to a single pass of synthetic groundwater containing Fe, Ca^{2+}, and Mg^{2+}(FCM) without NOM through the treatment system.

To determine the relative contributions of direct and indirect photolysis to the changes in NOM and iron upon UV irradiation, a series of experiments were conducted in which reactive intermediates (i.e., $HO^{\bullet}$, $^1O_2$, ^{3}NOM) produced by photoexcitation of NOM or H_2O_2 were scavenged (Figure 4.19).

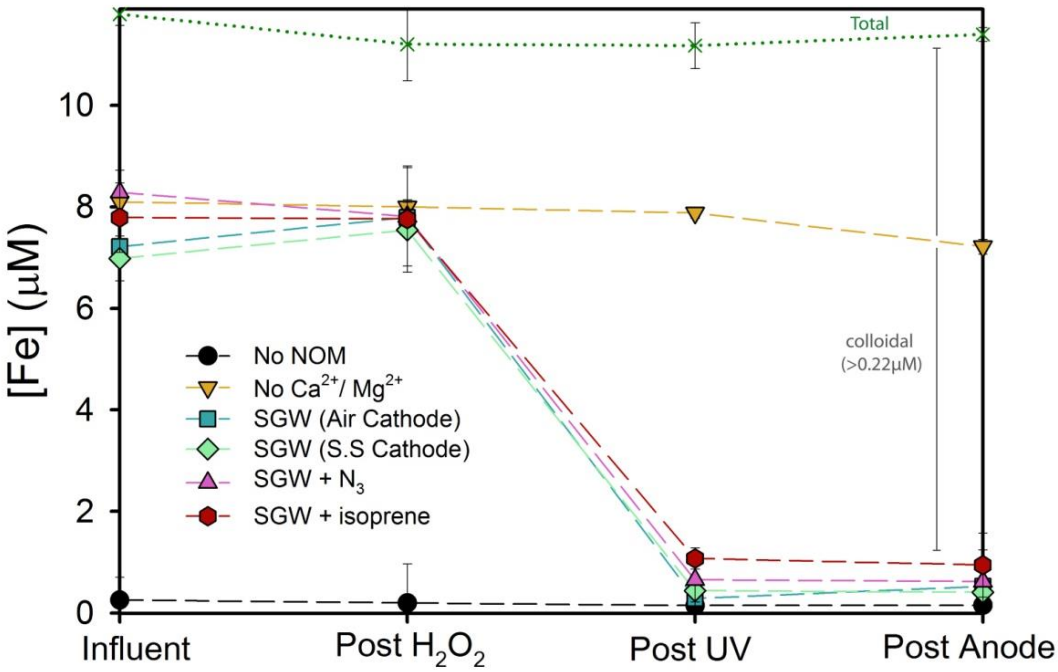

Figure 4.19: Speciation of dissolved and colloidal Fe in simulated electrolytes exposed to the combined EC/UV treatment system in the presence and absence of Ca^{2+} and Mg^{2+}, NOM, and reactive intermediate quenchers.

Experiments conducted with a stainless steel cathode (i.e., no production of H_2O_2) or in the presence of 1 mM tertiary butanol (i.e., enough to reduce $[HO^{\bullet}]_{SS}$ by approximately 70%) revealed no change in Fe removal, indicating that reactions with $HO^{\bullet}$ were not important (See

Section A.4.3 of the Appendix for calculations). Although the potential contribution of $HO^{\bullet}$ to Fe removal was hypothesized earlier in dark experiments, its negligible role in irradiated solutions is not unsurprising given the significant light screening of H_2O_2 by NOM (~82%) and limited fraction of $HO^{\bullet}$ reacting with NOM (i.e., ~ 12%) in the presence of other solutes (i.e., H_2O_2, HCO_3^-, CO_3^{2-}; See Section A.4.4 of the Appendix for calculations). Similarly, the presence of both 50 µM NaN_3 and 500 µM isoprene, enough to lower $[^1O_2]_{SS}$ and $[^3NOM]_{SS}$ by 17% and 50%, respectively, did not influence Fe removal. Collectively, these results suggest that direct photolysis of NOM were responsible for conversion of organically complexed Fe into forms that were removed upon filtration.

4.3.3 Effect of Solution Chemistry on Phototransformation of Fe(III)-NOM Complexes.

Previous research has shown that divalent cations (e.g., Ca^{2+}, Mg^{2+}) can impact iron oxide structural conformation, surface charge, as well as photolability of organically-complexed iron (van Genuchten *et al.*, 2014). For example, Ca^{2+} and Mg^{2+} promote the photochemical reduction of Fe(III)-EDTA complexes via formation of ternary complexes that increased the quantum yield (Fujii *et al.*, 2015). Treatment experiments performed in synthetic groundwater indicated that Fe removal increased with increasing concentrations of Ca^{2+} and Mg^{2+} (Figure 4.20).

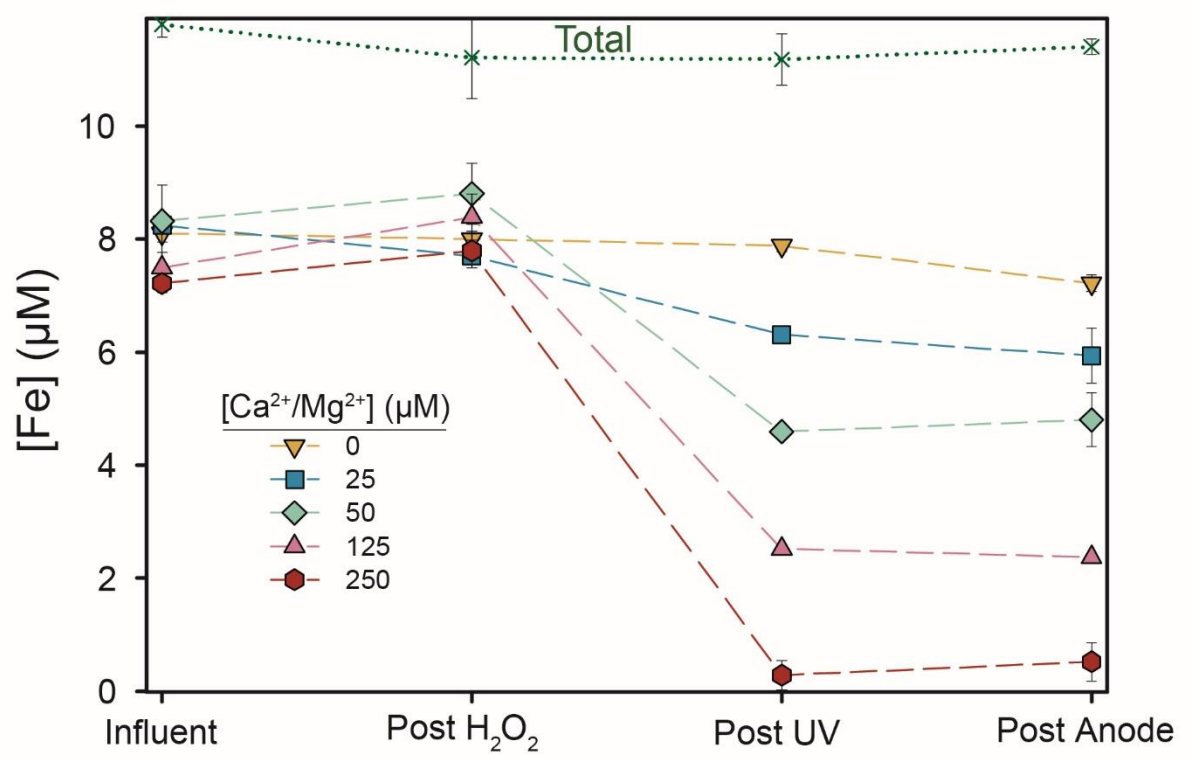

Figure 4.20: Concentration of dissolved and total (i.e., dissolved and colloidal) Fe in synthetic groundwater exposed to the combined EC/UV treatment system at varying concentrations of Ca^{2+} and Mg^{2+} (0 to 250 µM).

The possible role of divalent cation bridging of Fe(III)-NOM complexes (Delaire *et al.*, 2015) or metal exchange (Fujii *et al.*, 2015) of Ca^{2+} and Mg^{2+} with Fe(III) at NOM complexation

sites was assessed. Similar uptake of Ca^{2+} and Mg^{2+} (~ 40 µM of each cation) in the presence and absence of NOM suggests that Fe removal via divalent cation bridging of Fe(III)-NOM complexes was not important (Figure 4.21). In addition, increased Fe loss via metal exchange between Ca^{2+} and Mg^{2+} with Fe(III)-NOM complexes was deemed unimportant because Fe removal in dark experiments was not affected by the presence of divalent cations (Figure 4.22).

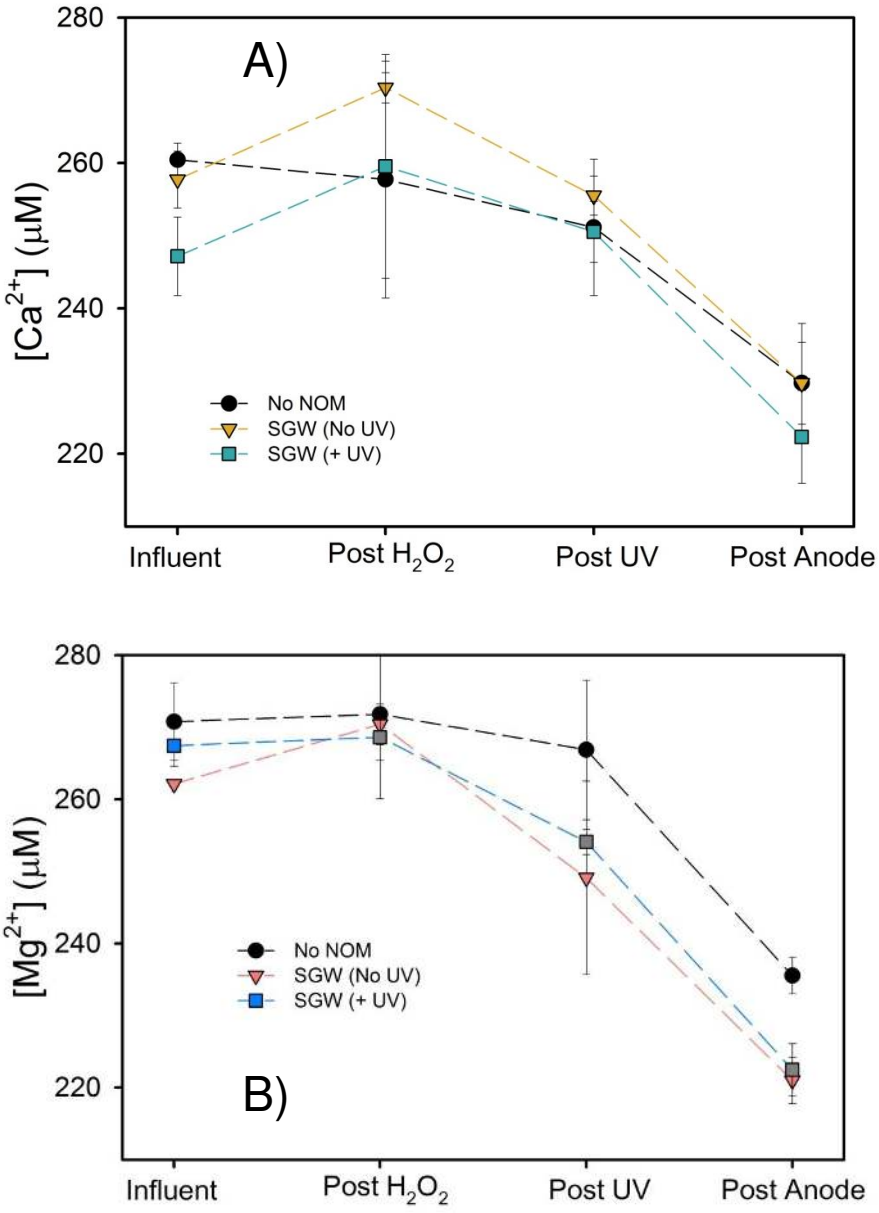

Figure 4.21: Concentration of (A) Ca^{2+} and (B) Mg^{2+} during treatment of synthetic groundwater in the presence and absence of UV light and natural organic matter.

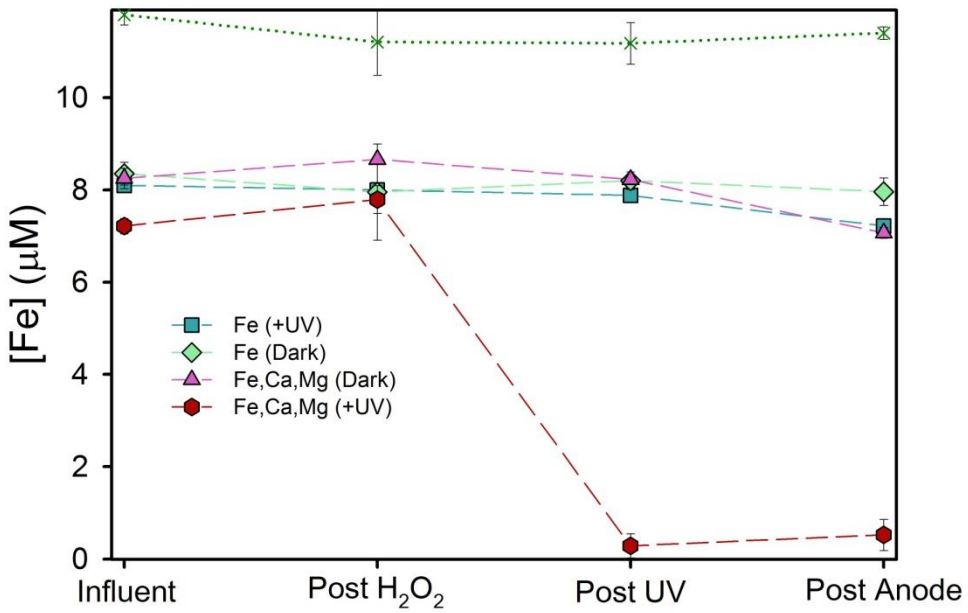

Figure 4.22: Concentration of dissolved (filterable) Fe in synthetic groundwater in the presence and absence of Ca^{2+} and Mg^{2+} exposed to treatment. Experiments were performed both with and without UV irradiation. Green dotted line corresponds to the average total iron (i.e., dissolved and colloidal).

Comparison of photodegradation experiments performed in synthetic groundwater revealed more rapid shifts in NOM chemical composition to aliphatic formulas (i.e., higher H:C ratios; Tables 4.5 and 4.6), more pronounced shifts in the distribution of peak intensities to lower molecular weight formulas (Figure 4.23), and greater UV-visible absorbance loss (Figures 4.24-4.27) in the presence of Ca^{2+} and Mg^{2+}, confirming the hypothesis that divalent cations increased the changes in NOM that occurred upon UV irradiation.

Table 4.5. FT-ICR characterization of Suwanee River NOM in the presence of 10 μM Fe exposed to UV irradiation.

			Molecular Weight (Da)		H/C Ratio		O/C Ratio	
	Individual Peaks		Average	Stdev	Average	Stdev	Average	Stdev
Total	Non-Irradiated	633	363.2800	76.1362	1.1865	0.2880	0.5240	0.1598
	Irradiated	761	348.0328	79.6796	1.1670	0.2462	0.5477	0.1374
	Individual Peaks		Average	Stdev	Average	Stdev	Average	Stdev
Common	Non-Irradiated	462	355.5242	67.3857	1.1929	0.2883	0.5239	0.1579
	Irradiated	462	344.3304	67.6283	1.1635	0.2209	0.5519	0.1257
	Individual Peaks		Average	Stdev	Average	Stdev	Average	Stdev
Unique	Non-Irradiated	171	426.5756	96.8935	1.1449	0.2775	0.5244	0.1723
	Irradiated	158	444.0306	110.1853	1.1431	0.2700	0.5437	0.1515

Table 4.6. FT-ICR characterization of Suwanee River NOM in the presence of 10 µM Fe, 250 µM Ca^{2+}, and 250 µM Mg^{2+} exposed to UV irradiation.

			Molecular Weight (Da)		H/C Ratio		O/C Ratio	
	Individual Peaks		Average	Stdev	Average	Stdev	Average	Stdev
Total	Non-Irradiated	731	381.5951	87.6638	1.1434	0.2164	0.5495	0.1301
	Irradiated	812	360.3240	74.7247	1.1666	0.2552	0.5440	0.1363
	Individual Peaks		Average	Stdev	Average	Stdev	Average	Stdev
Common	Non-Irradiated	536	364.0336	74.8980	1.1486	0.2142	1.1608	0.2405
	Irradiated	536	345.3787	74.2229	1.1608	0.2405	0.5556	0.1299
	Individual Peaks		Average	Stdev	Average	Stdev	Average	Stdev
Unique	Non-Irradiated	194	491.9768	76.1917	1.1136	0.2242	0.5315	0.1509
	Irradiated	214	365.1644	108.9100	1.1884	0.2960	0.4958	0.2060

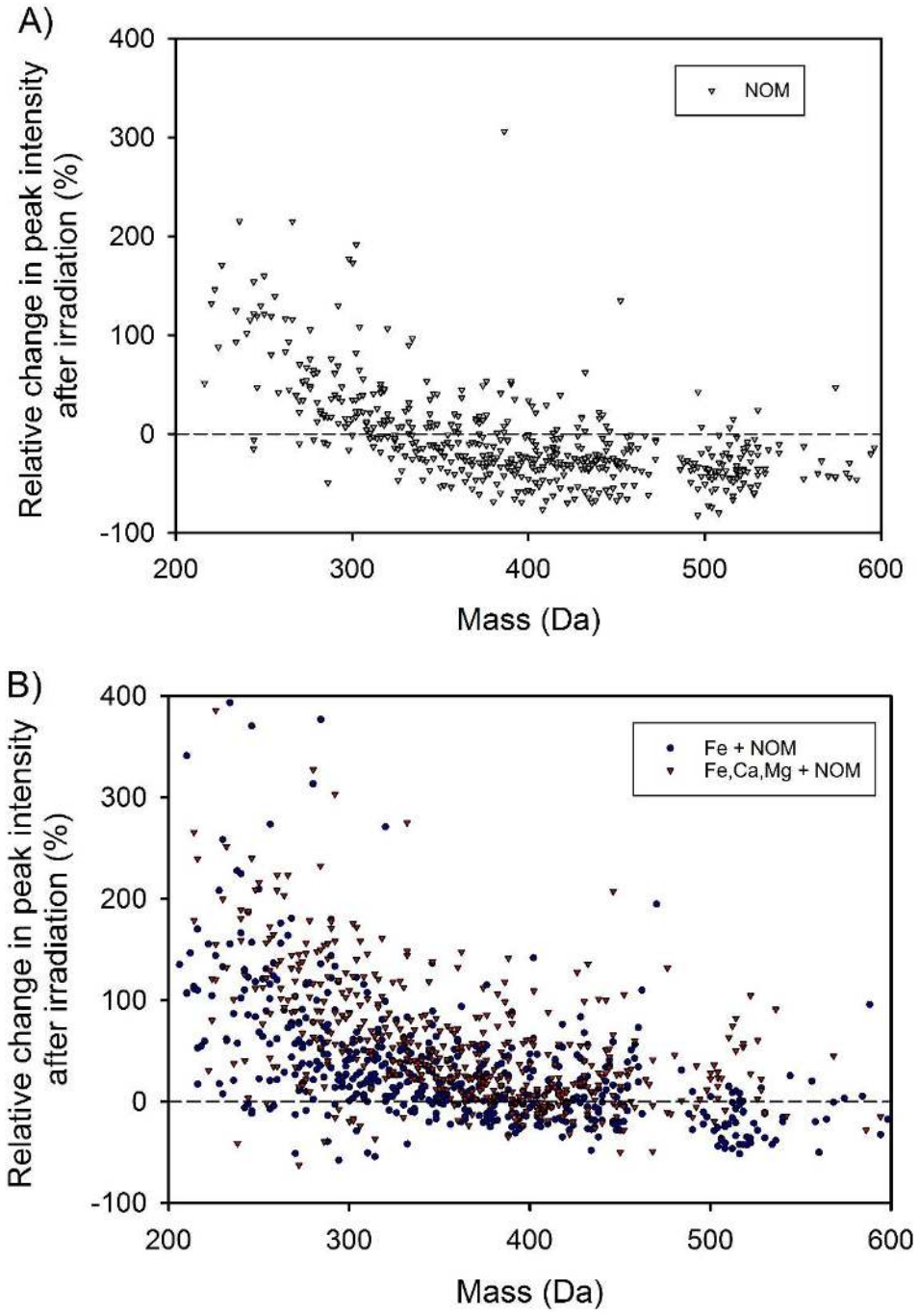

Figure 4.23: Changes in relative peak intensity after UV irradiation of formulas that were common to both the non-irradiated and irradiated synthetic solutions containing A) 1 mg L^{-1} Suwanee River NOM and B) 1 mg L^{-1} Suwanee River NOM with either Fe (10 µM) or Fe (10 µM), Ca^{2+} (250 µM), and Mg^{2+} (250 µM).

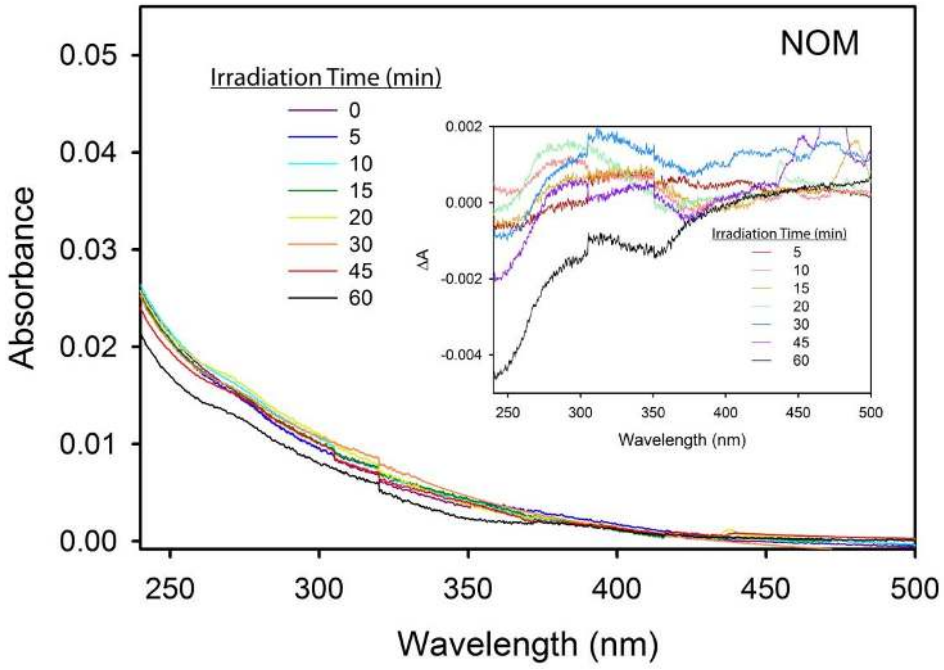

Figure 4.24: Changes in absorption spectra of synthetic groundwater containing 1 mg L^{-1} Suwannee River NOM with UV irradiation time. Inset: differential absorbance relative to non-irradiated solution (i.e., t=0). Experiments were performed in batch (V_{TOT} = 900 mL).

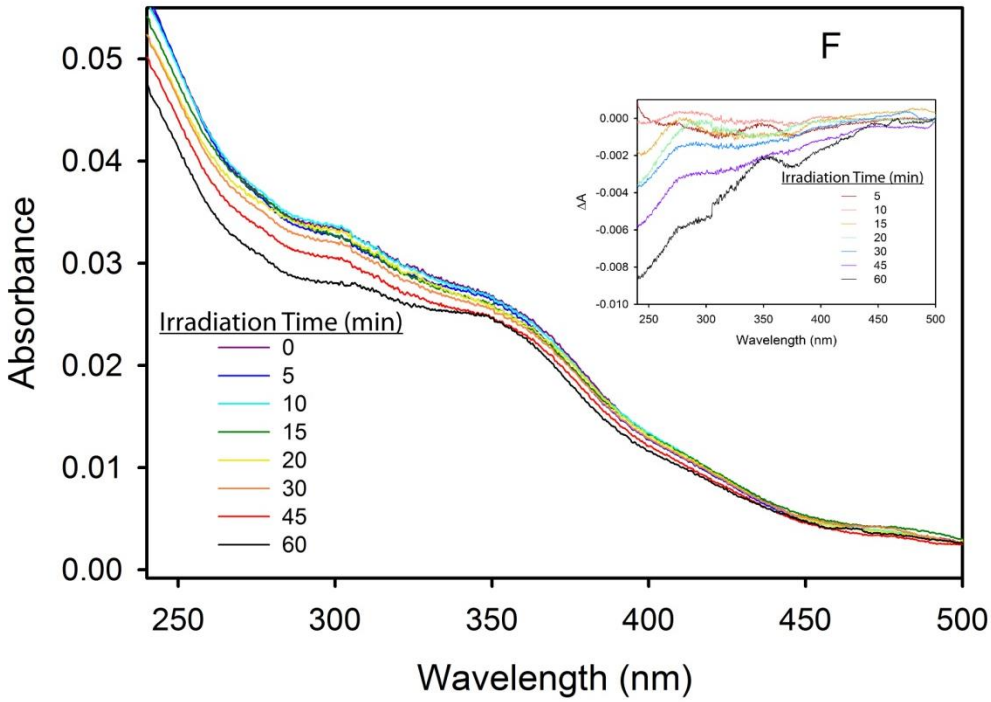

Figure 4.25: Changes in absorption spectra of synthetic groundwater containing 1 mg L^{-1} Suwannee River NOM and 10 µM Fe(II) with UV irradiation time. Inset: differential absorbance relative to non-irradiated solution (i.e., t=0). Experiments were performed in batch (V_{TOT} = 900 mL).

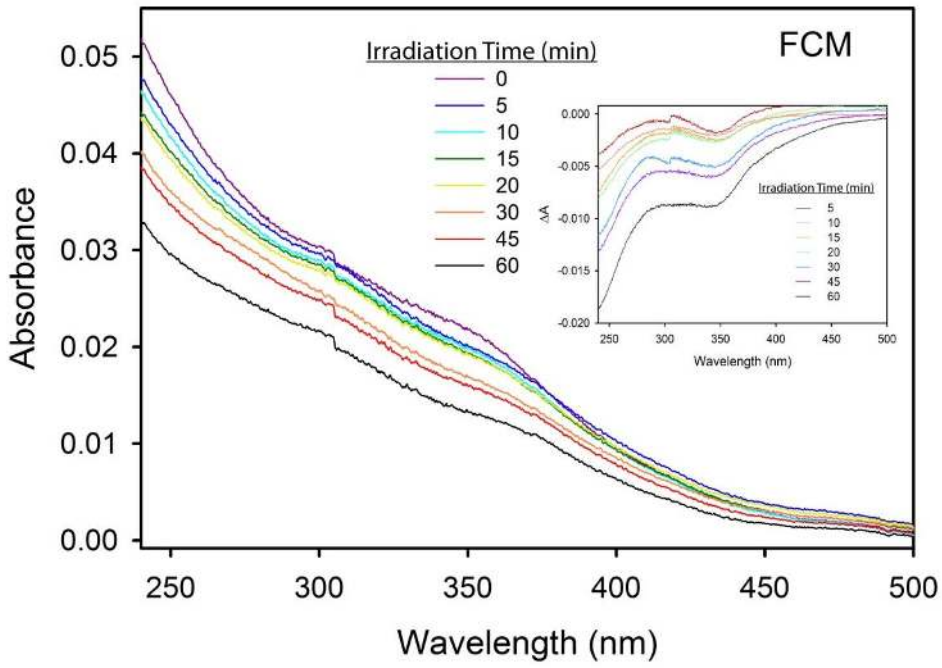

Figure 4.26: Changes in absorption spectra of synthetic groundwater containing 1 mg L^{-1} Suwannee River NOM, 10 µM Fe(II), and 250 µM Ca^{2+} and Mg^{2+} with UV irradiation time. Inset: differential absorbance relative to non-irradiated solution (i.e., t=0). Experiments were performed in batch (V_{TOT} = 900 mL).

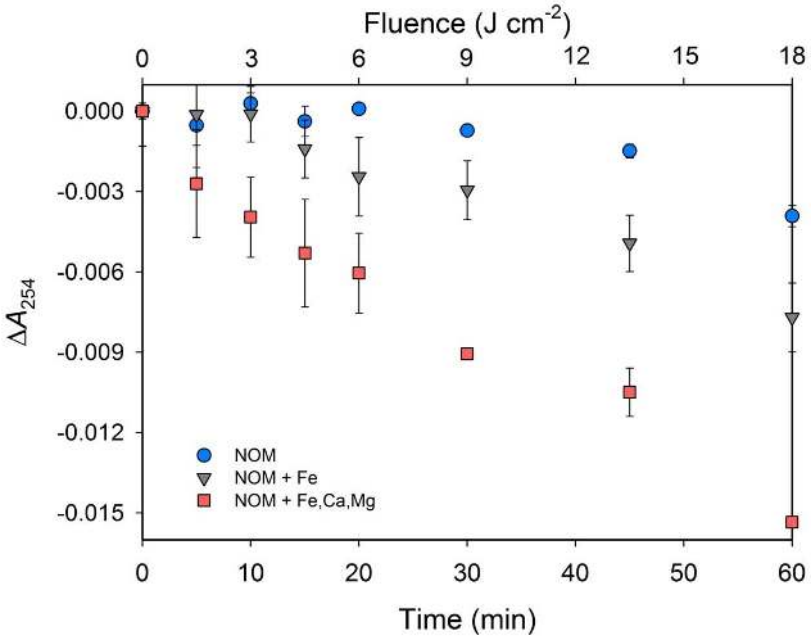

Figure 4.27: Differential absorbance at 254 nm during batch UV irradiation of synthetic groundwater containing NOM, Fe(III)-NOM, and Fe(III)-NOM-Ca^{2+}/Mg^{2+} complexes vs. UV irradiation time. Experiments were performed in batch (V_{TOT} = 900 mL). Iron was added as Fe(II). [NOM]= 1 mg L^{-1}; [Fe(II)] = 10 µM; [Ca^{2+}] = [Mg^{2+}] = 250 µM.

The enhanced photoreactivity of NOM may be attributable to conformational changes induced by divalent cation complexation that either accelerates LMCT reactions, resulting in the formation of Fe(II) and oxidation of the NOM-complexing functional group (Barbeau, 2006; Fujii *et al.*, 2008; Aiken *et al.*, 2011; Fujii *et al.*, 2015), or alters intramolecular charge transfer thereby decreasing light absorption and/or quantum yield (Aeschbacher *et al.*, 2012; Sharpless *et al.*, 2014). To provide insight into the governing mechanism, photochemical formation of Fe(II) and electron transfer kinetics were analyzed in the synthetic groundwater matrix. Initial photochemical production rates of Fe(II) under UV irradiation approached 4.42 ± 0.4 nM s^{-1} (Figure 4.28).

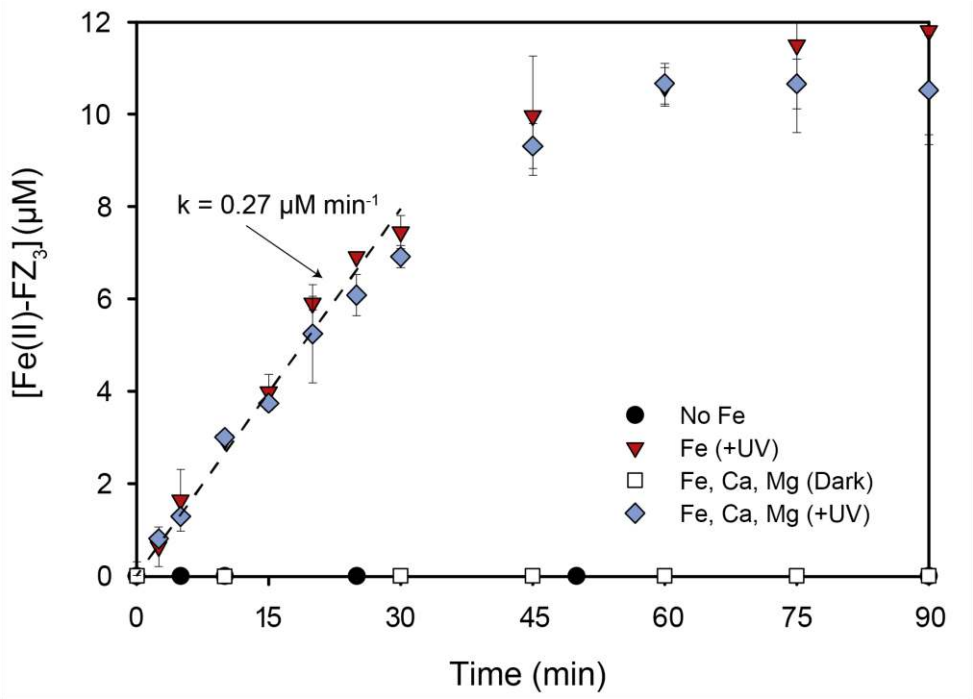

Figure 4.28: Rate of Fe(II) production during UV_{254} photolysis of Fe(III)-NOM complexes as well as dark controls as determined via production of ferrous iron-ferrozine complex (Fe(II)-FZ_3) measured at 562 nm (Stookey, 1970; Viollier *et al.*, 2000). Iron was initially added as 10 µM Fe(III). All solutions were at pH 6.5.

Considering the hydraulic conditions (i.e., 1.8 CSTRs-in-series) and residence time (~660 seconds) in the UV reactor during continuous treatment, approximately 3 µM of Fe(III) should have been reduced and subsequently oxidized to produce particulate Fe(III)-oxides. This is, however, less than half of the iron that was actually removed in the system. Furthermore, comparable Fe(II) production rates in the presence and absence of Ca^{2+} and Mg^{2+} do not support the hypothesis that divalent cations accelerate rates of the LMCT reactions (Figure 4.20). These findings are similar to results of experiments conducted with Suwannee River Fulvic Acid, in which divalent cations did not affect production of Fe(II) under solar photolysis conditions (Fujii *et al.*, 2008; Fujii *et al.*, 2015).

Intramolecular electron transfer between photoexcited acceptor moieties (i.e., carbonyls) and ground-state donor moieties (i.e., phenolates) stabilizes NOM and slows phototransformation rates (Parker *et al.*, 2013). Conformational changes of the NOM structure

by Ca^{2+} or Mg^{2+} complexation can disrupt this donor-acceptor electronic coupling (Sato *et al.*, 2001), leading to accelerated phototransformation of NOM. To evaluate this hypothesis, cyclic voltammetry experiments were performed using NOM, Fe-NOM, and Fe-NOM with added Ca^{2+} and Mg^{2+}(Figure 4.29). Although weakly defined, voltammograms for Suwannee River NOM contained a pair of cathodic peaks at -0.98 V and -1.32 V, which were consistent with the peak reduction potentials for *p*-benzoquinone (Figure 4.30). Thus, these peaks correspond to single electron reduction reactions to form an intermediate semiquinone radical ($E_{pc,1}$ = -0.75 V) and a quinone dianion ($E_{pc,2}$ = -1.33 V) (Nurmi & Tratnyek, 2002). Addition of Fe^{2+} to the NOM solution shifted the onset potential of the cathodic waves to more positive potentials ($\Delta E_{pc,1}$ = +0.140 V; $\Delta E_{pc,2}$ = +0.048 V) and increased the redox activity relative to the free ligand wave (i.e., NOM only) (Fimmen *et al.*, 2007). In the presence of Ca^{2+} and Mg^{2+}, however, reductive currents decreased and the second reduction peak disappeared. These results suggest inhibition of charge-transfer pathways between redox-active functional groups due to the formation of a divalent cation-semiquinone complex (Sato *et al.*, 2001; Yuasa *et al.*, 2006), suppressing intramolecular electron transfer and accelerating the phototransformation of NOM. These results, combined with those from spectroscopic and compositional analysis, provide evidence that divalent cations increased the photolability of the organic matter.

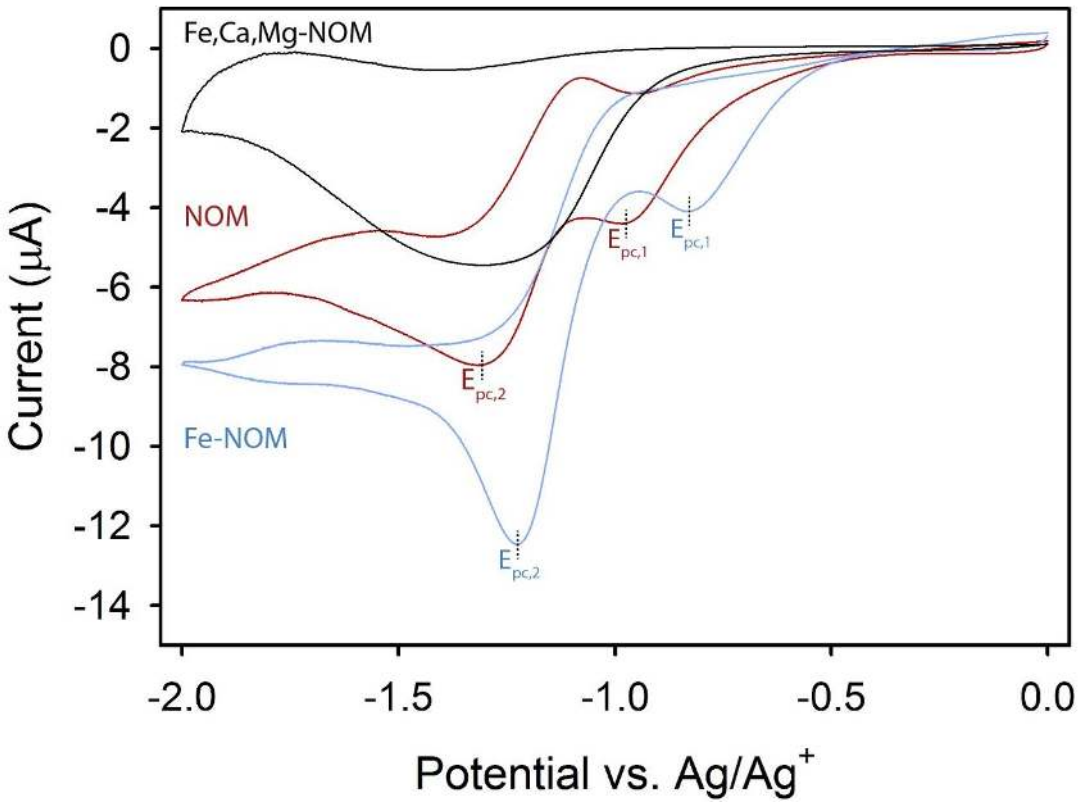

Figure 4.29: Cyclic Voltammograms of Suwannee River NOM (90 mg L^{-1}; ~ 45 mgC L^{-1}), Suwannee River NOM with 50 µM $Fe(Cl)_3$, and Suwannee River NOM with 50 µM $Fe(Cl)_3$, 500 µM $Ca(Cl)_2$, and 500 µM $Mg(Cl)_2$. E_{pc} refers to the cathodic peak potential.

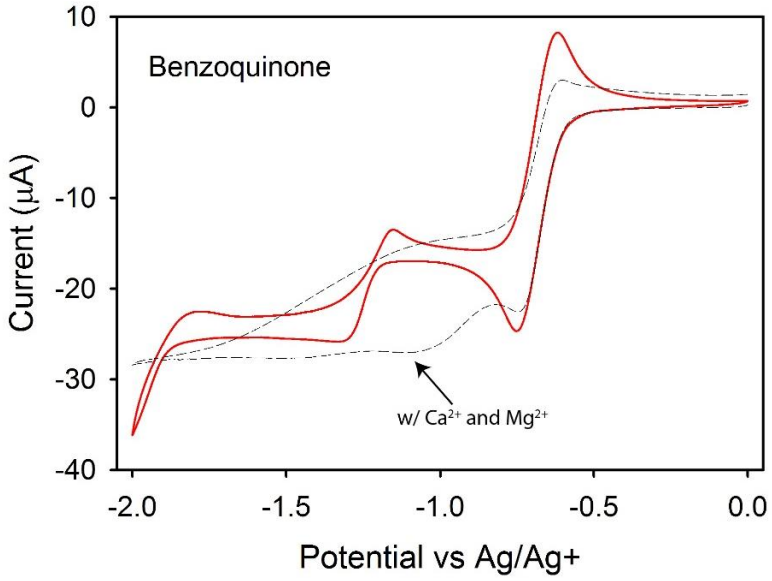

Figure 4.30: Cyclic Voltammogram of 500 µM p-benzoquinone. CV's were performed in anhydrous dimethyl sulfoxide (DMSO; 50 mL) containing 5 mM tetrabutylammonium hexaflurophosphate (NBu4PF6). Experiments were performed with a Pt wire working and counter electrode (0.25 mm diameter) and nonaqueous Ag/Ag^{+} reference electrode (BASi) at a scan rate of 10 mV s^{-1}.

4.3.4 Environmental Significance

Drinking water sources that are candidates for treatment by point-of-use devices will frequently contain iron, calcium, magnesium, and organic matter at concentrations comparable to those studied here. For instance, contamination of groundwater with arsenic typically involves the reductive dissolution of iron hydroxides, resulting in simultaneous release of arsenic and iron under anoxic conditions (Hug *et al.*, 2001; McArthur *et al.*, 2004). Similarly, water sources contaminated with Pb may also contain iron from the corrosion of galvanized pipes (McFadden *et al.*, 2011). In most groundwater, alkaline earth metals (e.g., Ca^{2+} and Mg^{2+}) and natural organic matter are also present. The technology described here is a simple, low-cost technology for distributed treatment of arsenic- and lead-contaminated waters suitable for these solution conditions. Considering only the electrical energy demand from the electrochemical cell and UV lamp, the treatment of water had an energy demand of 2.2 kWh m^{-3}. This device nearly completely remove a suite of trace organic contaminants (Barazesh *et al.*, 2015) from the authentic groundwater, while it removed 12 of the initial 28 µg L^{-1} of As (See Section A.4.5 of the Appendix for calculations). Thus, considering an As sorption capacity of 0.012 mol As per mol iron oxide (Figure 4.10), treating authentic groundwater containing 28 µg L^{-1} to below the World Health Organization Maximum Contaminant Level of 10 µg L^{-1} would require an additional dosing of 6.7 µM Fe. Irrespective of the source of the Fe, the system would only generate 1.1 mg L^{-1} of waste sludge (See Section A.4.6 of the Appendix for calculations). Challenges still remain in the development of a low-cost means of separating iron oxides after prolonged treatment, but methods employing gravitational settling and/or membrane filtration may be practical.

In addition to providing a standalone distributed treatment system, this research may offer substantial promise for decreasing operational costs and increasing process efficiency of iron-based electrocoagulation techniques by reducing electrolysis times, iron dosing, and sludge production simply though the integration of a UV treatment step. Additional research would be needed to assess the effectiveness of the treatment under those conditions. Macromolecular structure, binding capacity, and physicochemical properties of NOM are affected by solution chemistry (Aiken *et al.*, 2011), therefore additional research is needed to assess the behavior of metal-NOM complexes under varying pH values and metal-to-NOM ratios.

CHAPTER 5. Conclusions

5.1 Summary

Inadequate access to clean drinking water is one of the most globally pervasive problems. As water scarcity grows worse, addressing this problem will require novel approaches that allow people to access new sources of water including through the use of point-of-use and point-of-entry treatment devices. Distributed drinking water treatment systems hold promise for addressing many current water supply challenges. Onsite treatment systems decrease reliance on imported water through the local reuse of water sources. Moreover, they do not require the significant capital costs required to retrofit large-scale treatment plants to accommodate emerging contaminants, thereby allowing novel technological innovations to be implemented quickly. This is particularly needed given the increasing use of designer drugs and pesticides, which pose new challenges that cannot be met by conventional wastewater treatment plants (Eggen *et al.*, 2014). To avoid potential adverse health effects associated with the presence of trace organic contaminants and toxic trace elements in these water sources, innovative treatment methods are needed. Research that identifies cost-effective, robust solutions for providing potable drinking water without relying upon centralized drinking water treatment are critical.

The research described in this dissertation evaluated a new approach for using electrochemistry to treat water sources that are currently not being exploited. The following sections evaluate the technological and financial feasibility of two remote, drinking water electrolysis systems, address some of their major challenges, and identify appropriate design strategies for their adoption.

5.2 Electrochemical Transformation of Trace Organic Contaminants in the Presence of Halide and Carbonate Ions

In Chapter 2, transformation mechanisms, kinetics, product formation and production of byproducts were investigated during anodic oxidation of trace organic contaminants in matrices comparable to those that might be encountered in a distributed treatment system. The rate of removal of compounds in halide- and carbonate-containing matrices varied by over two orders of magnitude (i.e., 10^{-4} to 10^{-2} s^{-1}). Transformation rates for most contaminants increased in the presence of chloride and trace amounts of bromide; however, elevated concentrations of HCO_3^- often affected transformation rates through formation of selective oxidants (e.g., $CO_3^{\bullet-}$) that preferentially reacted with amine and phenolic moieties. Reactions on anode surfaces and with homogenous species (i.e., hypochlorous acid and hydroxyl radical) were studied separately to estimate their contributions to trace organic contaminant transformation rates under different solution conditions (e.g., varying carbonate, halide, and dissolved organic carbon concentrations). In a wastewater effluent sample, the model accurately predicted rates of removal of electron-rich contaminants but underestimated the transformation rates of compounds that exhibited low reactivity with HOCl and HOBr, indicating the possible contribution of previously unaccounted for species, such as adsorbed halogen radicals.

These results highlight two shortcomings of anodic oxidation. First, significant variability in transformation rates of organic contaminants is typically observed, particularly for electron-poor contaminants, due to chemical and contaminant mass transfer limitations given the low electro-active surface area relative to the volume of water being treated. Second, electrophilic

substitution reactions between HOCl and HOBr with organic contaminants results in the formation of halogenated transformation products. In some cases, sequential halogenation of parent compounds results in the formation of regulated halogenated disinfection byproducts (e.g., THMs and HAAs) at concentrations greatly in excess of their existing water quality standards, effectively substituting one contaminant for another. Given the attractiveness of employing anodic oxidation for highly conductive halide-containing waste streams, including industrial and municipal wastewater as well as reverse osmosis retentate, reactions with halogen species poses a challenge to anodically-driven decentralized drinking water systems that may limit its application.

5.3 Modular Advanced Oxidation Processes Enabled by Cathodic Hydrogen Peroxide Production

The research described in Chapter 3 presents an alternative approach exploiting cathodic generation of H_2O_2 from ambient air followed by UV photolysis to generate reactive hydroxyl radicals for contaminant degradation. H_2O_2 production was demonstrated in varying source waters over a combination of flow rates (35 - 350 L d^{-1}) and applied current densities (0 - 80 A m^{-2}). High O_2 fluxes (i.e., 0.57 L m^{-2} min^{-1}) through the gas permeable cathode and high Coulombic efficiencies (i.e., >85%) enabled H_2O_2 production at rates between 14.8 to 38.6 mg H_2O_2 L^{-1} min^{-1}, independent of solution chemistry. Although the extent of transformation of trace organic contaminants was affected by the current density and the concentrations of $HO^{\bullet}$ scavengers in the source water, the electrical energy per order (E_{EO}) ranged from 1 to 3 kWh m^{-3}, which was significantly lower than E_{EO} observed for the anodic oxidation of the same suite of contaminants. In addition, transformation of organic contaminants was accomplished without production of high concentrations of halogenated disinfection byproducts.

The fate of toxic trace elements in the electrochemical treatment system was investigated in Chapter 4. Toxic trace elements, including lead and arsenic, pose risks to human health, and thus, distributed treatment systems. Typically, removal of trace elements can occur through sorption onto iron oxide surfaces; however, under the conditions encountered in drinking water sources (e.g., relatively low dissolved Fe) the extent of iron oxide precipitation is influenced by the presence of metal complexing ligands (e.g., carboxylic and phenolic groups) present in natural organic matter. For example, authentic groundwater containing 1 mg L^{-1} of natural organic matter resulted in soluble iron concentrations over 100 times greater than predicted by thermodynamic calculations at circumneutral pH (i.e., 50 nM dissolved Fe).

The potential for using cathodically-produced H_2O_2 and UV light to oxidize these ligands in natural organic matter that prevent or slow iron precipitation was investigated by measuring dissolved iron and trace element concentrations throughout the treatment train under different conditions. Combined electrochemical and photochemical treatment of authentic groundwater resulted in nearly complete conversion of iron to forms that could be separated by membrane microfiltration or gravitational settling. Furthermore, a quantitative relationship was observed for the sorption and removal of Pb, Cu, and As on the iron oxide colloids. Decreases in solution absorbance and shifts in molecular composition of natural organic matter to lower oxygen:carbon ratios indicated that loss of iron-complexing ligands occurred primarily via photodecarboxylation reactions. The presence of Ca^{2+} and Mg^{2+} significantly increased the removal of iron and trace

elements following exposure to UV light due to the inhibition of intramolecular charge transfer reactions that had previously prevented stabilized the metal-NOM aggregate from photochemical breakdown and formation of filterable colloids. Overall, this chapter showed that the electrochemical system offers substantial benefits over other metal removal technologies, such as iron-based electrocoagulation, by reducing the volume of solids requiring disposal simply through the integration of a UV lamp.

5.4 Implications and Future Research

Collectively, the research described in this dissertation provides insight into the mechanisms and potential application of electrochemical water treatment technologies for distributed drinking water treatment systems. Specifically, the modular advanced oxidation system driven by cathodic hydrogen peroxide production may prove to be an important element of an easily adoptable, low-cost drinking water treatment system. However, further research is necessary for system optimization, reduction in energy demand, and assessment of long-term performance. These issues are detailed below along with suggestions for future research.

Currently, ~65% of the H_2O_2 produced makes it through the treatment train given the low molar absorptivity of H_2O_2 at 254 nm and limited quenching by HOCl in the anode chamber due to short anodic residence times and minimal chlorine production. Although H_2O_2 does not pose a health risk at these concentrations, its presence in potable water may be undesirable. While a solution could be achieved by either curtailing H_2O_2 production or increasing the fluence to destroy all the H_2O_2, this has a tradeoff of either lower transformation of organics or increasing energy demand, respectively. For point-of-use water treatment systems, it might be advantageous to investigate more catalytic materials for either activating H_2O_2 (i.e., converting it into $HO^{\bullet}$) or quenching residual H_2O_2. For example, anodic reactive electrochemical membranes that integrate physical separation with electrochemical oxidation have been described for water treatment as a means of maximizing contaminant transfer to the electrode (Zaky & Chaplin, 2013). Employing either a porous electrode in a dual cathode setup and/or as an anode could promote reduction of H_2O_2 to $HO^{\bullet}$ or oxidation of H_2O_2 to H_2O. The former approach could serve as a replacement for the energy-intensive UV lamp and potentially aid in the degradation of recalcitrant organics by promoting direct oxidation on the electrode (e.g., fluorinated organics) (Chaplin, 2014). Alternatively, it may be possible to remove excess H_2O_2 by passing it though activated carbon, a high surface area catalyst consisting of metal oxide (Salem *et al.*, 2000) or silver (Anipsitakis & Dionysiou, 2004), or a more catalytic anode for chlorine evolution (e.g., blue TiO_2 Nanotubes) (Yang & Hoffmann, 2016).

The majority of the energy required for operation comes is associated with the low-pressure mercury UV lamp, with only 8-14% of the energy attributable to the electrochemical production of H_2O_2. Significant room for improvement exists for optimizing the energy use during UV treatment. As discussed above, one possible strategy is to replace the UV lamp with a reactive electrochemical membrane, however, investigation into their efficiency of $HO^{\bullet}$ production from H_2O_2 is needed. Another potential approach involves the use of UV light emitting diodes (LEDs). Presently, the current power output, lifetimes, and costs of this technology preclude it from being a viable replacement of low-pressure UV lamps for drinking

water treatment, although substantial advances in the technology are projected in the next decade (Chatterley & Linden, 2010).

Investigation into the feasibility of the point-of-use treatment system to meet residential water demand (e.g., 200 L person^{-1} day^{-1}) and perform for extended durations under real-world conditions are needed to aid in its uptake. The 64 cm^2 cathode tested at the bench scale was able to accommodate flow rates up to 250 L d^{-1}, at which point the system was limited not by the cathode's ability to produce H_2O_2 but by high transmembrane pressure, which caused water to diffuse back through the pores. Modification of the gas diffusion electrode with more polytetrafluoroethylene binder could enhance the transmembrane strength of the electrode. Higher flow rates could also be accomplished by transitioning from a parallel plate design to a tubular design, which would increase the surface area of the cathode exposed to the air (Figure 5.1).

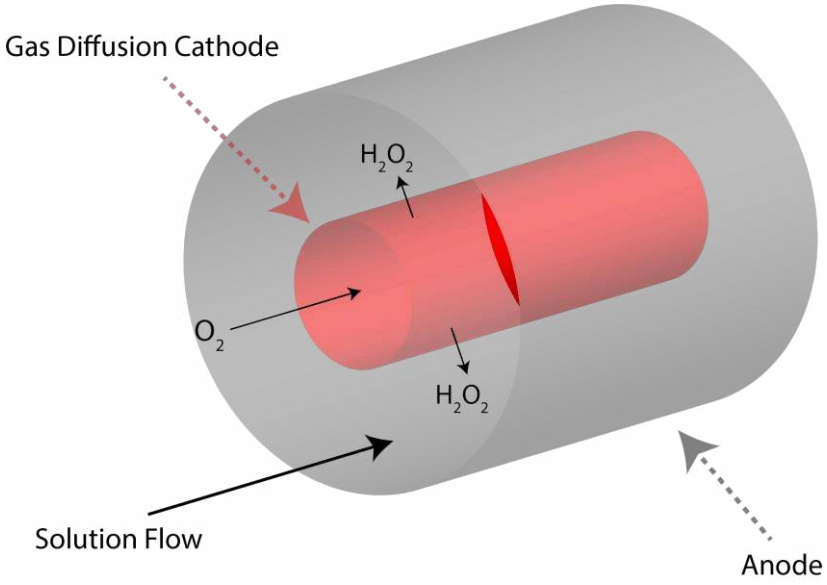

Figure 5.1: Proposed tubular design for the electrochemical cell

Additional research is needed to assess long-term system performance under realistic operating conditions. While the system was able to maintain H_2O_2 production rates through 6000 L of tap water, challenge tests with more heterogenous matrices such as wastewater treatment plant effluent are needed as a worst-case scenario.

In Chapter 2, we demonstrated that anodic oxidation of waters containing Cl^- and Br^- often produces a suite of toxic halogenated transformation products. While the modular treatment system driven by cathodic hydrogen peroxide production did not produce halogenated transformation products, oxidation by UV light and $HO^\bullet$ typically results in modification of the parent compound rather than complete mineralization (Prasse *et al.*, 2015). Transformation products of the test compounds that were identified typically accounted for less than 10% of the transformed parent compound. Although it is impractical to identify all transformation products, it may be beneficial to determine if compounds with known toxicity are being formed (e.g.,

aliphatic aldehydes). Such studies could be conducted using *in vitro* cytotoxicity and genotoxicity assays using mammalian cells (e.g., Chinese hamster ovary cells) (Jeong *et al.*, 2015).

Finally, the system described in Chapter 4 showed promise as a low-cost means of removing trace elements through sorption onto iron oxides that were formed during oxidation of soluble metal-NOM complexes. Challenges still remain in evaluating the mass of settled colloids that accumulate after prolonged treatment and potential low-cost means of removing them. Additionally, the treatment efficiency was dependent on the initial iron concentration in the contaminated aquifer, and thus, the effectiveness of the treatment system may be limited to certain aquifers. The findings of this research, however, may offer substantial promise for decreasing operational costs and increasing process efficiency of iron-based electrocoagulation techniques by reducing the need for electrode cleaning, replacement, and sludge disposal simply though integration of a UV lamp.

The effects of UV irradiation on iron oxide colloid formation at varying metal-to-NOM ratios are not well understood. In particular, under conditions where the concentration of dissolved metal ions exceed those of dissolved NOM, such as in electrocoagulation, NOM may compete with trace elements for mineral surfaces, alter colloid aggregation, and either enhance or inhibit dissolution (Aiken *et al.*, 2011). Therefore, investigation into the effect of UV photolysis under varying metal-to-NOM ratios is needed. Additional investigation may be needed into the fate and transformation of other metal-binding functional groups, such as amine and thiol moieties, during treatment.

References

Acero, J. L., Stemmler, K., & Von Gunten, U. (2000). Degradation kinetics of atrazine and its degradation products with ozone and OH radicals: A predictive tool for drinking water treatment. *Environmental Science & Technology, 34*(4), 591-597. doi:10.1021/es990724e

Aeschbacher, M., Graf, C., Schwarzenbach, R. P., & Sander, M. (2012). Antioxidant Properties of Humic Substances. *Environmental Science & Technology, 46*(9), 4916-4925. doi:10.1021/es300039h

Aiken, G. R., Hsu-Kim, H., & Ryan, J. N. (2011). Influence of Dissolved Organic Matter on the Environmental Fate of Metals, Nanoparticles, and Colloids. *Environmental Science & Technology, 45*(8), 3196-3201. doi:10.1021/es103992s

Allard, S., Fouche, L., Dick, J., Heitz, A., & von Gunten, U. (2013). Oxidation of Manganese(II) during Chlorination: Role of Bromide. *Environmental Science & Technology, 47*(15), 8716-8723. doi:10.1021/es401304r

American Public Health, A., Eaton, A. D., American Water Works, A., & Water Environment, F. (2005). *Standard methods for the examination of water and wastewater*. Washington, D.C.: APHA-AWWA-WEF.

Anglada, Á., Urtiaga, A., Ortiz, I., Mantzavinos, D., & Diamadopoulos, E. (2011). Boron-doped diamond anodic treatment of landfill leachate: Evaluation of operating variables and formation of oxidation by-products. *Water Research, 45*(2), 828-838. doi:https://doi.org/10.1016/j.watres.2010.09.017

Anipsitakis, G. P., & Dionysiou, D. D. (2004). Radical generation by the interaction of transition metals with common oxidants. *Environmental Science and Technology, 38*(13), 3705-3712. doi:10.1021/es035121o

Appiani, E., Page, S. E., & McNeill, K. (2014). On the Use of Hydroxyl Radical Kinetics to Assess the Number-Average Molecular Weight of Dissolved Organic Matter. *Environmental Science & Technology, 48*(20), 11794-11802. doi:10.1021/es5021873

Azizi, O., Hubler, D., Schrader, G., Farrell, J., & Chaplin, B. P. (2011). Mechanism of Perchlorate Formation on Boron-Doped Diamond Film Anodes. *Environmental Science & Technology, 45*(24), 10582-10590. doi:10.1021/es202534w

Baeza, C., & Knappe, D. R. U. (2011). Transformation kinetics of biochemically active compounds in low-pressure UV Photolysis and UV/H2O2 advanced oxidation processes. *Water Research, 45*(15), 4531-4543. doi:10.1016/j.watres.2011.05.039

Bagastyo, A. Y., Batstone, D. J., Rabaey, K., & Radjenovic, J. (2013). Electrochemical oxidation of electrodialysed reverse osmosis concentrate on Ti/Pt-IrO2, Ti/SnO2-Sb and boron-doped diamond electrodes. *Water Research, 47*(1), 242-250. doi:10.1016/j.watres.2012.10.001

Bagastyo, A. Y., Radjenovic, J., Mu, Y., Rozendal, R. A., Batstone, D. J., & Rabaey, K. (2011). Electrochemical oxidation of reverse osmosis concentrate on mixed metal oxide (MMO) titanium coated electrodes. *Water Research, 45*(16), 4951-4959. doi:10.1016/j.watres.2011.06.039

Balci, B., Oturan, N., Cherrier, R., & Oturan, M. A. (2009). Degradation of atrazine in aqueous medium by electrocatalytically generated hydroxyl radicals. A kinetic and mechanistic study. *Water Research, 43*(7), 1924-1934. doi:10.1016/j.watres.2009.01.021

Barazesh, J. M., Hennebel, T., Jasper, J. T., & Sedlak, D. L. (2015). Modular Advanced Oxidation Process Enabled by Cathodic Hydrogen Peroxide Production. *Environmental Science & Technology, 49*(12), 7391-7399. doi:10.1021/acs.est.5b01254

Barazesh, J. M., Prasse, C., & Sedlak, D. L. (2016). Electrochemical Transformation of Trace Organic Contaminants in the Presence of Halide and Carbonate Ions. *Environmental Science & Technology, 50*(18), 10143-10152. doi:10.1021/acs.est.6b02232

Barbeau, K. (2006). Photochemistry of Organic Iron(III) Complexing Ligands in Oceanic Systems. *Photochemistry and Photobiology, 82*(6), 1505-1516. doi:10.1111/j.1751-1097.2006.tb09806.x

Benotti, M. J., Trenholm, R. A., Vanderford, B. J., Holady, J. C., Stanford, B. D., & Snyder, S. A. (2008). Pharmaceuticals and endocrine disrupting compounds in U.S. drinking water. *Environmental Science and Technology, 43*(3), 597-603.

Benotti, M. J., Trenholm, R. A., Vanderford, B. J., Holady, J. C., Stanford, B. D., & Snyder, S. A. (2009). Pharmaceuticals and Endocrine Disrupting Compounds in US Drinking Water. *Environmental Science & Technology, 43*(3), 597-603. doi:10.1021/es801845a

Bergmann, M. E. H., Koparal, A. S., & Iourtchouk, T. (2014). Electrochemical Advanced Oxidation Processes, Formation of Halogenate and Perhalogenate Species: A Critical Review. *Critical Reviews in Environmental Science and Technology, 44*(4), 348-390. doi:10.1080/10643389.2012.718948

Bergmann, M. E. H., Rollin, J., & Iourtchouk, T. (2009). The occurrence of perchlorate during drinking water electrolysis using BDD anodes. *Electrochimica Acta, 54*(7), 2102-2107. doi:10.1016/j.electacta.2008.09.040

Bichai, F., Ryan, H., Fitzgerald, C., Williams, K., Abdelmoteleb, A., Brotchie, R., & Komatsu, R. (2015). Understanding the role of alternative water supply in an urban water security strategy: an analytical framework for decision-making. *Urban Water Journal, 12*(3), 175-189. doi:10.1080/1573062x.2014.895844

Bolton, J. R., Bircher, K. G., Tumas, W., & Tolman, C. A. (2001). Figures-of-merit for the technical development and application of advanced oxidation technologies for both electric- and solar-driven systems - (IUPAC Technical Report). *Pure and Applied Chemistry, 73*(4), 627-637. doi:10.1351/pac200173040627

Bolton, J. R., & Linden, K. G. (2003). Standardization of methods for fluence (UV dose) determination in bench-scale UV experiments. *Journal of Environmental Engineering-Asce, 129*(3), 209-215. doi:10.1061/(asce)0733-9372(2003)129:3(209)

Bolton, J. R., & Stefan, M. I. (2002). Fundamental photochemical approach to the concepts of fluence (UV dose) and electrical energy efficiency in photochemical degradation reactions. *Research on Chemical Intermediates, 28*(7-9), 857-870. doi:10.1163/15685670260469474

Bonvin, F., Jost, L., Randin, L., Bonvin, E., & Kohn, T. (2016). Super-fine powdered activated carbon (SPAC) for efficient removal of micropollutants from wastewater treatment plant effluent. *Water Research, 90*, 90-99. doi:https://doi.org/10.1016/j.watres.2015.12.001

Bradley, P. M., Journey, C. A., Romanok, K. M., Barber, L. B., Buxton, H. T., Foreman, W. T., . . . Villeneuve, D. L. (2017). Expanded Target-Chemical Analysis Reveals Extensive Mixed-Organic-Contaminant Exposure in U.S. Streams. *Environmental Science & Technology*. doi:10.1021/acs.est.7b00012

Brillas, E., Sires, I., & Oturan, M. A. (2009). Electro-Fenton process and related electrochemical technologies based on Fenton's reaction chemistry. *Chemical Reviews, 109*(12), 6570-6631. doi:10.1021/cr900136g

Brunmark, A., & Cadenas, E. (1987). Electronically excited state generation during the reaction of p-benzoquinone with H2O2: Relation to product formation: 2-OH-and 2, 3-epoxy-p-benzoquinone the effect of glutathione. *Free Radical Biology and Medicine, 3*(3), 169-180.

Butkovskyi, A., Jeremiasse, A. W., Leal, L. H., van der Zande, T., Rijnaarts, H., & Zeeman, G. (2014). Electrochemical conversion of micropollutants in gray water. *Environmental Science and Technology, 48*(3), 1893-1901. doi:10.1021/es404411p

Buxton, G. V., Bydder, M., Salmon, G. A., & Williams, J. E. (2000). The reactivity of chlorine atoms in aqueous solution. Part III. The reactions of Cl-center dot with solutes. *Physical Chemistry Chemical Physics, 2*(2), 237-245.

Buxton, G. V., Greenstock, C. L., Helman, W. P., & Ross, A. B. (1988). CRITICAL-REVIEW OF RATE CONSTANTS FOR REACTIONS OF HYDRATED ELECTRONS, HYDROGEN-ATOMS AND HYDROXYL RADICALS (.OH/.O-) IN AQUEOUS-SOLUTION. *Journal of Physical and Chemical Reference Data, 17*(2), 513-886.

Buxton, G. V., Greenstock, C. L., Helman, W. P., & Ross, A. B. (1988). Critical review of rate constants for reactions of hydrated electrons, hydrogen atoms, and hydroxyl radicals (.OH/.O-) in aqueous solution. *Journal of Physical and Chemical Reference Data, 17*(2), 513-886.

Campos-Martin, J. M., Blanco-Brieva, G., & Fierro, J. L. G. (2006). Hydrogen peroxide synthesis: An outlook beyond the anthraquinone process. *Angewandte Chemie-International Edition, 45*(42), 6962-6984. doi:10.1002/anie.200503779

Canonica, S., Kohn, T., Mac, M., Real, F. J., Wirz, J., & von Gunten, U. (2005). Photosensitizer Method to Determine Rate Constants for the Reaction of Carbonate Radical with Organic Compounds. *Environmental Science & Technology, 39*(23), 9182-9188. doi:10.1021/es051236b

Canonica, S., Meunier, L., & Von Gunten, U. (2008). Phototransformation of selected pharmaceuticals during UV treatment of drinking water. *Water Research, 42*(1-2), 121-128. doi:10.1016/j.watres.2007.07.026

Cater, S. R., Stefan, M. I., Bolton, J. R., & Safarzadeh-Amiri, A. (2000). UV/H2O2 treatment of methyl tert-butyl ether in contaminated waters. *Environmental Science & Technology, 34*(4), 659-662. doi:10.1021/es9905750

Celdran, R., & Gonzalezvelasco, J. J. (1981). OXIDATION MECHANISM OF ALLYL ALCOHOL ON AN AU-ELECTRODE IN BASIC SOLUTIONS. *Electrochimica Acta, 26*(4), 525-533. doi:10.1016/0013-4686(81)87033-8

Chaplin, B. P. (2014). Critical review of electrochemical advanced oxidation processes for water treatment applications. *Environmental Science-Processes & Impacts, 16*(6), 1182-1203. doi:10.1039/c3em00679d

Chatterley, C., & Linden, K. (2010). Demonstration and evaluation of germicidal UV-LEDs for point-of-use water disinfection. *Journal of Water and Health, 8*(3), 479-486. doi:10.2166/wh.2010.124

Chini, C. M., Schreiber, K. L., Barker, Z. A., & Stillwell, A. S. (2016). Quantifying Energy and Water Savings in the U.S. Residential Sector. *Environmental Science & Technology, 50*(17), 9003-9012. doi:10.1021/acs.est.6b01559

Cho, K., & Hoffmann, M. R. (2014). Urea Degradation by Electrochemically Generated Reactive Chlorine Species: Products and Reaction Pathways. *Environmental Science & Technology, 48*(19), 11504-11511. doi:10.1021/es5025405

Cho, K., Qu, Y., Kwon, D., Zhang, H., Cid, C. A., Aryanfar, A., & Hoffmann, M. R. (2014). Effects of Anodic Potential and Chloride Ion on Overall Reactivity in Electrochemical Reactors Designed for Solar-Powered Wastewater Treatment. *Environmental Science & Technology, 48*(4), 2377-2384. doi:10.1021/es404137u

Comninellis, C. (1994). ELECTROCATALYSIS IN THE ELECTROCHEMICAL CONVERSION/COMBUSTION OF ORGANIC POLLUTANTS FOR WASTE-WATER TREATMENT. *Electrochimica Acta, 39*(11-12), 1857-1862. doi:10.1016/0013-4686(94)85175-1

Comninellis, C., Kapalka, A., Malato, S., Parsons, S. A., Poulios, I., & Mantzavinos, D. (2008). Advanced oxidation processes for water treatment: advances and trends for R&D. *Journal of Chemical Technology & Biotechnology, 83*(6), 769-776. doi:10.1002/jctb.1873

Connick, R. E. (1947). The Interaction of Hydrogen Peroxide and Hypochlorous Acid in Acidic Solution containing Chloride Ion. *Journal of the American Chemical Society, 69*(6), 1509-1514. doi:10.1021/ja01198a074

Consonni, V., Trasatti, S., Pollak, F., & Ogrady, W. E. (1987). Mechanism of chlorine evolution on oxide anodes - study of pH effects. *Journal of Electroanalytical Chemistry, 228*(1-2), 393-406. doi:10.1016/0022-0728(87)80119-5

Dahlgren, E., Göçmen, C., Lackner, K., & van Ryzin, G. (2013). Small Modular Infrastructure. *The Engineering Economist, 58*(4), 231-264. doi:10.1080/0013791X.2013.825038

Daughton, C. G., & Ternes, T. A. (1999). Pharmaceuticals and personal care products in the environment: agents of subtle change? *Environmental Health Perspectives, 107*(Suppl 6), 907-938.

DDB Engineering, I. (2013). *Groundwater Replenishment System 2013 Annual Report*. Retrieved from

De Battisti, A., Ferro, S., & Dal Colle, M. (2001). Electrocatalysis at conductive diamond modified by noble-metal oxides. *Journal of Physical Chemistry B, 105*(9), 1679-1682. doi:10.1021/jp003216w

De Laurentiis, E., Prasse, C., Ternes, T. A., Minella, M., Maurino, V., Minero, C., . . . Vione, D. (2014). Assessing the photochemical transformation pathways of acetaminophen relevant to surface waters: Transformation kinetics, intermediates, and modelling. *Water Research, 53*, 235-248. doi:10.1016/j.watres.2014.01.016

Deborde, M., & von Gunten, U. (2008). Reactions of chlorine with inorganic and organic compounds during water treatment - Kinetics and mechanisms: A critical review. *Water Research, 42*(1-2), 13-51. doi:10.1016/j.watres.2007.07.025

Del Vecchio, R., & Blough, N. V. (2002). Photobleaching of chromophoric dissolved organic matter in natural waters: kinetics and modeling. *Marine Chemistry, 78*(4), 231-253. doi:https://doi.org/10.1016/S0304-4203(02)00036-1

Delaire, C., van Genuchten, C. M., Nelson, K. L., Amrose, S. E., & Gadgil, A. J. (2015). Escherichia coli Attenuation by Fe Electrocoagulation in Synthetic Bengal Groundwater: Effect of pH and Natural Organic Matter. *Environmental Science & Technology, 49*(16), 9945-9953. doi:10.1021/acs.est.5b01696

Dittmar, T., Koch, B., Hertkorn, N., & Kattner, G. (2008). A simple and efficient method for the solid-phase extraction of dissolved organic matter (SPE-DOM) from seawater. *Limnol. Oceanogr. Methods, 6*, 230-235.

Dixit, S., & Hering, J. G. (2003). Comparison of Arsenic(V) and Arsenic(III) Sorption onto Iron Oxide Minerals: Implications for Arsenic Mobility. *Environmental Science & Technology, 37*(18), 4182-4189. doi:10.1021/es030309t

Dodd, M. C., & Huang, C.-H. (2004). Transformation of the Antibacterial Agent Sulfamethoxazole in Reactions with Chlorine: Kinetics, Mechanisms, and Pathways. *Environmental Science & Technology, 38*(21), 5607-5615. doi:10.1021/es035225z

Dodd, M. C., & Huang, C. H. (2007). Aqueous chlorination of the antibacterial agent trimethoprim: Reaction kinetics and pathways. *Water Research, 41*(3), 647-655. doi:10.1016/j.watres.2006.10.029

Dodd, M. C., Zuleeg, S., Gunten, U. v., & Pronk, W. (2008). Ozonation of Source-Separated Urine for Resource Recovery and Waste Minimization: Process Modeling, Reaction Chemistry, and Operational Considerations. *Environmental Science & Technology, 42*(24), 9329-9337. doi:10.1021/es800560r

Doelsch, E., Rose, J., Masion, A., Bottero, J. Y., Nahon, D., & Bertsch, P. M. (2000). Speciation and crystal chemistry of iron (III) chloride hydrolyzed in the presence of SiO4 ligands. 1. An Fe K-edge EXAFS study. *Langmuir, 16*(10), 4726-4731.

Dong, M. M., & Rosario-Ortiz, F. L. (2012). Photochemical Formation of Hydroxyl Radical from Effluent Organic Matter. *Environmental Science & Technology, 46*(7), 3788-3794. doi:10.1021/es2043454

Dotson, A. D., Keen, V. S., Metz, D., & Linden, K. G. (2010). UV/H2O2 treatment of drinking water increases post-chlorination DBP formation. *Water Research, 44*(12), 3703-3713. doi:10.1016/j.watres.2010.04.006

Eaton, A. D., Clesceri, L. S., Greenberg, A. E., Franson, M. A. H., American Public Health, A., American Water Works, A., & Water Environment, F. (1998). *Standard methods for the examination of water and wastewater*. Washington, DC: American Public Health Association.

Eggen, R. I. L., Hollender, J., Joss, A., Schärer, M., & Stamm, C. (2014). Reducing the Discharge of Micropollutants in the Aquatic Environment: The Benefits of Upgrading Wastewater Treatment Plants. *Environmental Science & Technology, 48*(14), 7683-7689. doi:10.1021/es500907n

Eisenberg, G. M. (1943). Colorimetric determination of hydrogen peroxide. *Industrial and Engineering Chemistry, 15*(5), 327-328.

Englehardt, J. D., Wu, T., & Tchobanoglous, G. (2013). Urban net-zero water treatment and mineralization: Experiments, modeling and design. *Water Research, 47*(13), 4680-4691. doi:10.1016/j.watres.2013.05.026

Erenburg, R. G. (1984). MECHANISM OF THE CHLORINE REACTION OF RUTHENIUM-TITANIUM OXIDE ANODES. *Soviet Electrochemistry, 20*(12), 1481-1486.

Eversloh, C. L., Henning, N., Schulz, M., & Ternes, T. A. (2014). Electrochemical treatment of iopromide under conditions of reverse osmosis concentrates - Elucidation of the degradation pathway. *Water Research, 48*, 237-246. doi:10.1016/j.watres.2013.09.035

Eversloh, C. L., Schulz, M., Wagner, M., & Ternes, T. A. (2015). Electrochemical oxidation of tramadol in low-salinity reverse osmosis concentrates using boron-doped diamond anodes. *Water Research, 72*, 293-304. doi:10.1016/j.watres.2014.12.021

Farhat, A., Keller, J., Tait, S., & Radjenovic, J. (2015). Removal of Persistent Organic Contaminants by Electrochemically Activated Sulfate. *Environmental Science & Technology, 49*(24), 14326-14333. doi:10.1021/acs.est.5b02705

Faust, B. C., & Zepp, R. G. (1993). Photochemistry of aqueous iron(III)-polycarboxylate complexes: roles in the chemistry of atmospheric and surface waters. *Environmental Science & Technology, 27*(12), 2517-2522. doi:10.1021/es00048a032

Ferro, S., & Battisti, A. D. (2004). The Bromine Electrode. Part I: Adsorption Phenomena at Polycrystalline Platinum Electrodes. *Journal of Applied Electrochemistry, 34*(10), 981-987. doi:10.1023/B:JACH.0000042666.25746.e6

Ferro, S., & De Battisti, A. (2002). Electrocatalysis and Chlorine Evolution Reaction at Ruthenium Dioxide Deposited on Conductive Diamond. *The Journal of Physical Chemistry B, 106*(9), 2249-2254. doi:10.1021/jp012195i

Ferro, S., Orsan, C., & De Battisti, A. (2005). The bromine electrode Part II: reaction kinetics at polycrystalline Pt. *Journal of Applied Electrochemistry, 35*(3), 273-278. doi:10.1007/s10800-004-6773-8

Fimmen, R. L., Cory, R. M., Chin, Y.-P., Trouts, T. D., & McKnight, D. M. (2007). Probing the oxidation–reduction properties of terrestrially and microbially derived dissolved organic matter. *Geochimica Et Cosmochimica Acta, 71*(12), 3003-3015. doi:http://doi.org/10.1016/j.gca.2007.04.009

Foller, P. C., & Bombard, R. T. (1995). Processes for the production of mixtures of caustic soda and hydrogen-peroxide via the reduction of oxygen. *Journal of Applied Electrochemistry, 25*(7), 613-627.

Fujii, M., Rose, A. L., Waite, T. D., & Omura, T. (2008). Effect of divalent cations on the kinetics of Fe(III) complexation by organic ligands in natural waters. *Geochimica Et Cosmochimica Acta, 72*(5), 1335-1349. doi:http://dx.doi.org/10.1016/j.gca.2007.12.017

Fujii, M., Yeung, A. C. Y., & Waite, T. D. (2015). Competitive Effects of Calcium and Magnesium Ions on the Photochemical Transformation and Associated Cellular Uptake of Iron by the Freshwater Cyanobacterial Phytoplankton Microcystis aeruginosa. *Environmental Science & Technology, 49*(15), 9133-9142. doi:10.1021/acs.est.5b01583

Giguère, P. A., & Herman, K. (1976). A remarkably long-lived radical: The aminoperoxy, NH2O2. *Chemical Physics Letters, 44*(2), 273-276. doi:http://dx.doi.org/10.1016/0009-2614(76)80508-8

Gikas, P., & Tchobanoglous, G. (2009). The role of satellite and decentralized strategies in water resources management. *Journal of Environmental Management, 90*(1), 144-152. doi:10.1016/j.jenvman.2007.08.016

Gilbert, B. C., Stell, J. K., Peet, W. J., & Radford, K. J. (1988). Generation and reactions of the chlorine atom in aqueous solution. *Journal of the Chemical Society, Faraday Transactions 1: Physical Chemistry in Condensed Phases, 84*(10), 3319-3330. doi:10.1039/F19888403319

Gleeson, T., Wada, Y., Bierkens, M. F. P., & van Beek, L. P. H. (2012). Water balance of global aquifers revealed by groundwater footprint. *Nature, 488*(7410), 197-200. doi:http://www.nature.com/nature/journal/v488/n7410/abs/nature11295.html#supplementary-information

Goldstone, J. V., & Voelker, B. M. (2000). Chemistry of Superoxide Radical in Seawater: CDOM Associated Sink of Superoxide in Coastal Waters. *Environmental Science & Technology, 34*(6), 1043-1048. doi:10.1021/es9905445

Grebel, J. E., Pignatello, J. J., & Mitch, W. A. (2010). Effect of Halide Ions and Carbonates on Organic Contaminant Degradation by Hydroxyl Radical-Based Advanced Oxidation Processes in Saline Waters. *Environmental Science & Technology, 44*(17), 6822-6828. doi:10.1021/es1010225

Haag, W. R., & Mill, T. (1987). RATE CONSTANTS FOR INTERACTION OF 1O21Δg) WITH AZIDE ION IN WATER. *Photochemistry and Photobiology, 45*(3), 317-321. doi:10.1111/j.1751-1097.1987.tb05381.x

Held, A. M., Halko, D. J., & Hurst, J. K. (1978). Mechanisms of Chlorine Oxidation of Hydrogen Peroxide. *Journal of the American Chemical Society, 100*(18), 5732-5740. doi:10.1021/ja00486a025

Helms, J. R., Stubbins, A., Ritchie, J. D., Minor, E. C., Kieber, D. J., & Mopper, K. (2008). Absorption spectral slopes and slope ratios as indicators of molecular weight, source, and photobleaching of chromophoric dissolved organic matter. *Limnology and Oceanography, 53*(3), 955-969. doi:10.4319/lo.2008.53.3.0955

Hering, J. G., Waite, T. D., Luthy, R. G., Drewes, J. E., & Sedlak, D. L. (2013). A Changing Framework for Urban Water Systems. *Environmental Science & Technology, 47*(19), 10721-10726. doi:10.1021/es4007096

Hernandez-Leal, L., Temmink, H., Zeeman, G., & Buisman, C. J. N. (2011). Removal of micropollutants from aerobically treated grey water via ozone and activated carbon. *Water Research, 45*(9), 2887-2896.

Huang, L., Li, L., Dong, W., Liu, Y., & Hou, H. (2008). Removal of Ammonia by OH Radical in Aqueous Phase. *Environmental Science & Technology, 42*(21), 8070-8075. doi:10.1021/es8008216

Huber, M. M., Canonica, S., Park, G.-Y., & von Gunten, U. (2003). Oxidation of Pharmaceuticals during Ozonation and Advanced Oxidation Processes. *Environmental Science & Technology, 37*(5), 1016-1024. doi:10.1021/es025896h

Hug, S. J., Canonica, L., Wegelin, M., Gechter, D., & von Gunten, U. (2001). Solar Oxidation and Removal of Arsenic at Circumneutral pH in Iron Containing Waters. *Environmental Science & Technology, 35*(10), 2114-2121. doi:10.1021/es001551s

Jasper, J. T., Jones, Z. L., Sharp, J. O., & Sedlak, D. L. (2014). Biotransformation of trace organic contaminants in open-water unit process treatment wetlands. *Environmental Science and Technology, 48*(9), 5136-5144. doi:10.1021/es500351e

Jasper, J. T., & Sedlak, D. L. (2013). Phototransformation of Wastewater-Derived Trace Organic Contaminants in Open-Water Unit Process Treatment Wetlands. *Environmental Science & Technology, 47*(19), 10781-10790. doi:10.1021/es304334w

Jasper, J. T., Shafaat, O. S., & Hoffmann, M. R. (2016). Electrochemical Transformation of Trace Organic Contaminants in Latrine Wastewater. *Environmental Science & Technology, 50*(18), 10198-10208. doi:10.1021/acs.est.6b02912

Jeong, C. H., Postigo, C., Richardson, S. D., Simmons, J. E., Kimura, S. Y., Mariñas, B. J., . . . Plewa, M. J. (2015). Occurrence and Comparative Toxicity of Haloacetaldehyde Disinfection Byproducts in Drinking Water. *Environmental Science & Technology, 49*(23), 13749-13759. doi:10.1021/es506358x

Jeong, J., Kim, C., & Yoon, J. (2009). The effect of electrode material on the generation of oxidants and microbial inactivation in the electrochemical disinfection processes. *Water Research, 43*(4), 895-901. doi:10.1016/j.watres.2008.11.033

Jones, C. W. (1999). *Applications of hydrogen peroxide and derivates* Cambridge, U.K.: Royal Society of Chemistry.

Katsoyiannis, I. A., Canonica, S., & von Gunten, U. (2011). Efficiency and energy requirements for the transformation of organic micropollutants by ozone, O-3/H2O2 and UV/H2O2. *Water Research, 45*(13), 3811-3822. doi:10.1016/j.watres.2011.04.038

Kim, C., Kim, S., Choi, J., Lee, J., Kang, J. S., Sung, Y. E., . . . Yoon, J. (2014). Blue TiO2 Nanotube Array as an Oxidant Generating Novel Anode Material Fabricated by Simple Cathodic Polarization. *Electrochimica Acta, 141*, 113-119. doi:10.1016/j.electacta.2014.07.062

Kinniburgh, D. G., Milne, C. J., Benedetti, M. F., Pinheiro, J. P., Filius, J., Koopal, L. K., & Van Riemsdijk, W. H. (1996). Metal Ion Binding by Humic Acid: Application of the NICA-Donnan Model. *Environmental Science & Technology, 30*(5), 1687-1698. doi:10.1021/es950695h

Kiwi, J., Lopez, A., & Nadtochenko, V. (2000). Mechanism and kinetics of the OH-radical intervention during fenton oxidation in the presence of a significant amount of radical scavenger (Cl-). *Environmental Science & Technology, 34*(11), 2162-2168. doi:10.1021/es991406i

Koch, B. P., Dittmar, T., Witt, M., & Kattner, G. (2007). Fundamentals of molecular formula assignment to ultrahigh resolution mass data of natural organic matter. *Anal. Chem., 79*(4), 1758-1763. doi:10.1021/ac061949s

Kolpin, D. W., Furlong, E. T., Meyer, M. T., Thurman, E. M., Zaugg, S. D., Barber, L. B., & Buxton, H. T. (2002). Pharmaceuticals, Hormones, and Other Organic Wastewater Contaminants in U.S. Streams, 1999−2000: A National Reconnaissance. *Environmental Science & Technology, 36*(6), 1202-1211. doi:10.1021/es011055j

Kostich, M. S., Batt, A. L., & Lazorchak, J. M. (2014). Concentrations of prioritized pharmaceuticals in effluents from 50 large wastewater treatment plants in the US and implications for risk estimation. *Environmental Pollution, 184*, 354-359. doi:http://dx.doi.org/10.1016/j.envpol.2013.09.013

Krishtalik, L. I. (1981). KINETICS AND MECHANISM OF ANODIC CHLORINE AND OXYGEN EVOLUTION REACTIONS ON TRANSITION-METAL OXIDE ELECTRODES. *Electrochimica Acta, 26*(3), 329-337. doi:10.1016/0013-4686(81)85019-0

Kujawinski, E. B., & Behn, M. D. (2006). Automated analysis of electrospray ionization Fourier transform ion cyclotron resonance mass spectra of natural organic matter. *Anal. Chem., 78*(13), 4363-4373. doi:10.1021/ac0600306

Kumar, K., & Margerum, D. W. (1987). KINETICS AND MECHANISM OF GENERAL-ACID-ASSISTED OXIDATION OF BROMIDE BY HYPOCHLORITE AND HYPOCHLOROUS ACID. *Inorganic Chemistry, 26*(16), 2706-2711. doi:10.1021/ic00263a030

Kwan, W. P., & Voelker, B. M. (2002). Decomposition of hydrogen peroxide and organic compounds in the presence of dissolved iron and ferrihydrite. *Environmental Science & Technology, 36*(7), 1467-1476.

Larsen, A. T., Udert, K. M., & Lienert, J. (2013). *Source separation and decentralization for wastewater management*: IWA Publishing.

Larsen, T. A., Hoffmann, S., Lüthi, C., Truffer, B., & Maurer, M. (2016). Emerging solutions to the water challenges of an urbanizing world. *Science, 352*(6288), 928-933. doi:10.1126/science.aad8641

Larsen, T. A., Udert, K. M., & Lienert, J. (2013). *Source separation and decentralization for wastewater management*: IWA Publishing.

Laxminarayan, R., Duse, A., Wattal, C., Zaidi, A. K. M., Wertheim, H. F. L., Sumpradit, N., . . . Cars, O. (2013). Antibiotic resistance—the need for global solutions. *The Lancet Infectious Diseases, 13*(12), 1057-1098. doi:https://doi.org/10.1016/S1473-3099(13)70318-9

Lee, Y., Gerrity, D., Lee, M., Gamage, S., Pisarenko, A., Trenholm, R. A., . . . von Gunten, U. (2016). Organic Contaminant Abatement in Reclaimed Water by UV/H2O2 and a Combined Process Consisting of O-3/H2O2 Followed by UV/H2O2: Prediction of Abatement Efficiency, Energy Consumption, and Byproduct Formation. *Environmental Science & Technology, 50*(7), 3809-3819. doi:10.1021/acs.est.5b04904

Lee, Y., & von Gunten, U. (2010). Oxidative transformation of micropollutants during municipal wastewater treatment: Comparison of kinetic aspects of selective (chlorine, chlorine dioxide, ferrate(VI), and ozone) and non-selective oxidants (hydroxyl radical). *Water Research, 44*(2), 555-566. doi:10.1016/j.watres.2009.11.045

Lester, Y., Sharpless, C. M., Mamane, H., & Linden, K. G. (2013). Production of Photo-oxidants by Dissolved Organic Matter During UV Water Treatment. *Environmental Science & Technology, 47*(20), 11726-11733. doi:10.1021/es402879x

Liu, J., & Zhang, X. (2014). Comparative toxicity of new halophenolic DBPs in chlorinated saline wastewater effluents against a marine alga: Halophenolic DBPs are generally more toxic than haloaliphatic ones. *Water Research, 65*, 64-72. doi:http://dx.doi.org/10.1016/j.watres.2014.07.024

Liu, R. S. H., Turro, N. J., & Hammond, G. S. (1965). Mechanisms of Photochemical Reactions in Solution. XXXI. Activation and Deactivation of Conjugated Dienes by Energy Transfer. *Journal of the American Chemical Society, 87*(15), 3406-3412. doi:10.1021/ja01093a021

Liu, Y., Hejazi, M., Kyle, P., Kim, S. H., Davies, E., Miralles, D. G., . . . Niyogi, D. (2016). Global and Regional Evaluation of Energy for Water. *Environmental Science & Technology, 50*(17), 9736-9745. doi:10.1021/acs.est.6b01065

Lütke Eversloh, C., Schulz, M., Wagner, M., & Ternes, T. A. (2015). Electrochemical oxidation of tramadol in low-salinity reverse osmosis concentrates using boron-doped diamond anodes. *Water Research, 72*, 293-304. doi:https://doi.org/10.1016/j.watres.2014.12.021

Maizel, A. C., & Remucal, C. K. (2017). The effect of advanced secondary municipal wastewater treatment on the molecular composition of dissolved organic matter. *Water Res., 122*, 42-52.

Maizel, A. C., & Remucal, C. K. (2017). Molecular Composition and Photochemical Reactivity of Size-Fractionated Dissolved Organic Matter. *Environmental Science & Technology, 51*(4), 2113-2123. doi:10.1021/acs.est.6b05140

Malpass, G. R. P., Miwa, D. W., Machado, S. A. S., Olivi, P., & Motheo, A. J. (2006). Oxidation of the pesticide atrazine at DSA (R) electrodes. *Journal of Hazardous Materials, 137*(1), 565-572. doi:10.1016/j.jhazmat.2006.02.045

McArthur, J., Banerjee, D., Hudson-Edwards, K., Mishra, R., Purohit, R., Ravenscroft, P., . . . Talukder, T. (2004). Natural organic matter in sedimentary basins and its relation to arsenic in anoxic ground water: the example of West Bengal and its worldwide implications. *Applied Geochemistry, 19*(8), 1255-1293.

McFadden, M., Giani, R., Kwan, P., & Reiber, S. H. (2011). Contributions to drinking water lead from galvanized iron corrosion scales. *American Water Works Association. Journal, 103*(4), 76.

McKenzie, R. (1980). The adsorption of lead and other heavy metals on oxides of manganese and iron. *Soil Research, 18*(1), 61-73. doi:https://doi.org/10.1071/SR9800061

McNeill, K., & Canonica, S. (2016). Triplet state dissolved organic matter in aquatic photochemistry: reaction mechanisms, substrate scope, and photophysical properties. *Environmental Science: Processes & Impacts, 18*(11), 1381-1399. doi:10.1039/C6EM00408C

Mekonnen, M. M., & Hoekstra, A. Y. (2016). Four billion people facing severe water scarcity. *Science Advances, 2*(2). doi:10.1126/sciadv.1500323

Milne, C. J., Kinniburgh, D. G., van Riemsdijk, W. H., & Tipping, E. (2003). Generic NICA−Donnan Model Parameters for Metal-Ion Binding by Humic Substances. *Environmental Science & Technology, 37*(5), 958-971. doi:10.1021/es0258879

Mitch, W. A., Sharp, J. O., Trussell, R. R., Valentine, R. L., Alvarez-Cohen, L., & Sedlak, D. L. (2003). N-Nitrosodimethylamine (NDMA) as a Drinking Water Contaminant: A Review. *Environmental Engineering Science, 20*(5), 389-404. doi:10.1089/109287503768335896

Modin, O., & Fukushi, K. (2013). Production of high concentrations of H2O2 in a bioelectrochemical reactor fed with real municipal wastewater. *Environmental Technology, 34*(19), 2737-2742. doi:10.1080/09593330.2013.788041

Monteiro, S. C., & Boxall, A. B. A. (2010). Occurrence and Fate of Human Pharmaceuticals in the Environment *Reviews of Environmental Contamination and Toxicology* (pp. 53-154). New York, NY: Springer New York.

Morrissey, C. A., Mineau, P., Devries, J. H., Sanchez-Bayo, F., Liess, M., Cavallaro, M. C., & Liber, K. (2015). Neonicotinoid contamination of global surface waters and associated risk to aquatic invertebrates: A review. *Environment International, 74*, 291-303. doi:https://doi.org/10.1016/j.envint.2014.10.024

Nair, S., George, B., Malano, H. M., Arora, M., & Nawarathna, B. (2014). Water-energy-greenhouse gas nexus of urban water systems: Review of concepts, state-of-art and methods. *Resources Conservation and Recycling, 89*, 1-10. doi:10.1016/j.resconrec.2014.05.007

Neta, P., Huie, R. E., & Ross, A. B. (1988). RATE CONSTANTS FOR REACTIONS OF INORGANIC RADICALS IN AQUEOUS-SOLUTION. *Journal of Physical and Chemical Reference Data, 17*(3), 1027-1284.

Neta, P., Huie, R. E., & Ross, A. B. (1988). Rate constants for reactions of inorganic radicals in aqueous solution. *Journal of Physical and Chemical Reference Data, 17*(3), 1027-1284. doi:doi:http://dx.doi.org/10.1063/1.555808

Neta, P., Maruthamuthu, P., Carton, P. M., & Fessenden, R. W. (1978). Formation and reactivity of the amino radical. *The Journal of Physical Chemistry, 82*(17), 1875-1878. doi:10.1021/j100506a004

Niemuth, N. J., Jordan, R., Crago, J., Blanksma, C., Johnson, R., & Klaper, R. D. (2015). Metformin exposure at environmentally relevant concentrations causes potential endocrine disruption in adult male fish. *Environmental Toxicology and Chemistry, 34*(2), 291-296. doi:10.1002/etc.2793

Notre Dame Radiation Laboratory. Radiation Chemistry Data Center, Kinetics Database. (2002). Retrieved from www.rcrd.nd.edu

Nurmi, J. T., & Tratnyek, P. G. (2002). Electrochemical Properties of Natural Organic Matter (NOM), Fractions of NOM, and Model Biogeochemical Electron Shuttles. *Environmental Science & Technology, 36*(4), 617-624. doi:10.1021/es0110731

Oki, T., & Kanae, S. (2006). Global Hydrological Cycles and World Water Resources. *Science, 313*(5790), 1068-1072. doi:10.1126/science.1128845

Oturan, N., Brillas, E., & Oturan, M. A. (2012). Unprecedented total mineralization of atrazine and cyanuric acid by anodic oxidation and electro-Fenton with a boron-doped diamond anode. *Environmental Chemistry Letters, 10*(2), 165-170. doi:10.1007/s10311-011-0337-z

Oulton, R. L., Kohn, T., & Cwiertny, D. M. (2010). Pharmaceuticals and personal care products in effluent matrices: A survey of transformation and removal during wastewater treatment and implications for wastewater management. *Journal of Environmental Monitoring, 12*(11), 1956-1978. doi:10.1039/C0EM00068J

Park, H., Vecitis, C. D., & Hoffmann, M. R. (2009). Electrochemical Water Splitting Coupled with Organic Compound Oxidation: The Role of Active Chlorine Species. *Journal of Physical Chemistry C, 113*(18), 7935-7945. doi:10.1021/jp810331w

Parker, K. M., Pignatello, J. J., & Mitch, W. A. (2013). Influence of Ionic Strength on Triplet-State Natural Organic Matter Loss by Energy Transfer and Electron Transfer Pathways. *Environmental Science & Technology, 47*(19), 10987-10994. doi:10.1021/es401900j

Pastor, E., Schmidt, V. M., Iwasita, T., Arevalo, M. C., Gonzalez, S., & Arvia, A. J. (1993). THE REACTIVITY OF PRIMARY C3-ALCOHOLS ON GOLD ELECTRODES IN ACID-MEDIA - A COMPARATIVE-STUDY BASED ON DEMS DATA. *Electrochimica Acta, 38*(10), 1337-1344. doi:10.1016/0013-4686(93)80067-a

Pereira, V. J., Linden, K. G., & Weinberg, H. S. (2007). Evaluation of UV irradiation for photolytic and oxidative degradation of pharmaceutical compounds in water. *Water Research, 41*(19), 4413-4423. doi:10.1016/j.watres.2007.05.056

Pereira, V. J., Weinberg, H. S., Linden, K. G., & Singer, P. C. (2007). UV degradation kinetics and modeling of pharmaceutical compounds in laboratory grade and surface water via direct and indirect photolysis at 254 nm. *Environmental Science & Technology, 41*(5), 1682-1688. doi:10.1021/es061491b

Pinkston, K. E., & Sedlak, D. L. (2004). Transformation of aromatic ether-and amine-containing pharmaceuticals during chlorine disinfection. *Environmental Science & Technology, 38*(14), 4019-4025. doi:10.1021/es0353681

Prasse, C., Stalter, D., Schulte-Oehlmann, U., Oehlmann, J., & Ternes, T. A. (2015). Spoilt for choice: A critical review on the chemical and biological assessment of current wastewater treatment technologies. *Water Research, 87*, 237-270. doi:http://dx.doi.org/10.1016/j.watres.2015.09.023

Prasse, C., Wenk, J., Jasper, J. T., Ternes, T. A., & Sedlak, D. L. (2015). Co-occurrence of Photochemical and Microbiological Transformation Processes in Open-Water Unit Process Wetlands. *Environmental Science & Technology, 49*(24), 14136-14145. doi:10.1021/acs.est.5b03783

Purdom, C. E., Hardiman, P. A., Bye, V. V. J., Eno, N. C., Tyler, C. R., & Sumpter, J. P. (1994). Estrogenic Effects of Effluents from Sewage Treatment Works. *Chemistry and Ecology, 8*(4), 275-285. doi:10.1080/02757549408038554

R.P. Schwarzenbach, P. M. G., and D.M. Imboden. (2002). *Environmental Organic Chemistry*. New York: John Wiley & Sons.

Radjenovic, J., Escher, B. I., & Rabaey, K. (2011). Electrochemical degradation of the beta-blocker metoprolol by Ti/Ru0.7Ir0.3O2 and Ti/SnO2-Sb electrodes. *Water Research, 45*(10), 3205-3214. doi:10.1016/j.watres.2011.03.040

Radjenovic, J., & Sedlak, D. L. (2015). Challenges and Opportunities for Electrochemical Processes as Next-Generation Technologies for the Treatment of Contaminated Water. *Environmental Science & Technology, 49*(19), 11292-11302. doi:10.1021/acs.est.5b02414

Ray, J. R., Lee, B., Baltrusaitis, J., & Jun, Y.-S. (2012). Formation of Iron(III) (Hydr)oxides on Polyaspartate- and Alginate-Coated Substrates: Effects of Coating Hydrophilicity and Functional Group. *Environmental Science & Technology, 46*(24), 13167-13175. doi:10.1021/es302124g

Razavi, B., Song, W. H., Cooper, W. J., Greaves, J., & Jeong, J. (2009). Free-Radical-Induced Oxidative and Reductive Degradation of Fibrate Pharmaceuticals: Kinetic Studies and Degradation Mechanisms. *Journal of Physical Chemistry A, 113*(7), 1287-1294. doi:10.1021/jp808057c

Rice, J., Wutich, A., & Westerhoff, P. (2013). Assessment of De Facto Wastewater Reuse across the U.S.: Trends between 1980 and 2008. *Environmental Science & Technology, 47*(19), 11099-11105. doi:10.1021/es402792s

Rosario-Ortiz, F. L., & Canonica, S. (2016). Probe compounds to assess the photochemical activity of dissolved organic matter. *Environmental Science & Technology*.

Rosario-Ortiz, F. L., Wert, E. C., & Snyder, S. A. (2010). Evaluation of UV/H2O2 treatment for the oxidation of pharmaceuticals in wastewater. *Water Research, 44*(5), 1440-1448. doi:10.1016/j.watres.2009.10.031

Rose, A. L. (2003). Effect of Dissolved Natural Organic Matter on the Kinetics of Ferrous Iron Oxygenation in Seawater. *Environmental Science & Technology, 37*(21), 4877-4886. doi:10.1021/es034152g

Rose, J., Flank, A.-M., Masion, A., Bottero, J.-Y., & Elmerich, P. (1997). Nucleation and growth mechanisms of Fe oxyhydroxide in the presence of PO4 ions. 2. P K-edge EXAFS study. *Langmuir, 13*(6), 1827-1834.

Rozendal, R. A., Hamelers, H. V. M., & Buisman, C. J. N. (2006). Effects of membrane cation transport on pH and microbial fuel cell performance. *Environmental Science & Technology, 40*(17), 5206-5211. doi:10.1021/es060387r

Rozendal, R. A., Leone, E., Keller, J., & Rabaey, K. (2009). Efficient hydrogen peroxide generation from organic matter in a bioelectrochemical system. *Electrochemistry Communications, 11*(9), 1752-1755. doi:10.1016/j.elecom.2009.07.008

Salem, I. A., El-Maazawi, M., & Zaki, A. B. (2000). Kinetics and mechanisms of decomposition reaction of hydrogen peroxide in presence of metal complexes. *International Journal of Chemical Kinetics, 32*(11), 643-666. doi:10.1002/1097-4601(2000)32:11<643::aid-kin1>3.0.co;2-c

Salgado, R., Pereira, V. J., Carvalho, G., Soeiro, R., Gaffney, V., Almeida, C., . . . Noronha, J. P. (2013). Photodegradation kinetics and transformation products of ketoprofen, diclofenac and atenolol in pure water and treated wastewater. *Journal of Hazardous Materials, 244*, 516-527. doi:10.1016/j.jhazmat.2012.10.039

Sansalone, J. J., & Buchberger, S. G. (1997). Partitioning and first flush of metals in urban roadway storm water. *Journal of Environmental Engineering-Asce, 123*(2), 134-143. doi:10.1061/(asce)0733-9372(1997)123:2(134)

Sato, A., Takagi, K., Kano, K., Kato, N., Duine, J. A., & Ikeda, T. (2001). Ca(2+) stabilizes the semiquinone radical of pyrroloquinoline quinone. *Biochemical Journal, 357*(Pt 3), 893-898.

Schwarzenbach, R. P., Escher, B. I., Fenner, K., Hofstetter, T. B., Johnson, C. A., von Gunten, U., & Wehrli, B. (2006). The Challenge of Micropollutants in Aquatic Systems. *Science, 313*(5790), 1072-1077. doi:10.1126/science.1127291

Shannon, M. A., Bohn, P. W., Elimelech, M., Georgiadis, J. G., Marinas, B. J., & Mayes, A. M. (2008). Science and technology for water purification in the coming decades. *Nature, 452*(7185), 301-310.

Sharpless, C. M., Aeschbacher, M., Page, S. E., Wenk, J., Sander, M., & McNeill, K. (2014). Photooxidation-Induced Changes in Optical, Electrochemical, and Photochemical Properties of Humic Substances. *Environmental Science & Technology, 48*(5), 2688-2696. doi:10.1021/es403925g

Sharpless, C. M., & Linden, K. G. (2003). Experimental and model comparisons of low- and medium-pressure Hg lamps for the direct and H2O2 assisted UV photodegradation of N-nitrosodimethylamine in simulated drinking water. *Environmental Science & Technology, 37*(9), 1933-1940. doi:10.1021/es025814p

Shi, Z., & Stone, A. T. (2009). PbO2(s, Plattnerite) Reductive Dissolution by Aqueous Manganous and Ferrous Ions. *Environmental Science & Technology, 43*(10), 3596-3603. doi:10.1021/es8034686

Shi, Z., & Stone, A. T. (2009). PbO2(s, Plattnerite) Reductive Dissolution by Natural Organic Matter: Reductant and Inhibitory Subfractions. *Environmental Science & Technology, 43*(10), 3604-3611. doi:10.1021/es802441g

Shu, Z. Q., Bolton, J. R., Belosevic, M., & El Din, M. G. (2013). Photodegradation of emerging micropollutants using the medium-pressure UV/H2O2 Advanced Oxidation Process. *Water Research, 47*(8), 2881-2889. doi:10.1016/j.watres.2013.02.045

Snyder, S. A., Adham, S., Redding, A. M., Cannon, F. S., DeCarolis, J., Oppenheimer, J., . . . Yoon, Y. (2007). Role of membranes and activated carbon in the removal of endocrine disruptors and pharmaceuticals. *Desalination, 202*(1), 156-181. doi:http://dx.doi.org/10.1016/j.desal.2005.12.052

Solomon, J. L., & Madix, R. J. (1987). KINETICS AND MECHANISM OF THE OXIDATION OF ALLYL ALCOHOL ON AG(110). *Journal of Physical Chemistry, 91*(24), 6241-6244. doi:10.1021/j100308a034

Solomon, K. R., Baker, D. B., Richards, R. P., Dixon, D. R., Klaine, S. J., LaPoint, T. W., . . . Williams, W. M. (1996). Ecological risk assessment of atrazine in North American surface waters. *Environmental Toxicology and Chemistry, 15*(1), 31-74. doi:10.1897/1551-5028(1996)015<0031:eraoai>2.3.co;2

Steenken, S., & Neta, P. (1982). One-electron redox potentials of phenols. Hydroxy- and aminophenols and related compounds of biological interest. *The Journal of Physical Chemistry, 86*(18), 3661-3667. doi:10.1021/j100215a033

Stenson, A. C., Landing, W. M., Marshall, A. G., & Cooper, W. T. (2002). Ionization and fragmentation of humic substances in electrospray ionization Fourier transform-ion cyclotron resonance mass spectrometry. *Analytical Chemistry, 74*(17), 4397-4409.

Stookey, L. L. (1970). Ferrozine-a new spectrophotometric reagent for iron. *Analytical Chemistry, 42*(7), 779-781.

Szpyrkowicz, L., Kaul, S. N., Neti, R. N., & Satyanarayan, S. (2005). Influence of anode material on electrochemical oxidation for the treatment of tannery wastewater. *Water Research, 39*(8), 1601-1613. doi:10.1016/j.watres.2005.01.016

Ternes, T. A., Stüber, J., Herrmann, N., McDowell, D., Ried, A., Kampmann, M., & Teiser, B. (2003). Ozonation: a tool for removal of pharmaceuticals, contrast media and musk fragrances from wastewater? *Water Research, 37*(8), 1976-1982. doi:https://doi.org/10.1016/S0043-1354(02)00570-5

Tojo, S., Tachikawa, T., Fujitsuka, M., & Majima, T. (2004). Oxidation processes of aromatic sulfides by hydroxyl radicals in colloidal solution of TiO2 during pulse radiolysis. *Chemical Physics Letters, 384*(4–6), 312-316. doi:http://dx.doi.org/10.1016/j.cplett.2003.11.109

Tomcsányi, L., De Battisti, A., Hirschberg, G., Varga, K., & Liszi, J. (1999). The study of the electrooxidation of chloride at RuO2/TiO2 electrode using CV and radiotracer techniques and evaluating by electrochemical kinetic simulation methods. *Electrochimica Acta, 44*(14), 2463-2472. doi:http://dx.doi.org/10.1016/S0013-4686(98)00381-8

Toze, S. (2006). Reuse of effluent water—benefits and risks. *Agricultural Water Management, 80*(1–3), 147-159. doi:https://doi.org/10.1016/j.agwat.2005.07.010

Trasatti, S. (1987). PROGRESS IN THE UNDERSTANDING OF THE MECHANISM OF CHLORINE EVOLUTION AT OXIDE ELECTRODES. *Electrochimica Acta, 32*(3), 369-382. doi:10.1016/0013-4686(87)85001-6

Trasatti, S., & Petrii, O. A. (1991). REAL SURFACE-AREA MEASUREMENTS IN ELECTROCHEMISTRY. *Pure and Applied Chemistry, 63*(5), 711-734. doi:10.1351/pac199163050711

Twardowski, M. S., Boss, E., Sullivan, J. M., & Donaghay, P. L. (2004). Modeling the spectral shape of absorption by chromophoric dissolved organic matter. *Marine Chemistry, 89*(1–4), 69-88. doi:http://dx.doi.org/10.1016/j.marchem.2004.02.008

van Genuchten, C. M., Addy, S. E. A., Peña, J., & Gadgil, A. J. (2012). Removing Arsenic from Synthetic Groundwater with Iron Electrocoagulation: An Fe and As K-Edge EXAFS Study. *Environmental Science & Technology, 46*(2), 986-994. doi:10.1021/es201913a

van Genuchten, C. M., Pena, J., Amrose, S. E., & Gadgil, A. J. (2014). Structure of Fe(III) precipitates generated by the electrolytic dissolution of Fe(0) in the presence of groundwater ions. *Geochimica Et Cosmochimica Acta, 127*, 285-304. doi:10.1016/j.gca.2013.11.044

Vecitis, C. D., Gao, G., & Liu, H. (2011). Electrochemical Carbon Nanotube Filter for Adsorption, Desorption, and Oxidation of Aqueous Dyes and Anions. *The Journal of Physical Chemistry C, 115*(9), 3621-3629. doi:10.1021/jp111844j

Viollier, E., Inglett, P. W., Hunter, K., Roychoudhury, A. N., & Van Cappellen, P. (2000). The ferrozine method revisited: Fe(II)/Fe(III) determination in natural waters. *Applied Geochemistry, 15*(6), 785-790. doi:http://dx.doi.org/10.1016/S0883-2927(99)00097-9

Von Gunten, U., & Oliveras, Y. (1998). Advanced oxidation of bromide-containing waters: Bromate formation mechanisms. *Environmental Science & Technology, 32*(1), 63-70. doi:10.1021/es970477j

VonGunten, U., & Oliveras, Y. (1997). Kinetics of the reaction between hydrogen peroxide and hypobromous acid: Implication on water treatment and natural systems. *Water Research, 31*(4), 900-906. doi:10.1016/s0043-1354(96)00368-5

Vörösmarty, C. J., Green, P., Salisbury, J., & Lammers, R. B. (2000). Global Water Resources: Vulnerability from Climate Change and Population Growth. *Science, 289*(5477), 284-288. doi:10.1126/science.289.5477.284

Wang, H. J., Bakheet, B., Yuan, S., Li, X., Yu, G., Murayama, S., & Wang, Y. J. (2015). Kinetics and energy efficiency for the degradation of 1,4-dioxane by electro-peroxone process. *Journal of Hazardous Materials, 294*, 90-98. doi:10.1016/j.jhazmat.2015.03.058

Ward, C. P., & Cory, R. M. (2016). Complete and Partial Photo-oxidation of Dissolved Organic Matter Draining Permafrost Soils. *Environmental Science & Technology, 50*(7), 3545-3553. doi:10.1021/acs.est.5b05354

Warner, N. R., Christie, C. A., Jackson, R. B., & Vengosh, A. (2013). Impacts of Shale Gas Wastewater Disposal on Water Quality in Western Pennsylvania. *Environmental Science & Technology, 47*(20), 11849-11857. doi:10.1021/es402165b

Watts, M. J., Hofmann, R., & Rosenfeldt, E. J. (2012). Low-pressure UV/Cl-2 for advanced oxidation of taste and odor. *Journal American Water Works Association, 104*(1), 47-48. doi:10.5942/jawwa.2012.104.0006

Weinberg, H. S., Krasner, S. W., Richardson, S. D., & Thruston Jr, A. D. (2002). The occurrence of disinfection by-products (DBPs) of health concern in drinking water: results of a nationwide DBP occurrence study. *National Exposure Research Laboratory, United States Environmental Protection Agency, Athen, GA*, 460.

Wenk, J., Aeschbacher, M., Salhi, E., Canonica, S., von Gunten, U., & Sander, M. (2013). Chemical Oxidation of Dissolved Organic Matter by Chlorine Dioxide, Chlorine, And Ozone: Effects on Its Optical and Antioxidant Properties. *Environmental Science & Technology, 47*(19), 11147-11156. doi:10.1021/es402516b

Wenk, J., & Canonica, S. (2012). Phenolic Antioxidants Inhibit the Triplet-Induced Transformation of Anilines and Sulfonamide Antibiotics in Aqueous Solution. *Environmental Science & Technology, 46*(10), 5455-5462. doi:10.1021/es300485u

Wenk, J., von Gunten, U., & Canonica, S. (2011). Effect of Dissolved Organic Matter on the Transformation of Contaminants Induced by Excited Triplet States and the Hydroxyl Radical. *Environmental Science & Technology, 45*(4), 1334-1340. doi:10.1021/es102212t

Weston, D. P., & Lydy, M. J. (2014). Toxicity of the Insecticide Fipronil and Its Degradates to Benthic Macroinvertebrates of Urban Streams. *Environmental Science & Technology, 48*(2), 1290-1297. doi:10.1021/es4045874

Winid, B. (2015). Bromine and water quality – Selected aspects and future perspectives. *Applied Geochemistry, 63*, 413-435. doi:http://dx.doi.org/10.1016/j.apgeochem.2015.10.004

World Water Assessment Programme. 2012. *The United Nations World Water Development Report 4: Managing Water under Uncertainty and Risk*. Paris, UNESCO

Xie, Y. (2001). Analyzing haloacetic acids using gas chromatography/mass spectrometry. *Water Research, 35*(6), 1599-1602.

Yan, H., Fangong, K., Shoujuan, W., & Guihua, Y. (2014). Novel gas diffusion electrode system for effective production of hydrogen peroxide. *Applied Mechanics and Materials, 496-500*, 159-162. doi:10.4028/www.scientific.net/AMM.496-500.159

Yang, Y., & Hoffmann, M. R. (2016). Synthesis and Stabilization of Blue-Black TiO2 Nanotube Arrays for Electrochemical Oxidant Generation and Wastewater Treatment. *Environmental Science & Technology, 50*(21), 11888-11894. doi:10.1021/acs.est.6b03540

Yuasa, J., Suenobu, T., & Fukuzumi, S. (2006). Binding Modes in Metal Ion Complexes of Quinones and Semiquinone Radical Anions: Electron-Transfer Reactivity. *ChemPhysChem, 7*(4), 942-954. doi:10.1002/cphc.200500640

Zafiriou, O. C., Voelker, B. M., & Sedlak, D. L. (1998). Chemistry of the Superoxide Radical (O2-) in Seawater: Reactions with Inorganic Copper Complexes. *The Journal of Physical Chemistry A, 102*(28), 5693-5700. doi:10.1021/jp980709g

Zaky, A. M., & Chaplin, B. P. (2013). Porous Substoichiometric TiO2 Anodes as Reactive Electrochemical Membranes for Water Treatment. *Environmental Science & Technology, 47*(12), 6554-6563. doi:10.1021/es401287e

Zepp, R. G., Hoigne, J., & Bader, H. (1987). NITRATE-INDUCED PHOTOOXIDATION OF TRACE ORGANIC-CHEMICALS IN WATER. *Environmental Science & Technology, 21*(5), 443-450. doi:10.1021/es00159a004

Zhai, H., Zhang, X., Zhu, X., Liu, J., & Ji, M. (2014). Formation of Brominated Disinfection Byproducts during Chloramination of Drinking Water: New Polar Species and Overall Kinetics. *Environmental Science & Technology, 48*(5), 2579-2588. doi:10.1021/es4034765

Zhang, F., Pant, D., & Logan, B. E. (2011). Long-term performance of activated carbon air cathodes with different diffusion layer porosities in microbial fuel cells. *Biosensors and Bioelectronics, 30*(1), 49-55. doi:10.1016/j.bios.2011.08.025

Zhang, R., Sun, P., Boyer, T. H., Zhao, L., & Huang, C.-H. (2015). Degradation of Pharmaceuticals and Metabolite in Synthetic Human Urine by UV, UV/H2O2, and UV/PDS. *Environmental Science & Technology, 49*(5), 3056-3066. doi:10.1021/es504799n

Zhu, X., Ni, J., Xing, X., Li, H., & Jiang, Y. (2011). Synergies between electrochemical oxidation and activated carbon adsorption in three-dimensional boron-doped diamond anode system. *Electrochimica Acta, 56*(3), 1270-1274. doi:https://doi.org/10.1016/j.electacta.2010.10.073

Zhuo, Q., Deng, S., Yang, B., Huang, J., & Yu, G. (2011). Efficient Electrochemical Oxidation of Perfluorooctanoate Using a Ti/SnO2-Sb-Bi Anode. *Environmental Science & Technology, 45*(7), 2973-2979. doi:10.1021/es1024542

Appendix

A.2. Electrochemical Transformation of Trace Organic Contaminants in the Presence of Halide and Carbonate Ions.

A.2.1 Mass Spectroscopy Parameters

Trace organic compounds were separated by an Agilent 1200 HPLC using a 3.0 mm × 150 mm Phenomenex Synergi Hydro-RP 4 µm column, after a 3.00 mm × 4 mm AQ C18 SecurityGuard guard cartridge. The column was eluted with 0.6 mL min^{-1} methanol and 0.1% acetic acid in water with the following gradient: 0 minutes, 0% methanol; 2 minutes, 0% methanol; 8 minutes, 60% methanol; 11 minutes, 95% methanol; 12 minutes, 95% methanol; 12.1 minutes, 0% methanol; 17 minutes, 0% methanol. Compounds were detected with an Agilent 6460 MS-MS using electrospray ionization (ESI) with a gas temperature of 350°C, a sheath gas temperature of 400°C, a gas flow rate of 11 L/min at 50 psi, and a capillary voltage of 3600 V. Compound-specific parameters are given in Table A.1.

Table A.1. Compound-Specific Mass Spectrometry Parameters[a]

compound	precursor ion (amu)	fragmentor voltage (V)	product ions (amu)	collision energy (V)	cell accelerator (V)	ionization mode
Abacavir	287	90	191 150	15 35	2	positive
Acyclovir	226	75	152 135	10 45	2	positive
Acetaminophen	152.1	90	110 65	10 30	6 8	positive
Atenolol	267	130	145 190	24 16	7	positive
Atrazine	216.1	100	173.9 104	30 15	3	positive
Carbamazepine	237	120	179 194	35 15	7	positive

Isoproturon	207.2	100	164.9 133.9	8 20	7	positive
Metoprolol	268	130	159 116	17 14	7	positive
Propranolol	260	98	116 183	13 12	7	positive
Sulfa-methoxazole	254	110	92 156	25 10	7	positive
Trimethoprim	291	140	123 261	20 17	7	positive

[a]All compounds were analyzed using a drying gas temperature of 350˚ C, a gas flow of 6 L min^{-1}, a nebulizer pressure of 45 psi, a sheath gas temperature of 350 ˚ C, a sheath gas flow of 8 L min^{-1}, a nozzle voltage of 300 V, a positive capillary voltage of 3600 V, and a dwell time of 7 ms.

A.2.2 Estimation of HO• Produced During Electrolysis

The reversible redox reaction for water oxidation occurring at an anode can be given by:

$$H_2O \leftrightarrow HO^{\bullet} + H^+ + e^-$$

where the reactions in the cathodic and anodic directions occur simultaneously. The production of $HO^{\bullet}$ is governed by the difference between the applied potential (E) and the equilibrium potential ($E_H°$). The difference between the applied potential and equilibrium potential (Nerst Equation) dictates the thermodynamic equilibrium between the concentration of products to reactants (i.e., E >> $E_H°$ means there is driving force to produce [$HO^{\bullet}$]). The observed $HO^{\bullet}$ production, however, is affected by the kinetics of the reaction which are dependent on the electrode material. Therefore, the Nerst equation estimates the thermodynamic maximum production. The calculation of the production of $HO^{\bullet}$ at pH 8 was performed through manipulation of the Nerst equation:

$$[HO^{\bullet}] = \left[10^{\left(\frac{E-E_H^{\circ}}{-0.0592}\right)}[H^+]\right]^{-1}$$

where E_H° is the standard reduction potential of $HO^{\bullet}/H_2O$ (2.59V) (Neta *et al.*, 1988).

A.2.3 Bimolecular Rate Constants of Trace Organic Contaminants with Reactive Oxidants

Table A.2. Bimolecular rate constants for the reaction between HOCl, HOBr, and radical species for the trace organic contaminants and probes used in this study.

		Rate Constant (M^{-1} s^{-1})				
	Compound	k_{OH}•	k_{CO_3}•- (pH 8)	k_{HOCl} (pH 8)[a]	k_{HOBr} (pH 8)[a]	k_{Cl_2}•-
Trace Organic Contaminants	carbamazepine	9.1×10^9 (± 13%)	3.9×10^6 (± 22%)	2.6×10^{-2} (± 6%)	1.4×10^0 (± 23%)	-
	isoproturon	7.9×10^9 (± 1%)	3×10^7 (± 13%)	9.3×10^{-2} (± 5%)	7.1×10^0 (± 11%)	-
	atrazine	3.0×10^9 (± 15%)	3.7×10^6 (± 48%)	5.2×10^{-3} (± 6%)	$<1.0 \times 10^0$	-
	atenolol	7.5×10^9 (± 4%)	5.9×10^7 (± 27%)	6.6×10^{-2} (± 7%)	1.1×10^1 (± 7%)	-
	metoprolol	8.4×10^9 (± 1%)	8.4×10^6 (± 61%)	1.2×10^{-2} (± 7%)	9.5×10^0 (± 17%)	-
	propranolol	1.1×10^{10} (± 2%)	7.7×10^7 (± 15%)	6.0×10^{-1} (± 18%)	1.5×10^2 (± 27%)	-
	trimethoprim	8.7×10^9 (± 2%)	2.3×10^7 (± 48%)	1.1×10^1 (± 2%)	3.2×10^2 (± 15%)	-
	sulfamethoxazole	5.9×10^9 (± 11%)	1.5×10^8 (± 20%)	1.1×10^2 (± 7%)	1.6×10^3 (± 19%)	-
	acetaminophen	2×10^9 (± 29%)	3.8×10^8 (± 29%)	3.8×10^1 (± 11%)	5.7×10^2	-
	acyclovir	5×10^9 (± 2%)	1.1×10^8 (± 2%)	9.9×10^0 (± 24%)	1.5×10^3 (± 16%)	-
	abacavir	1.1×10^{11} (± 3%)	1.2×10^9 (± 4%)	7.1×10^0 (± 13%)	1.7×10^3 (± 21%)	-
Probes	*p*CBA	5×10^9	-	-	-	3×10^6
	Allyl Alcohol	6×10^9	2.5×10^5	1.0×10^{-1} (± 98%)	-	3.2×10^7 [a]
	t-buOH	6×10^8	-	-	-	7×10^2

[a]Values determined in this study.

A.2.4 Relevance of Different Oxidation Pathways towards Organic Contaminant Removal during Electrolysis

Table A.3. Percent contribution of different oxidation pathways to the transformation of trace organic contaminants in 10 mM NaCl at pH 8 on Ti-IrO_2.

	DET[a]	$HO•_{ads}$[(c)]	Bulk HO•[(b)]	HOCl[(d)]	$Cl•_{ads}$[(e)]
Atrazine	0.2	2.5	5.7	18.6	73.0
Isoproturon	5.2	3.5	1.4	15.3	74.8
Carbamazepine	3.8	1.8	2.1	8.1	84.2
Atenolol	4.6	9.6	6.0	67.2	12.6
Metoprolol	8.6	11.7	5.5	23.8	50.3
Propranolol	4.4	6.9	0.6	22.7	65.4
Trimethoprim	1.8	10.9	0.8	82.1	4.4
Sulfamethoxazole	1.0	19.9	0.5	78.6	<1.0
Acetaminophen	1.3	10.4	0.4	88.6	<1.0
Acyclovir	1.4	12.5	0.6	88.9	<1.0
Abacavir	1.4	10.1	9.2	43.4	35.9

[a]DET was calculated using the removal rate due to Borate + AA. [b]Bulk HO• was calculated from the product of the contaminant-specific bimolecular rate constant of dissolved HO• with the steady-state bulk HO• concentration determined from pCBA measurements. [c]Oxidation due to $HO•_{ads}$ was determined from the current efficiency for water oxidation (77%) in 10 mM NaCl with the contribution of $HO•_{ads}$ determined in the borate buffer. [d]See experimental in Section A.2.7 below for contribution of HOCl. [e]$Cl•_{ads}$ was determined as the difference between the total observed degradation in 10 mM NaCl from the contributions of direct electron transfer, $HO•_{ads}$, bulk HO•, and HOCl. All percentages were determined by dividing the pseudo-first order removal rates from the specific oxidation pathway (s^{-1}) by the total observed degradation rate (s^{-1}).

A.2.5 Production of HOCl in the Presence of NOM

The production of HOCl in the presence of NOM can be described by:

$$\frac{d[HOCl]}{dt} = k'_{HOCl} - k[NOM][HOCl]$$

where k'_{HOCl} is the zero-order production rate of HOCl in the presence of 10 mM NaCl, and k is the bimolecular rate constant of NOM with HOCl. At short electrolysis times, low [HOCl] concentrations means that the term k[NOM][HOCl] is small and the production of HOCl is roughly equal to k'_{HOCl} (See Figure 2.24A of the main text). This suggests that the Volmer-Heyrovsky formation of chlorine on the anode (k'_{HOCl}) is not affected by NOM. At large electrolysis times, k[NOM][HOCl] is sufficiently large so the production of HOCl deviates from linearity.

A.2.6 Branching ratio for HO• with SRHA and contaminants

Using a rate constant of $k_{HO\bullet,SRHA} = 5.7 \times 10^8$ L M_C^{-1} s^{-1} (Appiani et al. 2014) for the interaction of HO• with SRHA and $k_{HO\bullet,organic} = 5 \times 10^9$ M^{-1} s^{-1} as an average rate constant for HO• with organic contaminants, we have:

$$\frac{k_{HO\bullet,organic}[organics]}{k_{HO\bullet,SRHA}[SRHA]} = \frac{(5 \times 10^9 M^{-1} s^{-1})(4 \times 10^7 M)}{(5.7 \times 10^8 \text{ L } M_C^{-1} s^{-1})\left(\frac{1 M_C}{1200 \text{ mgC}}\right)(5 \text{ mgC } L^{-1})} = 0.85\%$$

A.2.7 Determination of the Predicted Removal of Contaminants during Electrolysis.

Borate. The contributions of direct electron transfer and adsorbed hydroxyl radical toward contaminant oxidation can be determined during the electrolysis of borate buffered electrolyte, where the only species contributing to oxidation are:

$$k_{borate} = k_{DET} + k_{HO^\bullet_{ads}} + k_{HO\bullet}[HO^\bullet]_{SS}$$

Removal of the selective hydroxyl radical probe, pCBA, in all the electrolytes except ammonia indicated that $[HO^\bullet]_{SS}$ had a negligible contribution to contaminant transformation. Therefore, dissolved hydroxyl radical can be ignored here on out and the contributing species in borate electrolysis are:

$$k_{borate} \approx k_{DET} + k_{HO^\bullet_{ads}}$$

Tertiary butanol or allyl alcohol can be used as selective probes to discern between the contributions of $HO^\bullet_{ads}$ and DET.

HOCl. The predicted transformation of contaminants in the presence of Cl^- was calculated as follows:

$$k_{HOCl} = k_{DET} + k_{HO^\bullet_{ads}} + k_{HOCl}[HOCl]$$

where k_{HOCl} is the bimolecular rate constant of the HOCl with trace organic contaminants. HOCl production is pseudo-zeroth order with respect to Cl^- and can be expressed as:

$$[HOCl] = k'_{HOCl}t$$

$$k_{HOCl} = k_{DET} + k_{HO^\bullet_{ads}} + k_{HOCl}k'_{HOCl}t$$

k_{DET} and $k_{HO^\bullet_{ads}}$ were determined previously in the borate buffered electrolyte and k_{HOCl} is given in Table A.2. The value of t was selected as the time needed for roughly 95% of the compound removal (using the pseudo-first order observed removal rates) in the 10 mM NaCl electrolyte.

$$t_{95\%} = \frac{\ln(0.05)}{k_{obs}}$$

Differences in the predicted and observed removal were ascribed to reactive chlorine species ($Cl^\bullet_{ads}$ and $Cl_2^{\bullet-}$). Due to limited rate constants of these species with contaminants and a lack of probe compounds to determine their steady state concentrations, they were ignored from the model.

HOCl and HOBr. The predicted transformation of contaminants in the presence of Cl^- and Br^- was calculated as follows:

$$k_{obs} \approx k_{borate} + k_{HOCl}[HOCl] + k_{HOBr}[HOBr]$$

where k_{HOCl} and k_{HOBr} are the bimolecular rate constants of the oxidants with trace organic contaminants. Given the fast oxidation of bromide with HOCl and considering the rapid rate of HOCl production (i.e., HOCl is in excess), it is likely that essentially all of the Br^- was converted to HOBr within seconds of the initiation of electrolysis (i.e., $[HOBr] \approx [Br^-] = 20\ \mu M$) and is continually re-oxidized after HOBr reacts with contaminants. As a result, we rewrite the expression for the observed degradation as:

$$k_{obs} \approx k_{borate} + k_{HOCl}[k'_{HOCl}t - 20\mu M] + k_{HOBr}[20\mu M]$$

The value of t was selected as the time needed for roughly 95% of the compound removal (using the pseudo-first order observed removal rates) in the 10 mM NaCl/20μM Br^- electrolyte.

Wastewater. To predict the removal of contaminants in EBMUD effluent, the contributions of direct electron transfer, $[HO^\bullet]_{SS}$, and $CO_3^{\bullet-}$ were also taken into consideration. Direct electron transfer and adsorbed hydroxyl radical were taken as those observed removal rates in the borate buffered electrolyte. Due to the inability to quantify $[CO_3^{\bullet-}]_{SS}$ with probe compounds (i.e., *N,N*-dimethylaniline) (Neta *et al.*, 1988; "Notre Dame Radiation Laboratory. Radiation Chemistry Data Center, Kinetics Database," 2002; Jasper & Sedlak, 2013) in the presence of HOCl

(Deborde & von Gunten, 2008), the influence of $CO_3^{\bullet-}$ towards removal rates was estimated using scaling factors determined in Figure 2.19 of the main text (i.e., $k_{Br,HCO_3}/ k_{Br}$):

$$k_{obs} \approx \frac{k_{Br,HCO_3}}{k_{Br}} \times (k_{borate} + k_{HOCl}[k'_{HOCl}t - 20\mu M] + k_{HOBr}[20\mu M])$$

A.3. Modular Advanced Oxidation Processes Enabled by Cathodic Hydrogen Peroxide Production

A.3.1 Energy per Volume Treated for the Electrochemical Cell and UV Lamp

At a current density of 4.14 A m^{-2}, the highest cell potential was for the poorly conductive groundwater (2.67 V). Assuming the cell runs continuously for a day:

$$\left(\frac{4.14\ A}{m^2}\right)(0.0064\ m^2)(2.67\ V) = 0.071\ W = \frac{0.071\ J}{s}$$

$$\left(\frac{0.071\ J}{s}\right)(86400s)\left(\frac{Wh}{3600J}\right) = 1.7\ Wh$$

The energy per volume of water treated was calculated using the power output of the UV lamp (9W) and the flow rate of the system (120 L d^{-1})

$$(0.009\ kW)\left(\frac{1d}{120L}\right)\left(\frac{24h}{d}\right)\left(\frac{1000L}{m^3}\right) = 1.8\ kWh\ m^{-3}$$

A.3.2 Raw Data Values for the Transformation of Trace Organic Contaminants

Table A.3.1. Normalized Total System Pharmaceutical Transformation for Electrolyte

	Atenolol	Trimethoprim	Metoprolol	Sulfamethoxazole	Propranolol	Carbamazepine	Atrazine	Ibuprofen	TCC	Gemfibrozil
No EC/ NO UV	1.00 ± 0	1.00 ± 0	1.00 ± 0	1.00 ± 0	1.00 ± 0	1.00 ±0	1.00 ± 0	1.00 ± 0	1.00 ± 0	1.00 ± 0
0 + UV	0.758 ± 0.027	0.689 ± 0.030	0.684 ± 0.015	0.000	0.447 ± 0.023	0.724 ± 0.053	0.162 ± 0.013	0.630 ± 0.057	0.383 ± 0.060	0.782 ± 0.060
5+ UV	0.00	0.000	0.014 ± 0.010	0.000	0.006 ± 0.002	0.000	0.06 ± 0.008	0.033 ± 0.007	0.328 ± 0.085	0.018 ± 0.010
10 + UV	0.00	0.000	0.004 ± 0.006	0.000	0.003 ± 0.002	0.000	0.0531 ± 0.009	0.017 ± 0.017	0.678 ± 0.359	0.000
15+ UV	0.00	0.000	0.00 ± 0.001	0.000	0.003 ± 0.002	0.000	0.052 ± 0.007	0.022 ± 0.014	0.439 ± 0.190	0.000
20+ UV	0.00	0.000	0.000	0.000	0.001 ± 0.001	0.000	0.058 ± 0.002	0.018 ± 0.011	0.449 ± 0.288	0.000
25+UV	0.00	0.000	0.001 ± 0.002	0.000	0.000	0.000	0.068 ± 0.007	0.027 ± 0.005	0.319 ± 0.143	0.000

Table A.3.2. Normalized Total System Pharmaceutical Transformation for Synthetic Groundwater

	Atenolol	Trimethoprim	Metoprolol	Sulfamethoxazole	Propranolol	Carbamazepine	Atrazine	Ibuprofen	TCC	Gemfibrozil
No EC/ NO UV	1.00 ± 0	1.00 ± 0	1.00 ± 0	1.00 ± 0	1.00 ± 0	1.00 ±0	1.00 ± 0	1.00 ± 0	1.00 ± 0	1.00 ± 0
0 + UV	0.829 ± 0.030	0.622 ± 0.016	0.734 ± 0.020	0.016 ± 0	0.011 ± 0.012	0.838 ± 0.012	0.180 ± 0.001	0.676 ± 0.03	0.226 ± 0.127	0.725 ± 0.035
5+ UV	0.153 ± 0.013	0.0131 ± 0.005	0.125 ± 0.006	0	0.0018 ± 0	0.215 ± 0.012	0.104 ± 0.004	0.265 ± 0.015	0.288 ± 0.099	0.212 ± 0.01
10 + UV	0.066 ± 0.01	0.0064 ± 0.007	0.071 ± 0.01	0	0.0035 ± 0	0.118 ± 0.014	0.098 ± 0.014	0.151 ± 0.032	0.394 ± 0.218	0.155 ± 0.02
15+ UV	0.041 ± 0	0	0.032 ± 0.028	0	0.0017 ± 0	0.07 ± 0	0.090 ± 0.002	0.133 ± 0.009	0.3 ± 0.064	0.118 ± 0
20+ UV	0.0175 ± 0.003	0	0.032 ± 0.001	0	0.0055 ± 0	0.047 ± 0.04	0.082 ± 0.004	0.133 + 0.01	0.241 ± 0.08	0.093 ± 0.005
25+UV	0.009 ± 0.003	0	0.025 ± 0.002	0	0.002 ± 0	0.013 ± 0.01	0.077 ± 0.002	0.089 ± 0.03	0.333 ± 0.118	0.081 ±0.002

Table A.3.3. Normalized Total System Pharmaceutical Transformation for Wastewater Effluent

	Atenolol	Trimethoprim	Metoprolol	Sulfamethoxazole	Propranolol	Carbamazepine	Atrazine	Ibuprofen	TCC	Gemfibrozil
No EC/ NO UV	1.00 ± 0	1.00 ± 0	1.00 ± 0	1.00 ± 0	1.00 ± 0	1.00 ±0	1.00 ± 0	1.00 ± 0	1.00 ± 0	1.00 ± 0
0 + UV	0.871 ± 0.033	0.866 ± 0.015	0.831 ± 0.029	0.042 ± 0.002	0.585 ± 0.013	0.858 ± 0.022	0.316 ± 0.010	0.725 ± 0.040	0.386 ± 0.123	0.882 ± 0.023
5+ UV	0.577 ± 0.083	0.553 ± 0.083	0.523 ± 0.071	0.022 ± 0.006	0.195 ± 0.028	0.485 ± 0.049	0.264 ± 0.01	0.501 ± 0.071	0.285 ± 0.067	0.559 ± 0.068
10 + UV	0.443 ± 0.018	0.429 ± 0.025	0.382 ± 0.029	0.010 ± 0.01	0.090 ± 0.011	0.331 ± 0.025	0.250 ± 0.024	0.429 ± 0.093	0.241 ± 0.052	0.441 ± 0.073
15+ UV	0.400 ± 0.051	0.390 ± 0.042	0.331 ± 0.047	0.005 ± 0.004	0.055 ± 0.007	0.271 ± 0.029	0.239 ± 0.015	0.374 ± 0.071	0.463 ± 0.131	0.366 ± 0.041
20+ UV	0.378 ± 0.060	0.359 ± 0.061	0.313 ± 0.055	0.013 ± 0.002	0.051 ± 0.008	0.260 ± 0.057	0.289 ± 0.021	0.228 ± 0.144	0.349 ± 0.246	0.209 ± 0.189
25+UV	0.324 ± 0.039	0.313 ± 0.036	0.265 ± 0.025	0.009 ± 0	0.032 ± 0.006	0.215 ± 0.019	0.278 ± 0.011	0.234 ± 0.133	0.515 ± 0.221	0.179 ± 0.144

Table A.3.4. Normalized Total System Pharmaceutical Transformation for Surface Water

	Atenolol	Trimethoprim	Metoprolol	Sulfamethoxazole	Propranolol	Carbamazepine	Atrazine	Ibuprofen	TCC	Gemfibrozil
No EC/ NO UV	1.00 ± 0	1.00 ± 0	1.00 ± 0	1.00 ± 0	1.00 ± 0	1.00 ±0	1.00 ± 0	1.00 ± 0	1.00 ± 0	1.00 ± 0
0 + UV	0.706 ± 0.12	0.737 ± 0.06	0.632 ± 0.10	0.063 ± 0.014	0.414 ± 0.06	0.781 ± 0.050	0.320 ± 0.024	0.762 ± 0.1	0.463± 0.123	0.792 ± 0.13
5+ UV	0.181 ± 0.033	0.156 ± 0.006	0.155 ± 0.029	0.024 ± 0.002	0.065 ± 0.014	0.160 ± 0.012	0.193 ± 0.016	0.172 ± 0.0166	0.205 ± 0.095	0.043 ± 0.006
10 + UV	0.081 ± 0.016	0.086 ± 0.008	0.065 ± 0.017	0.015 ± 0.004	0.036 ± 0.087	0.080 ± 0.010	0.148 ± 0.012	0.134 ± 0.027	0.406 ± 0.194	0.117 ± 0.033
15+ UV	0.074 ± 0.004	0.072 ± 0.003	0.068 ± 0.003	0.012 ± 0.001	0.048 ± 0.007	0.074 ± 0.005	0.144 ± 0.005	0.084 ± 0.030	0.465 ± 0.35	0.071 ± 0.022
20+ UV	0.076 ± 0.024	0.087 ± 0.021	0.063 ± 0.02	0.020 ± 0.007	0.043 ± 0.012	0.065 ± 0.000	0.190 ± 0.0276	0.193 ± 0.073	0.368 ± 0.154	0.157 ± 0.064
25+UV	0.068 ± 0.013	0.070 ± 0.017	0.058 ± 0.017	0.010 ± 0.005	0.040 ± 0.012	0.067 ± 0.01	0.152 ± 0.020	0.166 ± 0.034	0.251 ± 0.013	0.113 ± 0.024

A.3.3 Calculation for the Fraction of HO• going to Contaminants

$$\text{fraction HO}^{\bullet} \text{ to contaminants} = \frac{\sum k_{HO\bullet,cont}[Cont]}{\sum k_{HO\bullet,s}[S]}$$

A sample calculation for the fraction of the HO• to trace organic contaminants in the groundwater for pH 8 in the presence of 3 mg L^{-1} (0.09 mM) has been provided using the bimolecular rate constants in Table 3.1 of the main text. At pH 8, of the 3.9 mEq L^{-1} of the TIC in the ground water, 3.8 mM is at HCO_3^- while 0.02 mM is as CO_3^{2-}.

$$\frac{\sum k_{HO\bullet,cont}[Cont]}{\sum k_{HO\bullet,cont}[Cont] + k_{HO\bullet,H2O2}[H_2O_2] + k_{HO\bullet,DOC}[DOC] + k_{HO\bullet,HCO3}[HCO_3^-] + k_{HO\bullet,CO32-}[CO_3^{2-}]}$$

$$\frac{(2.99E3\ s^{-1})}{(2.99E3\ s^{-1}) + (2.7E7\ M^{-1}\ s^{-1})(9*10^{-5}\ M) + (9.8E3\ L\ mgC^{-1}\ s^{-1})(0.1\ mgC\ L^{-1}) + (8.5E6\ M^{-1}\ s^{-1})(3.8*10^{-3}\ M) + (3.9E8\ M^{-1}\ s^{-1})(0.02*10^{-5}\ M)}$$

= 6.5% of available HO•

A.3.4 Reduction in Direct Photolysis from H_2O_2 Light Screening

The pseudo-first order rate constant for direct photolysis of compounds in the absence of H_2O_2, k'_d, is given by:

$$k'_d = \frac{E^{\circ}_{254}\varepsilon_{254}\varphi_{254}[1-10^{-\alpha z}]}{\alpha z}$$

where E°_{254} is the incident photon fluence rate (Ei m^{-2} s^{-1}) at 254 nm, ε_{254} is the decadic molar extinction coefficient of the organic compound at 254 nm (M^{-1} cm^{-1}), ϕ_{254} is the quantum yield at 254 nm (mol Ei^{-1}), α is the solution absorbance (cm^{-1}), and z is the light path length (cm). In the presence of H_2O_2, the direct photolysis rate decreases due to additional absorbance of incident light by H_2O_2. The pseudo-first order rate constant for direct photolysis of compounds in the presence of H_2O_2, $k'_{d,H2O2}$, is given by:

$$k'_{d,H2O2} = \frac{E^{\circ}_{254}\varepsilon_{254}\varphi_{254}[1-10^{-(\alpha+\varepsilon_{H2O2}[H_2O_2])z}]}{(\alpha+\varepsilon_{H2O2}[H_2O_2])z}$$

where ε_{H2O2} is the decadic molar extinction coefficient of the H_2O_2 at 254 nm (M^{-1} cm^{-1}). Comparing the two rates, we get:

$$\frac{k'_{d,H2O2} - k'_d}{k'_d} = \frac{\left(\frac{[1-10^{-(\alpha+\varepsilon_{H2O2}[H_2O_2])z}]\alpha}{(\alpha+\varepsilon_{H2O2}[H_2O_2])}\right) - [1-10^{-\alpha z}]}{[1-10^{-\alpha z}]}$$

For WWTP effluent at 25 A m^{-2}: α = 0.137 cm^{-1}, ε_{H2O2}= 18.6 $M^{-1}cm^{-1}$, $[H_2O_2]$ = 0.54 mM , z = 0.043 m. As a result, the direct photolysis rate in the presence of H_2O_2 decreased by 3.8% for the suite of trace organic contaminants.

$$\frac{k'_{d,H2O2} - k'_d}{k'_d} = 0.0378$$

A.3.5 pH Dependence of H_2O_2 Reaction with HOCl

The primary mechanisms for the reaction of HOCl with H_2O_2 are:

$$HOCl + HO_2^- \xrightarrow{k_1=4.4E7\ M^{-1}\ s^{-1}} Cl^- + O_2 + H_2O$$

$$OCl^- + H_2O_2 \xrightarrow{k_2=3.4E3\ M^{-1}\ s^{-1}} Cl^- + O_2 + H_2O$$

The removal of either $HOCL_{total}$ or $H_2O_{2\ total}$ can be given by

$$\frac{-d[HOCl_{total}]}{dt} = (k_1\alpha_{0,HOCl}\alpha_{1,H202} + k_2\alpha_{1,HOCl}\alpha_{0,H202})[HOCl_{total}][H_2O_{2_{total}}]$$

Where the pH dependent biomolecular rate constant is just:

$$k'_{pH} = (k_1\alpha_{0,HOCl}\alpha_{1,H202} + k_2\alpha_{1,HOCl}\alpha_{0,H202})$$

Given the $pK_{a,HOCl} = 7.6$ and $pK_{a,H2O2} = 11.6$, we can calculate the alpha speciation values.

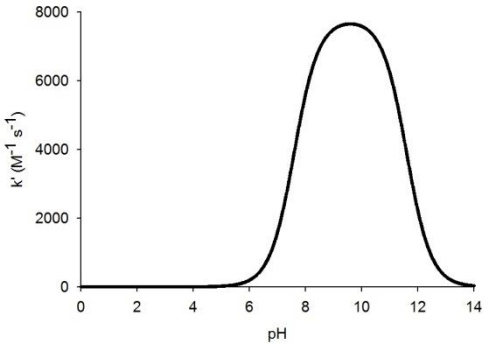

Figure A.3.1: pH-dependent bimolecular rate constant for the reaction between HOCl and H_2O_2.

A.4. Trace Element Removal in Distributed Drinking Water Treatment Systems by Cathodic H_2O_2 Production and UV Photolysis

A.4.1 $HO^\bullet$ yield from UV photolysis of NO_3^- counter-ions

$HO^\bullet$ is formed through the photolysis of H_2O_2, NO_3^-, and NOM. The formation rate of $HO^\bullet$ from the photolysis of H_2O_2 can be expressed as:

$$R_{form,HO,H_2O_2} = 2k'_{H2O2}$$

$$k'_{H2O2} = S_{254}\frac{E^\circ_{254}\varepsilon_{254}\varphi_{254}[1 - 10^{-\alpha z}]}{\alpha z}[H2O2]$$

where E°_{254} is the incident photon fluence rate (Ei m^{-2} s^{-1}) at 254 nm, ε_{254} is the decadic molar extinction coefficient of the organic compound at 254 nm (M^{-1} cm^{-1}), ϕ_{254} is the quantum yield at 254 nm (mol Ei^{-1}), α is the solution absorbance (cm^{-1}), and z is the light path length (cm). S_{254} is the screening factor of the water due to light absorption from NOM and other constituents that absorb light at 254 nm:

$$S_{254} \approx \frac{[1-10^{-\alpha z}]}{(2.3)(1.2)\alpha z}$$

R_{form,HO,NO_3^-} and $R_{form,HO,DOM}$ are the formation rates (M s^{-1}) of $HO^{\bullet}$ from NO_3^-, and NOM, which may be calculated using:(Jasper & Sedlak, 2013)

$$R_{form,HO,NO_3^-} = S_{254}\frac{E^{\circ}_{254}\varepsilon_{NO_3^-,254}\varphi_{NO_3^-,254}[1-10^{-\alpha z}]}{\alpha z}[NO_3^-]$$

$$R_{form,HO,DOM} = \frac{E^{\circ}_{254}\varphi_{DOM,254}[1-10^{-\alpha z}]}{\alpha}$$

Compound specific parameters are listed below (Table A.4.1). Trace metals and divalent cations from 1% Nitric acid stocks (0.159 M) were diluted 670 times into the 4 L influent vessel.

Table A.4.1. Concentrations, molar absorptivities, and quantum yields of solution constituents.

Species	**H_2O_2** *(a)*	**NO_3^-** *(b)*	**NOM** *(c)*
ε_{254} (M^{-1} cm^{-1})	18.6	4	-
φ_{254}	1	1.6×10^{-2}	3.7×10^{-5}
Conc (M)	$\sim 0.5 \times 10^{3}$	240×10^{6}	1 *d*

a (Barazesh et al., 2015). [b] (Zepp et al., 1987). [c] (Jasper & Sedlak, 2013). [a]NOM concentration is given in mg L^{-1}.

Given z = 0.043 m, where E°_{254} = 106.9 μEi m^{-2} s^{-1}, and α= 3.93 m^{-1}, we obtain:

$$R_{form,HO,H_2O_2} = 6.18 \times 10^{-4}\ M\ s^{-1}$$

$$R_{form,HO,NO_3^-} = 1.03 \times 10^{-6}\ M\ s^{-1}$$

$HO^{\bullet}$ formed from the photolysis of NO_3^- amounts to 0.17% of the $HO^{\bullet}$ formed from the photolysis of H_2O_2 and therefore considered to have a negligible effect on the transformation processes.

A.4.2 NOM Characterization by Mass Spectroscopy

NOM average molecular weight ($MW_{NOM,Avg}$), H/C ratio ($MW_{H/C,Avg}$), and O/C ratio ($MW_{O/C,Avg}$), were calculated as the weighted average of the peak intensity of a given chemical formula with either the molecular weight, H/C ratio, or O/C ratio, respectively:

$$MW_{NOM,Avg} = \frac{\sum MW_i \times P_i}{\sum P_i}$$

$$MW_{H/C,Avg} = \frac{\sum H/C_i \times P_i}{\sum P_i}$$

$$MW_{O/C,Avg} = \frac{\sum O/C_i \times P_i}{\sum P_i}$$

where MW_i, H/C_i, and O/C_i are the molecular weight, H/C ratio, and O/C ratio of a distinct chemical formula, i, and P_i is the peak intensity. An example calculation to determine weighted standard deviations is provided below:

$$MW_{NOM,STD} = \sqrt{\frac{\sum P_i \times (MW_i - MW_{NOM,Avg})^2}{\left(\frac{N-1}{N}\right)\sum P_i}}$$

where N is the number of observations.

A.4.3 Reduction of steady-state concentrations of reactive intermediates in the presence of quenchers.

$HO^\bullet$ may be formed from the photolysis of H_2O_2, chromophoric dissolved organic matter, or NO_3^-. $HO^\bullet$ is primarily scavenged by DOM, H_2O_2, HCO_3^-, and CO_3^{2-}. Therefore, $[HO^\bullet]_{SS}$ can be calculated by:

$$[HO^\bullet]_{SS} = \frac{R_{form,HO,H_2O_2} + R_{form,HO,CDOM} + R_{form,HO,NO_3^{3-}}}{k_{HO,DOM}[DOM] + k_{HO,H_2O_2}[H_2O_2] + k_{HO,HCO_3^-}[HCO_3^-] + k_{HO,CO_3^{2-}}[CO_3^{2-}]}$$

where R_{form,HO,H_2O_2} , $R_{form,HO,CDOM}$, and $R_{form,HO,NO_3^{3-}}$ are the formation rates (M s^{-1}) of $HO^\bullet$ and $k_{HO,DOM}$, k_{HO,H_2O_2}, k_{HO,HCO_3^-}, and $k_{HO,CO_3^{2-}}$ are the second-order reaction rate constants between $HO^\bullet$ and water constituents. Assuming the formation rate is unaffected by the presence of the radical quencher (in this case tertiary butanol), then the percent reduction in the steady-state concentration of $HO^\bullet$ can be expressed as the ratio of the denominator in the presence and absence of tertiary butanol(i.e., $k_{HO,tbuoH}[tbuOH]$):

$$\text{Reduction in } [HO^\bullet]_{SS} = \frac{k_{HO,DOM}[DOM] + k_{HO,H_2O_2}[H_2O_2] + k_{HO,HCO_3^-}[HCO_3^-] + k_{HO,CO_3^{2-}}[CO_3^{2-}]}{k_{HO,DOM}[DOM] + k_{HO,H_2O_2}[H_2O_2] + k_{HO,HCO_3^-}[HCO_3^-] + k_{HO,CO_3^{2-}}[CO_3^{2-}] + k_{HO,tbuoH}[tbuOH]}$$

At pH 9.3, the alpha values for carbonate speciation are: $\alpha_1 = 0.914$, $\alpha_2 = 0.085$. Considering 5 mM $[HCO_3]_{TOTAL}$, 0.5 mM H_2O_2, and 1 mgC L^{-1} DOM, and using the rate constants provided in below in Table A.4.2, one gets a reduction in $HO^\bullet$ of **71.8%.**

Table A.4.2. Rate Constants for hydroxyl radical and water constituents.

Rate Constant	Value	Citation
$k_{HO,DOM}$ (mgC L^{-1} s^{-1})	1.7×10^4	Jasper et al. 2013
k_{HO,H_2O_2} (M^{-1} s^{-1})	2.7×10^7	Buxton et al. 1988
k_{HO,HCO_3^-} (M^{-1} s^{-1})	8.5×10^6	Buxton et al. 1988
$k_{HO,CO_3^{2-}}$ (M^{-1} s^{-1})	3.9×10^8	Buxton et al. 1988
$k_{HO,tbuoH}$ (M^{-1} s^{-1})	6×10^8	Buxton et al. 1988

A similar approach can be applied for ^{3}NOM. In surface waters, the primary loss mechanism is through reaction with dissolved oxygen (roughly 250 µM for oxygenated waters), which has a rate constant of 2×10^9 M^{-1} s^{-1}(Rosario-Ortiz & Canonica, 2016). Although we cannot find an exact bimolecular rate constant between ^{3}NOM and isoprene, previous researchers have observed using flash spectroscopic studies that conjugated dienes quench high energy sensitizers (i.e., ^{3}NOM) at rates close to diffusion controlled limits (Liu *et al.*, 1965; McNeill & Canonica, 2016). Therefore, assuming a reaction rate constant of 1×10^9 M^{-1} s^{-1} and 500 µM isoprene, one gets a reduction in steady-state ^{3}NOM of **50%.**

For $^1O_2$, the percent reduction in steady-state values is a combination of reduction in the formation rate due to light screening (~7%) and the increase in scavenging rate due to by 50 µM NaN_3. The primary scavenger in the absence of NaN_3 is quenching by water, which has a decay rate of 2.5×10^5 s^{-1} (Haag & Mill, 1987). As the second order reaction rate constant between $^1O_2$ and NaN_3 is 5×10^8 M^{-1} s^{-1}, the decrease in steady-state $^1O_2$ due to quenching is ~10%. Therefore, the total decrease in steady-state $^1O_2$ can be estimated to be close to ~17%. Note, that quenching rate obtained with NaN_3 need to be interpreted with caution, due to the formation of azide radicals. However, as $^1O_2$ are formed through reactions of O_2 with ^{3}NOM, the previous example using isoprene which quenches 50% of the ^{3}NOM should also lower the steady state $^1O_2$ by 50%. Collectively, the observed results (i.e., Figure 4.19) and calculations rule out the importance of reactive radical species to the removal of Fe from the system.

A.4.4 Light Screening and Branching Ratio for Hydroxyl Radical

The absorbance of 510 µM H_2O_2 at pH 9 at 254 nm is approximately 0.0114 while the absorbance of NOM in the authentic water at 254 nm, when corrected for background constituents, is approximately 0.061. Therefore, the fraction of UV light at 254 nm going to the photolysis of H_2O_2 is **18%**. In other words, NOM screen ~82% of the incident light at 254 nm.

The fraction of $HO^{\bullet}$ going to NOM can be expressed as:

$$= \frac{k_{HO\bullet,NOM}[NOM]}{k_{HO\bullet,NOM}[NOM] + k_{HO\bullet,HCO3}[HCO_3^-] + k_{HO\bullet,CO32-}[CO_3^{2-}] + k_{HO\bullet,H2O2}[H_2O_2]}$$

Where $k_{HO\bullet,NOM} = 1.7 \times 10^4$ mgC^{-1} L^{-1}, $k_{HO\bullet,HCO3} = 8.5 \times 10^6$ M^{-1} L^{-1}, $k_{HO\bullet,CO32-} = 3.9 \times 10^8$ M^{-1} L^{-1}, and $k_{HO\bullet,H2O2} = 2.7 \times 10^7$ M^{-1} L^{-1}. In groundwater at pH 9.1 in the presence of 510 µM H_2O_2, ~5 mM TIC, and 0.5 mgC L^{-1} NOM, approximately **11.7%** of $HO^{\bullet}$ react with NOM.

A.4.5 System Energy Calculations

The total system power (P_{total},W) is a combination of the UV lamp power and the electrochemical cell power, which can be expressed as a product of the current density (I, A m^{-2}), cell potential (V_{cell}), and the electrode surface area (A, m^2) :

$$P_{total} = I * A * V_{cell} + P_{lamp}$$

At a current density of 25 A m^{-2}, cell potential of 13.6 V, flow rate of 121 L d^{-1}, and lamp power of 9 W, the total power demand of the treatment system was 0.01175 kW. The energy demand per m^3 can be calculated as the power demand divided by the system flow rate, which yields an energy demand per m^3 of 2.21 kWh m^{-3}.

A.4.6 Iron Dosing and Sludge Calculations

The amount of Fe needed to reduce the arsenic concentration from 28 µg L^{-1} to below the World Health Organization Maximum Contaminant Level of 10 µg L^{-1} in authentic groundwater can be calculated using the arsenic sorption capacity of iron oxides determined in Figure 2 (i.e., 0.0123 mol_{As}: mol_{Fe}). Using the ambient iron in the system (approximately 10 µM), the arsenic was reduced to 16.2 µg L^{-1}. Therefore, to remove an additional 6.2 µg L^{-1} of As if would require:

$$\left(\frac{6.2\ \mu g\ As}{L}\right)\left(\frac{1\ \mu M\ As}{\frac{74.9\ \mu g\ As}{L}}\right)\left(\frac{1\ \mu MFe}{0.0123\ \mu MAs}\right) = 6.73\ \mu M\ Fe$$

The total amount of iron oxide sludge produced per liter of treated water would be

$$\left(\frac{10.5 + 6.73\ \mu mol\ Fe}{L}\right)\left(\frac{54.55\ \mu g\ Fe}{1\ \mu mol\ Fe}\right) = 1.07\ mg\ Fe\ L^{-1}$$